MEASUREMENT OF COPOLAR ATTENUATION THROUGH THE BRIGHT BAND AT 4 & 7 GHz

by

JACK A. VAN DER STAR

BASc., The University of British Columbia, 1977

A THESIS SUBMITTED IN PARTIAL FULFILLMENT OF

THE REQUIREMENTS FOR THE DEGREE OF

MASTER OF APPLIED SCIENCE

in

THE DEPARTMENT OF ELECTRICAL ENGINEERING

We accept this thesis as conforming

to the required standard

THE UNIVERSITY OF BRITISH COLUMBIA

April 1982

In presenting this thesis in partial fulfilment of the requirements for an advanced degree at the University of British Columbia, I agree that the Library shall make it freely available for reference and study. I further agree that permission for extensive copying of this thesis for scholarly purposes may be granted by the head of my department or by his or her representatives. It is understood that copying or publication of this thesis for financial gain shall not be allowed without my written permission.

Department of Electrical Engineering

The University of British Columbia
1956 Main Mall
Vancouver, Canada
V6T 1Y3

Date April 15, 1982

ABSTRACT

This thesis describes an experiment designed to measure microwave propagation through the bright band at 4 and 7 GHz. The path is located approximately 100 kilometers east of Vancouver, British Columbia, Canada, forming part of the Trans Canada Telephone System microwave network. The path is coastal and mountainous in nature, 41.3 kilometers in length and experiences an average annual rainfall of 1600 mm/year. Due to these factors and an elevation differential of 1227 m between transmitting and receiving sites, the 0°C isotherm and hence bright band effect normally exist along the path from November to April.

A measurement system based on remote telemetry is used to obtain high resolution and accurately time-correlated data. Received signal levels are taken from five selected 4 and 7 GHz microwave channels which are sampled at a rate of 10 Hz. Meteorological information is obtained from five locations along the path and sampled at a rate of 1 Hz. The data thus collected are then time-correlated as it arrives at the University of British Columbia (Vancouver) recording site where it is analyzed using high-level language routines developed as part of a propagation data base management system. A detailed description of both the measurement system and the data management system are provided in the thesis.

Results from several precipitation systems indicate that bright band attenuation can be many times (in dB per kilometer) greater than attenuation due to equivalent amounts of rain. This is described by an Excess Attenuation

Ratio (EAR) defined as the ratio of the excess attenuation in dB/km calculated using the Laws and Parson distribution at 0°C. The experimental results compare favourably with those predicted by the theoretical model of Matsumoto and Nishitsuji.

A scintillation type fading phenomenon superimposed on the broad-band fade has also been observed during bright band propagation conditions. From the preliminary results this phenomenon appears to be correlated with sudden changes in differential temperature between transmitter and receiver sites and thus a corresponding change in the thickness of the bright band.

TABLE OF CONTENTS

	Page
ABSTRACT	ii
TABLE OF CONTENTS	iv
LIST OF ILLUSTRATIONS	vii
LIST OF TABLES	xiv
ACKNOWLEDGEMENTS	xv
I. INTRODUCTION	1
1.1 The Importance of Microwave Propagation in the Design of Microwave Systems	1
1.2 Factors Affecting Microwave Propagation	2
1.2.1 Path Factors	3
1.2.2 Rain Attenuation	5
1.2.3 Multipath Fading	10
1.2.4 Other Propagation Factors	12
1.3 Improving Reliability in Path Design	13
1.4 Bright Band Effects	15
1.5 Scope of Thesis	21
1.5.1 The Research Program	21
1.5.2 Thesis Objectives	23
1.5.3 Thesis Outline	24
II. THE EXPERIMENT	26
2.1 Introduction	26
2.2 The Path	26
2.3 Received Signal Monitoring	26
III. METEOROLOGICAL INSTRUMENTATION	35
3.1 System Design	35
3.1.1 Measurement Criteria	35
3.1.2 Site Selection	35
3.2 Meteorological Measurements	39
3.2.1 Rain	39
3.2.2 Temperature Transducer	41
3.2.3 Wind Velocity and Wind Direction Transducer	42
3.3. Meteorological-Data Sampling	42

		Page
IV.	DATA ACQUISITION SYSTEM	45
4.1	Design Criteria for a Real Time Data Acquisition System	45
4.2	Site Selection	47
4.2.1	Received Signal Site	47
4.2.2	Meteorological Sites	48
4.3	Data Collection Network Design	49
4.3.1	Data Statistics	49
4.3.2	Link Capacities	49
4.3.3	Node Considerations	50
4.3.4	Implementation of the Network Topology	51
4.4	Real Time Data Storage	52
4.4.1	Microprocessor Considerations	52
4.4.2	Data Storage Formats	52
4.5	Allowance for Future Data Requirements	54
4.6	An Alternate Data Acquisition System Using Chart Recorders.	54
V.	DATA BASE MANAGEMENT SYSTEM	55
5.1	Specifications	55
5.2	Design Considerations for DBMS Relative to Existing and Future Systems	57
5.3	A System Description of DBMS	59
5.3.1	Data Transfer and Handling	59
5.3.2	Estimate of DBMS Data Volumes	61
VI.	RESULTS	62
6.1	Some Initial Results Obtained Using Chart Recording	62
6.2	Events Measured Using Remote Telemetry Showing Bright Band Propagation	66
6.2.1	January 23, 1982, 7:30-11:30 p.m.	66
6.2.2	January 23, 1982, 2:00-4:30 p.m.	70
6.2.3	February 19, 1982, 7:30-9:00 a.m.	79
VII.	CONCLUSIONS AND DIRECTIONS FOR FUTURE RESEARCH	84
7.1	Conclusions	84
7.2	Directions for Future Research	85

		Page
APPENDIX A	Automatic Gain Control (AGC) Calibrations	89
APPENDIX B	Details of the Data Acquisition System Layout	95
APPENDIX C	Equipment and Site Layouts	106
APPENDIX D	Meteorological Transducers	122
APPENDIX E	Signal Conditoning Units	127
APPENDIX F	Analog to Digital Convertor	136
APPENDIX G	Digital to Analog Convertor	142
APPENDIX H	Modem Units	145
APPENDIX I	Microprocessor Units	150
APPENDIX J	Microprocessor Software	169
APPENDIX K	The Bright Band Propagation Experiment's Data Base Management System	190
REFERENCES	. . . . .	200

LIST OF ILLUSTRATIONS

Figure		Page
1.0	Path Factors	3
1.1	Specific attenuation as a function of frequency for coherent wave propagation through uniform rain. The curves are based on the Laws and Parsons dropsize distribution and the terminal velocities of Gunn and Kinzer. — — — — Rain temperature of 20°C. — — — — Rain temperature of 0°C.	8
1.2	A microwave system diagram illustrating space diversity, equipment diversity and frequency diversity	14
1.3	The character and classification of snow as it passes through the bright band as seen on water-blue paper	18
1.4	Falling velocity vs. radii of raindrops and snowflakes . . .	19
1.5	Relative bright band geometries between slant path terrestial and earth space links	22
2.0	Geographical layout of the bright band propagation experiment	27
2.1	Path profile: Ryder Lake to Dog Mountain	28
2.2	Path photographs	29
2.3	Frequency selection plan and receiver equipment used at receiver site	31
2.4	4 GHz receiver microwave transmission block diagram	32
2.5	7 GHz microwave transmission system block diagram	33
3.0	Measurement system layout	36
3.1	Path cross-section showing relative locations of the weather station sites	38
3.2	Weather station inter-site distances	40
3.3	Photograph of the U.B.C. Weatherlog microprocessor and meteorological signal conditioning unit	43

Figure		Page
4.0	The data acquisition system block diagram with component areas identified	46
4.1	Data collection network topology	51
4.2	Photograph of the Video Terminal Displaying Incoming Data . .	53
5.0	The bright band experiment data system flow chart	56
5.1	DBMS in relation to other propagation data management systems	58
5.2	User flowchart to process time series data on the DBMS software system	60
6.0	Recordings of received signal at 7 GHz during bright band propagation: a) Event "A" (January 11-12, 1980) b) Event "B" (February 2, 1980)	63
6.1	The Agassiz temperature and 7.142 GHz signal level versus time	67
6.2	Agassiz rain rate and the 7.496 GHz signal level versus time	68
6.3	The 3.550 and 7.496 GHz signal levels versus time	71
6.4	The Dog Mountain transmitter site temperature and the 7.496 GHz reveiver levels versus time	72
6.5	The Ryder Lake receiver site temperature and the 7.496 GHz receiver level versus time.	73
6.6	An expanded view at approximately 80 minutes into the event showing the Ryder Lake temperature and 7.496 GHz receiver level versus time	74
6.7	Ryder Lake differential temperature and 7.496 GHz received signal level versus time showing the fade discontinuity 80 minutes into the event	75
6.8	Ryder Lake differential temperature and 7.496 GHz received signal level versus time showing discontinuities 30 minutes into the event.	76

Figure		Page
6.9	Ryder Lake windspeed, temperature and the 3.550 GHz received signal level versus time	77
6.10	An expanded view of the Ryder windspeed and 3.550 GHz received signal level versus time approximately 90 minutes into the event.	78
6.11	Ryder Lake and Dog Mountain Temperature, Ryder Lake Windspeed and the 7.496 GHz receive signal level versus time.	80
6.12	Agassiz rain rate and the 7.496 and 4.010 GHz receive signals versus time	81
6.13	Ryder Lake differential temperature and the 7.496 GH receive signal level versus time.	83
7.0	Proposed system configuration to incorporate the digital radio monitoring system	88
A-1	3550 MHz receiver AGC calibration	90
A-2	3790 MHz " " "	91
A-3	4010 MHz " " "	92
A-4	7142 MHz " " "	93
A-5	7496.5 MHz receiver AGC calibration	94
B-1	Path system layout for U.B.C. microwave propagation experiment	97
B-2	Path profile Ruby Creek to Ryder Lake	98
B-3	Path profile: Bear Mountain to Ryder Lake	98
B-4	Circuit layout from Dog Mountain to Ryder Lake	99
B-5	Circuit layout from the Agassiz Experimental Farm to Ryder Lake	99
B-6	Schematic for the Ryder Lake to U.B.C. data circuit	100
B-7	The RS232 interface for the Ryder Lake to U.B.C. data circuit	101

Figure		Page
C-1	Ryder Lake site photograph	102
C-2	Ryder Lake site equipment configuration	103
C-3	Ryder Lake site layout	104
C-4a	Dog Mountain site photograph	105
C-4b	A photograph showing damage to the anemometer caused by severe icing conditions at Dog Mountain	106
C-5	Dog Mountain site equipment configuration	107
C-6	Dog Mountain site layout	108
C-7	Agassiz Experimental Farm site photograph	109
C-8	Agassiz Experimental Farm site equipment configuration . . .	110
C-9	Agassiz Experimental Farm site layout	111
C-10	Ruby Creek site photograph	112
C-11	Ruby Creek site equipment configuration	113
C-12	Ruby Creek site layout	114
C-13	Bear Mountain site photograph	115
C-14	Bear Mountain site equipment configuration	117
C-15	Bear Mountain site layout	118
C-16	The University of British Columbia site photograph	119
C-17	The University of British Columbia equipment configuration .	120
C-18	The University of British Columbia site layout	121
D-1	A photograph of the anemometer	122
D-2	Anemometer circuit and wiring diagram	123
D-3	A typical rain bucket and tipping assembly	124
D-4	Photograph of the temperature probe	125

Figure		Page
E-1	Top view Photograph of the meteorological signal conditioning unit	127
E-2	Circuit schematic for the meteorological signal conditioning unit	128
E-3	Front and rear views of the meteorological signal	129
E-4	Circuit schematic for the Bear Mountain signal conditioning card	132
E-5	Circuit schematic for the receiver signal conditioning card .	134
F-1	Photographs showing the A/D convertor separately and installed	137
F-2	Circuit schematic and physical layout for the Weatherlog analog to digital convertor	139
F-3	Control signal timing diagram for the A/D convertor	140
F-4	Sample oscilloscope traces of the A/D output during calibration	140
F-5	A/D calibration program	141
G-1	Circuit schematic for the D/A convertor	143
G-2	Listing of the program to provide chart recordings from the receiver data using the D/A converter	144
H-1	Photograph of an installed modem transmit unit	145
H-2	Interface schematic for a Weatherlog modem transmit unit . .	147
H-3	Physical drawing of the Ryder Lake receiver unit showing top, front and rear views	148
H-4	Interface schematic for one of the modem receiver units . . .	149
I-1	Physical drawing of the UBC data formatting (P#1) micro-processor showing front, top and rear views	151
I-2	Physical drawing of the UBC data processing (P#2) micro-processor showing front, top and rear views	152

Figure		Page
I-3	Photograph showing the interior layout of the data formatting (μP#1) and data processing (μP#2) microprocessors	153
I-4	Circuit schematic and physical layout of the asynchronous interface (ACIA) card	156
I-5	Physical drawing of the Ryder Lake microprocessor unit showing front, top and rear views	160
I-6	Physical drawing of the Weatherlog microprocessor showing front, top and rear views	162
I-7	Photograph showing the interior layout of a typical UBC Weatherlog microprocessor unit	163
I-8	Physical drawing of the low power microprocessor unit used at Bear Mountain	165
I-9	Photograph showing the interior layout of the Bear Mountain microprocessor unit	166
I-10	Equipment configuration to transfer data from the cassette tape drive to the NOVA 840 magnetic tape drive	167
I-11	Circuit diagram of the RS232C to current loop interface . . .	168
J-1a	Program flow chart for μP#1; the UBC data formatter	171
J-1b	Data formatter buffer memory organization	172
J-2	Program flow charts for μP#2; the UBC data processor microprocessor unit	173
J-3	Diagram showing the structure of the time series queue (TSQ)	176
J-4	Data acquisition flow chart for the Ryder Lake datalog 6800 microprocessor	183
J-5	Program flow chart for the UBC Weatherlog 8085 data acquisition microprocessors	185
J-6	Data acquisition and control program flow chart for the remote Bear Mountain 1802 microprocessor unit	187
J-7	Program flow chart to transfer data from cassette tapes to magnetic tape using the NOVA 840	189

Figure		Page
K-1	DBMS functional flow chart showing completion status	192
K-2	DBMS main program flow chart	193
K-3	Sample Plotting Run	199

LIST OF TABLES

Table		Page
1.0	Attenuation Multipliers Due to Watery Snow	20
2.0	Microwave Transmission Calculations	34
3.0	Geographical and Functional Site Details	37
3.1	Inter-Site Distances as a Function of Path Length	40
4.0	Data Acquisition System Link Capacities	54
5.0	DBMS Data Volume Estimates	61
6.0	Preliminary Results	64
6.1	Bright Band Excess Attenuation Ratio (EAR) Results	64
6.2	January 23, 1982 Results (7 GHz)	69
6.3	Bright-Band Excess Attenuation (EAR) Results	69
6.4	February 19, 1982 Results	82
6.5	February 19, 1982 EAR Results	82
A-1	Receiver Frequencies Polarizations and Associated AGC Curves.	89
B-1	VHF Radio Path Transmission Calculations	96
E-1	The Resistor Values Used in the Differential Gain Block for Optimum Gain	133
F-1	A/D Convertor Channel Assignment Table	138
H-1	Modem Center Frequency Assignments	146
I-1	I/O Port Address assignments for the Data Formatter Unit μP#1	154
I-2	I/O Port Address assignments for the Data Processor Unit μP#2	155
I-3	6800 Interrupt Vectors	157
I-4	Analog to Digital (A/D) Convertor Channel Assignments	159
I-5	I/O Port Address Assignments for the Ryder Lake Unit	161
J-1	RAM Time Assignments (μP#1)	178
J-2	Time Series Block Format	179
J-3	Data Format for the Distribution Buffer	180
K-1	Data Directory for the Time Series Format	195

ACKNOWLEDGEMENTS

I would like to acknowledge my appreciation to Dr. M.M.Z. Kharadly who has provided me with much needed support, supervision and suggestions throughout the course of this research.

A grateful acknowledgement is also extended to Mr. Neville Owen of the British Columbia Telephone Company for his much appreciated assistance, his field coordination and his advice throughout my thesis work. I would also like to thank the following people at the British Columbia Telephone Company for their invaluable contributions made during this research:

Mr. Bill Squans
Mr. Stan Dahl
Mr. Red Matthews
Mr. George Gatt
Mr. Dwight Chan
Mr. Peter Claydon

In the same way I would like to thank the following staff at the Communications Research Centre in Ottawa for their numerous suggestions, for their continued support and for providing a stimulating working environment during my stay:

Dr. Stewart McCormick
Dr. Rod Olsen
Dr. Dick Butler
Dr. Ben Segal
Dr. John Strickland
Mr. Neville Reed
Mr. Hassen Kheirallah
Mr. Joe Schlesak

My gratitude is also extended to the following people at the Agassiz Experimental Farm for generously providing valuable back up meteorological data from their weather station, for maintaining the UBC chart recordings and looking after the UBC Weatherlog computer:

Mr. Frank DeZwaan
Ms. Moira Jewell

I would like to give many thanks to Dr. Terry Enegren and Mr. David Michelson, for implementing the integration phase of the remote telemetry and DBMS systems, making the results possible. I would also like to express my gratitude to the following staff at the Department of Electrical Engineering for their contributions:

Mr. James Johnston
Mr. Eric Minch
Mr. Edwin Lee
Mr. Jun Lee

Thanks are due to Ms. Sherry Lashmar and Mrs. Kathy Brindamour for typing the manuscript, Mr. Ben Van der Star for his help in assembling the electronics and to Mr. Len Smart for the development of the entry procedure and plotting routine packages.

I would also like to thank all my friends and colleagues, particularly Dr. Basil Peters, Mr. Peter van der Gracht, Mr. Konrad Mauch and Mr. Frank Peabody for creating an enjoyable and stimulating working environment. I would like to greatfully acknowledge, as well, the Agassiz Experimental Farm and the Canadian Broadcasting Corporation for their cooperation in allowing the use of their facilities at intermediate valley sites along the path.

This work was supported by the British Columbia Telephone Company through contract number 000708 (NO/KO), the Communications Research Centre in Ottawa through contract numbers OSU 79-00061, OSU 80-00146 and 81-00112 and The National Science and Engineering Research Council of Canada through grant number A-3344.

Finally, I would like to thank my wife Kathy for her continued patience, encouragement and support during my master's program.

CHAPTER 1

INTRODUCTION

1.1 The Importance of Microwave Propagation in the Design of Microwave Systems

Microwave propagation parameters affect the reliability (availability) of terrestrial and satellite communication systems and thus have a major influence on their economics [1]. Therefore, techniques to confidently estimate this reliability are essential before system planners and designers can implement cost effective and economically viable microwave transmission systems [2].

Microwave transmission systems below 10 GHz include both satellite and terrestrial networks with common carriers and CATV operators being the main users. The least demanding from an availability viewpoint is the CATV operator. His performance requirements are deemed satisfactory if the system is available for more than 99.8% of the time, which represents an outage of approximately 1000 minutes per year [3]. On the other hand, the most demanding user of communication systems are the common carriers who presently operate at 4, 6 and 7 GHz and propose to start operations in the 8 GHz band [4]. An example of a typical common carrier system specification is the one proposed for the Vancouver to Halifax, 8 GHz digital circuit. The system is specified to be available for more than 99.98% of the time [5], where the unavailability of less than 0.02% has been allocated with an allowance of 1/2 (.01%) for equipment failures, 1/4 (.005%) for rain outages and 1/4 (.005%) for multi-path fading outage. On an average per-hop basis this represents an

unavailability requirement of less than .0002% (63.2 seconds) of the time, where the combined propagation outage factors of rain and fading may not account for more than .0001% (31.6 seconds). Therefore, accurate estimation of the propagation reliability is essential before installation since propagation factors not accounted for in the original design could prevent meeting the total system availability objective. In this light, the work described by this thesis was started to study factors associated with bright-band propagation at 4 and 7 GHz, for which no account has yet been made.

1.2 Factors Affecting Microwave Propagation

Microwave propagation for frequencies below 10 GHz are largely affected by a path's geometry and associated weather characteristics. Microwave propagation is affected by the path's geometry in the way of free space attenuation, curvature changes due to variations in the refractivity profile and obstruction losses. Propagation factors related to meteorological conditions along a microwave path result in rain attenuation, multipath fading, and reductions in received signal levels due to the presence of the bright-band. Other factors such as gaseous absorption by water vapour oxygen and fog also exist to a minor extent below 10 GHz. A discussion of these factors and their determination is the subject of this next section.

1.2.1 Path Factors

Figure 1.0 shows an example of a line-of-sight microwave path which would form a segment in a common-carrier's back-bone microwave system. It would typically have a hop length of 40 to 60 km, a fade margin of 40 dB and an operating frequency between 4 and 10 GHz [5].

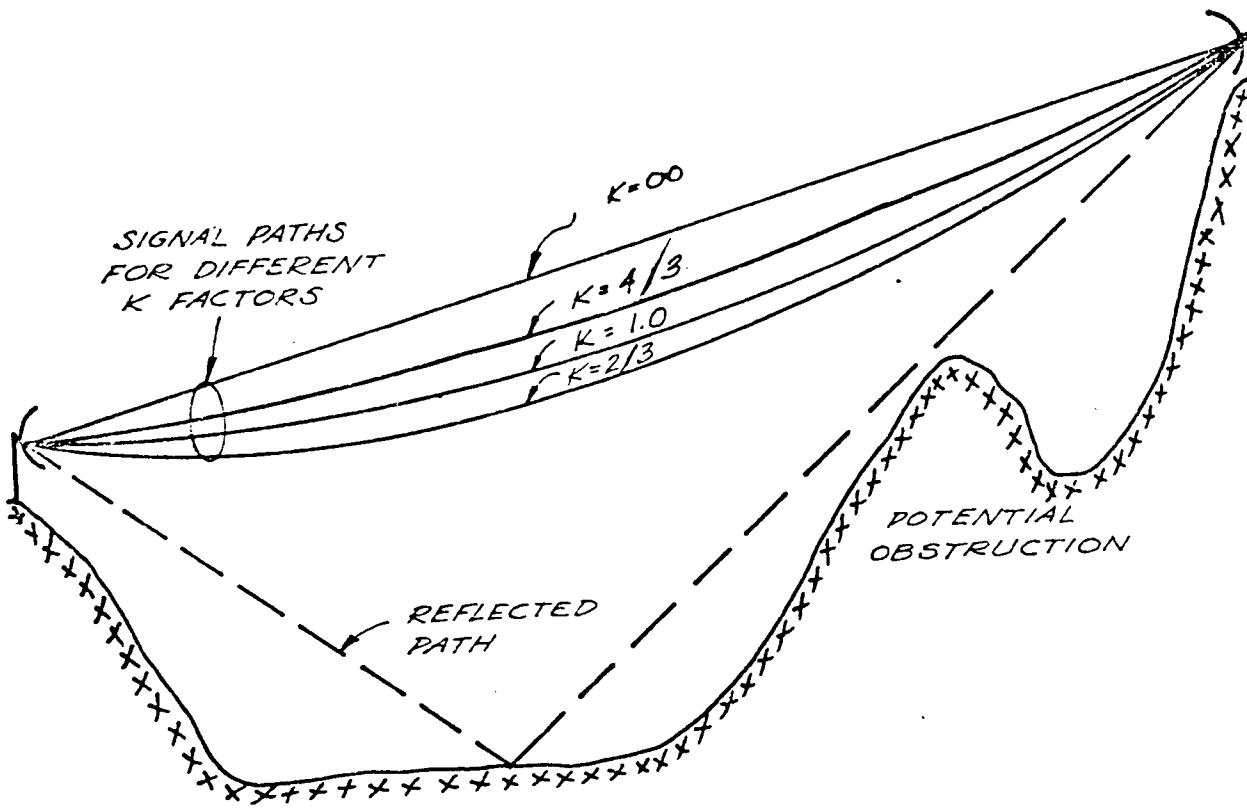

Figure 1.0 Path Factors

The Effect Due to Changes in Refractivity

Although a microwave path is often termed to be "line-of-sight", the beam does not travel in a straight line through the atmosphere from the transmitter to the receiver but rather bends as a result of a slight decrease in the atmospheric refractive index with height. This bending is described by a "K" or equivalent earth radius factor which, if multiplied by the actual earth radius r_o, gives the ficticious earth curve, r, travelled by the propagating microwave beam. Therefore, variations in atmospheric refractivity cause corresponding changes in the K factor and are described as a function of atmospheric temperature and water vapour content, as follows [6]:

$$N = (n-1)\ 10^6 = \underbrace{77.6\ \frac{P}{T}}_{\text{dry term}} + \underbrace{\frac{3.73\ 10^5\ e}{T^2}}_{\text{wet term}} \qquad (1\text{-}1)$$

where N: refractivity (N units)

n: refractive index

P: atmospheric pressure (m bar)

T: absolute temperature (°K)

e: water vapour pressure (m bar)

If a point is taken at a fixed elevation the radius of curvature of the beam, r, relative to the earth's radius r_o can be expressed as a function of the vertical index of refraction gradient dn/dh to give the following expression for the K factor [7]:

$$K = \frac{r}{r_o} \simeq \left(1 + r_o \frac{dn}{dh}\right)^{-1} = \left(1 + \frac{dN}{dh} / 157\right)^{-1} \Bigg|_{r_o = 6370\ \text{km}} \qquad (1\text{-}2)$$

Published maps on world atmospheric radio refractivity and refractivity

gradients are available [8,9,10].

Calculation of the Free Space Attenuation

The attenuation to a microwave signal emitted from an isotropic radiator can be determined as a function of frequency and distance by the following expression, [2]:

$$A_{dB} = 92.4 + 20 \log_{10} f + 20 \log_{10} D \qquad (1\text{-}3)$$

where, A_{dB}: free space attenuation (dB)

f: frequency (GHz)

D: distance (km)

Obstruction Losses

Obstruction losses vary according to a path's characteristic profile and operating frequency which allows their estimation, eg. Bullington [11].

1.2.2 Rain Attenuation

Early theoretical estimates of rain attenuation on microwave propagation were made by Ryde and Ryde [12,13] during World War II and were based on a first-order forward-scattering model that used a uniform distribution of equi-diameter spheres. The resulting expression for attenuation for a plane wave is given in equation (1-4):

$$\alpha = 0.4343 \times N \times \pi \times D^2 \times f_a \ (D/\lambda, m) \ dB/km \qquad (1\text{-}4)$$

where, α: attenuation (dB/Km)

N: density (m^{-3})

D: drop diameter (mm)

m: n-jnx, the complex refractive index of water

f_a: ratio of energy absorbed and scattered to that incident upon the projected area of the drop.

Medhurst, in his review [14], corrected the numerical calculations derived by Ryde using this model but found a large variation, greater than expected, in experimental measurements [15,16,17,18]. Medhurst suggested that some of this variation could be attributed to multiple scattering processes but further theoretical analysis by Crane [19] and Rogers & Olsen [20] determined that this effect would be insignificant and the "single scattering" model for rain attenuation was, in fact, valid for frequencies lower than 20 GHz. The discrepancy between theory and experiment which Medhurst observed has since been attributed to inaccurate rain rate measurements. Most researchers at present acknowledge that good agreement between theoretical estimates and carefully obtained experimental observations are possible [21].

In order to allow the calculation of the attenuation coefficient using path-average rain rate data, a relation between the rain rate, the density and the drop diameter is required. This is given in terms of the terminal velocity of a falling drop in (1-5):

$$R = 1.885 \times v \times N \times D^3 \text{ (mm/hr)} \qquad (1\text{-}5)$$

where, R: rain rate (mm/hr)

v: terminal velocity (m/sec)

N: density (m^{-3})

D: drop diameter (mm)

The terminal velocity is related to the drop diameter, as measured by Gunn and Kinzer [14], and therefore the calculation of the attenuation coefficient is

possible for uniform rain for a single drop size using (1-4). Physically, rain is composed of drop-sizes exhibiting a continuous range of diameters from 0.5 mm to 7 mm. Integrating the specific attenuation relation for a single drop size (1-4) over the whole drop size distribution for various rain rates gives the attenuation by actual rain vs. rain rate. Figure 1.1, taken from [22], provides a graph of the specific attenuation versus frequency at various rain rates using this approach.

The applicability of the results derived using the Ryde model is dependent on the diameter of the spheres used and, therefore, the proper selection of the drop size distribution is important. For most temperate-continental rainfall types the Laws and Parson distribution provides a good correlation between the Ryde model and experiment [23]. Other drop size distributions are available for differing applications which include the Marshall and Palmer distribution [24] and the Joss et al. distributions [25] for drizzle, wide spread rain and thunderstorms.

A Simplified Empirical Model for Rain Attenuation as a Function of Rain Rate

Further improvements to the calculation of specific attenuation as a function of rain rate have been made by Olsen, Rodgers and Hodge [22], who have developed the simplifying empirical formula in (1-6), known as the A - R relation:

$$A = a R^{b} \qquad (1\text{-}6)$$

where, A: attenuation (dB/Km)

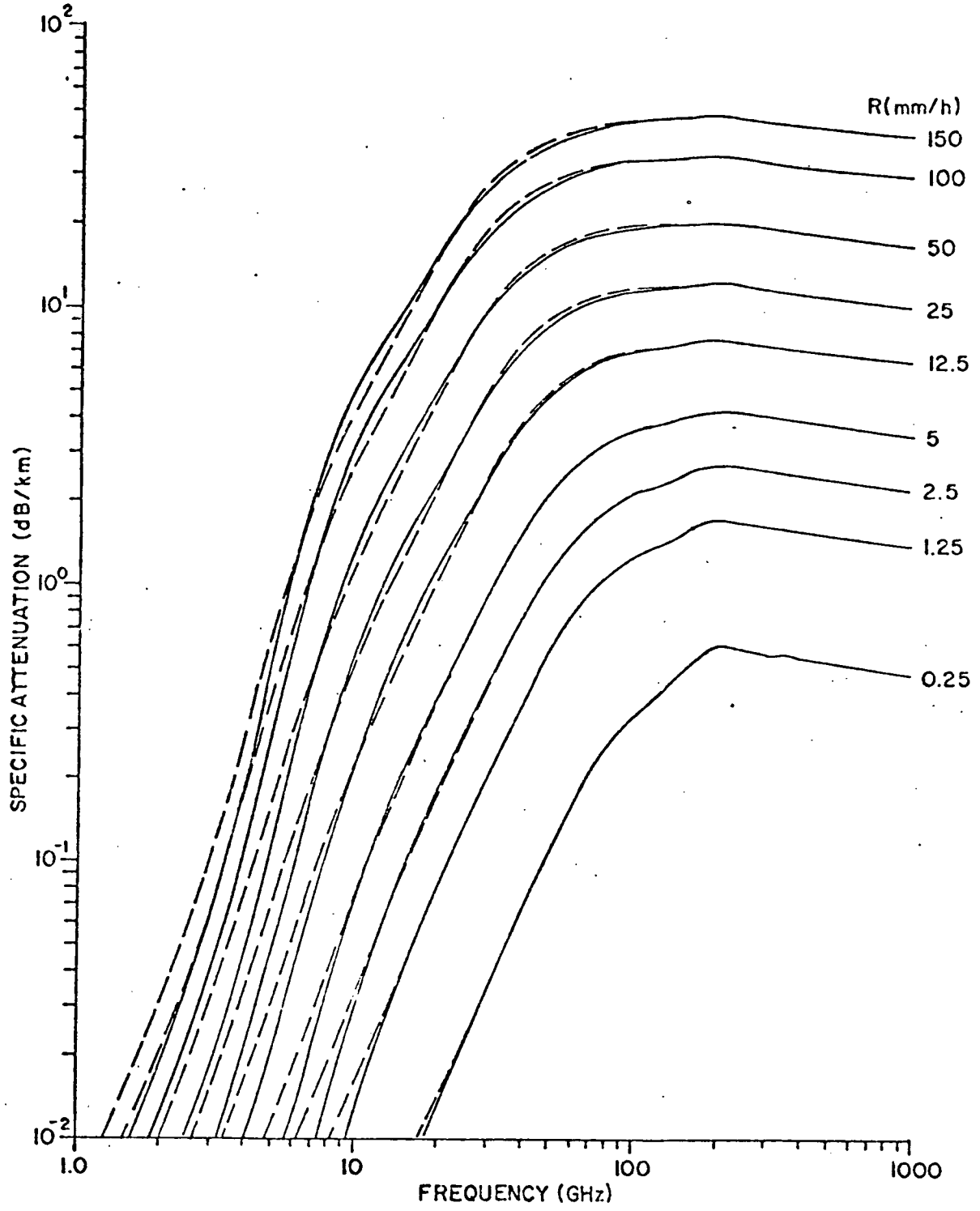

Figure 1.1 Specific attenuation as a function of frequency for coherent wave propagation through uniform rain. The curves are based on Laws and Parsons dropsize distribution and the terminal velocities of Gunn and Kinzer.

——— Rain temperature of 20°C.

- - - - - - - Rain temperature of 0°C.

R: rain rate (mm/hr)

a,b: frequency and rain temperature dependent parameters tabulated in [26]

Rain Rate Measurement

The determination of path attenuation due to rainfall requires the accurate measurement of path average rain rate. This is complicated by the fact that rain is non-uniform in nature and often consists of rain cells of limited extent [21]. Therefore, to obtain an accurate path average rain rate, the individual rain rates must be sampled at as many locations along the path as possible [26,27] or be estimated using synthetic storm techniques [59-62].

In a distributed system of rain guages, the path can be treated in segments where the total path attenuation due to rain is the sum of the individual segment attenuations, as follows:

$$A = \sum_{i=1}^{n} A_i = \sum_{i=1}^{n} \alpha_\lambda(R_i)\ell_i \qquad (1\text{-}7)$$

where, R_i: rain rate at guage i (mm/hr)

ℓ_i: length of segment i as a percentage of path length

(R_i): specific attenuation in dB/km at rain rate R_i

An approximation to (1-7) is usually adopted, (1-8), which uses the path average rain rate directly through the assumption that variations in rain rate segments are sufficiently small that the inter-segment specific attenuations are linearly related.

$$A \cong \alpha_\lambda \underbrace{\left(\sum_{i=1}^{n} \frac{R_i \times \ell_i}{L} \right)}_{*} \times L \qquad (1\text{-}8)$$

where, A: total path attenuation

α_λ: specific attenuation for a determined path average rain rate (dB/km)

R_i: rain rate for segment i (mm/hr)

ℓ_i: length of segment i

L: total path length (km)

*: path average rain rate

1.2.3 Multipath Fading

Under normal atmospheric conditions a line-of-sight hop provides one propagation path between transmitter and receiver antennas. If certain changes in the refractivity profile occur, additional propagation paths can result parallel to the main beam [6,28]. When these arrive together at the receiver, they add together according to their phase relationship producing variations in the received signal known as multipath fading. For N multiple propagation paths of amplitude a_n and delay τ_n the transfer function describing this phenomenon can be expressed as follows [6]:

$$H(f) = \sum_{n=1}^{N} a_n e^{-j\pi f \tau_n} \qquad (1\text{-}9)$$

Measurement Techniques and Physical Models

Investigations of multipath have either used a time-domain radar technique where the arrival of pulses are monitored by number, amplitude and time delay or used a frequency-domain technique where the path is swept in frequency and Fourier transformations are used to obtain the time-domain responses [29,30,31,32]. The conclusion from these experiments was that the number of propagation paths depends strongly on the links' meteorological conditions and that the frequency of a multipath fade increases with fade depth. Sanberg, using results from frequency swept measurements concluded that no multipath events occurred which could not be characterized by four or fewer rays [33]. Other swept measurements conducted by Martin [34] concluded that fades of the order of 20 dB are primarily due to two path propagation while deeper fades, of the order of 40 dB or more are due to the existence of at least three paths.

Models based on these physical parameters have been verified experimentally for ducting and for specialized types of atmospheric layering [35] but a general model which can be applied empirically from directly measured multipath parameters has yet to be developed [6].

Estimation of Multipath Propagation Outages

In order to characterize multipath propagation in a manner which allows path availabilities to be estimated, a general formula has been developed by Barnett [36] to calculate multipath outage probabilities as follows:

$$U = a \times b \times 6.0 \times 10^{-7} \times f \times D^3 \times 10^{[-F/10]} \qquad (1\text{-}10)$$

where, U: fade probability below fade margin

a: path roughness factor (4 for very smooth, 1 for average with some roughness and 1/4 for very rough mountainous terrain.)

b: factor to convert worst month probability to annual probability (1/2 for hot humid, 1/4 for average inland and 1/8 for very dry mountainous)

f: frequency (GHz)

D: path length (km)

F: fade margin under normal operation

Availability

For propagation factors such as multipath the availability is given by (1-11) [2].

$$A = (1-U) \times 100\% \qquad (1\text{-}11)$$

where: A - Availability defined as the percentage of time the received signal is useable

U - fade probability defined as the fraction of time the received signal is not useable.

1.2.4 Other Propagation Factors

Gaseous Absorption by Water Vapour, Oxygen and Fog

A minor effect on radio wave propagation near the earth's surface for frequencies lower than 10 GHz is due to the absorption by water vapour and oxygen. This effect increases with higher frequencies. At 10 GHz the attenuation is .007 dB/km at 20°C for oxygen absorption and .0045 dB/km at 20°C

for water vapour absorption [10]. The attenuation, therefore, amounts to less than one dB for an average 50 km microwave path. Fog also attenuates microwaves by the same scattering mechanism as rain but due to the much smaller drop diameters involved the amount of attenuation is minimal. Measured attenuations of 1 dB/km at 90 GHz are reported [37] which means for an average link the attenuation is considerably less than one dB for frequencies lower than 10 GHz.

Bright Band Effects

There is increasing evidence to suggest that the bright band causes attenuation in excess of what is normally predicted by a rain model. This is discussed in detail in section 1.4.

1.3 Improving Reliability in Path Design

Path reliability (availability) is a combined function of the propagation and equipment reliabilities and therefore both need to be considered in the design of a microwave link [2]. Improvements in propagation reliability can be achieved through careful path selection and the use of frequency and space diversity to minimize the effects of multipath and rain attenuation, while improvements in equipment availability are accomplished by using reliable system components and redundant configurations. Figure 1.2 illustrates these techniques.

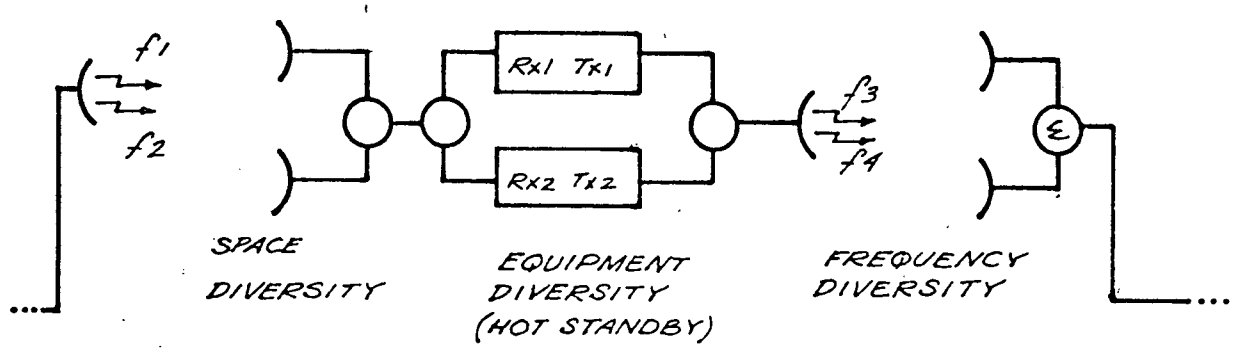

Figure 1.2 A Microwave System Diagram Illustrating Space Diversity, Equipment Diversity and Frequency Diversity.

For a typical non-diversity path of given path distance, fade margin, frequency and rain statistics the outage probabilities due to rain and multi-path fading can be calculated from equations (1-6) and (1-10) respectively. If further propagation reliability improvement is required space diversity and/or frequency diversity can be used on the link. The relationship used to calculate the space diversity improvement factor is given by Vigants [38] as follows:

$$I_{SD} = (1.2 \times 10^{-3} \times f \times S^2 \times 10^{[\bar{F}/10]})/D \qquad (1\text{-}12)$$

where, I_{SD}: space diversity improvement factor

S: vertical antenna spacing in meters

D: path length in kilometers

$\bar{F}$: fade margin associated with the second antenna

f: frequency in GHz.

Frequency Diversity

Similarly, a relation to calculate the frequency diversity improvement factor is given by Barnett [36]:

$$I_{FD} = a \times [\Delta f/f] \times 10^{[F/10]} \qquad (1\text{-}13)$$

where, I_{FD}: frequency diversity improvement factor

a: frequency band factor

(3 for the 890 - 960 MHz band
1 for the 2 GHz band
1/2 for the 4 GHz band
1/4 for the 6 GHz band
1/8 for the 7 & 8 GHz bands
and 1/12 for the 12 GHz band)

f: frequency (Hz)

Δf: frequency spacing (Hz)

F: fade margin (dB)

1.4 Bright Band Effects

The bright band is the transition region immediately below the 0°C isotherm where falling snowflakes melt and are turning into rain. Thus, bright-band propagation occurs when a microwave beam passes through precipitation in this region. It was named during World War II when high radar returns resulting from this melting layer region caused a "bright band" on the radar screens.

From a propagation point of view, there is increasing evidence which suggests that, during wet snow or sleet events, low angle microwave beams in temperate marine climates experience attenuation in excess of values predicted due to rain [39,40,41]. It has been postulated that the excess attenuation is a result of increased absorption and scattering upon transmission through the 0°C isotherm or bright band. Accurate direct measurement of this excess attenuation is difficult and there have been only few reported cases where quantitative results are given. Oomeri and Aoyagi [40] from propagation tests carried out Sapporo and Hokuriku, Japan, indicate that sleetfall attenution (in dB) to be six to seven times as large as the attenuation that can be predicted for the equivalent amount of rain. Watson [39], in his survey, cites propagation studies carried out in the USSR [41] which found similar results. Measurements taken using radar also shows excessive attenuation in the presence of bright band [42-47]. In addition to these published results, there are some reports in Canada, Scandanavia and the United Kingdom of excessive attenuation in the presence of sleet or wet snow [39].

Recently, by using stallite beacon signals to measure direct attenuation together with proven radar prediction methods for rain attenuation, more accurate measurements of bright band attenuation have been taken [44,47,48]. In this technique the rain attenuation is calculated to the base of the bright band and then this value is subtracted from the total attenuation to give an amount attributable to bright-band attenuation. Measurements taken by Hendry Antar, Schlesak and Olsen [47] using a dual-channel polarization diversity radar show a correlation of increased excess attenuation ascribed to the melt-

ing layer with an increase in the vertical thickness of the bright band layer for a given precipitation rate. They also found that the percentage of preferred orientation of the particles in the melting layer to be typically 20% as opposed to 65% to 85%, for rain.

An attempt to model the bright band has been made in a series of paper by Nishitsuji and Matsumoto [49,50,51] using the Ryde and Ryde approach [12,13]. Their first paper [49] establishes a set of Nrs density distribution tables of snowflake-size distributions for various classifications of snow similar to the tables of Laws and Parson. These distribution tables were prepared for four snow classifications: namely, dry snow, moist snow, wet snow and watery snow of which the last three represent snow types present in the bright band. Figure 1.3 taken from this paper illustrates these progressive changes in the character of snowflakes as they would appear on water-blue paper for snow as it passes through the bright band. In addition, Nishitsuji and Matsumoto measured the falling velocity corresponding to each snowflake diameter and for each snow classification. A graph of these results is presented in Figure 1.4 taken from [49].

The precipitation rate (P) can then be related to the density (Nrs), fall velocity (Vrs) and the radius (r_r) to allow the calculation of the snow attenuation for each snow classification as follows [51]:

$$P = \frac{4}{3} \pi \Sigma r_r^3 V_{rs} N_{rs} \qquad (1\text{-}14)$$

The greatest attenuation for equal precipitation rates was then found to be due to watery snow in the frequency range between 4 and 7 GHz. In terms of attenuation relative to rain of the same precipitation rate the attenuation

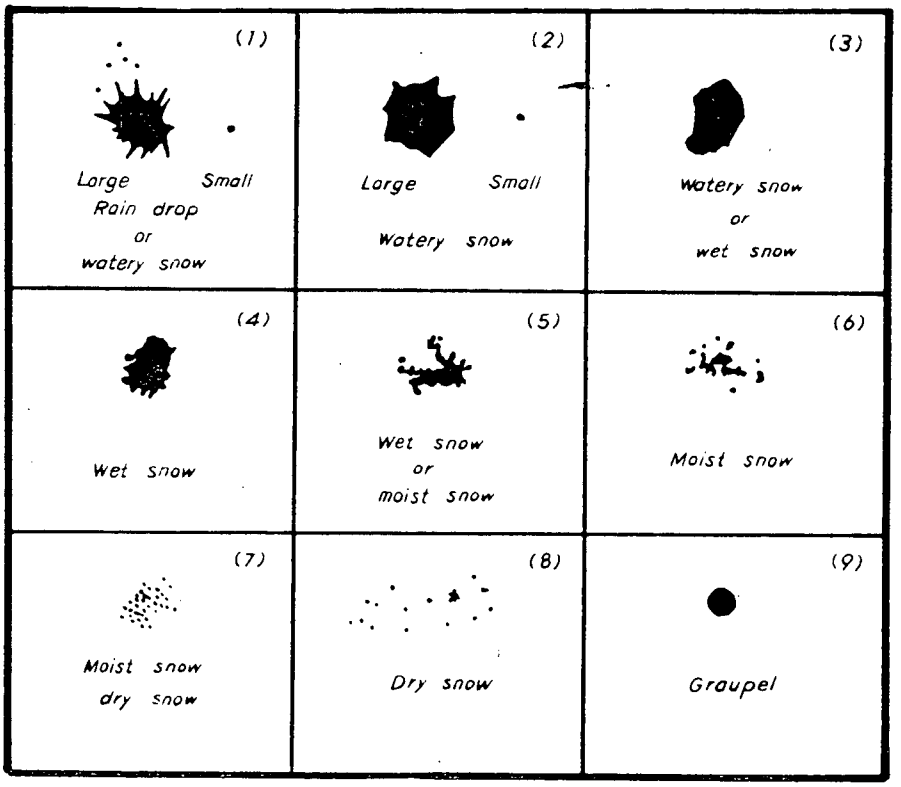

Figure 1.3 The Character and Classification of Snow as it passes through the Bright Band as seen on Water-Blue Paper.

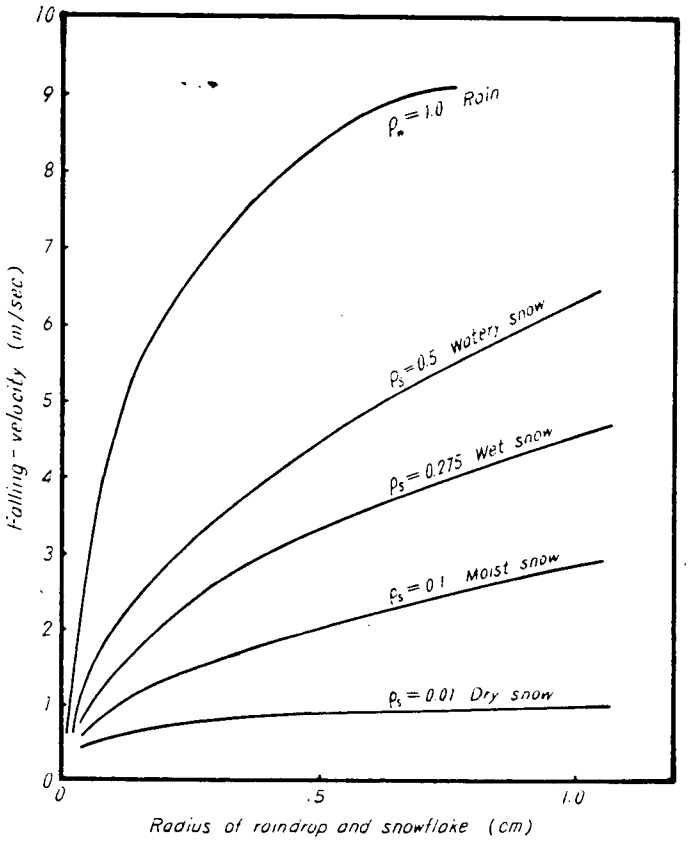

Figure 1.4 Falling Velocity vs. Radii of Raindrops and Snowflakes

due to watery snow in this range was calculated to be 15 times in dB's per kilometer. Table 1.0 presents these multiplier's in dB's per kilometer for various frequencies as derived from the model for wet snow [51].

Table 1.0 Attenuation Multipliers Due to Watery Snow.

Frequency (GHz)	Attenuation Multiplier (dB/km)
1	0.2
2	4.6
4	15.1
7	15.0
11	12.1
24	7.3
35	7.0
50	6.5

There are several supporting physical reasons why the attenuation at a fixed precipitation rate for watery and wet snow is greater than that due to rainfall [50]:

a) for a raindrop and watery snowflake of the same weight the latter has the greater radius;

b) the rate of fall of watery snow as compared to a raindrop is smaller so that the number of snowflakes in a unit volume is greater than that of rain;

c) snowflakes do not break up during their fall through the melting layer since the drop size spectrum just above the melting layer is similar in shape to that just below it [53];

d) the distribution of raindrop radii is semilogarithmic while that of watery snow is the sum of the same semilogarithm due to aggregation at the top of the melting layer [52-57], which means there are many large sized snowflakes in the bright band. This greatly impacts attenuation since the increase is proportional to the cube of the diameter of a snowflake or raindrop.

Possible Impact on Microwave Transmission Systems

For paths such as earth-space links and slant paths in temperate marine climates the bright band could have a significant effect which suggests that allowances should be made for this type of attenuation when predicting propagation reliability. Excess attenuation as a result of propagation through the bright band appears to be increasingly more important to account for as frequencies greater than 8 GHz are used. Examples showing the geometries associated with an earth-space link and a slant-path terrestial link relative to the bright band are shown in Figure 1.5

1.5 Scope of Thesis

1.5.1 The Research Program

The objectives of the present propagation research program which is being carried out in association with the Canadian Research Centre in Ottawa and the British Columbia Telephone Company in Vancouver are as follows:

1) To provide the facilities to perform research into the various aspects of both analog and digital microwave propagation.
2) To select and fully instrument a suitable path(s) for the monitoring of a number of factors that affect microwave propagation.

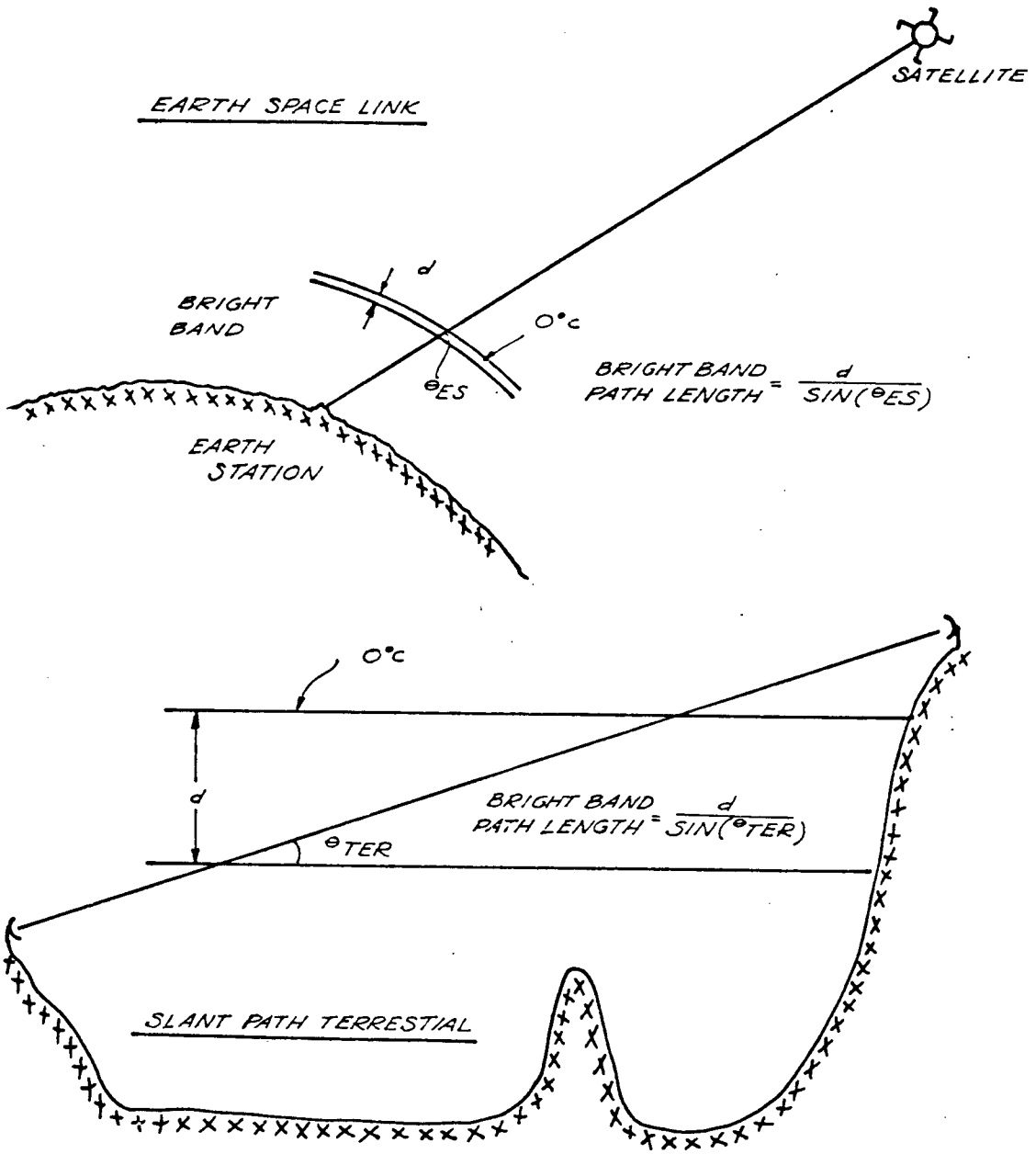

Figure 1.5 Relative Bright Geometries Between Slant Path Terrestial and Earth-Space Links

3) To establish the necessary data collection and data analysis infrastructure to efficiently store, retrieve and analyze large amounts of propagation data.
4) To establish the relationship, if any, between the occurrence of bright band and multipath fading phenomenon and the performance of certain microwave links.
5) To be able to determine a statistical model which takes into account bright band attenuation factors that would enable improved availability design for both terrestrial and earth space paths.

1.5.2 Thesis Objectives

The main objectives of the work in this thesis may be stated as follows:

1) Identification and measurement of the parameters affecting bright band propagation.
2) Development and implementation of a working telemetry based data collection system which can accurately measure, time correlate and preprocess large amounts of received signal and meteorological data.
3) Development of a data base management system to store and analyze the data collected.
4) Analysis of the data collected to determine bright-band propagation effects in the 4 and 7 GHZ range and provide a comparison to the theoretical model

1.5.3 Thesis Outline

A description of the path selected is the subject of Chapter II. Included is a path profile, a summary of the path's previous propagation history as well as the calculated and measured system performance characteristics.

Chapter III deals with the criteria for meteorological site selection and includes a description of the wind direction, wind speed, temperature and rain transducers through which the meteorological parameters affecting excess path attenuation can be measured.

Chapter IV deals with the data handling aspects of collecting the data from received signal and meteorological sensors and the network design for doing this in real time. Included are sections dealing with the data statistics, the link capacities, the microprocessors and the preprocessed time series and distribution series formats.

Chapter V deals with the specification, the design and the implementation of a data base management system. This is discussed in relation to software systems presently in existence, to the current bright band system and to future propagation research software requirements. Included is an illustration of the total data processing and handling system and the economics associated with using this system.

Chapter VI presents results of copolar attenuation through the bright band at 4 and 7 GHz. One set of these results has been taken from chart recordings during January-February 1980. Another set of results taken during January-February 1982 using the telemetry based data collection system as described in Chapters III, IV, and V, are also presented in this chapter.

These results represent a limited set to convey the character of the data measured and the nature of bright band propagation and to illustrate possible correlations to meteorological parameters.

Conclusions based on both the chart recorder and the telemetry based system are presented in Chapter VII as well as suggestions to further develope the measurement system and the analysis techniques used in this thesis.

CHAPTER II

THE EXPERIMENT

2.1 Introduction

This chapter provides a description of the path selected, the equipment used and the system fade margin parameters.

2.2 The Path

The path under investigation is part of the Trans Canada Telephone System microwave network and is located approximately 100 kilometers east of Vancouver, B.C., Canada. It is coastal and mountainous in nature, 41.3 kilometers in length and lies between site elevations of 236 m and 1436 m above mean sea level. Because the path has an elevation differential of 1227 m and an annual average rainfall of 1600 mm/yr., there is a high probability that the 0°C isotherm (and hence bright band) will exist at an intermediate elevation between the transmitter and receiver sites. The geographical layout and profile of the path are shown in Figures 2.0 and 2.1 respectively. Photographs are also provided looking directly down the path from the transmitter site (Figure 2.2(a)) and directly up the path from the receiver site (Figure 2.2(b)).

2.3 Received Signal Monitoring

At the receiver site, signal levels from five microwave channels are monitored and sampled at a rate of 10 Hz. These were selected on the basis of obtaining maximum information with respect to broadband and narrowband multi-

Figure 2.0 Geographical Layout of the Bright Band Propagation Experiment.

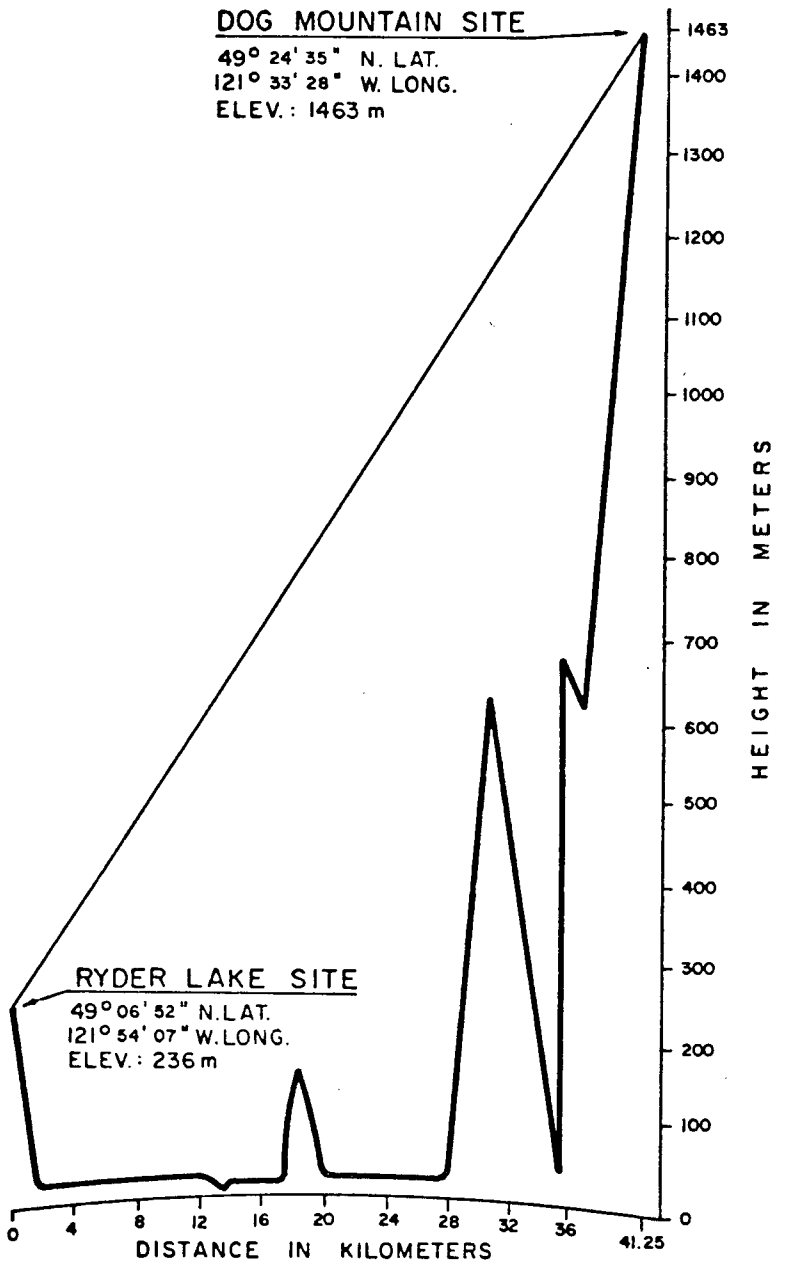

Figure 2.1 Path Profile: Ryder Lake to Dog Mountain.

a) From Transmitter Site: (Dog Mountain) Looking South
"+" indicates location of Receiver Site

b) From Receiver Site:
(Ryder Lake) Looking North
"+" indicates location of
Transmitter Site.

Figure 2.2 Path Photographs.

path fading, copolar attenuation and cross-polar effects. Four of the channels are of horizontal polarization and were selected at each end of the 4 and 7 GHz bands. The remaining channel is at 4 GHz and has a vertical polarization.

Specific information on the frequencies selected and the radio equipment used are given in Figure 2.3.

A sampling rate of 10 Hz has been selected as a compromise between the capacity of the high speed data link and maintaining the integrity of the received signal data during fast fade events. Fade rates of 50 to 60 dB/sec have been observed on a similar experimental link in British Columbia [57]. Therefore, a 10 Hz receiver signal sampling rate has been chosen to avoid losing this fade information and yet maintain the data flow within the capacity of the data link.

The block diagrams are given for both the 4 and 7 GHz transmission systems used in this experiment as shown in Figures 2.4 and 2.5 respectively. These are used to calculate the received signal levels, fade margins and resulting annual outage probabilities in the transmission calculations of Table 2.0. In both the 4 and 7 GHz cases the measured and calculated received signal levels agree to within 1 dB. The resulting outage probability due to propagation events is estimated to be 4.4 minutes/year for the 4 GHz system and 31.6 minutes/year for the 7 GHz system.

The received signal level is monitored from the Automatic Gain Control (AGC) feedback voltage which is proportional to the magnitude of the incoming signal. The variation of the AGC voltage versus receiver input signal level is given in Appendix A for the five microwave receivers monitored.

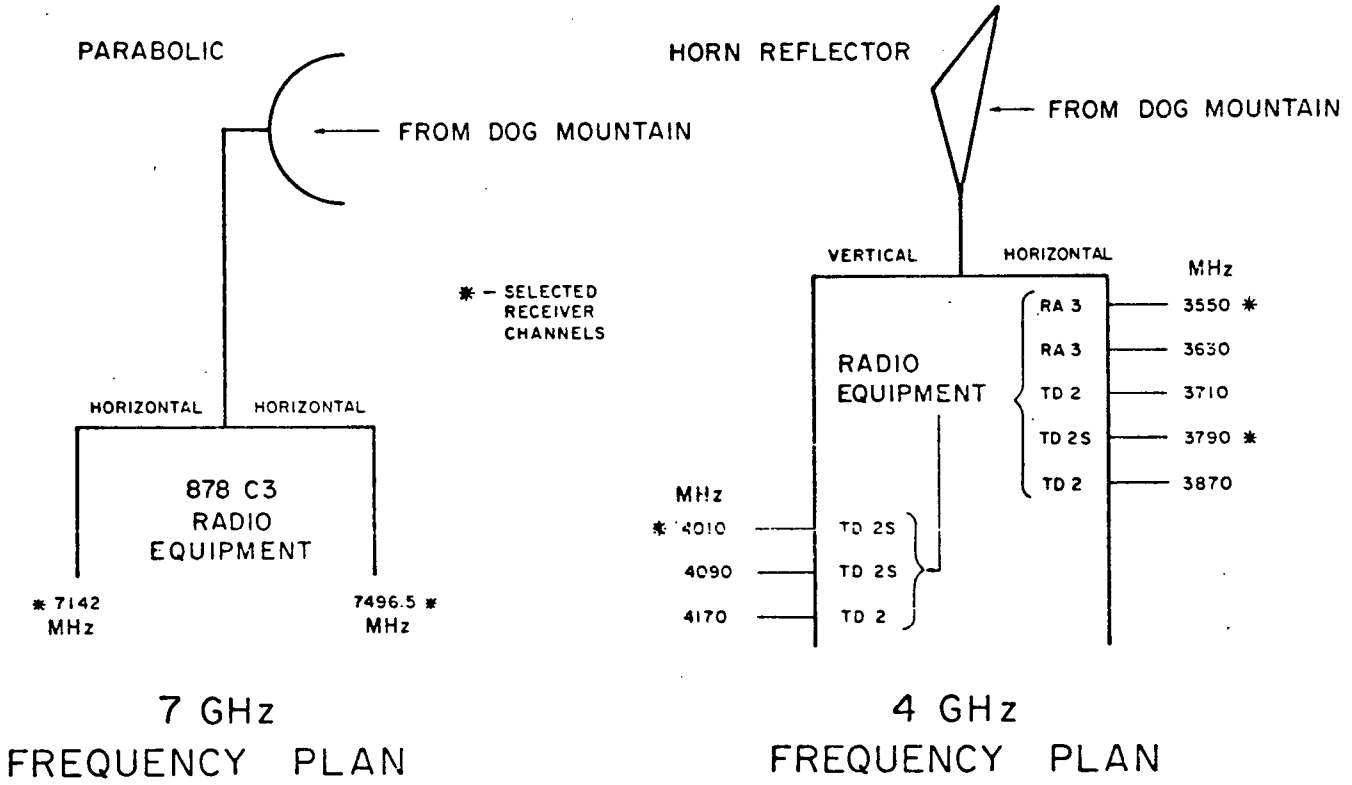

Figure 2.3 Frequency Selection Plan and Receiver Equipment used at Receiver Site.

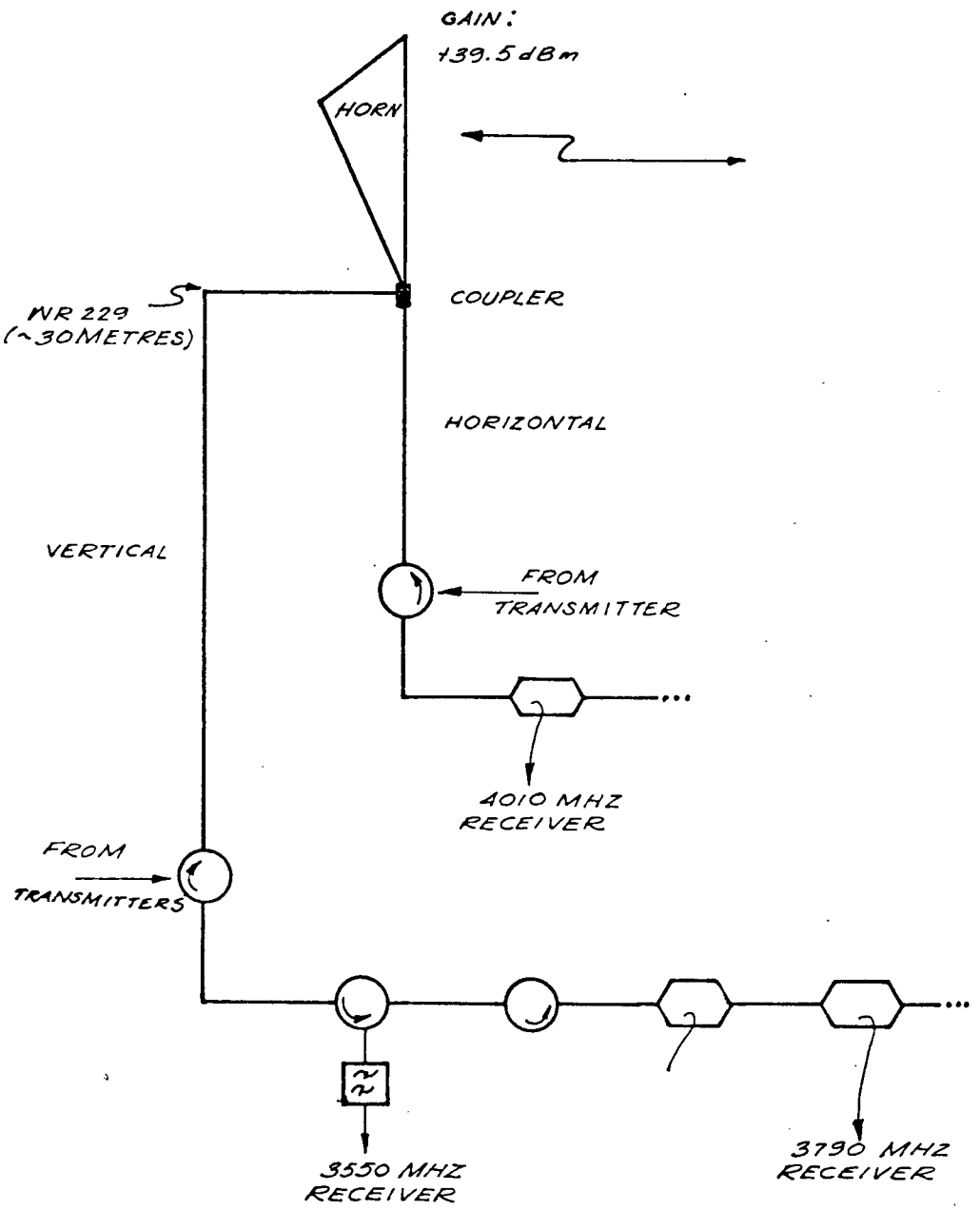

Figure 2.4 4 GHz. Microwave Transmission Block Diagram

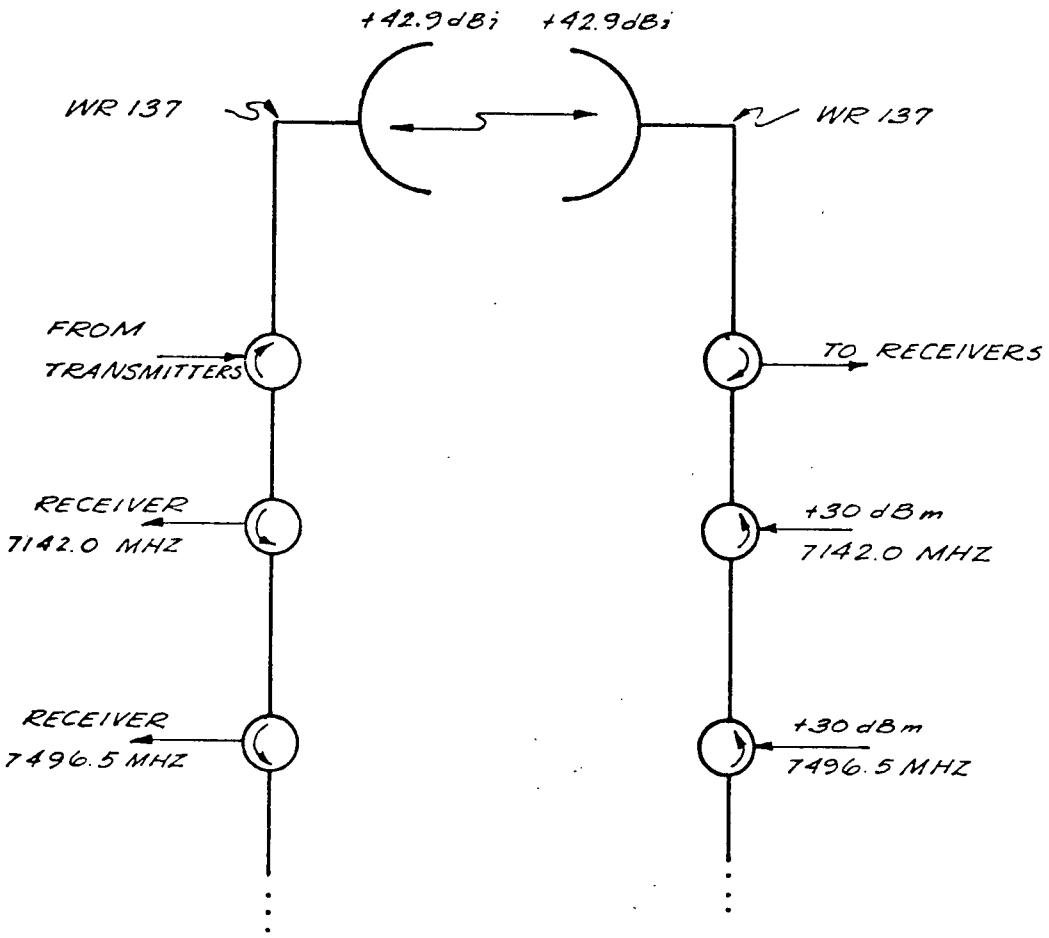

Figure 2.5 7 GHz. Microwave Transmission System Block Diagram

Table 2.0 Microwave Transmission Calculations

1)	Locations	Dog Mtn.	Ryder Lake	Dog Mtn.	Ryder Lake
2)	Latitude °N	49°24'35"	49°06'52"	49°24'35"	49°06'52"
3)	Longitude °W	121°33'28"	121°54'07"	121°33'28"	121°54'07"
4)	Elevation (meters)	1463m	235m	1463m	236m
5)	Antenna Height (meters)	20m	20m	9m	8m
6)	Azimuth (°T)	217.5		217.5	
8)	Frequency (MHz)	4010		7496.5	
9)	Path Length (km)	41.3		41.3	
10)	Path Attenuation (dB)	136.8		142.3	
11)	Misc. Losses (dB)	1.0		1.0	
12)	Transmission Line Type	WR229	WR229	WR137	WR137
13)	Transmission Line Loss	0.8	0.8	1.8	3.8
14)	Circulator Loss	0.6	0.6	0.8	0.8
15)	Filter Loss	-	-	-	-
16)	Connector Loss	0.4	0.4	0.6	0.6
17)	Radome Loss	1.0	1.0	1.0	1.0
18)	Total Loss (dB)	-143.4		-153.7	
19)	Antenna Type	Horn Reflector	Horn Reflector	Parabolic	Parabolic
20)	Antenna Gain (dBi)	+39.5	+39.5	+42.9	+42.9
21)	Transmitter Power (dBm)	+33.0		+30.0	
22)	Received Signal Level (18+20+21)	-31.4 (-31.0 Measured)		-37.9 (-38.5 Measured)	
23)	Receiver Threshold (dBm)	-68.5		-69.5	
24)	Fade Margin (22-23)	-37.1 (-37.5 Measured)		31.6 (-31.0 Measured)	
25)	Propagation Availability % (Annual)*	99.9992		99.994	
26)	Annual Outage Estimate	4.4 Min/Year		31.6 Min/Year	

*The propagation availability on line 25 has been calculated using the following formula [2,36,58]:

$$\text{Propagation Availability } \% = 100[1-ab(6.0\times10^{-7}\times f\times D^{3}\times10^{(-F/10)})]$$

where a = Terrian roughness factor (1 = average)
b = Climate Factor (1/4 = normal temperate)
f = frequency in Gigahertz
D = distance in kilometers
F = fade margin in dB

CHAPTER III

METEOROLOGICAL INSTRUMENTATION

3.1 System Design

3.1.1 Measurement Criteria

In order to measure the effects of copolar propagation through the bright band it is important to be able to monitor the presence of the 0°C isotherm along the path, to determine the thickness of the bright-band region and to measure the precipitation rates through the band. The presence of the bright band can be detected by establishing the temperature differential between the transmitter and receiver sites to see if the 0°C isotherm is included. The thickness of the bright-band region, once detected, is then determined indirectly by establishing the temperature gradient through the 0°C isotherm. The precipitation rates can be monitored directly through a network of rain gauges or indirectly using synthetic storm techniques [59-62]. The latter requires the measurement of windspeed and wind direction, preferably at several points along the path to determine precipitation cell locations as a function of time.

3.1.2 Site Selection

In order to meet the measurement criteria of obtaining detailed temperature gradient, point rainfall rate information and wind information, five weather stations have been selected between transmitter and receiver sites. These sites are shown in Fig. 3.0 with their geographical and functional site

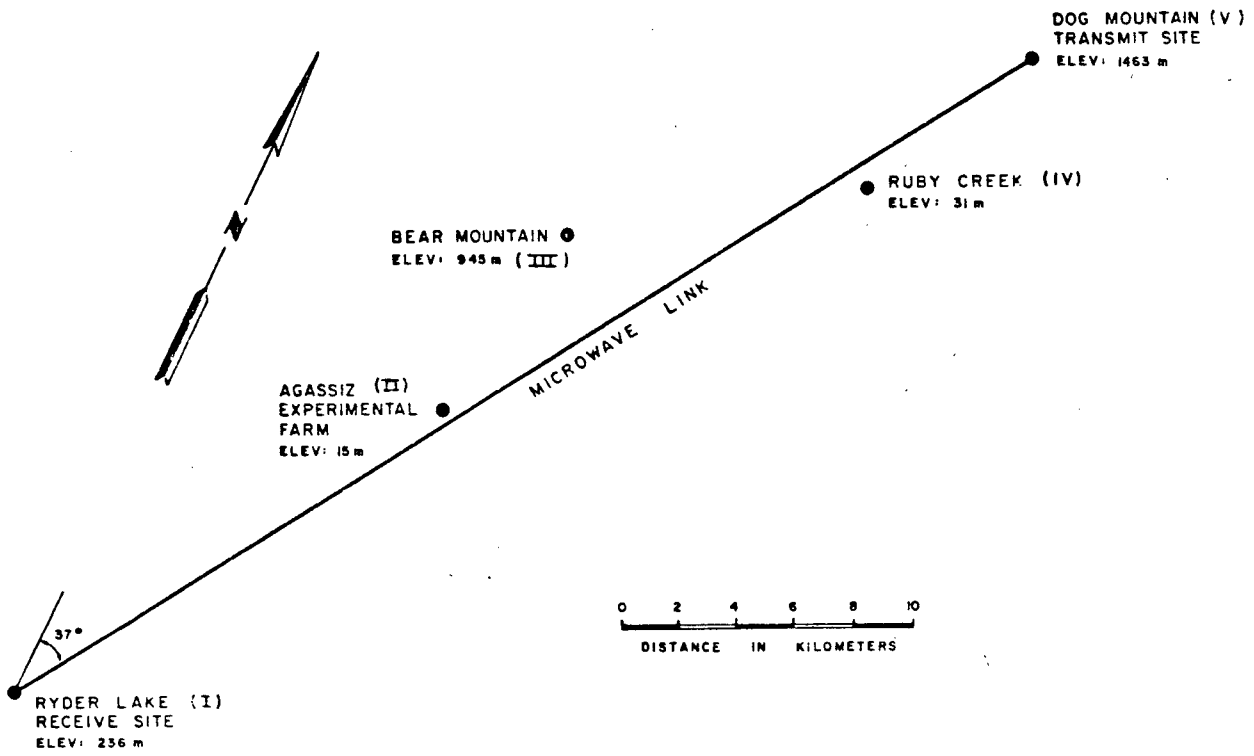

Figure 3.0 Measurement System Layout.

information provided in Table 3.0. Detailed site plans, equipment configurations and site photographs are available for each site in Appendix C.

The temperature gradient can be determined from the three sites located at beam elevation, with one at the transmitter site (V), one at mid-path (III) (at suitable elevation) and one at the receiver site (I). The point rainfall rate information is obtained from these as well as from the two remaining weather stations (II and IV) situated at intermediate sites along the valley floor beneath the path. These intermediate sites are valuable since they allow the measurement of the melted precipitation rates directly under the

Table 3.0 Geographical and Functional Site Details

	SITE	Coordinates & Elevation	Data Collected	Primary Importance
I.	Ryder Lake	49 06' 52" N. Lat. 121 54' 07" W. Long. Elevation: 236 m	Receiver Signals 2-4 GHz. Hor. Pol. 1-4 GHz. Ver. Pol. 2-7 GHz. Hor. Pol. Meteorological	. Multiplex's Field data . Receiver Site . Receiver Signals . Rain Rate . Temperature
II.	Agassiz Experi-mental	49 14' 40" N. Lat. 121 47' 18" W. Long. Elevation: 15 m	Meteorological	. Rain Rate . Intermediate Site on Valley Floor
III.	Bear Mtn.	49 18' 25" N. Lat. 121 41' 30" W. Long. Elevation: 945 m	Meteorological	. Temperature . Intermediate Site at Path Elevation
IV.	Ruby Creek	49 21' 15" N. Lat. 121 36' 45" W. Long. Elevation: 31 m	Meteorological	. Rain Rate . Intermediate Site on Valley Floor
V.	Dog. Mtn.	49 24' 35" N. Lat. 121 33' 28" W. Long. Elevation: 1463 m	Meteorological	. Temperature . Transmitter Site

path during bright band activity. This is possible due to their much lower and hence warmer site elevations. Fig. 3.1 provides a cross-section view of the path showing the relative locations of the weather station sites selected.

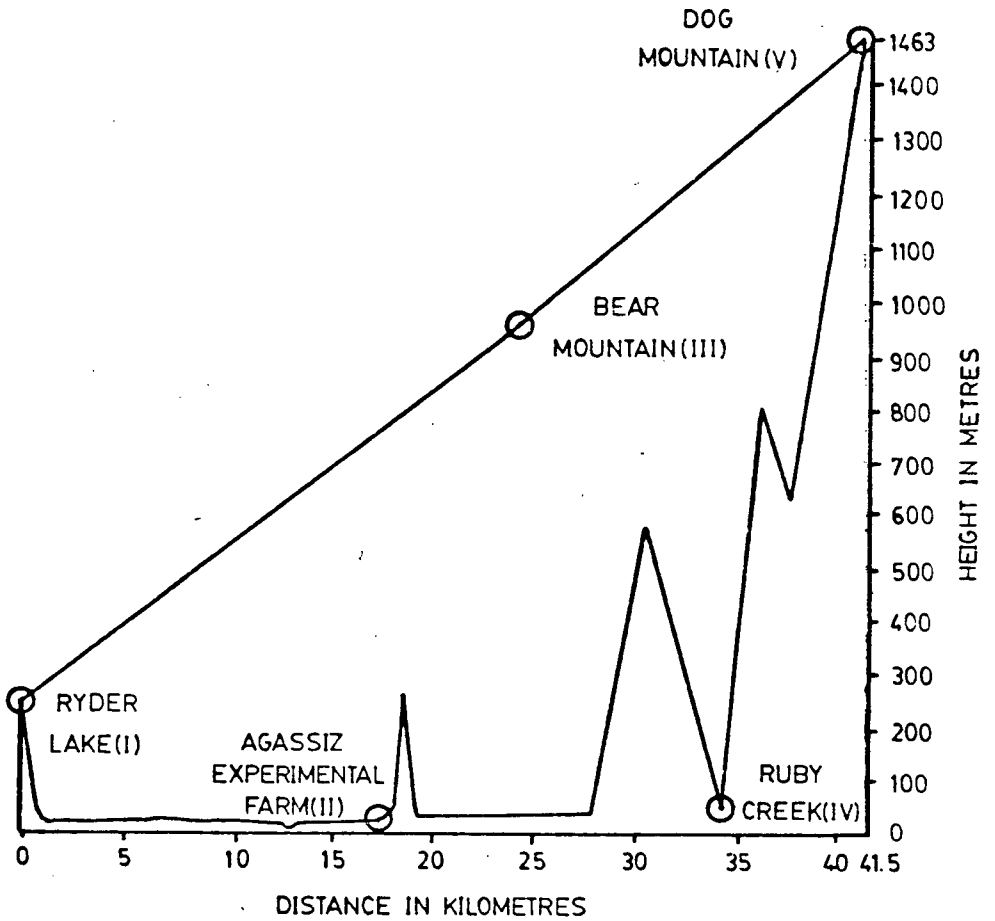

Figure 3.1 Path Cross-section Showing Relative Locations of the Weather Station Sites.

3.2 Meteorological Measurements

3.2.1 Rain

The rain gauges used in this thesis are of the tipping-bucket variety capable of measuring point rain rates of up to 400mm/hour. Accurate measurement above this rate is not important because of the low probability of such events in the path area [63,64].

The rain bucket tips after each 0.318mm of rain which generates a pulse by momentarily closing a glass encapsulated reed switch relay. The pulse thus generated is latched using a signal conditioning circuit for sampling by the microprocessor after which time the latch is cleared to await the next bucket tip. For a detailed description of the signal conditioning circuit with respect to circuit schematics, physical specifications and photograph refer to Appendix E.

With the path being located approximately 100 kilometers east of Vancouver, it was essential that the tipping buckets require low maintenance. For this reason a molded plastic unit which is inherently corrosion resistant was acquired. Appendix D-3 provides a detailed description and photograph of this unit.

Five rain gauges were installed along the path at each of the weather station sites. Figure 3.2 and Table 3.1 show the inter-site spacings and the spacings as a function of total path length.

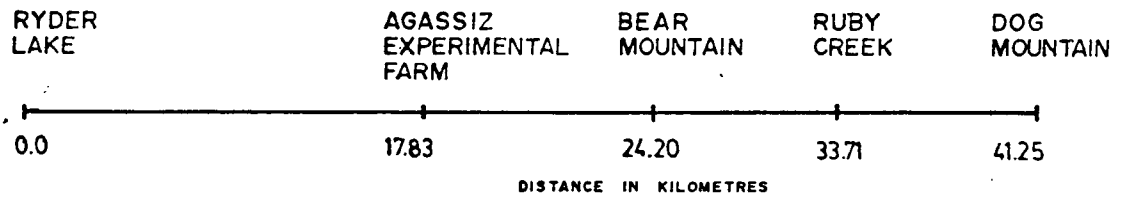

Figure 3.2 Weather Station Inter-Site Distances.

Table 3.1 Inter-Site Distances as a Function of Path Length

	Ryder Lake	Agassiz Exp.Farm	Bear Mtn.	Ruby Creek	Dog Mtn.
Ryder Lake	-	.43	.59	.82	1.0
Agassiz Exp. Farm		-	.15	.39	.57
Bear Mountain			-	.23	.41
Ruby Creek					.18
Dog Mountain					-

The total rain rate for the path is determined using a distance weighted average from the rain rates at each of the sites. The rain rate between any two interval bucket tips at a working gauge is first determined by equation 3-1.

$$RR_{\text{site 1}} = \frac{\text{tip size}}{\Delta T_{\text{tip}}} \qquad (3\text{-}1)$$

where

Tip Size = 0.318mm

ΔT_{tip} = time interval between two tips.

Then "path averaged rain rate" (RR path) calculated using equation (3-2).

$$RR_{path} = \frac{(RR_{site\ 1} + RR_{site\ 2}) \times (\%\ Path)_{site\ 1 - site\ 2}}{2} + \frac{(RR_{site\ 2} + RR_{site\ 3}) \times (\%\ Path)_{site\ 1 - site\ 2}}{2} + \ldots. + (RR_{site\ N-1} + RR_{site\ N}) \times (\%\ Path)_{site\ N-1\ -\ Site\ N}$$

It is important to calculate this rain rate with only those gauges which are operational and not affected by accumulations of snow.

An attempt has been made to minimize errors due to these factors by rejecting rain information from gauges where no activity is observed during the passage of a precipitation event.

3.2.2 Temperature Transducer

Temperature transducers were placed at all the sites to measure the outside ambient temperature. As a system, these transducers determine the presence of the 0°C isotherm and hence the bright band along the path as well as indirectly determining the thickness of the bright band region by establishing the temperature gradient between transmitter and receiver site elevations.

Their design is based on the linear temperature coefficient of a semiconductor junction when forward biased with a constant current source. The transducer is conditioned to provide a switch selectable output of 0.01 volts per degree centigrade or per degree fahrenheit allowing for single point calibration. Further details are given in Appendix D describing the unit as well as providing the calibration procedure.

3.2.3 Wind Velocity and Wind Direction Transducer

All the sites, except Ruby Creek and Bear Mountain, are equipped with a propeller type anemometer with the purpose of monitoring both wind velocity and wind direction. The velocity is derived from the output of the unit's propeller-driven dc generator which exhibits a linear windspeed-voltage characteristic. The azimuth, on the other hand, is provided by the linear output voltage which is proportional to the angle relative to true north based on the output of a gear-driven potentiometer.

The wind velocity and wind speed information obtained from these transducers is required to be able to apply synthetic storm techniques [59-62] in the processing of the propagation data for research purposes. More detailed information on the anemometer unit is given in Appendix D.

3.3 Meteorological-Data Sampling

The basic ac powered weather sites of the Agassiz Experimental Farm, Ruby Creek and Dog Mountain are each equipped with one U.B.C. Weatherlog Microprocessor and one Meteorological Signal Conditioning Unit. A photograph of these units is presented in Figure 3.3. Details on these units is given in Appendix I for the weatherlog processor and in Appendix E for the signal conditioning unit.

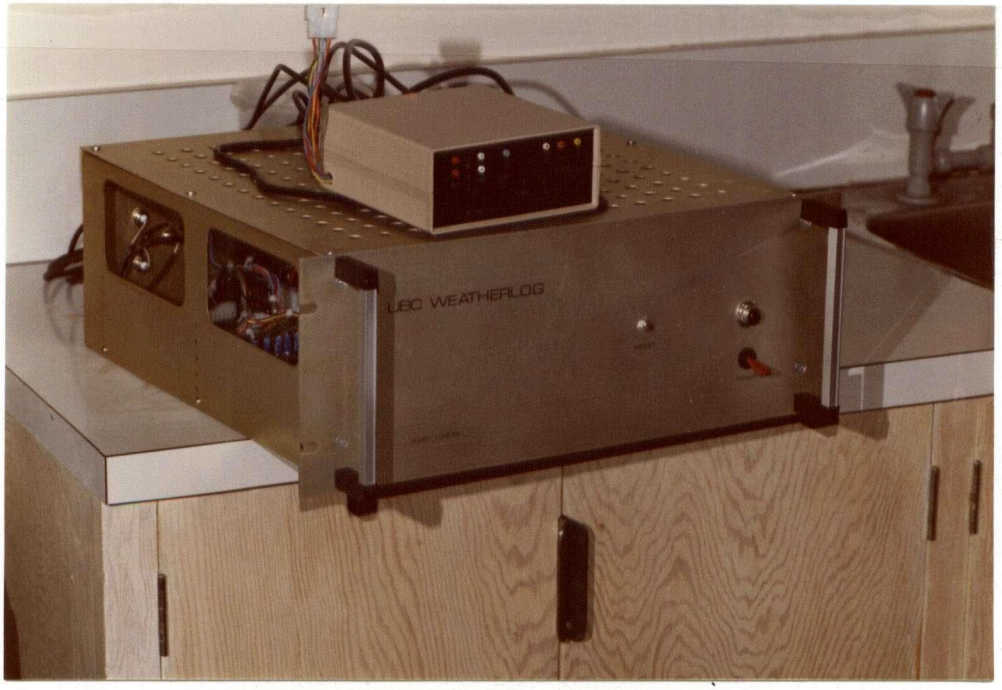

Figure 3.3 Photograph of the U.B.C. Weatherlog Microprocessor and Meteorological Signal Conditioning Unit.

The weatherlog has been programmed so that it samples the meteorological variables of wind direction, wind velocity, temperature and rainfall on a one-second software-determined interval. The output of the unit is a voice frequency FSK modulated signal. The sampling of the meteorological variables at the Ryder Lake and Bear Mountain sites follow the same "weatherlog" system design, but use other microprocessor configurations at these sites due to differing monitoring requirements and power availability constraints.

In choosing the optimum sampling rate, a trade-off is made between losing information of fast varying variables, transmitting data within the maximum link capacity and minimizing the design complexity of the signal conditioning unit. The compromise reached was to use a 1 Hz sampling rate, to transmit the data at 110 bps and design the conditioning unit to latch bucket tips until

sampled. This is a reasonable compromise since the information for all the variables except the fastest changes in wind velocity and wind direction are retained and little information is lost in the most important variables of temperature or rainfall. This leaves a growth allowances of 120% for future data requirements as additional transducers are needed.

CHAPTER IV

DATA ACQUISITION SYSTEM

4.1 Design Criteria for a Real Time Data Acquisition System

The data acquisition system must be capable of acquiring in real time the sampled meteorological and received signal level data and then be able to store this data in a format compatible for processing on a general purpose computer. To do this the data must be routed from the sites, shown in Figure 3.0, through a series of data links to arrive at the University of British Columbia for real time correlation.

The design of the data acquisition system comprises three basic areas:

I) The on-site data acquisition

II) The data collection network

III) The real-time storage, formatting and coordination of the data.

Figure 4.0 shows the data acquisition system block diagram with each of the three component areas identified. Component area I, the on-site data acquisition, deals with the type of data, the analog to digital (A/D) sampling rates and the interface to the outgoing data link. Component area II, the data-collection network, is concerned with minimizing system cost and delay time under certain link-capacity, link-flow and routing contraints. Component area III, the real-time storage, formatting and coordination of the data, is concerned with the time correlation of the incoming data and the processing of the data into suitable time series and distribution series storage formats.

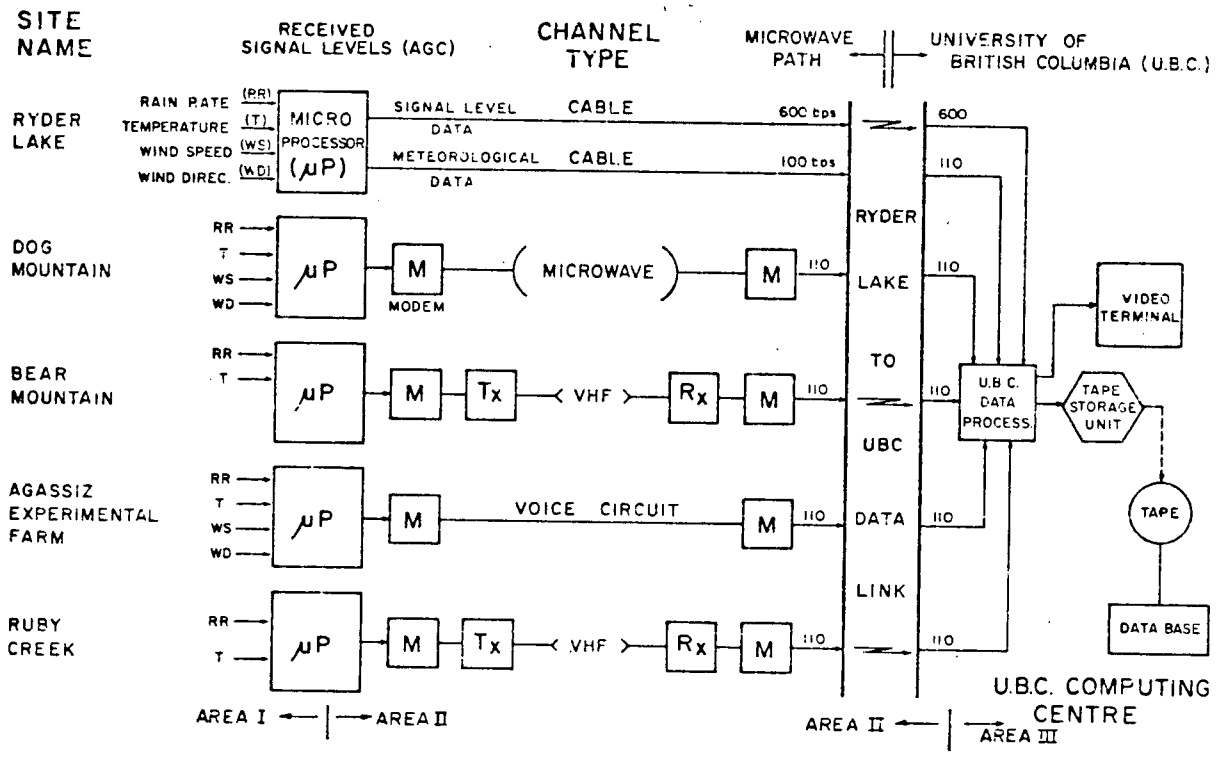

Figure 4.0 The Data Acquisition System Block Diagram With Component Areas Identified.

4.2 Site Selection

4.2.1 Received Signal Site

The Ryder Lake data acquisition equipment, which monitors the received signal levels, must provide sufficient samples and quantization resolution to accurately reconstruct the received signal levels from the outgoing data stream. This applies particularly to fast fades which have previously been observed at rates up to 50-60 dB per second on similar paths in the region [57]. The received signal data transmitted must also allow easy formatting, must be sent at a rate which is equal to or less than the outgoing link capacity and must maintain overall system timing. To meet these design objectives, an accurately determined sampling rate of 10 Hz was chosen, the received signal levels were conditioned to +0-5 volts matching the input range of the A/D and the number of outputted quantization bits were limited to eight bits to meet system data formats. The resulting data rate of 600 bits per second from the five monitored received signal levels is calculated as follows:

(One - 8 bit synch byte + five - 8 bit receiver
samples + 1 start bit/byte + 1 stop bit/byte)
all times 10 sampling cycles per second = 600 bps.

For more information concerning the receiver signal conditioning units refer to Appendix E, and for a detailed description of the Ryder Lake received signal level data acquisition microprocessor refer to Appendix I.

4.2.2 Meteorological Sites

The purpose of the data acquisition equipment at the meteorological sites is to sample the weather variables of wind direction, wind velocity, temperature and rainfall at one second intervals and send these back via the site's outgoing communication channel into the data collection network. The data acquisition equipment consists basically of a microprocessor which coordinates the sampling (see Appendix I), a meteorological signal conditioning unit which provides a full range, +0-5 volt, input to the A/D (see Appendix E) and a modem which encodes the data as a frequency shift keyed (FSK) output to the data channel (see Appendix H).

The outgoing data rate of 110 bps was chosen keeping future data growth requirements in mind. At present, the data sent for a one second sampling cycle includes four - 8 bit bytes, one - 8 bit synchronization byte as well as one start bit and one stop bit for each of these bytes to give a net data rate of 50 bps. This leaves an excess capacity of 60 bps for future use.

The type of communications channels used from the meteorological sites are shown in the system block diagram of Figure 4.0 and includes VHF radio channels from the Bear Mountain (III) and Ruby Creek (IV) sites, a microwave radio channel from Dog Mountain (V), a telephone circuit from the Agassiz Experimental Farm (II) and a cable at Ryder Lake (I). The organization of these communication channels into a data collection network is the subject of the next section.

4.3 Data Collection Network Design

4.3.1 Data Statistics

From section 4.2 it is evident that the data collection system must handle the statistically-different receiver and meteorological data packets. A packet of receiver signal level data is sent from site I every one-tenth of a second, consisting of 5 samples (the 3550, 3790, 4010, 7142.0 and 7496.5 GHz AGC voltages), followed by a synchronization byte. The net arrival rate for this receiver amplitude data including the start and stop bits is 600 bps. A data packet of meteorological data, on the other hand, is sent from each of the five weather station sites, consisting of four samples (wind direction, wind velocity, temperature and rainfall), followed by synchronization byte. The net data rate for the meteorological data on a per site basis including start and stop bits is 50 bps.

4.3.2 Link Capacities

In order to define a network topology, the link capacities and cost for each of the outgoing communication channels were considered. Several alternatives exist for each site but the link and associated communications channel providing for the best cost-capacity trade-off are as follows:

i) Ryder Lake to UBC (telephone circuit)

This link was restricted to an order-wire type telephone circuit channel available from the telephone company's existing network. This link corresponds to a conditioned telephone circuit with a data capacity of 2400 bps.

ii) Other Telephone Circuits

Other telephone circuit channels were easily obtained from the Agassiz Experimental Farm and from the Dog Mountain site (via microwave) to the Ryder Lake site. The circuit from Agassiz is a dedicated unconditioned telephone circuit through the regions switched network with a capacity of 1200 bps (see Figure B-5). The Dog Mountain circuit uses the lower frequency portion of a network alarm channel and has maximum capacity of 300 bps (see Figure B-4).

iii) Radio Channels

Two VHF radio licenses were obtained to provide the remaining two communication channels from Ruby Creek and Bear Mountain to Ryder Lake. These utilize the voice frequency pass band of the VHF radios providing a maximum link capacity of 600 bps.

For detailed information on all these data links please refer to Appendix B where their circuit schematics, path profiles and transmission calculations are given.

4.3.3 Node Considerations

Individual node design must be consistent with the overall data acquisition objective to coordinate and time correlate all collected data. This implies that no data storage or buffers at any of the collector or acquisition nodes can delay the arrival of data at the storage node (UBC) and that the sampled data should be sent immediately (as it is monitored).

4.3.4 Implementation of the Network Topology

The final data acquisition topology was largely determined by the constraints of cost, capacity and availability of the communication channels between nodes. The resulting topology is presented in Figure 4.1.

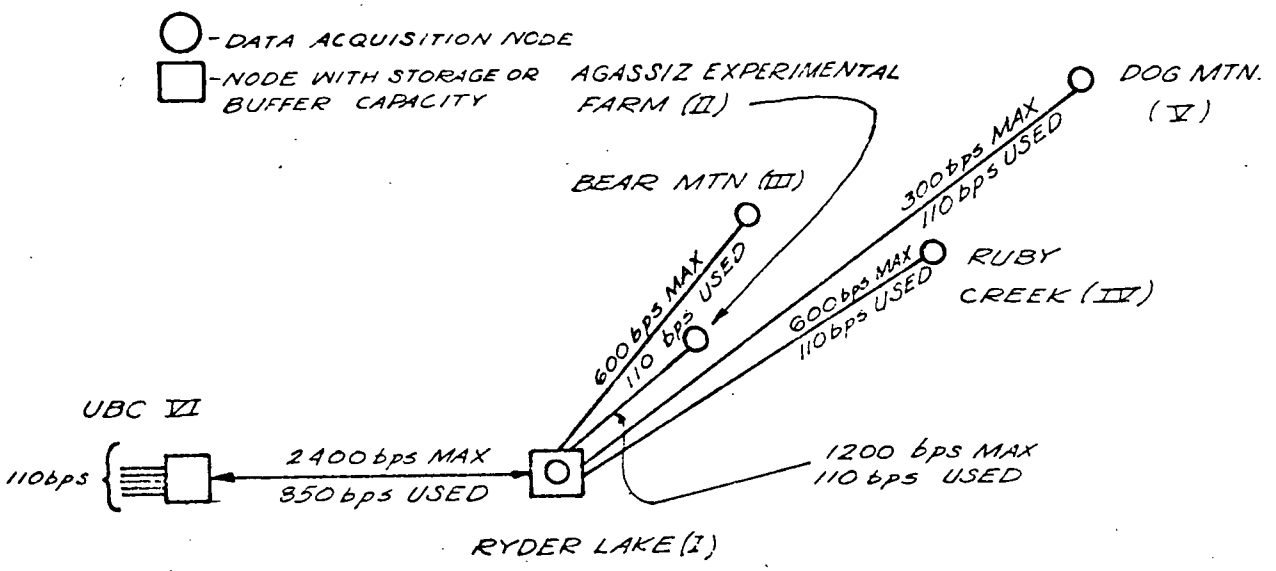

Figure 4.1 Data Collection Network Topology

4.4 Real Time Data Storage

4.4.1 Microprocessor Considerations

The acquisition system data storage microprocessor is located at UBC and handles the administrative tasks of tagging the data with real time as it arrives, of organizing the data into useful data storage formats and of outputting the processed data onto a magnetic tape and onto a video monitor. This processor's main objective is to reduce the volume of data to manageable levels by selecting only desirable time series intervals as well as compressing the data using hourly distributions. This technique reduces the stored data volume to approximately 10% of the total incoming data so that under normal operating conditions a 4.5 megabyte data cassette will record approximately 10 days of system output.

To make it effective, the UBC computer is interfaced using RS 232 ports and uses two CPU's to distribute the tasks of processing, formatting and data selection. A video monitor has been added to allow the real time display of incoming data as shown in Figure 4.2. Refer to Appendix I for a complete description of the UBC microprocessor hardware and to Appendix J for a discussion of the UBC processor programs.

4.4.2 Data Storage Formats

The data which arrives at UBC is stored in two basic formats; one for time series data and another for distribution data. The time series data includes all the arriving data whereas the distribution data format provides a cumulative hourly total of each variable for the number of samples taken at a given value. The time series data is only stored when an event occurs and

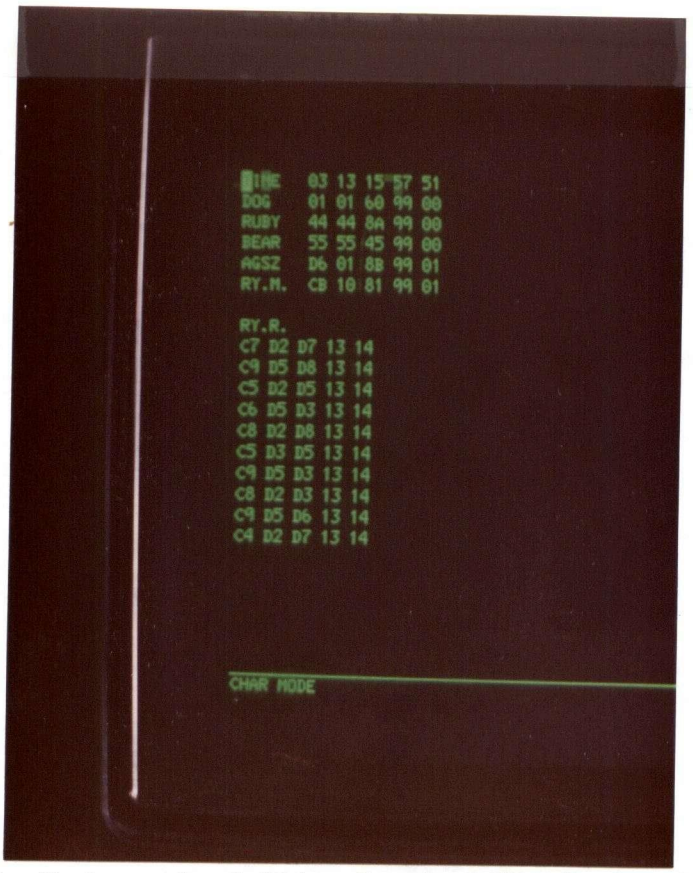

Figure 4.2 Photograph of Video Terminal Displaying Incoming Data

therefore time series dumps are random in nature and vary in length whereas the distribution buffer is dumped hourly and has a fixed length of 3890 bytes. The time series data is organized into a queue comprised of 12 complete one second blocks where each one second block is composed of 80 bytes. The distribution data is comprised of 5 types of data (wind direction, wind velocity, temperature, rainfall and receiver amplitude) with 5 double byte distributions for each meteorological data type and 5 double byte distributions for each receiver amplitude. Of these, each meteorological distribution has 64 double byte "bins" and each receiver signal amplitude distribution has 128 double byte "bins". Each bin represents a certain sampled value. The format used for the time series queue is given in Table J-2 and the format for the distribution series queue is provided in Table J-3 of Appendix J.

4.5 Allowance for Future Data Requirements

The present data acquisition system design has left a substantial amount of data capacity unused as shown in Table 4.0. This was intended to provide the capability of adding additional propagation experiments to the network as the program progresses. If the assumption is made that the network capacity is largely determined by the Ryder Lake to UBC link then there is 65% or 1550 bps of unused data handling capacity. This is calculated based on using effective total data rates since a statistical data multiplex is used on the Ryder Lake to UBC link.

Table 4.0 Data Acquisition System Link Capacities

	LINK	TOTAL CAPACITY	CAPACITY USED		CAPACITY UNUSED	
			bps	%	bps	%
1)	Ryder to UBC	2400	850	35	1550	65
2)	Dog to Ryder	300	50	17	250	83
3)	Ruby to Ryder	600	50	8	550	92
4)	Bear to Ryder	600	50	8	550	92
5)	Agassiz to Ryder	900	50	6	850	94

4.6 An Alternate Data Acquisition System Using Chart Recorders

Prior to the implementation of the automated data acquisition system a system of chart recorders were used to monitor two 7 GHz microwave channels at the receive site and meteorological variables from four stations located along the path. This system produced the first preliminary results which were presented in two papers [65,66] and are given in this thesis in section 6.1.

CHAPTER V

DATA BASE MANAGEMENT SYSTEM

5.1 Specifications

The data base management system (DBMS) has been developed as part of this research to provide an efficient means, through the use of a general purpose computer, to handle the analysis and storage of large volumes of meteorological and propagation data. Within the overall data handling problem, as far as the bright-band research is concerned, DBMS takes over data handling at the point where the 800 bpi, 9-track raw data tape is transfered from the NOVA 840 to the UBC computing center. This interface is illustrated in the data system flow chart of Figure 5.0.

In developing the specifications for DBMS, several general issues were considered. First, DBMS must be easy to use so that a researcher with minimal familiarity to MTS can utilize it. Second, DBMS must be flexibile to allow different propagation data series formats to be handled and yet require a minimum amount of software revision to incorporate the necessary changes. Third, DBMS must make maximum use of existing software packages developed for the 74 GHz experiment [66,70] and the library routines resident on the MTS system. Finally, DBMS must use "time" as the universal field of access to system data records since it is inherently a common variable for all propagation data.

In addition to these general specifications DBMS must satisfy four functional requirements:

1. It must enter new data onto the system (ENTER),

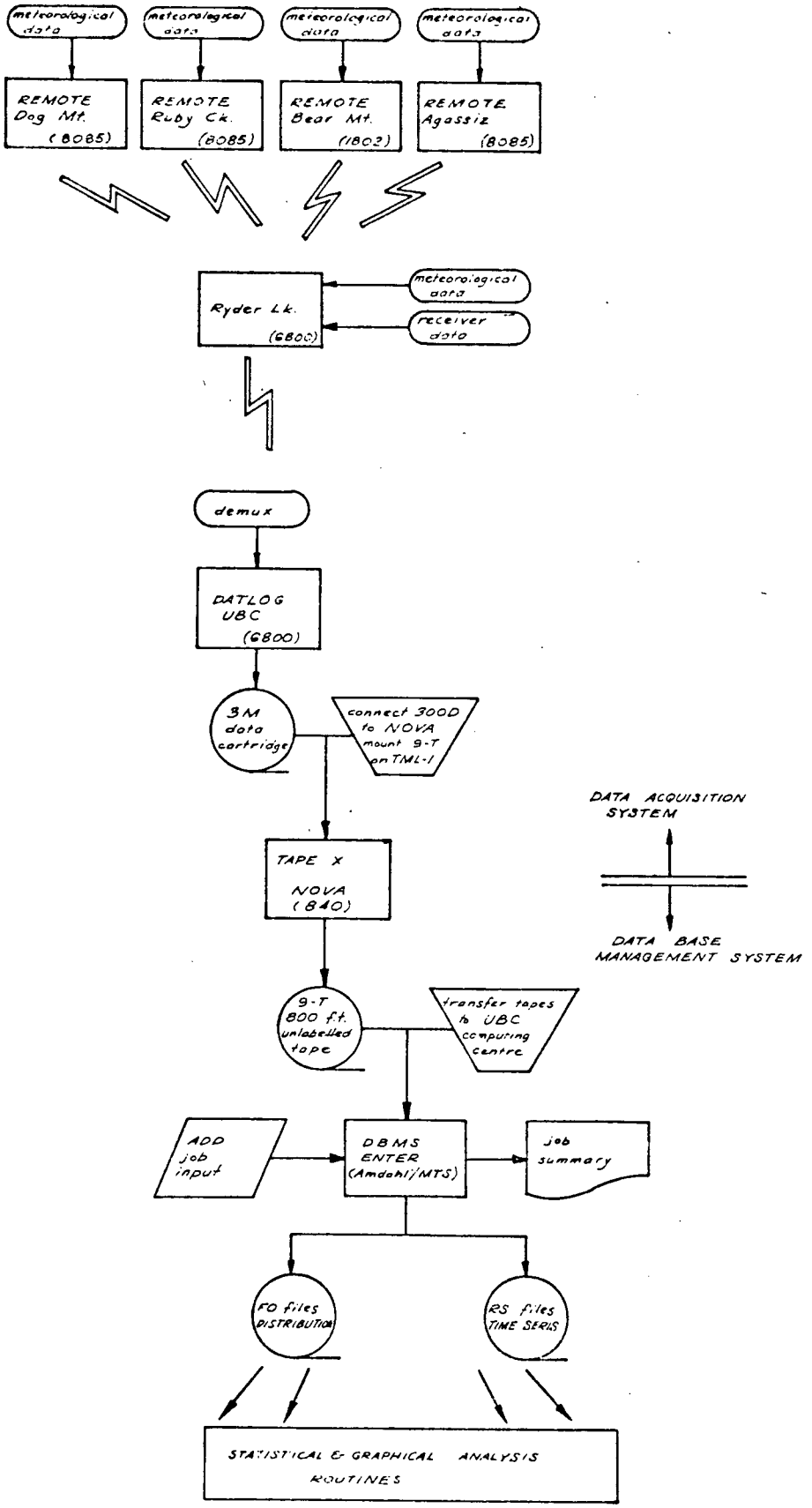

Figure 5.0 The Bright Band Experiment Data System Flow Chart

2. It must be capable of limited perusal and data selection from summarized results (SCAN),
3. It must be able to extract specified data records from the data base for independent analysis (EXTRACT),
4. It must allow easy application of graphical and statistical analysis routines (PLOT).

For a detailed description of the ENTER, the SCAN, the EXTRACT and the (PLOT) routines, refer to Appendix K.

5.2 Design Considerations for DBMS Relative to Existing and Future Systems

In the design of DBMS, several other experiments and data base storage systems (in progress or proposed) were considered in relation to each other as shown in Figure 5.1. At the present time the 74 GHz and the bright band experiments contribute data to the UBC data base while the B.C. Telephone Company monitoring system develops its own data base. In the future, the proposed digital radio propagation experiment will contribute data to both these data bases as well as to the one at the Communications Research Centre, Ottawa, Ontario. Therefore, it would be desirable to transfer data between the systems in order to allow researchers at one location to have access to data from the other.

There are several methods which can be used to transfer these data between systems, as illustrated in Figure 5.1. The most reliable method, which is also the most universal, is to transfer the raw data cassettes between systems. This method is desirable since the data processing would be under the control of the researcher who wants the results. Another reason, adding to this method's universality is that the cassette recording formats

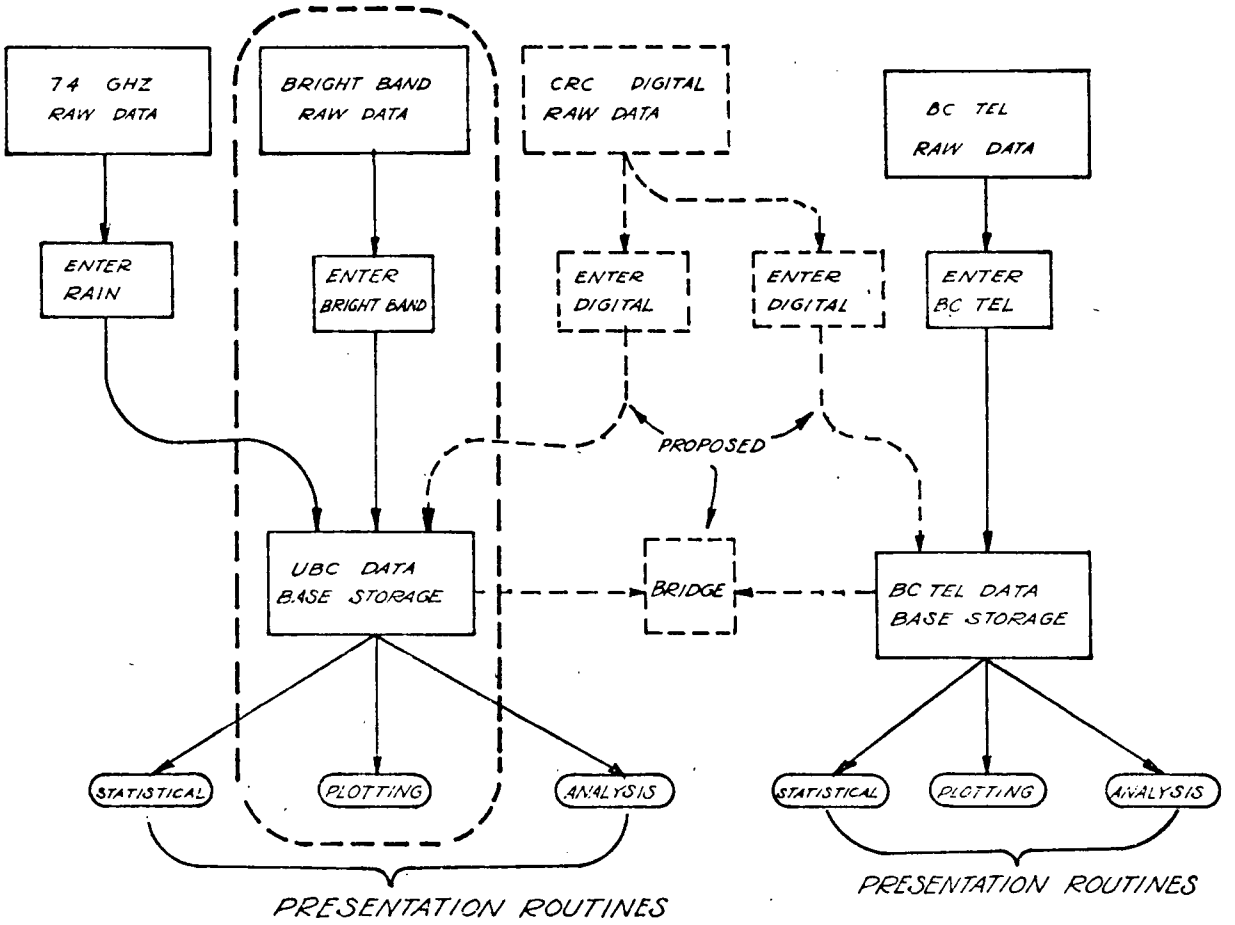

Figure 5.1 DBMS in Relation to Other Propagation Data Management Systems.

are the same as other Canadian propagation experiments.

The most efficient method to interface the two data bases would be to transfer the data on magnetic tapes between computing centers and use a bridging routine to reformat the data. This method is workable provided a large number of bridging routines are not required and the number of tapes to be transferred is not excessive.

5.3 A System Description of DBMS

5.3.1 Data Transfer and Handling

DBMS starts inputting data by evoking the "ENTER" mode. This inputs raw data of either time series or distribution series formats for processing from an unlabelled magnetic tape, previously transferred on the NOVA system at a density of 800 bpi in half word hexidecimal format from the cassettes. Once inputted the data is entered on a disc file. For the distribution series data one preprocessing scan is made and for the time series data two preprocessing scans are made. In the latter case the first scan processes the bucket-tip information to determine rain rates and the second scan converts the data using scaling factors and look-up tables to provide the engineering units. The converted disc files can then be outputted to a labelled 6450 bpi data tape using the MTS "FILESAVE" system or further processed by evoking the "PLOT" mode to display the data in one of several options. These include time series plots of windspeed, temperature, temperature gradient, differential temperature and receiver signal strength.

Figure 5.2 gives a block diagram of the DBMS software system to process the time series data. At the present time the routines to process the distribution series data have yet to be implemented.

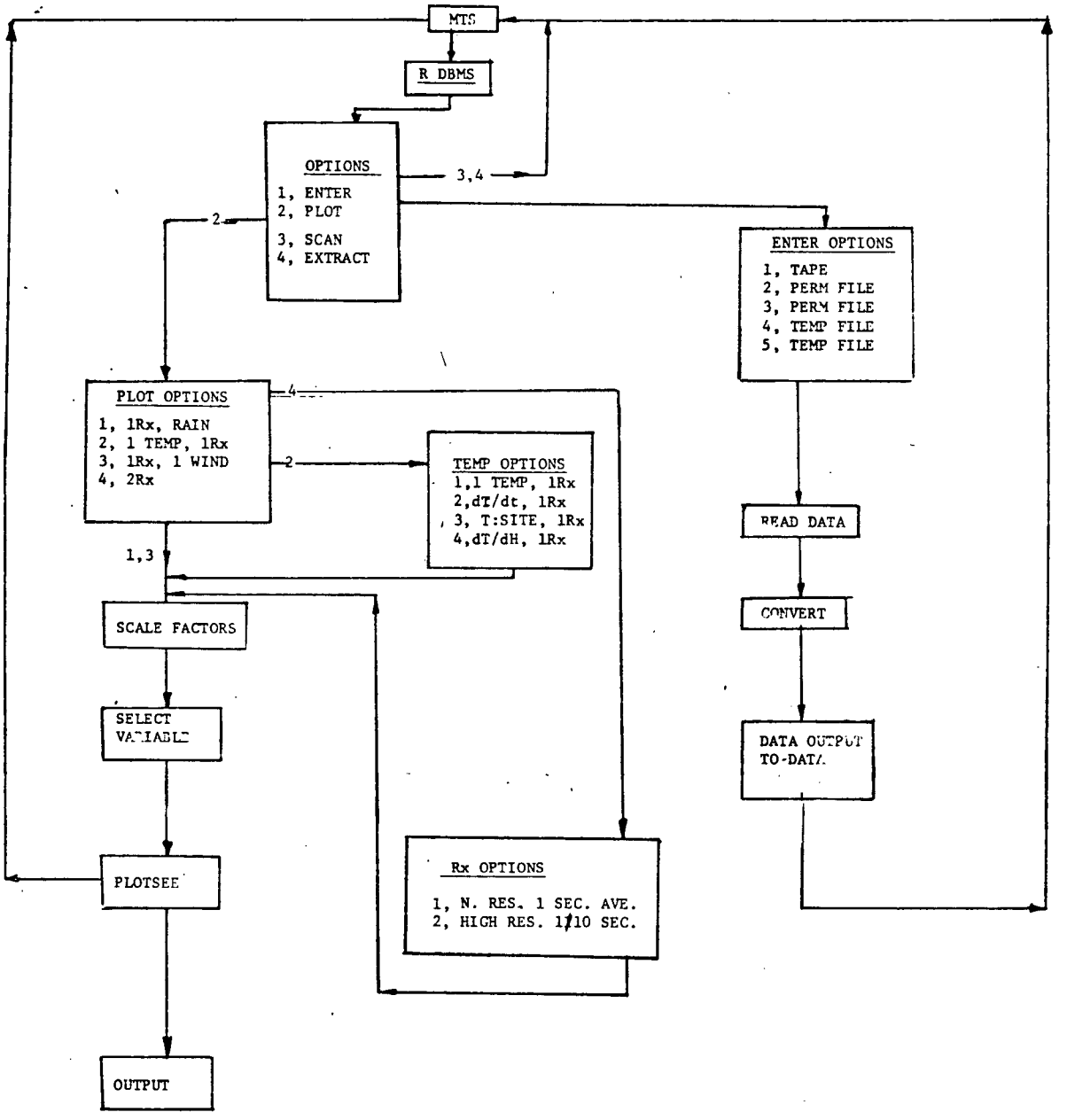

Figure 5.2 User Flowchart to Process time series data on the DBMS software system.

5.3.2 Estimate of DBMS Data Volumes

Size estimates for the bright-band data base are of interest. The amount of data acquired is determined mainly by the event criteria set to record time series data. Assuming that the event criteria is set so that on an average, 5% of the time series data is recorded the corresponding yearly data volume estimates are presented in Table 5.0. It is estimated that two 6250 bpi 2400 foot magnetic tapes per year is necessary to store the distribution data and six 6250 bpi 2400 foot magnetic tapes per year are required to store the time series data.

Table 5.0 DBMS Data Volume Estimates

Distribution Volumes (in bytes)	Time Series Volumes (@ 5% in bytes
3,890/hr.	14,580/hr.
93,360/day	349,920/day
653,520/wk.	2,449,440/wk.
2,800,800/mo.	10,497.600/mo.
33,609,600/yr.	125,971,200/yr.

CHAPTER VI

RESULTS

6.0 Introduction

Results are presented from two series of measurements. The first series were taken in early 1980 using chart recorders from which two events are analyzed exhibiting opposite dynamics in the movement of the 0°C isotherm. These results are presented in section 6.1. The second series of measurements were taken in early 1980 and uses the remote telemetry system as described in Chapters II, IV and V. Results from three events are analysed in section 6.3 showing various aspects of bright band propagation phenomenon.

6.1 Some Initial Results Obtained Using Chart Recordings

Prior to completion of the telemetry based system data was collected from January 3, 1980 to March 30, 1980, using chart recorders. During this time a number of events were recorded showing the presence of bright-band effects. Table 6.0 shows two sets of data taken during separate bright-band events.

The two events selected show opposite dynamics associated with the vertical movement of the 0°C isotherm. Charts of the received signal data are shown in Figure 6.1 along with the corresponding sampling intervals that were used in Table 6.0 and 6.1. Event "A", recorded on January 11-12, 1980, shows the 0°C isotherm rising in elevation from below the path while event "B", recorded on February 2, 1980, shows the 0°C isotherm descending in elevation from above the path. The presence of the bright band is verified by temperature recordings and rain gauge activity at the transmitter and receiver sites.

a) EVENT 'A'

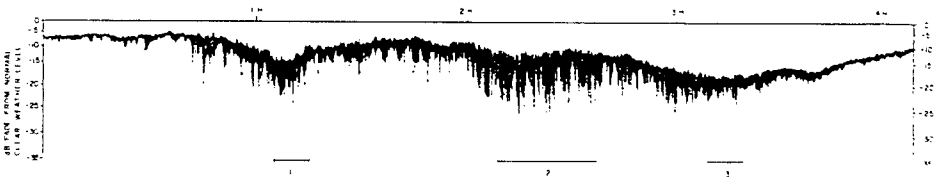

b) EVENT 'B'

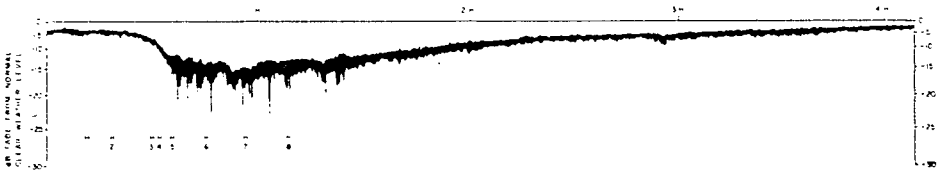

Figure 6.0 Recordings of Received Signal at 7 GHz During Bright-Band Propagation

a) Event "A" (January 11-12, 1980)
b) Event "B" (February 2, 1980)

Table 6.0 Preliminary Results

Event & Sample No.		Average Rain Rate (mm/hr)	Average Attenuation in dB		
			Meas.	Rain*	Excess Atten.
"A"	1	13.4	16.6	4.3	12.3
	2	9.5	13.5	2.3	11.2
	3	13.4	20.0	4.3	15.7
	4	3.8	9.0	1.0	8.0
	5	13.3	15.5	4.3	11.2
"B"	1	8.1	2.9	2.4	0.5
	2	8.0	3.8	2.4	1.4
	3	17.7	6.9	6.2	0.7
	4	19.1	10.9	6.8	4.1
	5	9.3	15.0	2.5	12.5
	6	7.2	16.6	2.1	14.5
	7	5.5	17.4	1.6	15.8
	8	4.3	10.4	1.1	9.3

*Derived using the Laws and Parson Distribution for 0°C

Table 6.1 Bright-Band Excess Attenuation Ratio (EAR) Results

Event No.		Average Rain Attenuation dB/km	Bright-band Attenuation dB/km	Excess Attenuation Ratio (EAR)
"A"	1	0.104	0.851	8.2
	2	0.056	0.775	13.9
	3	0.104	1.086	10.5
	4	0.024	0.553	23.1
	5	0.104	0.775	7.5
"B"	1	0.058	0.036	0.6*
	2	0.058	0.097	1.8*
	3	0.150	0.048	0.3*
	4	0.164	0.291	1.7*
	5	0.060	0.865	13.1
	6	0.051	1.003	19.7
	7	0.039	1.093	28.0
	8	0.027	0.643	23.8

*The 0°C isotherm is above the transmitter site for these data points.

These results show that the measured attenuation is considerably above that predicted by a rain model and, at this frequency, could only be attributed to excess bright-band attenuation. The radar reflectivity profiles presented by Dissanayake and McEwan [44] show that the bright band can be expected to occur for approximately 35% of the total path length.

In this thesis, the excess attenuation has been defined in terms of a ratio of the excess attenuation in dB/km attributable to bright band divided by the rain attenuation in dB/km using the Laws and Parson distribution at 0°C [23]. The ratio thus defined will be referred to as the Excess Attenuation Ratio (EAR). The EAR's for the corresponding sampling intervals used in Table 6.0 have been calculated and are presented in Table 6.1.

The excess attenuation ratios for event "A" are generally lower than for event "B", both being determined assuming rain along the whole path. This may be explained as follows. In event "B" the 0°C isotherm started from above the transmitter site with rain attenuation occurring along the whole path. Since wet snow or sleet would have been falling at the transmitter site during event "B", a contribution to the excess attenuation may also have come from accumulations on the radome. Taking these factors into account, the EAR's for event "A" would be lower and more in line with the EAR's found in event "A". Radome accumulations for event "A" would have been minimal since "dry" snow was present at the transmitter site and rain was falling at the receiver site for the sampling intervals selected.

In both events, rapid scintillation type fluctuations of 5 to 10 Hz appeared on the received signal recordings. These fluctuations coincided with the occurrence of heavy bright-band fading and were estimated to be up to 15

dB in depth. It has been suggested that these fast fades are due to refractive multipath as a result of propagation through the bright band region.* Although these spikes were present in the recordings, the measured attenuation in Table 6.0 was averaged along a baseline assuming that the spikes were not present. In order to study the cause of these scintillations in more detail, to determine the bright-band EAR's with greater resolution and to minimize errors due to radome snow accumulation, an improved experimental design based on remote telemetry was implemented. A description of this improved measurement system has been presented in Chapters II, IV and V and some preliminary results from this system are given in Section 6.2.

6.2 Remote Telemetry Results Showing Bright Band Propagation

6.2.1 January 23, 1982, 7:30-11:30 p.m.

These results were taken after a major storm front moved easterly through the path during a period of evenly distributed wide spread precipitation. An increase in attenuation is evident as the 0°C isotherm moves into the path as shown in Figure 6.1. The precipitation rates were measured for the decaying portion of the event as shown by the rain rate and attenuation plots in Figure 6.3. Excess Attenuation Ratios (EAR's) were calculated for the sampling points shown in Figure 6.2 and the results are presented in Tables 6.2 and 6.3. These range from 10.4 to 19.8 and agree favourably to the EAR of 15 predicted by theory [50]. The presence of the bright band was verified by temperature recordings at the transmitter and receiver sites.

* Private discussions with R.K. Crane at the URSI, Commission F, Symposium held at Lennoxville, Quebec, May 1980.

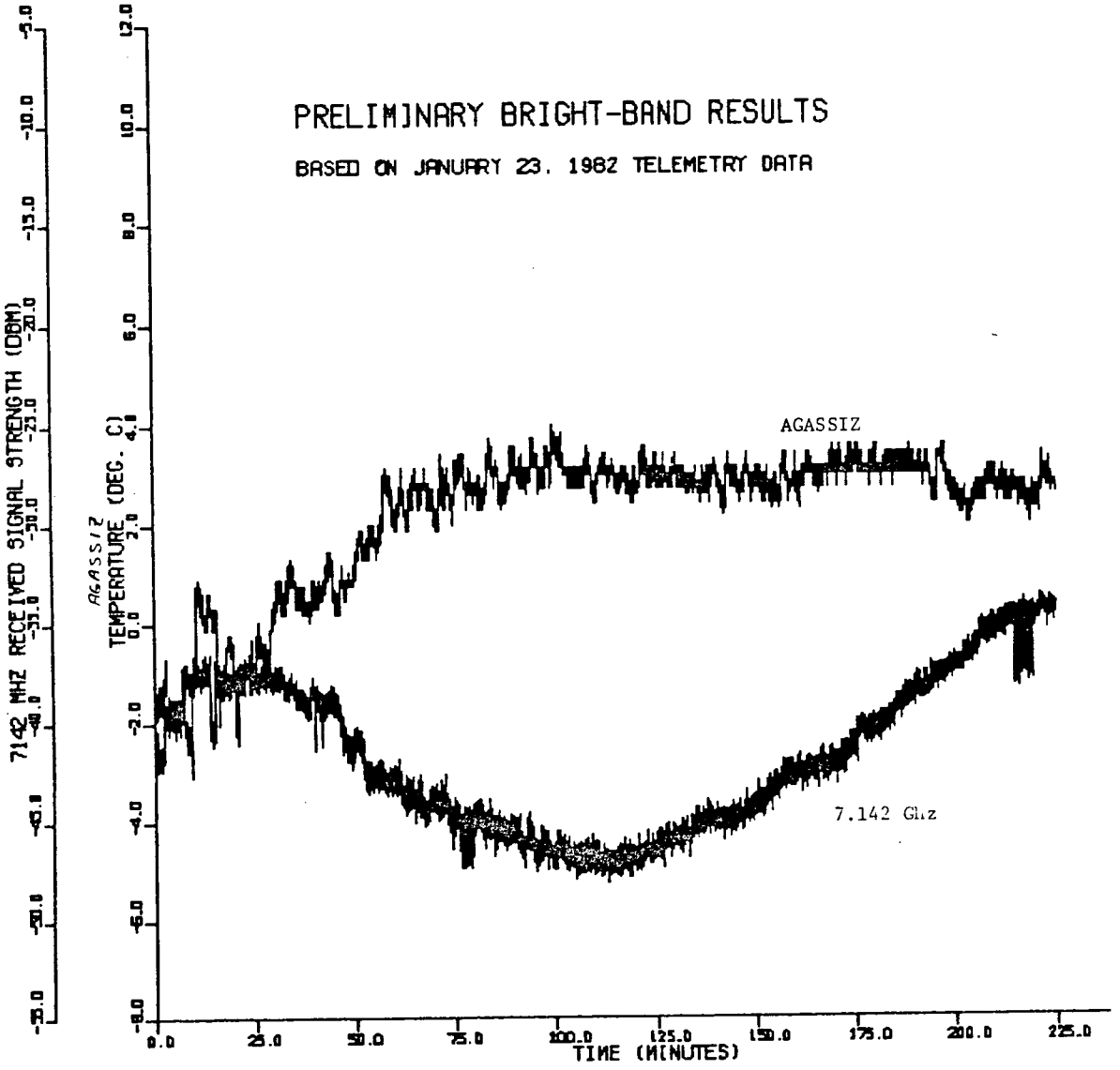

Figure 6.1 The Agassiz Temperature and 7.142 GHz Signals Versus Time

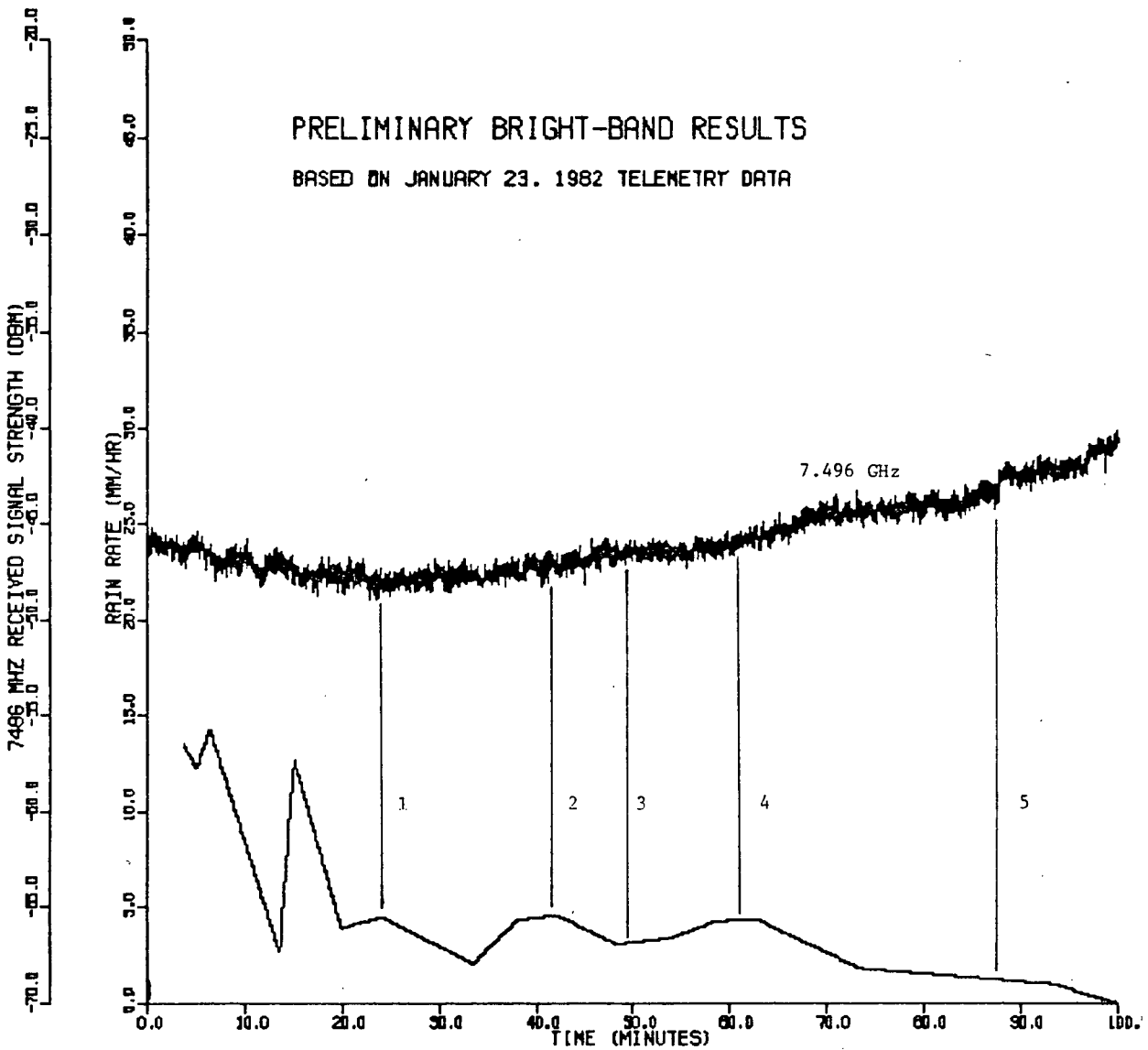

Figure 6.2 Agassiz Rain Rate and The 7.496 GHz Signal Level Versus Time

Table 6.2 January 23, 1982 Results (7 GHz)

Event & Sample No.	Average Rain Rate (mm/hr)	Average Attenuation in dB		
		Meas.	Rain*	Excess Atten.
1	4.4	8.8	1.5	7.3
2	4.4	7.8	1.5	6.3
3	3.5	7.1	1.1	6.0
4	4.4	6.9	1.5	5.4
5	1.3	3.0	0.4	0.2

*Derived using the Laws and Parson Distribution for 0°C

Table 6.3 Bright-Band Excess Attenuation Ratio (EAR) Results

Event & Sample No.	Average Rain Attenuation dB/km	Bright-band Attenuation dB/km	Excess Attenuation Ratio (EAR)
1	0.036	0.51	14.0
2	0.036	0.44	12.1
3	0.027	0.42	15.4
4	0.036	0.37	10.4
5	0.009	0.18	19.8

*The 0°C isotherm is above the transmitter site for these data points.

These results show that the measured attenuation is considerably above that predicted by a rain model and again as in the chart recordings could only be attributed at this frequency to excess bright-band attenuation.

Although rain information was taken at only one site the uniform and widespread nature of this event's precipitation gives consistent results with theory.

In this event which is similar to the later part of event B in Figure 6.0, no rapid scintillation type fluctuations were observed. This corresponded to gradual changes in temperature over this period.

6.2.2 January 23, 1982, 2:00-4:30 p.m.

The system front for the event on January 23, 1982, passed through the microwave link between 2:00 and 4:30 p.m. producing fades of up to 30 dB on the 7 GHz receivers and up to 19 dB on the 4 GHz receivers, as shown in Figure 6.3. The bright band was present along the path as indicated by the temperature recordings for the Dog Mountain transmitter site and the Ryder Lake receiver site in Figures 6.4 and 6.5 respectively.

As shown on Figure 6.5, there appears to be a correspondence between the passage of the temperature through 0°C at Ryder Lake site with the discontinuities in received signal level recordings at 7 GHz. Figure 6.6 shows an expanded view of Figure 6.5 around 80 minutes into the event showing details of this correspondence.

Expanded views of the differential temperature around the discontinuities shows a corresponding increase in the rate of change of temperature at these points. Figure 6.7 shows the increase in differential temperature for the fade discontinuity 80 minutes into the event and Figure 6.8 shows discontinuities earlier in the event around 30 minutes.

A similar correspondence is seen in the Ryder temperature and the rapid changes in the 3.550 GHz signal as shown in Figure 6.9. These changes show that as the 0°C isotherm moves into and out of the path there are corresponding rapid changes in received signal attenuation.

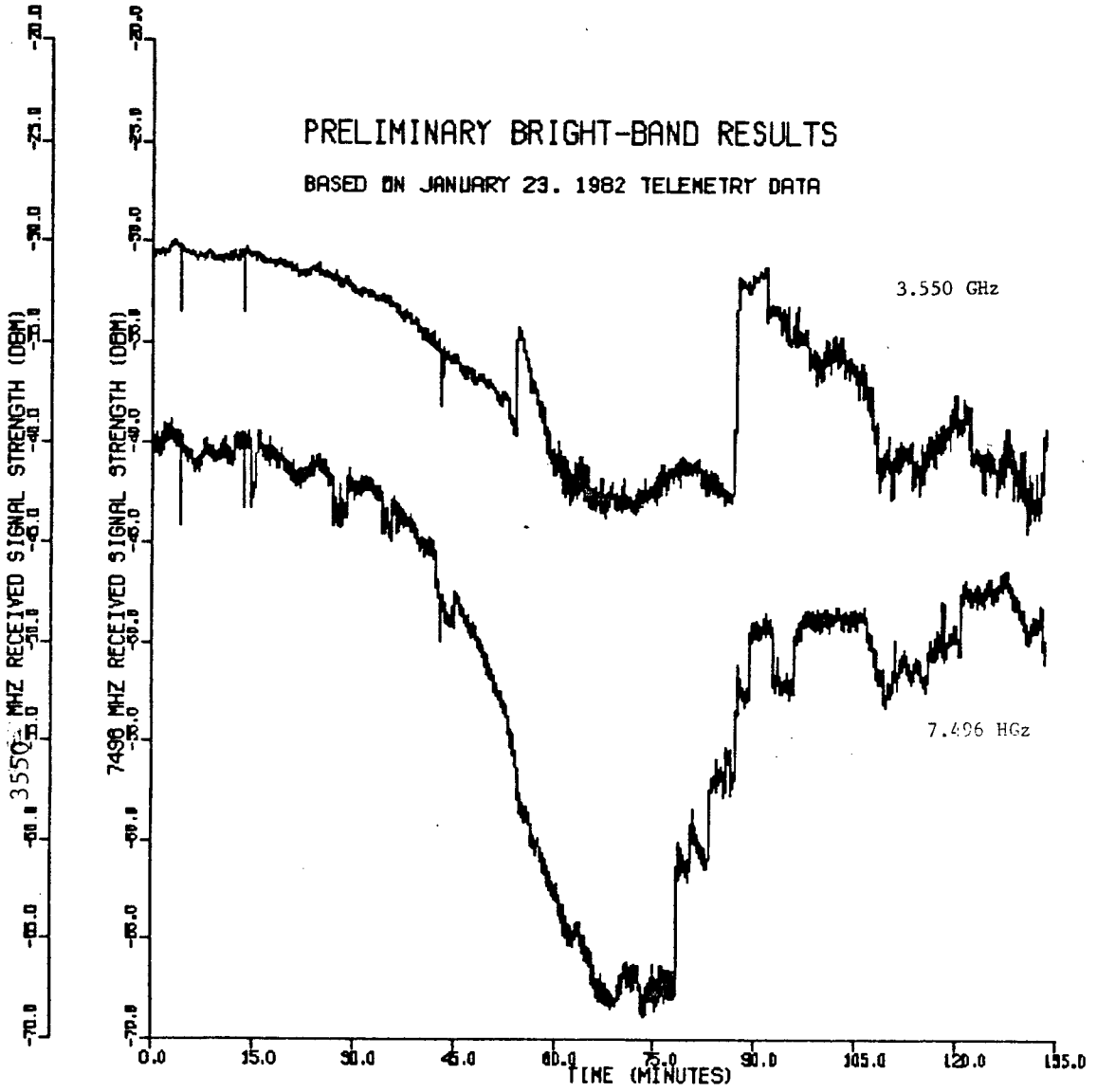

Figure 6.3 The 3.550 GHz and 7.496 GHz Signal Levels Versus Time

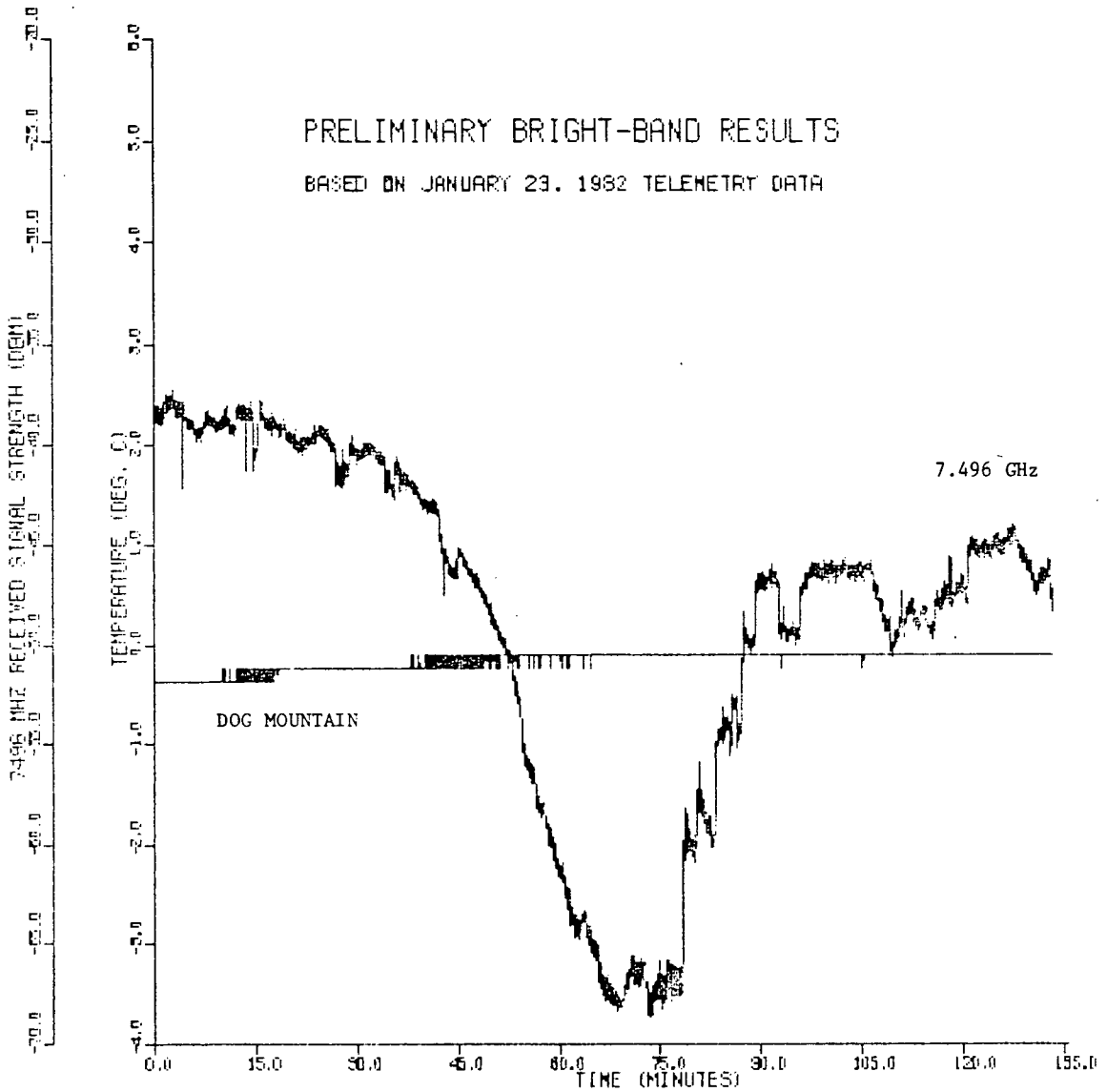

Figure 6.4 The Dog Mountain Transmitter Site Temperature and The 7.496 GHz Receiver Level Versus Time

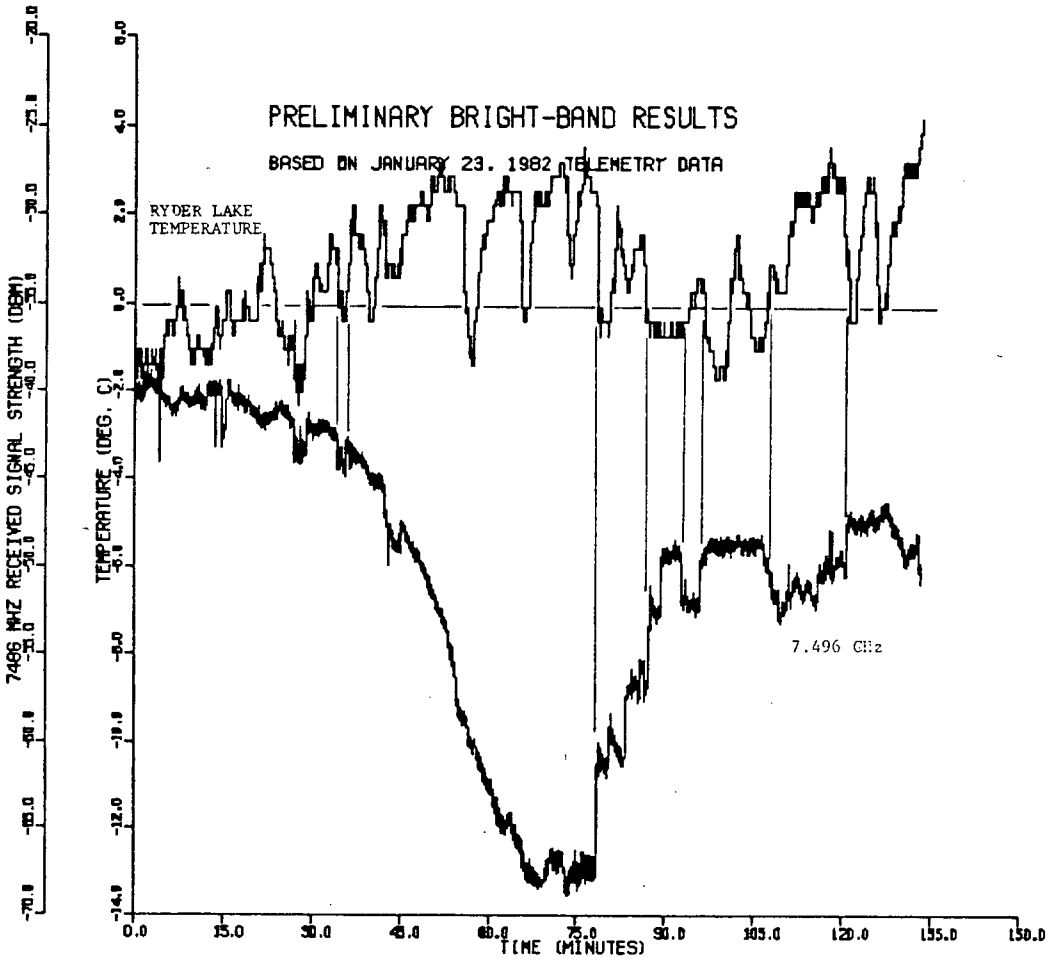

Figure 6.5 The Ryder Lake Receiver Site Temperature and The 7.496 GHz Signal Reciever Level Versus Time

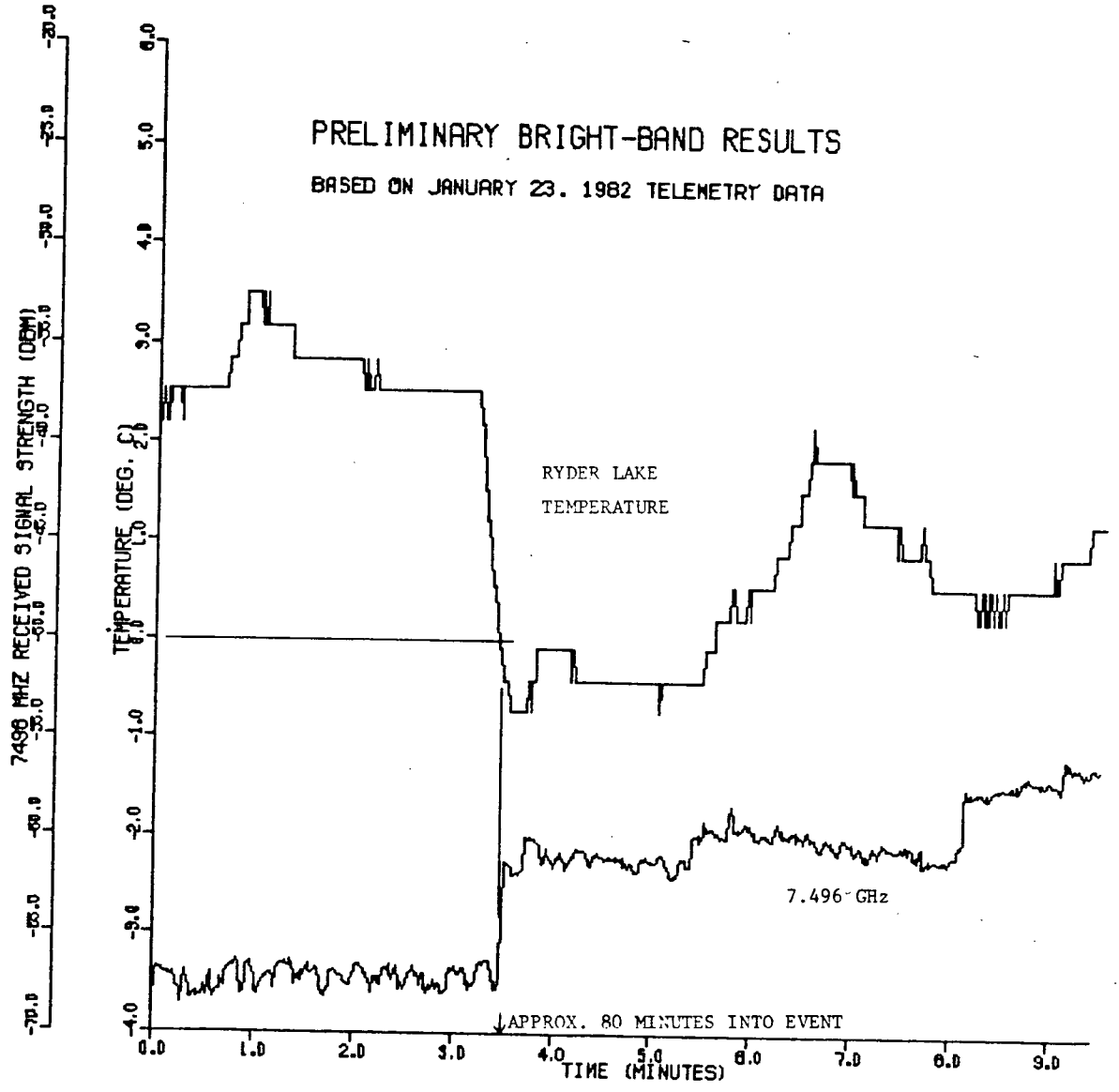

Figure 6.6 An Expanded View At Approximately 80 Minutes Into The Event Showing The 7.496 GHz Receiver Signal Level Versus Time

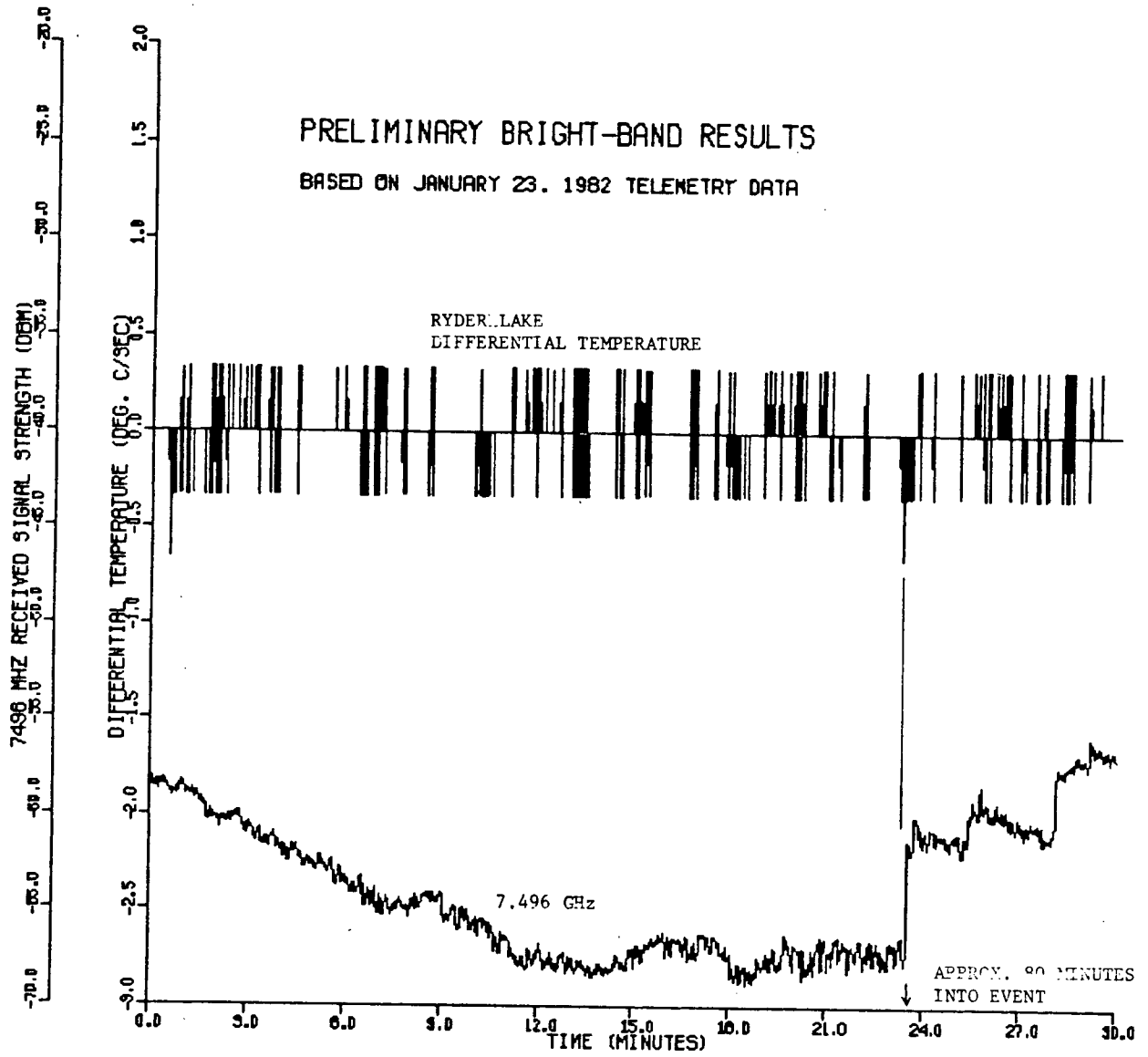

Figure 6.7 Ryder Lake Differential Temperature and 7.496 GHz Receiver Signal Level Versus Time Showing The Discontinuity 80 Minutes Into The Event

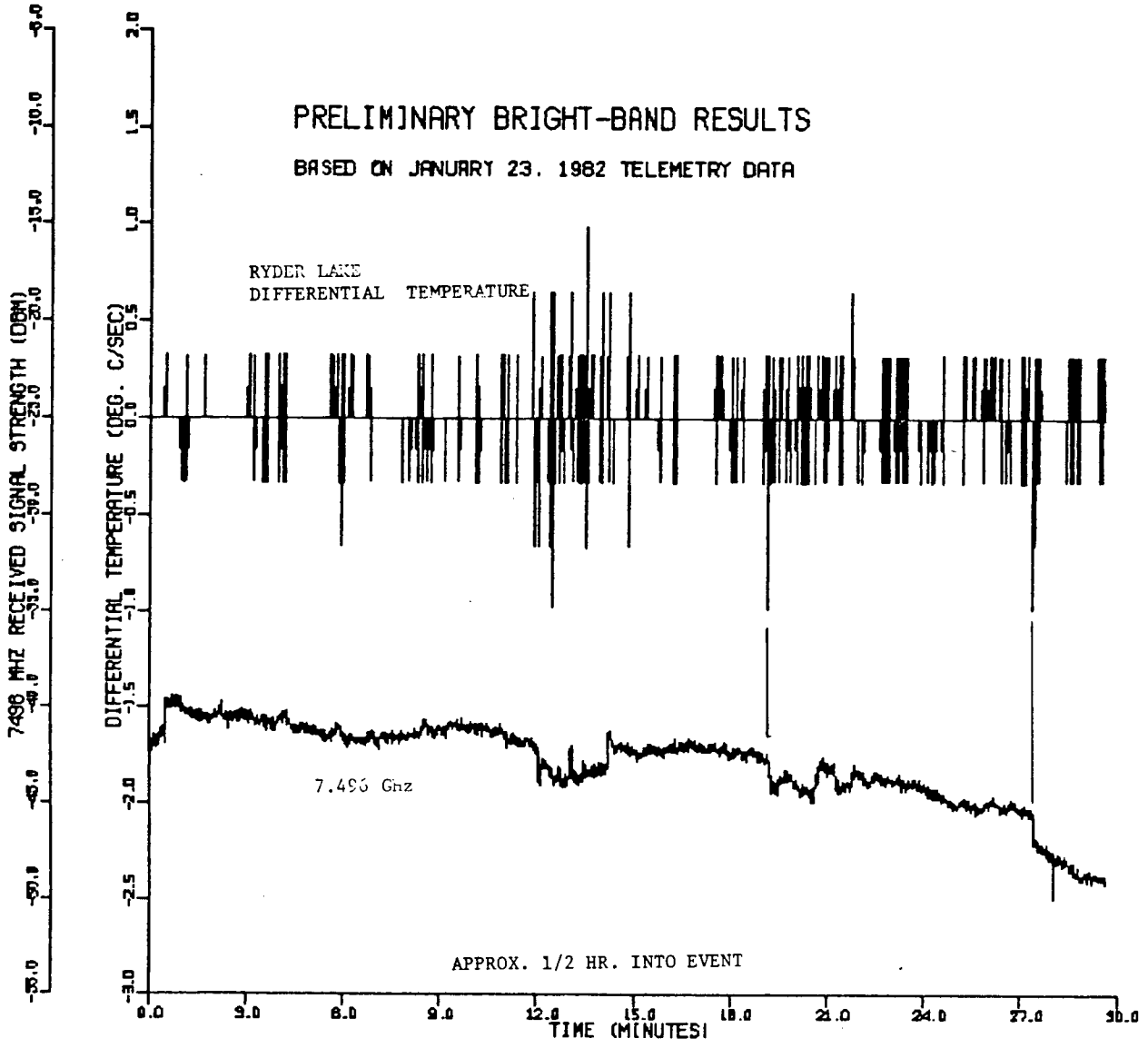

Figure 6.8 The Ryder Lake Differential Temperature and 7.496 GHz Receiver Signal Level Versus Time Showing Discontinuities 30 Minutes Into The Event.

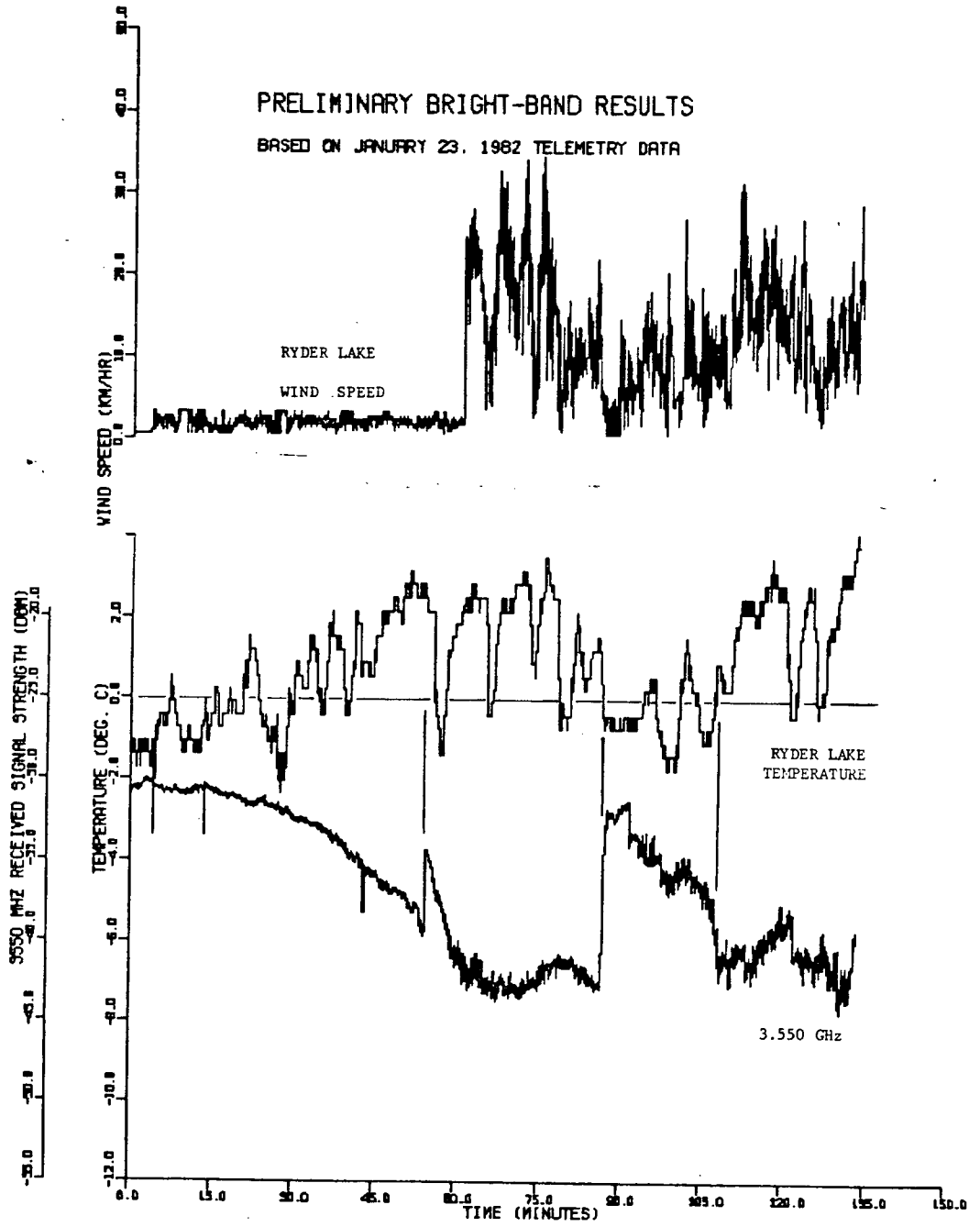

Figure 6.9 Ryder Lake Windspeed, Temperature, and The 3.550 GHz Reciever Signal Level Versus Time

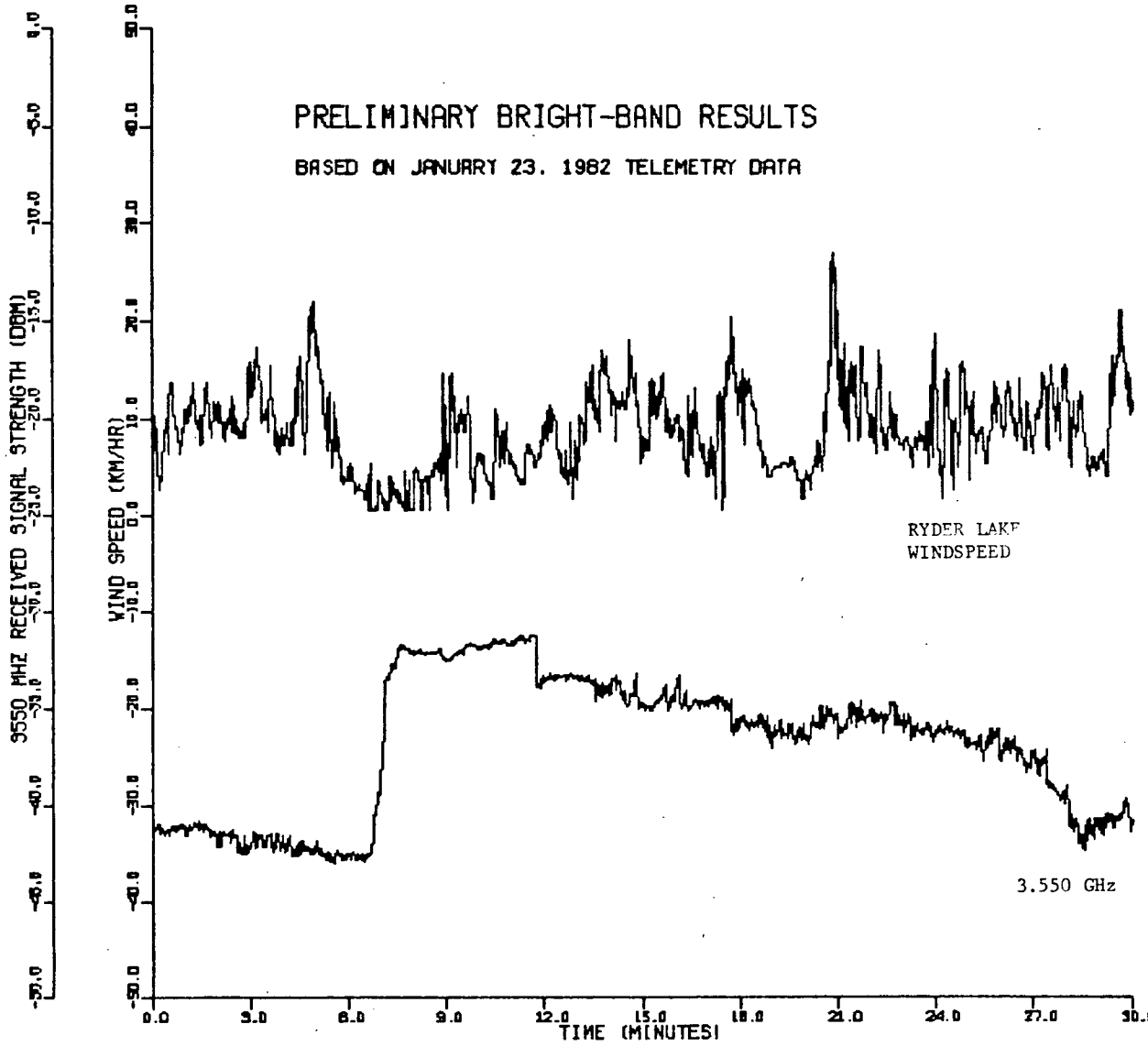

Figure 6.10 An Expanded View Of The Ryder Lake Windspeed and 3.550 GHz Receiver Signal Level Versus Time Approximately 90 Minutes Into The Event

Figure 6.10 shows an expanded view of the Ryder windspeed and 3.550 GHz signal versus time starting before the 90 minute discontinuity. The sudden reduction in received signal level was preceded by a sudden drop in the windspeed.

Rain information for this portion of the event was not available since the rain buckets were obstructed by ice.

6.2.3 February 19, 1982, 7:30-9:00 a.m.

These results were taken during the easterly passage of a storm front through the path on February 19, 1982. The presence of the 0°C isotherm during this event is indicated by the temperature recordings for the transmitter and receiver site in Figure 6.11. Excess Attenuation Ratios were calculated for both 4 and 7 GHz and are presented in Tables 6.4 and 6.5 according to the sample points shown in the received signal level and rain rate plots in Figure 6.12.

These results generally show that the measured attenuation during the presence of the bright band is significantly greater than that due to pure rain. Although there is a great variability in the Excess Attenuation Ratios for this event this could be attributed to rain rate for the path being taken at only one site (Agassiz) and to the turbulent nature of the storm front as it passed through. Evidence of the turbulent make-up of this event is observed in the rapid fluctuations of the Ryder Lake temperature and windspeed plots shown in Figure 6.11.

Scintillation like fading phenomenon which appeared first on the chart recordings in section 6.1 also were observed in this event in the 7.496 received signal levels. More observations and analysis needs to be undertaken

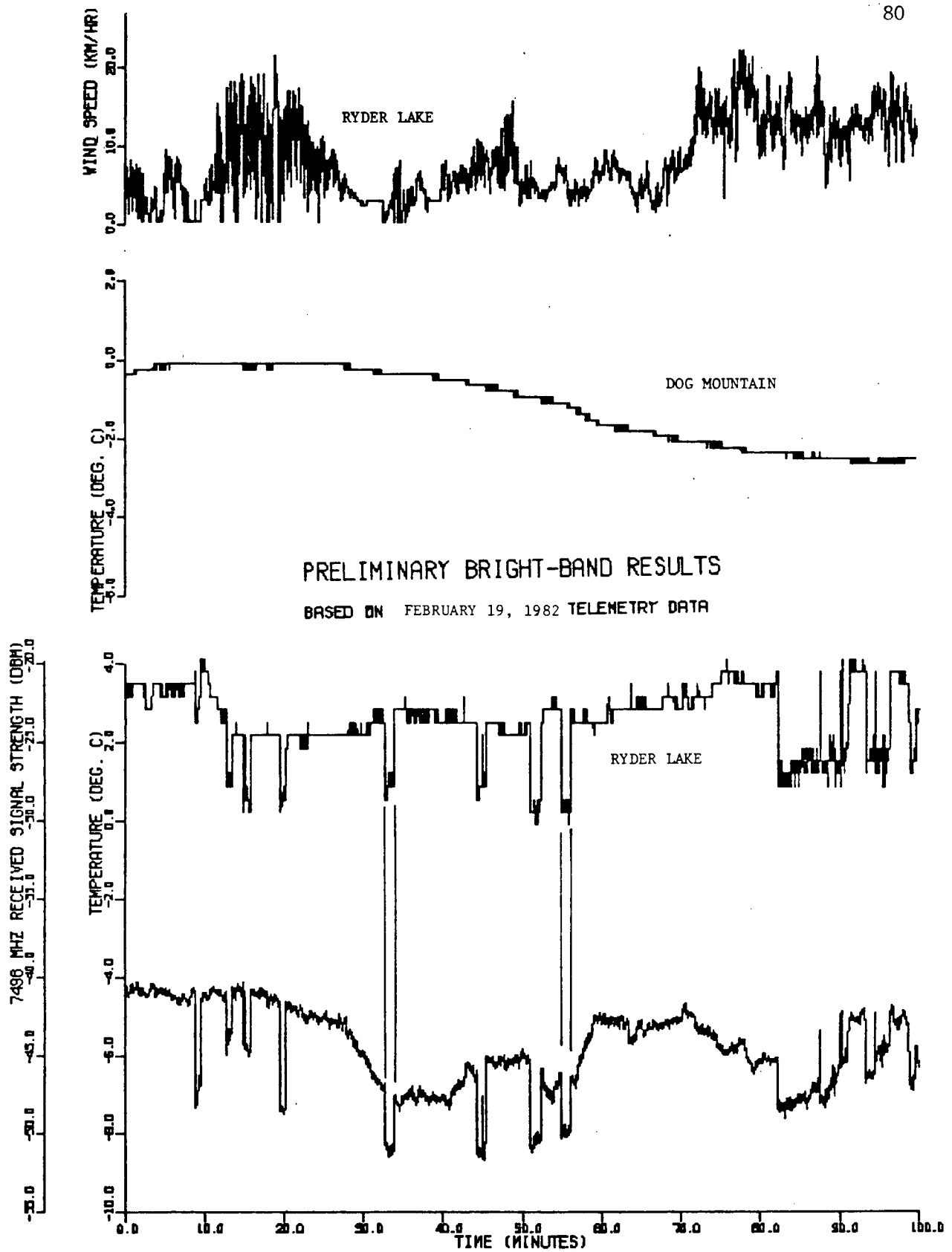

Figure 6.11 Ryder Lake and Dog Mountain Temperatures, Ryder Lake Windspeed and The 7.496 GHz Receiver Signal Level Versus Time

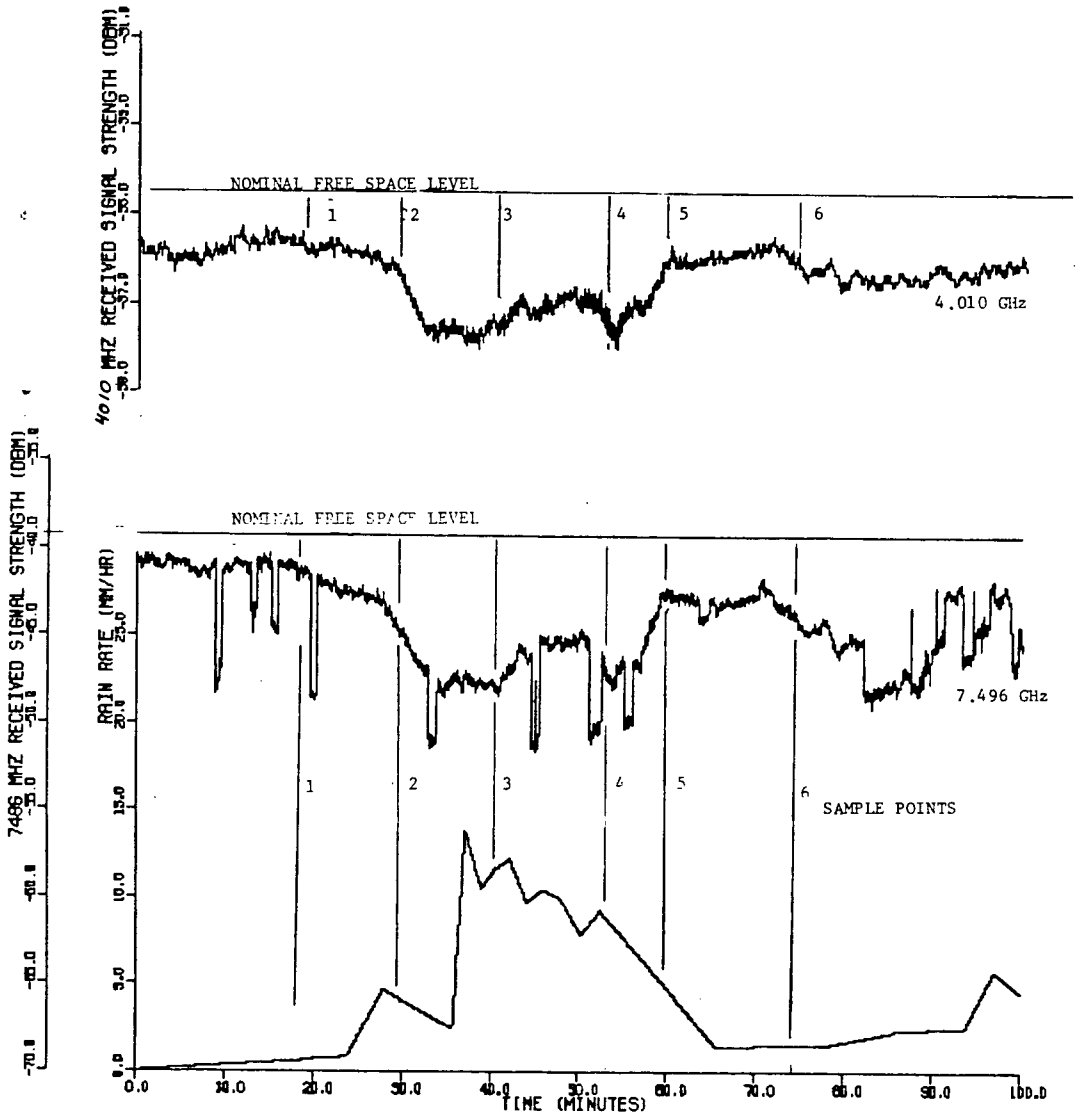

Figure 6.12 Agassiz Rain Rate, The 7.496 GHz and 4.010 GHz Receiver Signals Versus Time

Table 6.4 February 19, 1982 Results

Frequency & Sample No.	Average Rain Rate (mm/hr)	Average Attenuation in dB		
		Meas.	Rain*	Excess Atten.
4.010				
1	0.6	0.6	.04	0.56
2	4.0	1.6	.20	1.40
3	11.2	2.5	.57	1.93
4	9.0	2.4	.45	1.95
5	4.0	1.0	.20	0.80
6	1.2	0.7	.06	0.64
7.495				
1	0.6	1.5	0.17	1.33
2	4.0	6.0	1.36	4.64
3	11.2	8.5	4.50	4.00
4	9.0	6.5	3.50	3.00
5	4.0	3.0	1.36	1.64
6	1.2	3.7	0.36	3.31

*Derived using the Laws and Parson Distribution for 0°C

Table 6.5 February 19, 1982 Results

Frequency & Sample No.	Average Rain Attenuation dB/km	Bright-band Attenuation dB/km	Excess Attenuation Ratio (EAR)
4.010			
1	.00103	.044	42.7
2	.0048	.097	20.2
3	.0137	.134	9.8
4	.0110	.135	12.3
5	.0048	.056	11.7
6	.00145	.044	30.3
7.496			
1	.0041	.092	22.4
2	.0329	.321	9.8
3	.1110	.277	2.5
4	.0860	.208	2.4
5	.0329	.114	3.5
6	.0088	.229	26.0

before definite conclusions as to the cause of these scintillations can be determined. This data does suggest, however, that these rapid fades correspond to rapid changes in temperature and that these could result in changes to the thickness of the bright band along the path. The spikes in the temperature plot change at rates of up to 2°C per second at each side of the fade transition as shown in Figure 6.13. The feasibility of differential temperature physically changing at these rates is shown by Thompson et al. in their paper on atmospheric turbulence measurements [71].

In this particular event the temperature fluctuations decrease to just above 0°C which would suggest that the thickness of the bright band would increase due to a reduction in temperature gradient for these periods. Further research is being carried out to find the cause of this scintillation phenomenon.

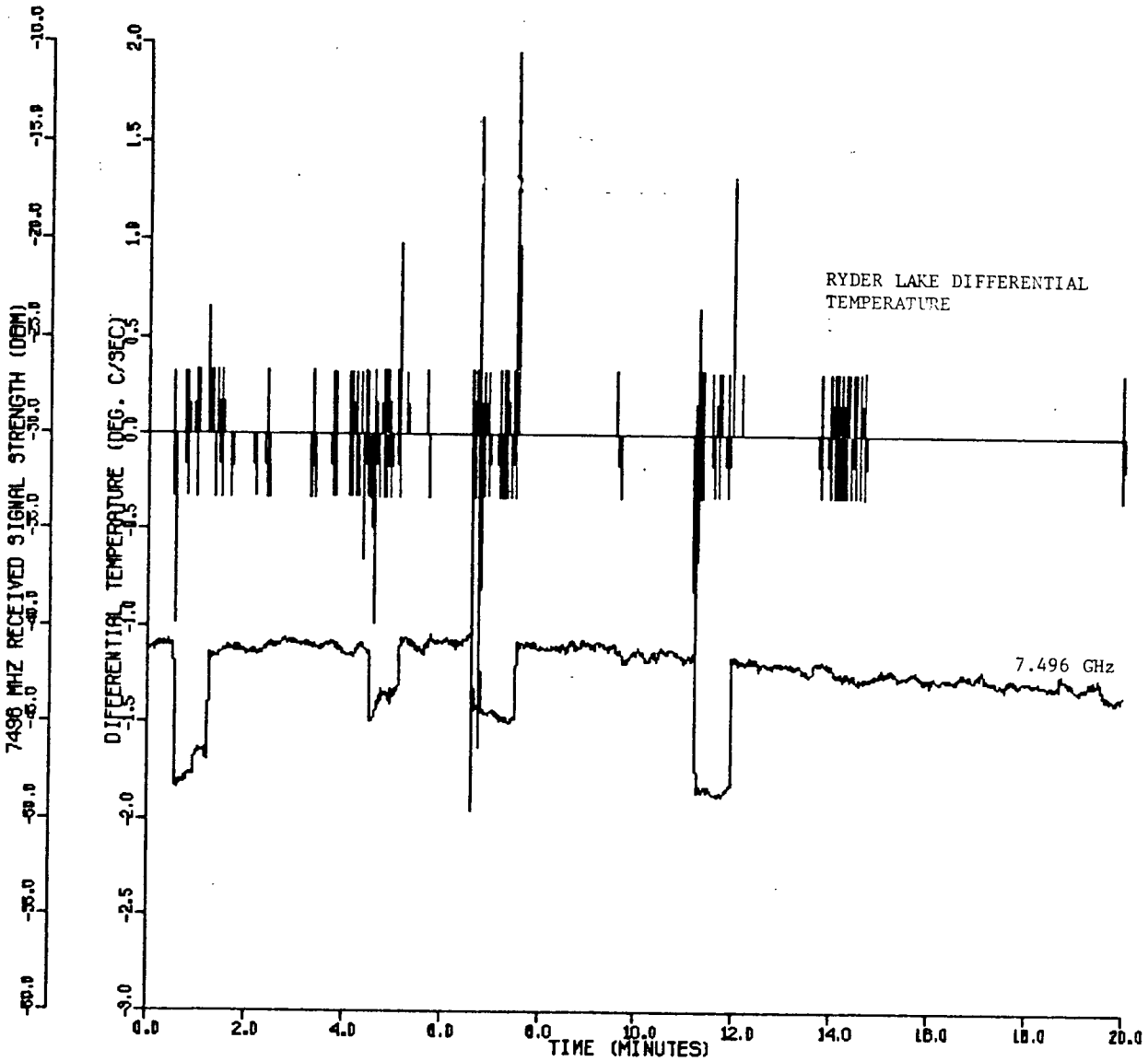

Figure 6.13 Ryder Lake Differential Temperature and The 7.496 GHz Receiver Signal Level Versus Time

CHAPTER VII

CONCLUSIONS AND DIRECTIONS FOR FUTURE WORK

7.1 Conclusions

Previous observations using chart recordings [64,65] showed that excess attenuation at 7 GHz due to the bright band is considerable with the magnitudes being consistent with those predicted by Nishitsuji and Matsumoto for watery snow. Based on these preliminary observations, the excess attenuation ratios ranged from 7 to 28 times (in dB) while the model for watery snow predicts an excess attenuation ratio of 15 at 7 GHz. The large variance between the measured values from those predicted can be attributed to several factors; first, the inaccuracies which can be attributed to a low density rain bucket network for determining rain rates in turbulent events, second, deviation of the thickness of the bright band from the assumed 400 m and third, differences between the path averaged precipitation rate from that of a precipitation rate averaged solely within the bright band.

The results, however, suggested that the Nishitsuji and the Matsumoto model for watery snow was applicable and therefore variations between measurement and that predicted by theory would most likely be attributable to the experimental methods used.

The remote-telemetry-based measurement system provided accurate correlations between meteorological phenomenon and received signal levels, confirmed the scintillation phenomenon superimposed on the broad band fade previously observed with the chart recorders and showed that bright band propagation was affected by the turbulent meteorological phenomenon during the

first phases of a storm system which became more stable as the storm decayed. Excess Attenuation Ratios consistent with theory were obtainable during the decaying phases of a storm where widespread uniform precipitation rates were occurring. Under these conditions (unfortunately only one was operating) a single rain bucket near the center of the path generally provided sufficient information. However, when the path was influenced by a storm front the rain information from a single site was not enough to obtain consistent results.

The scintillation phenomenon during fading appeared to correspond with rapid fluctuations in temperature around 0°C but further measurements and analysis are required to draw firm conclusions regarding the physical mechanisms resulting in these observations.

7.2 Directions for Future Research

This thesis lays the groundwork to evaluate the proposed 8 GHz digital radio with respect to its availability under various propagation conditions. During this intial bright-band study it has become clearer that factors which can be attributed to the bright band may also significantly impact the propagation of the 8 GHz digital radio on certain slant paths. For example, the rapid scintillations observed during deep bright band fading may affect the bit error rate performance [5,6] of the radio. Another factor of considerable concern is that the EAR is expected to be 15 at 8 GHz [51] and since rain attenuation starts becoming a significant factor at this frequency it makes bright band attenuation even more important. As shown by the recordings in Figure 6.0 under heavy widespread rain conditions a bright band fade can last for several hours making it an important design variable. Therefore

to derive maximum benefit from the next phase in this research program, the digital radio and the bright band experiment should be run concurrently.

Figure 7.0 gives two alternate system block diagrams to accomplish this, the first uses the data link to send the real time clock as data and the second option uses a WWVB time recorder at each site.

In terms of improving the present system, the following suggestions can be made:

(a) The temperature measurements at Ryder Lake (I) should be made to provide greater resolution around 0°C and be sampled at 10 Hz to retain information on its variations.

(b) A sturdier anemometer and radiant heater should be installed at the Dog Mountain site.

(c) A time-lapse camera should monitor the Dog Mountain transmit antenna radomes for accumulations during precipitation events.

(d) A heating system should be developed to eliminate accumulations of snow in the rain buckets.

(e) The code for the SCAN and EXTRACT features of DBMS needs to be implemented.

(f) A graphical routine could be developed to plot temperature contours on a path cross section.

(g) A statistical routine needs to be incorporated in DBMS to determine fade probabilities from the distribution series data.

Long term objectives in the area of bright band propagation research should include:

(a) A detailed evaluation of other slant paths such as earth-space links with respect to bright band effects and their potential effect on system availability.

(b) The Nishitsuji and Matsumoto models describing snow attenuation by snow classification should be extended to the bright band. This extension should determine attenuation for the bright band by first establishing its characteristic snow profile in terms of moist, wet and watery snow and then calculating the attenuation as a function of temperature gradient (or bright band thickness) and precipitation rate.

(c) A model needs to be developed to account for the scintillation type which corresponded to rapid changes in temperature.

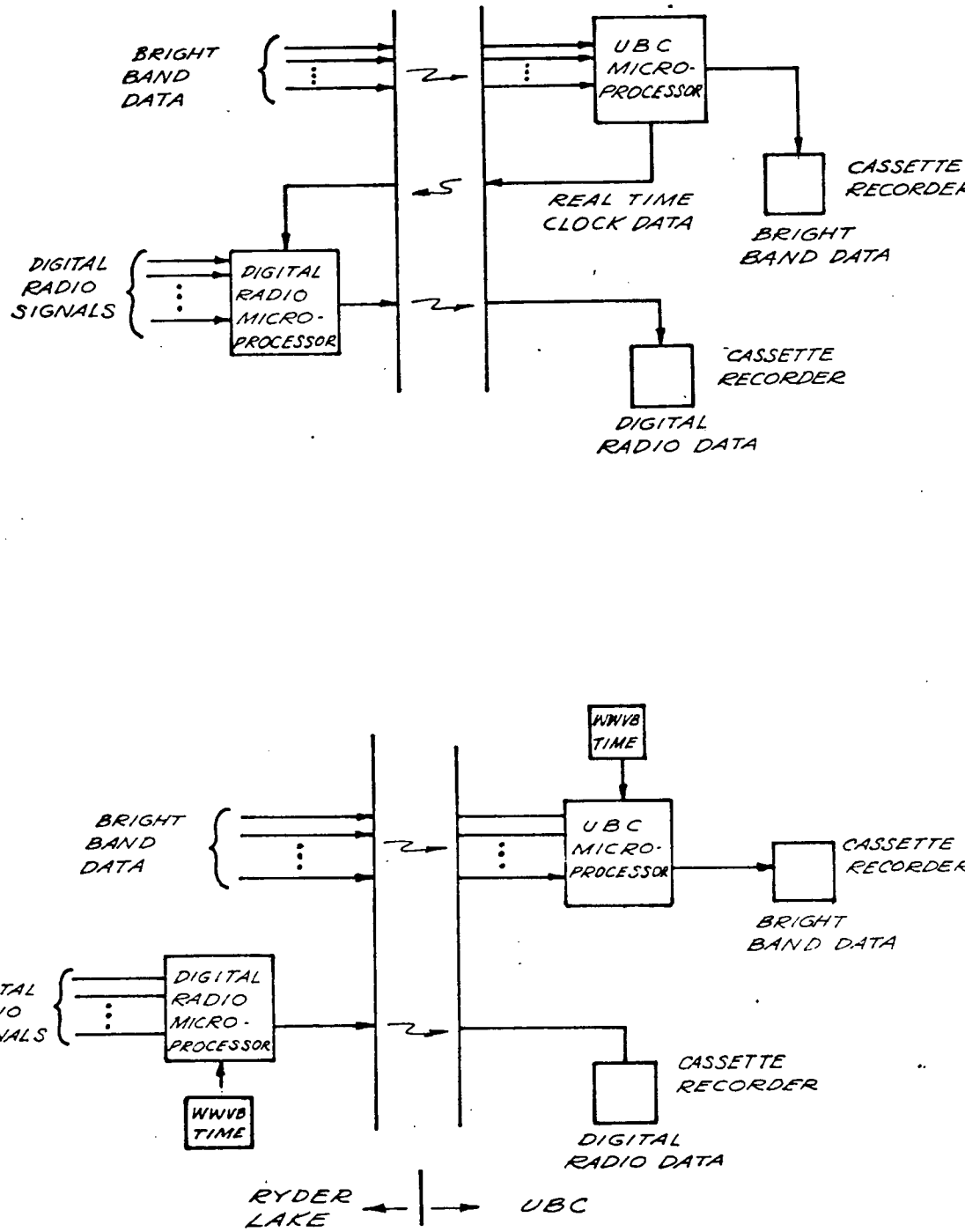

Figure 7.0 Proposed System Configurations to Incorporate the Digital Radio Monitoring System

APPENDIX A

AUTOMATIC GAIN CONTROL (AGC) CALIBRATIONS

To obtain accurate received signal level values the AGC feedback voltage must be accurately calibrated. This is achieved by inserting a known signal level of the correct frequency into the input of the microwave receiver and monitoring the AGC voltage output. In this experiment the AGC voltages were monitored at the output of the receiver signal conditioning circuit (see Appendix E) and plotted against the receiver input signal level to produce the AGC curves shown in Figures A-1 to A-5. These curves then form the basis for the look up tables and interpolation routines used as part of the entry procedure software in the data base management system as described in Chapter V and Appendix K. The receiver frequencies, polarizations and associated AGC curves used in this experiment are given in Table A-1.

TABLE A-1 Receiver Frequencies Polarizations and Associated AGC Curves

Receiver Frequency (MHz)	Polarization V = Vertical H = Horizontal	Associated AGC Curve by Figure #
3550	H	A-1
3790	H	A-2
4010	V	A-3
7142.0	H	A-4
7496.5	H	A-5

FIGURE A - I

3550 MHZ RECEIVER AGC CALIBRATION

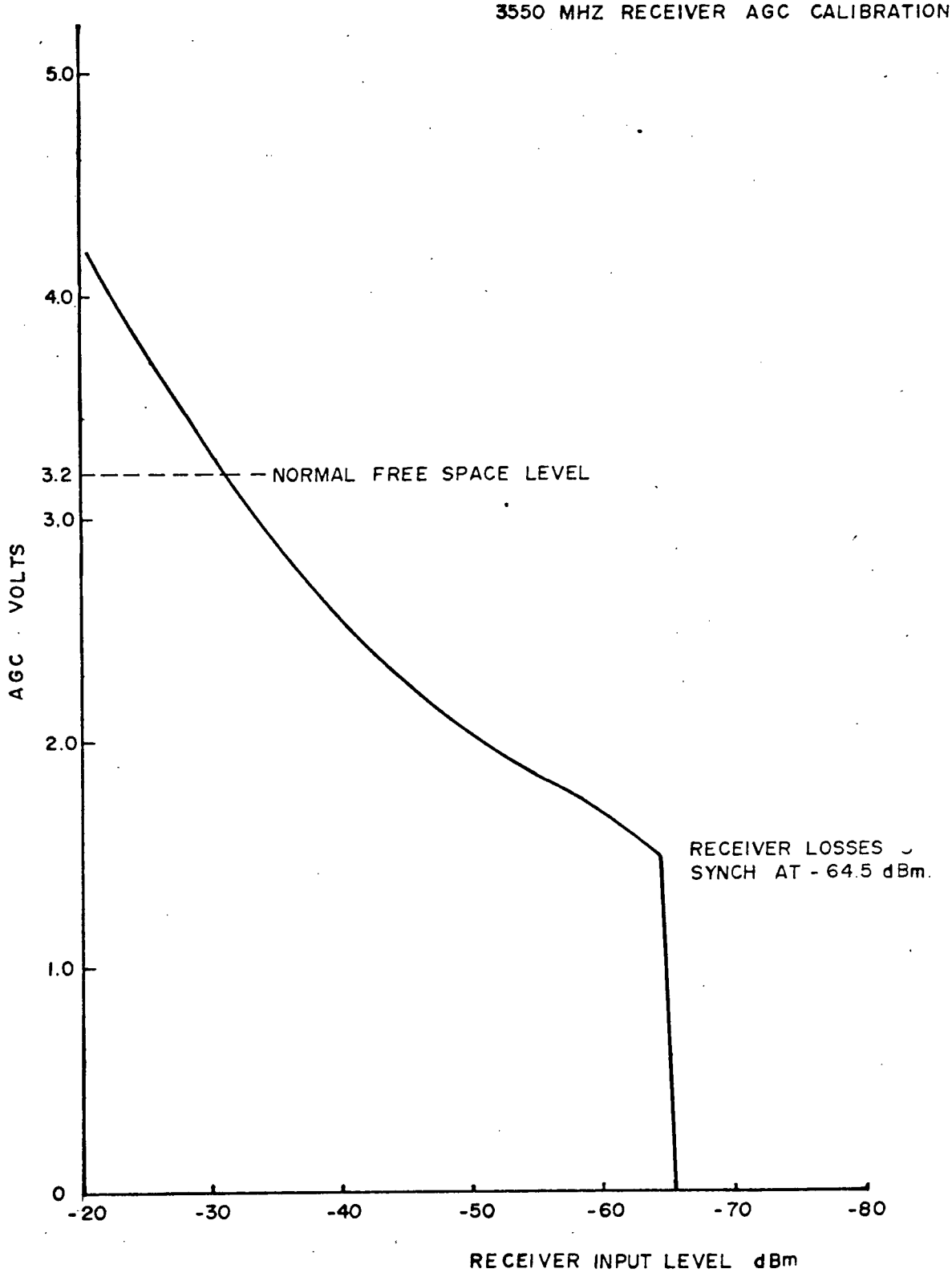

FIGURE A-2

3790 MHZ RECEIVER AGC CALIBRATION

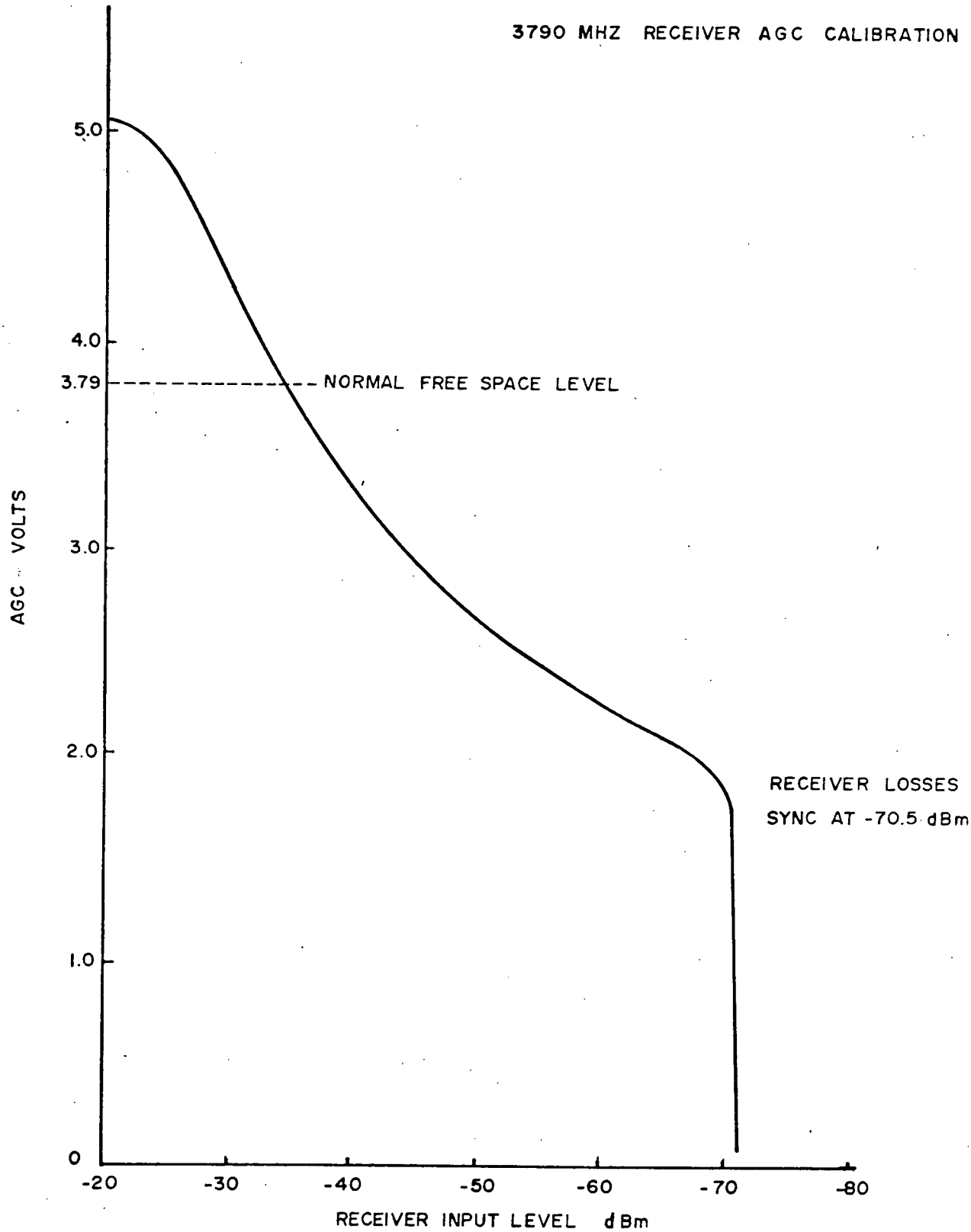

FIGURE A - 3

4010 MHZ RECEIVER AGC CALIBRATION

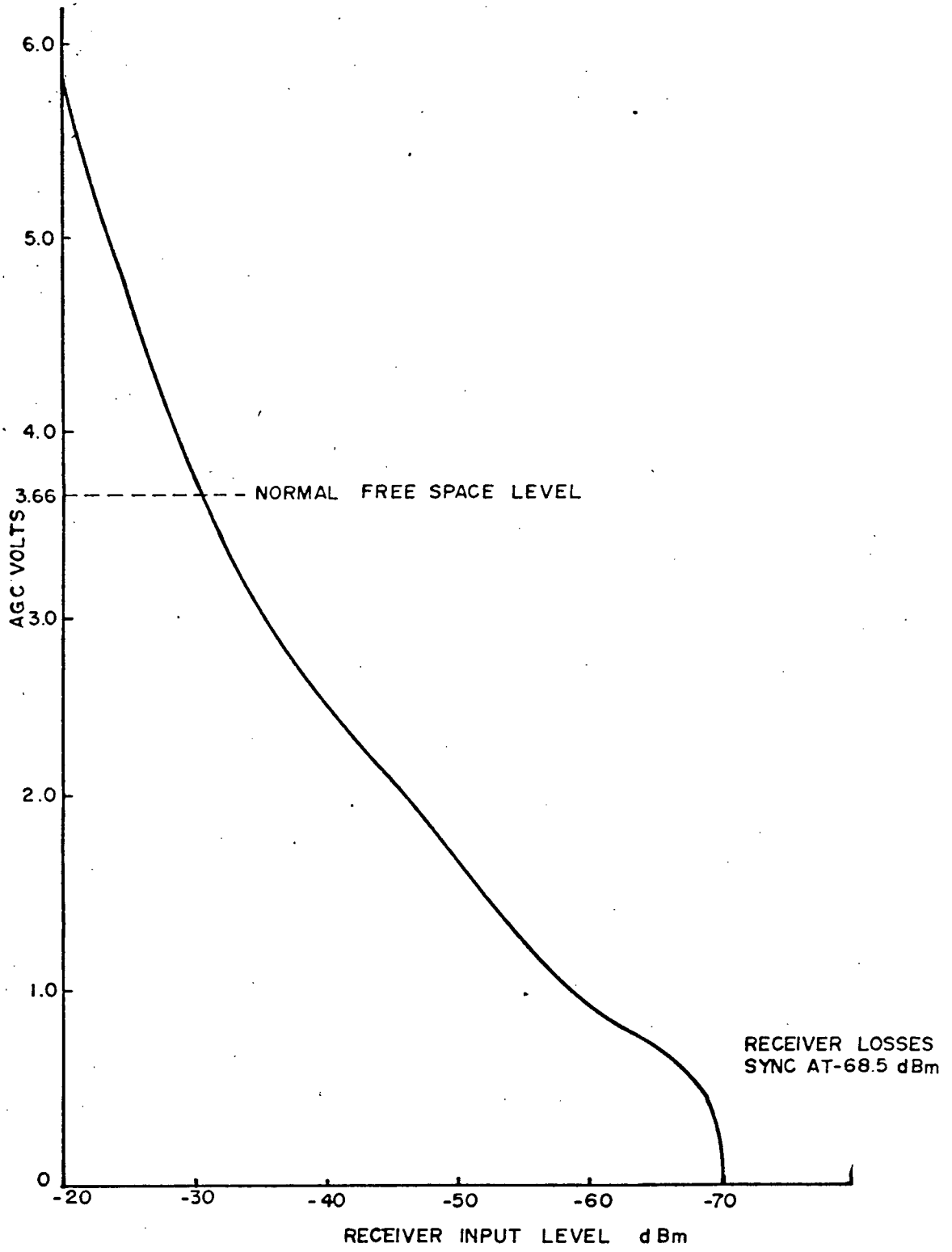

FIGURE A-4

7142 MHz. RECEIVER AGC CALIBRATION

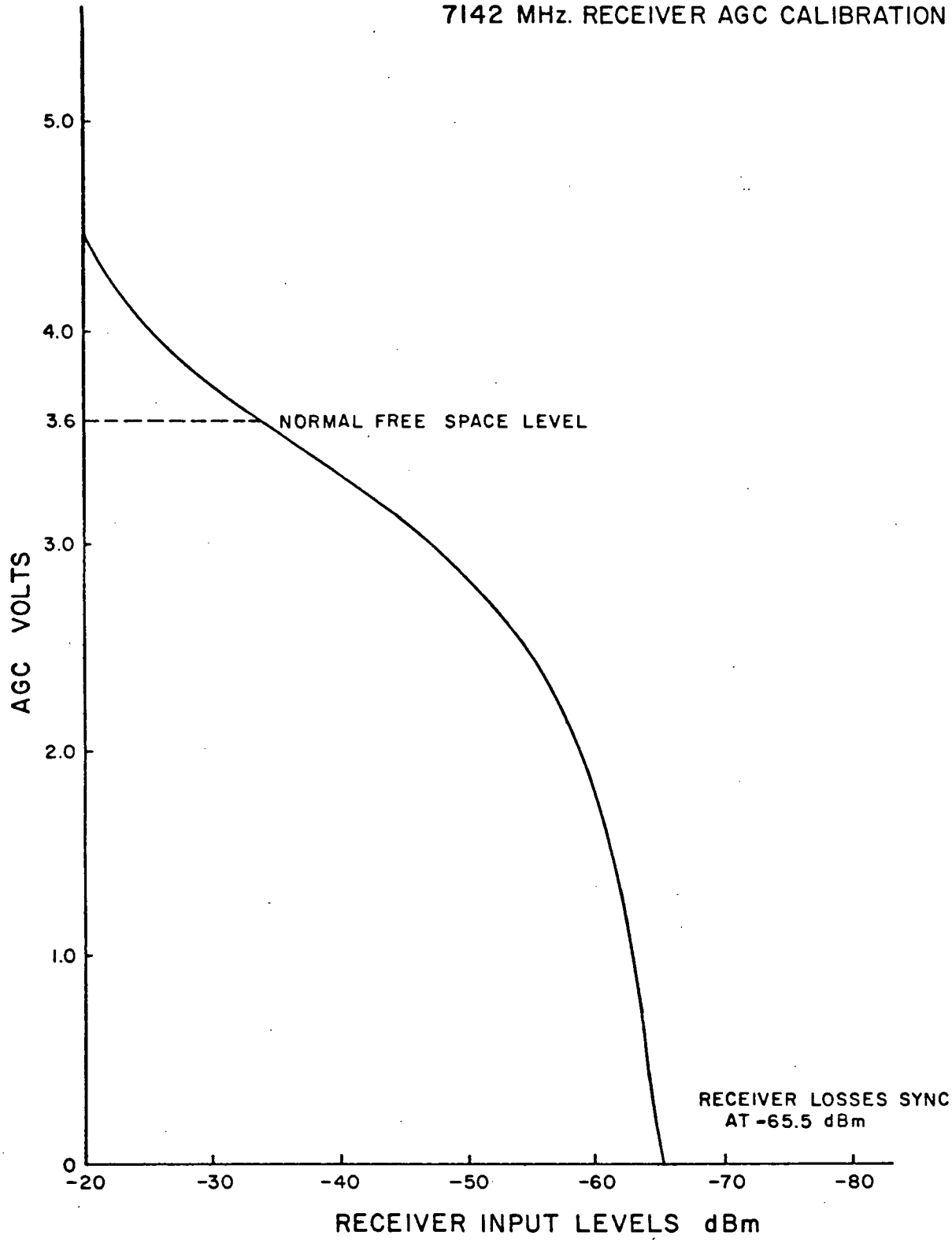

FIGURE A-5

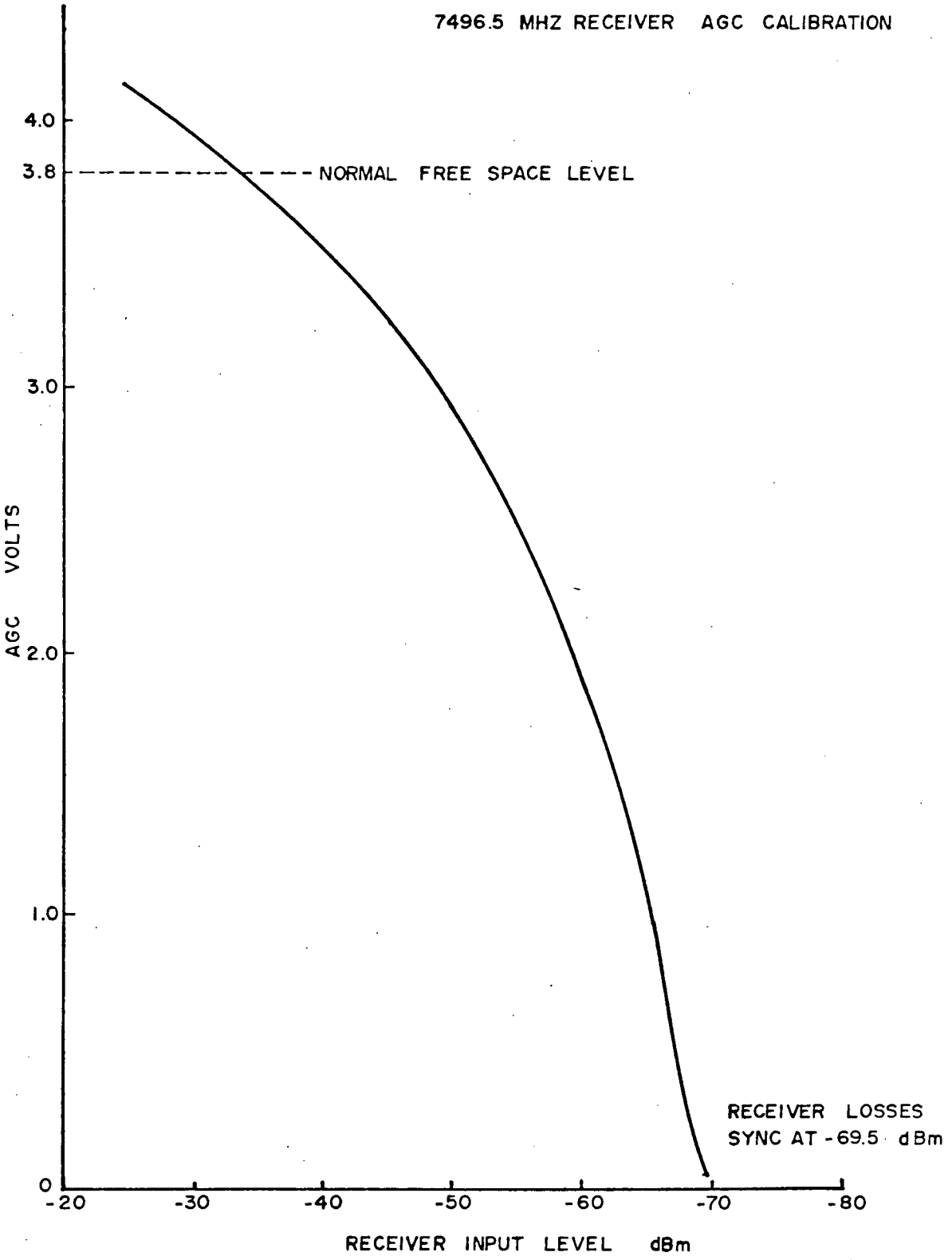
7496.5 MHZ RECEIVER AGC CALIBRATION
4.0
3.8
NORMAL FREE SPACE LEVEL
3.0
AGC VOLTS
2.0
1.0
0
RECEIVER LOSSES
SYNC AT -69.5 dBm
-20
-30
-40
-50
-60
-70
-80
RECEIVER INPUT LEVEL dBm

APPENDIX B

DETAILS OF THE DATA ACQUISITION SYSTEM LAYOUT

Figure B-1 gives a 1:250,000 topographical map showing the system layout for the UBC microwave propagation experiment including all the sites and associated data links. These include the Dog Mountain to Ryder Lake microwave path, the outgoing high speed data link to UBC and the end-links to the intermediate sites of Ruby Creek, Bear Mountain and the Agassiz Experimental Farm. A more detailed description for all these links is given in Figure B-2 to Figure B-7. Figures B-2 and B-3 provide detailed path profiles on 4/3 earth paper for the VHF radio links from Bear Mountain to Ryder Lake and from Ruby Creek to Ryder Lake, respectively. Table B-1 presents the VHF transmission calculations for these two paths using techniques developed by Bullington [11,67] and Okumura et al. [68]. Detailed circuit layouts, showing levels, entry points and routing, are provided in Figures B-4 and B-5 for the links from Dog Mountain to Ryder Lake and from the Agassiz Experimental Farm to Ryder Lake, respectively. Finally, a detailed circuit and routing diagram for the Ryder Lake to UBC data link is shown in Figure B-6 and a detailed illustration of the associated RS 232 interface configurations between the microprocessors and the statistical multiplex units is given in Figure B-7.

TABLE B-1 VHF Radio Path Transmission Calculations

1)	Locations	Bear Mountain	Ryder Lake	Ruby Creek	Ryder Lake
2)	Latitude °N	49°18'25"	49°06'52"	49°21'15"	49°06'52"
3)	Longitude °W	121°41'30"	121°54'07"	121°36'45"	121°54'07"
4)	Elevation (Meters)	945	236	31	236
5)	Antenna Height (Meters)	7	15	10	15
6)	DOC Call Sign	VGK 927	VGK 928	VGK 926	VGK 928
7)	Azimuth (°T)	218°T		212°T	
8)	Frequency (MHz)	160.11		151.79	
9)	Path Length (km)	26.1		33.7	
10)	Path Attenuation (dB)	-104.7		-102.4	
11)	Shadow Loss (dB)	0.0		26.0	
12)	Transmission Line Type	RG 58	RG 58	RG 58	RG 58
13)	" Line Loss (dB)	-1.0	-2.5	-5.0	-2.5
14)	Connector Loss (dB)	-1.0	-3.5	-1.0	-3.5
5)	Misc. Loss (dB)	-0.5	-0.5	-0.5	-0.5
16)	Total Losses (dB)	-113.7		-141.4	
17)	Antenna Gain (dBd)	+ 9.0	+11.0	+9.0	+11.0
18)	Transmitter Power (dBw)	-5.2		+ 4.8	
19)	Received Signal Level (dBw) (16+17+18)	-98.9		116.6	
20)	Threshold @ 12 dB SINAD (dBw)	-149.0		-149.0	
21)	Fade Margin (dB) SINAD (dBw)	50.1		32.4	
22)	Availability % Annual [67,68,69]	99.9998		99.989	

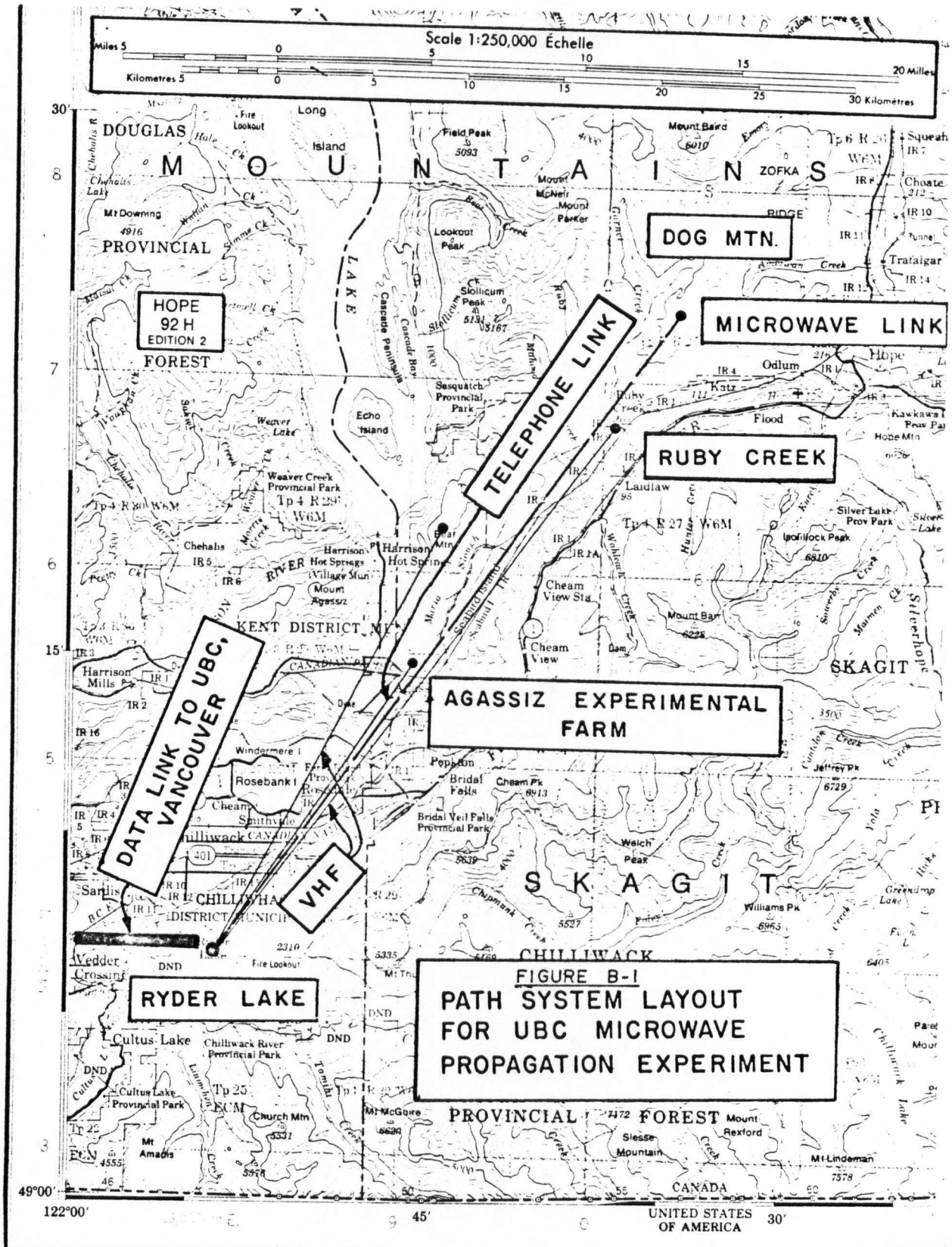

FIGURE B-1
PATH SYSTEM LAYOUT FOR UBC MICROWAVE PROPAGATION EXPERIMENT

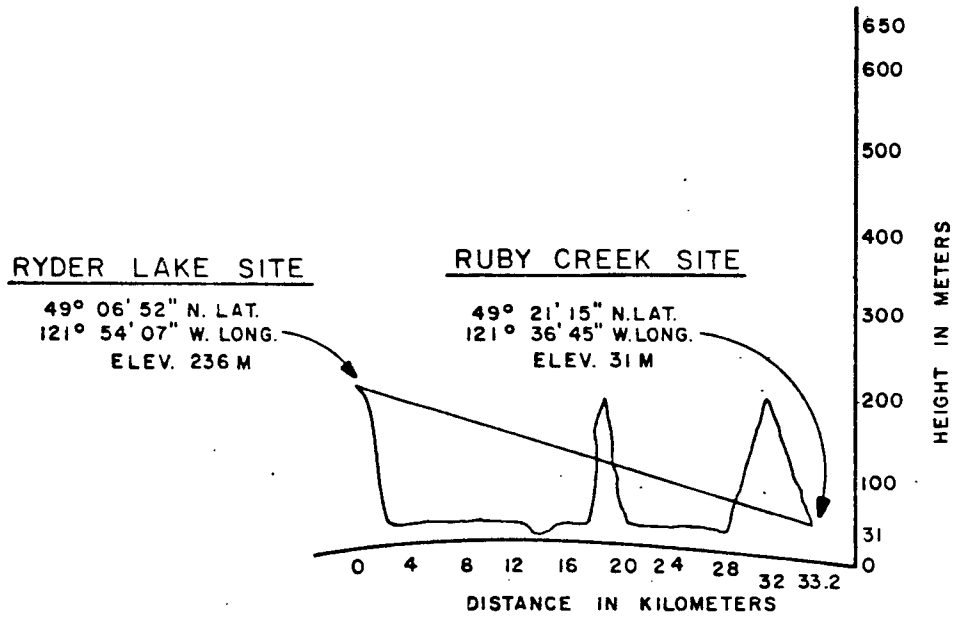

Figure B-2 Path Profile: Ruby Creek to Ryder Lake

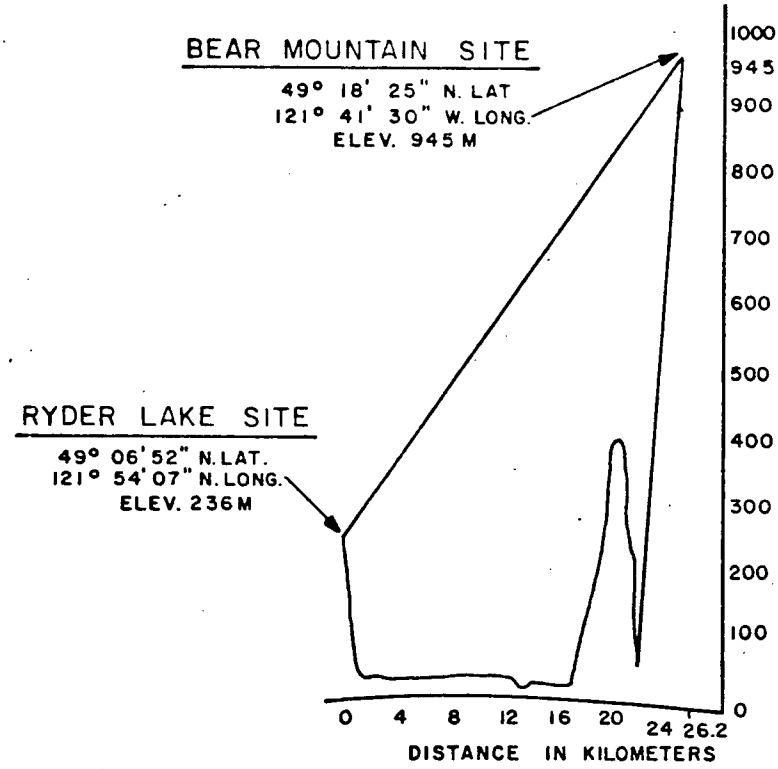

Figure B-3 Path Profile: Bear Mountain to Ryder Lake

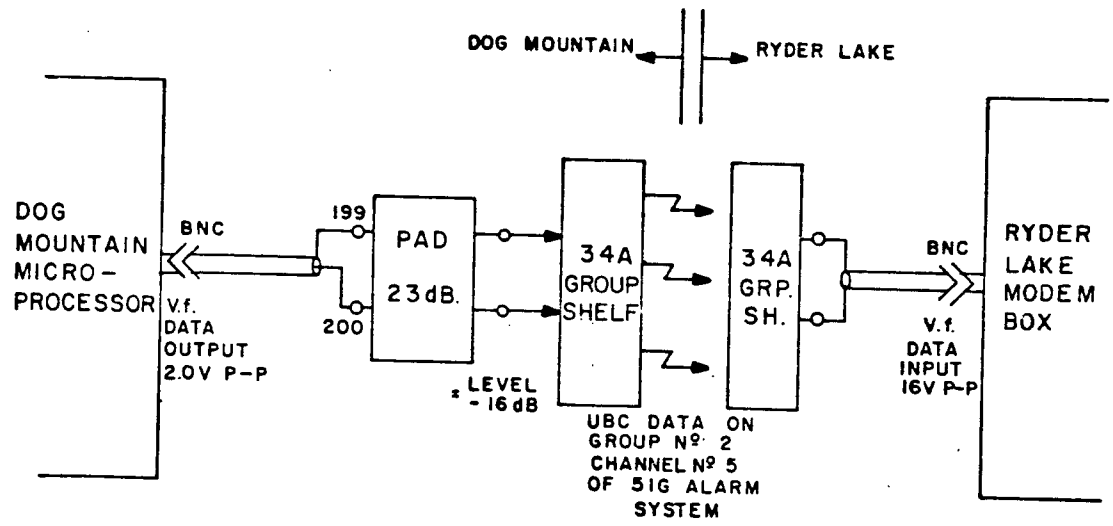

Figure B-4 Circuit Layout from Dog Mountain to Ryder Lake

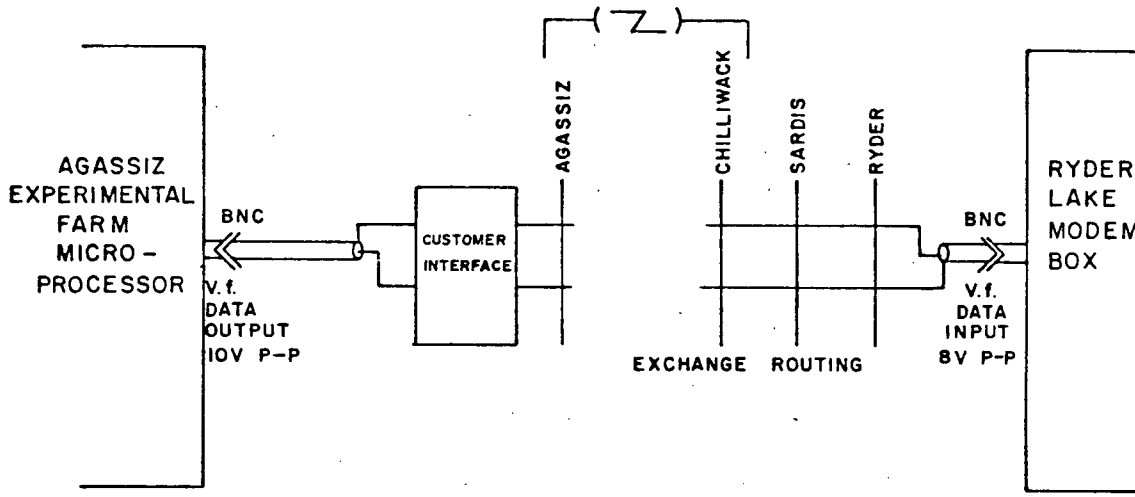

Figure B-5 Circuit Layout from the Agassiz Experimental Farm to Ryder Lake

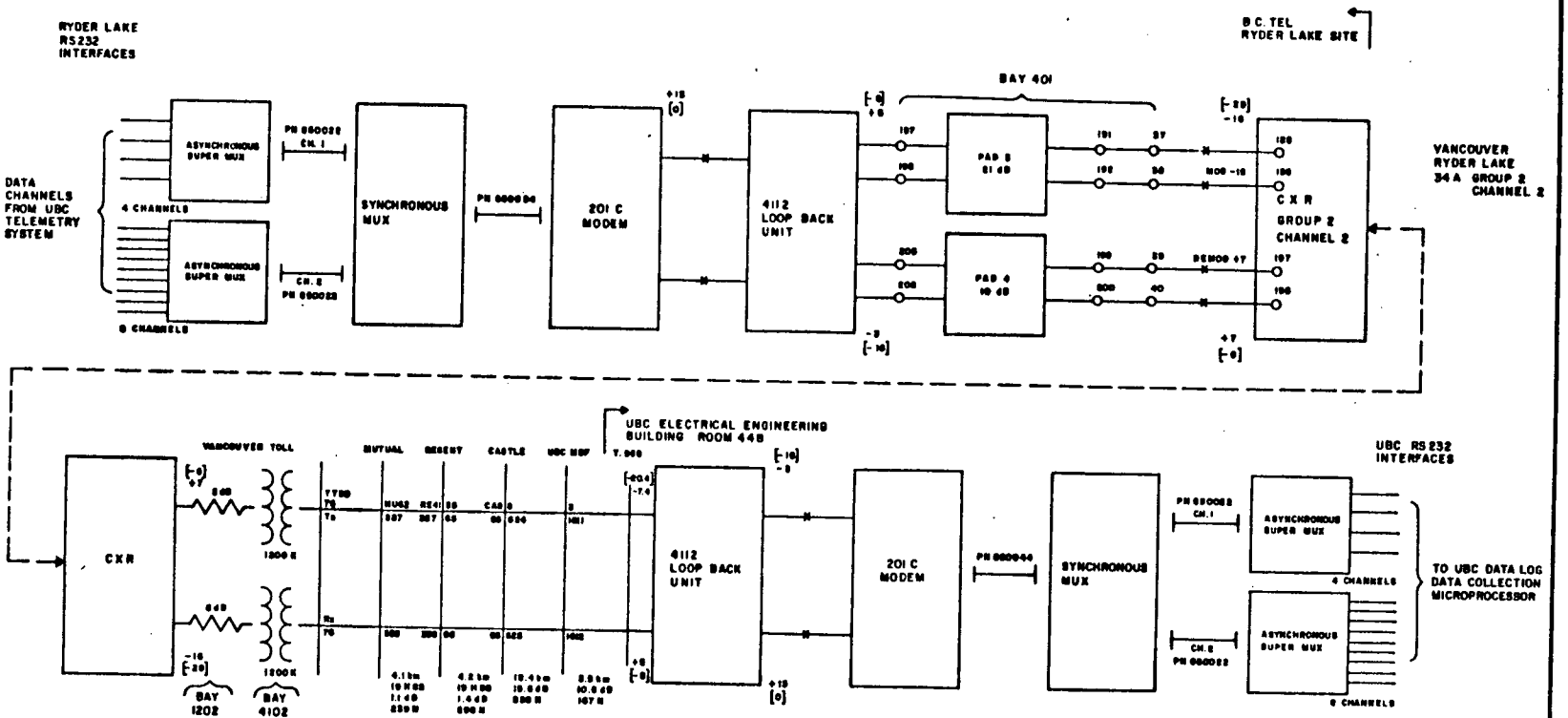

SCHEMATIC FOR THE RYDER LAKE TO UBC DATA CIRCUIT

FIGURE B-6

ISSUE 1

FEB. 28, 1981

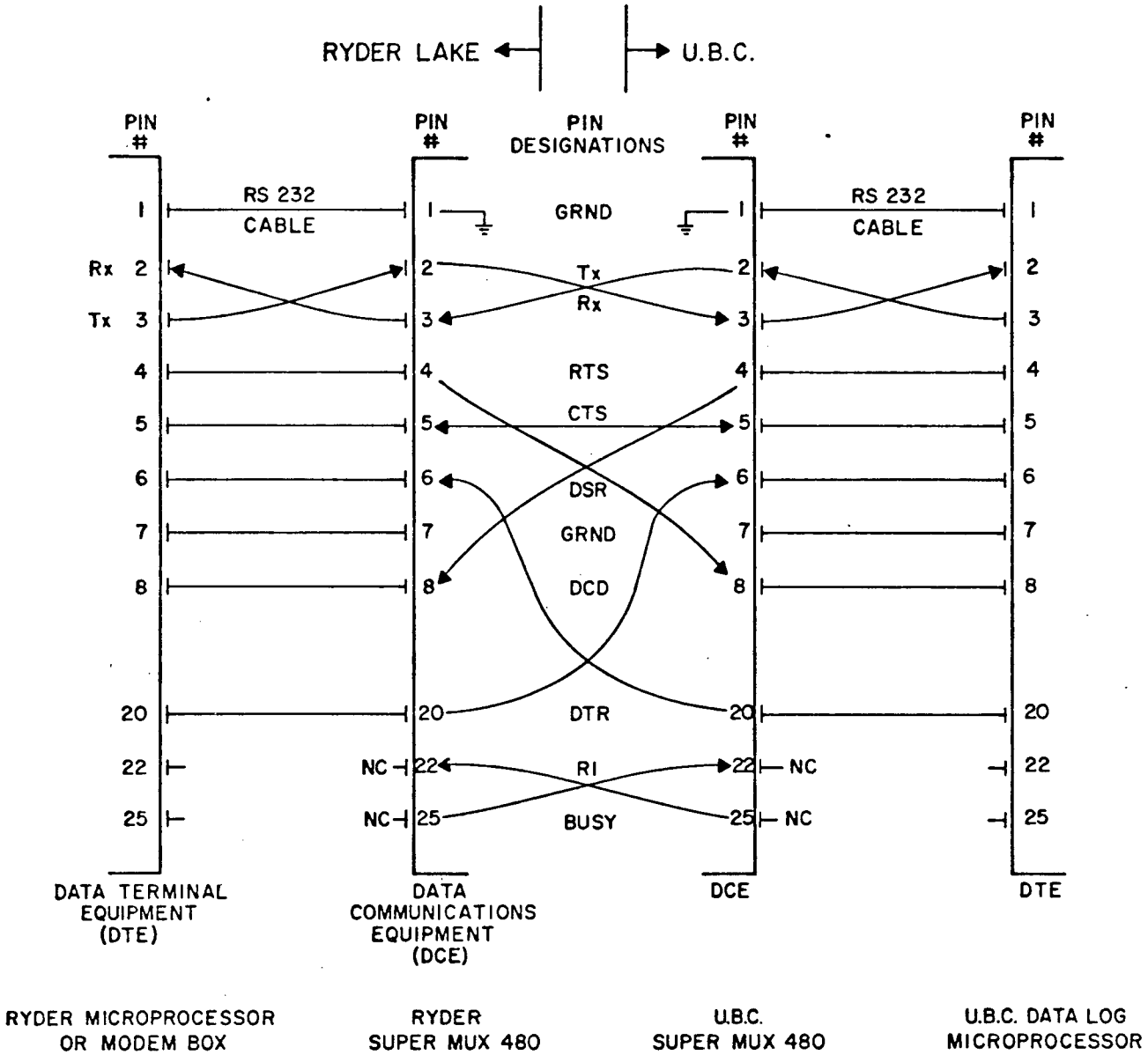

Figure B-7 The RS232C Interface for the Ryder Lake to UBC Data Circuit

APPENDIX C

EQUIPMENT AND SITE LAYOUTS

C-1 Ryder Lake

This site is the data concentration node where all the experimental field data are collected before being statistically multiplexed onto a telephone circuit for transmission to the University of British Columbia. The on-site data acquisition system serves two main purposes: first, to collect received signal level data from five selected 4 and 7 GHz microwave channels and, second, to monitor the wind speed, wind direction, temperature and rain rate variables at the site. Figure C-1 is a photograph of the site, Figure C-2 shows the equipment configuration and Figure C-3 illustrates the site layout.

Figure C-1 Ryder Lake Site Photograph

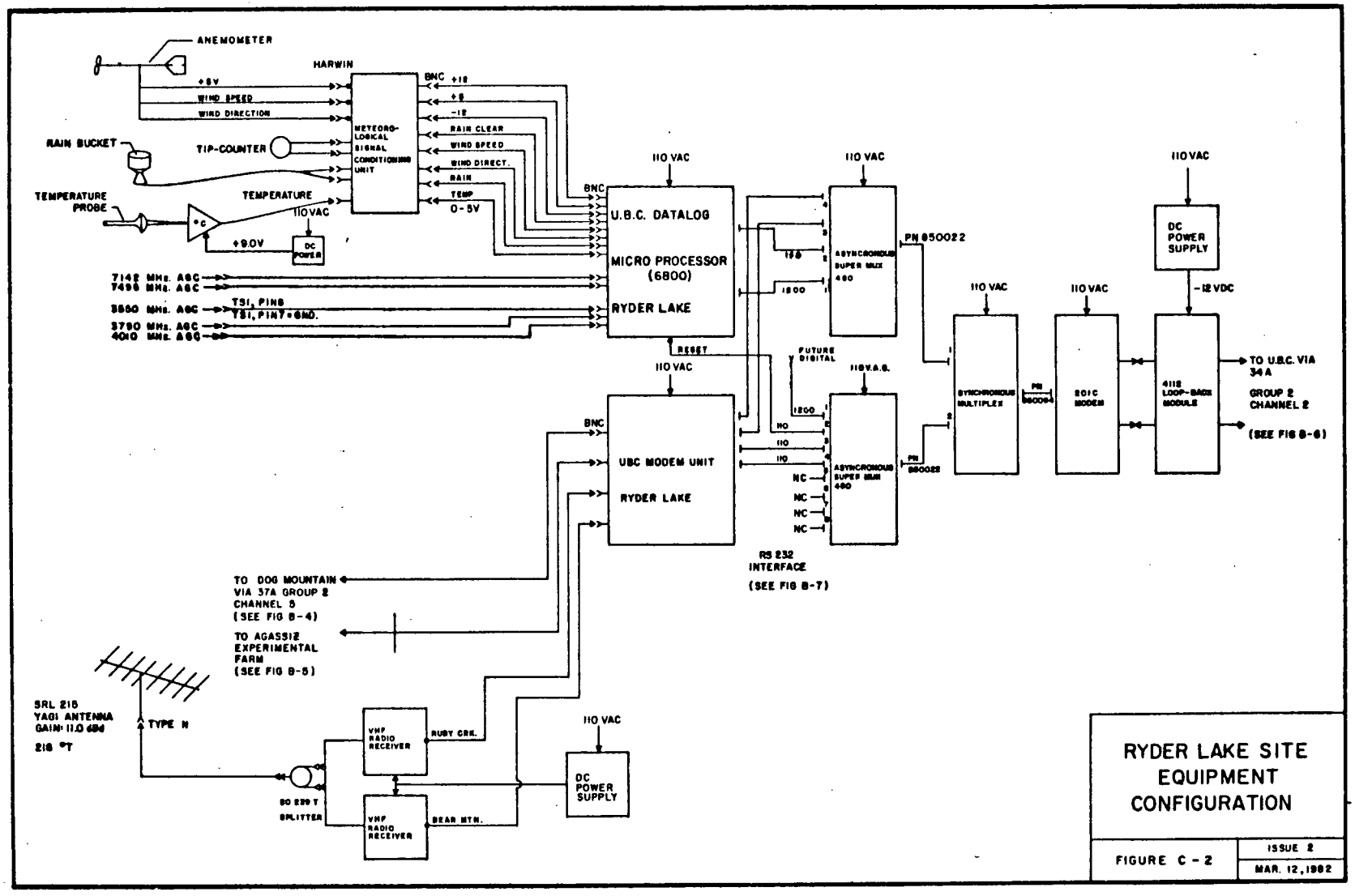

RYDER LAKE SITE EQUIPMENT CONFIGURATION

FIGURE C - 2

ISSUE 2

MAR. 12, 1982

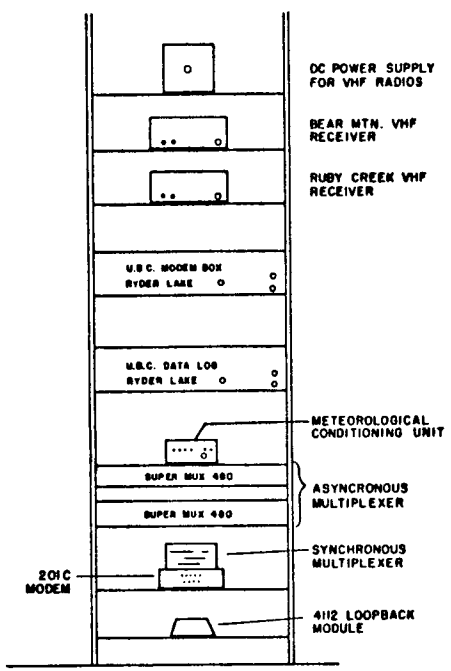

FRONT VIEW OF
THE UBC EQUIPMENT BAY
AT RYDER LAKE

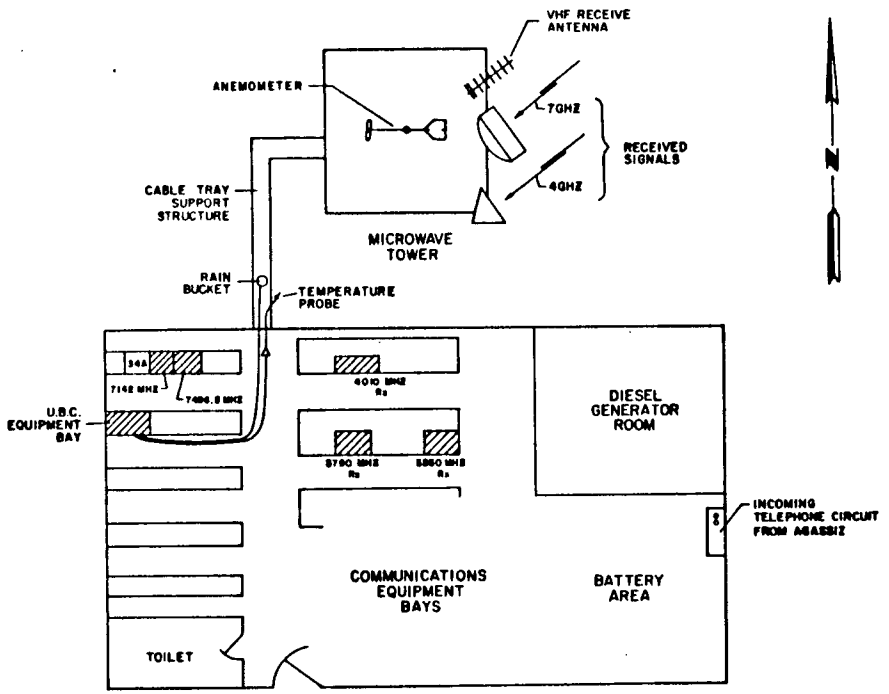

PLAN VIEW OF
THE RYDER LAKE SITE

RYDER LAKE
SITE LAYOUT

FIGURE C-3

ISSUE 2
MAR 12, 1982

C-2 Dog Mountain

The Dog Mountain site which is the transmitter site and the northern terminus of the microwave link under investigation, has an elevation of 1463m. A weather station located there senses meteorological information and sends it back to Vancouver via a spare data channel on the 51G alarm system to the Ryder Lake site. At Ryder Lake this information is statistically multiplexed for retransmission to UBC. Access to the site is by cable car as shown in the site photograph, Figure C-4a.

Figure C-4a Dog Mountain Site Photograph

The equipment configuration is given in Figure C-5 and a site layout (relevant to this work) is shown in Figure C-6.

This site experiences severe icing conditions which have caused the destruction of the experiment's initial anemometer, as shown in Figure C-4b. To prevent this destructive ice build-up in the future it is recommended that a radiant heater be installed directed at the anemometer*. The weather microprocessor could be used to control the heater during icing conditions by turning it on only during a -5°C to +3°C temperature range.

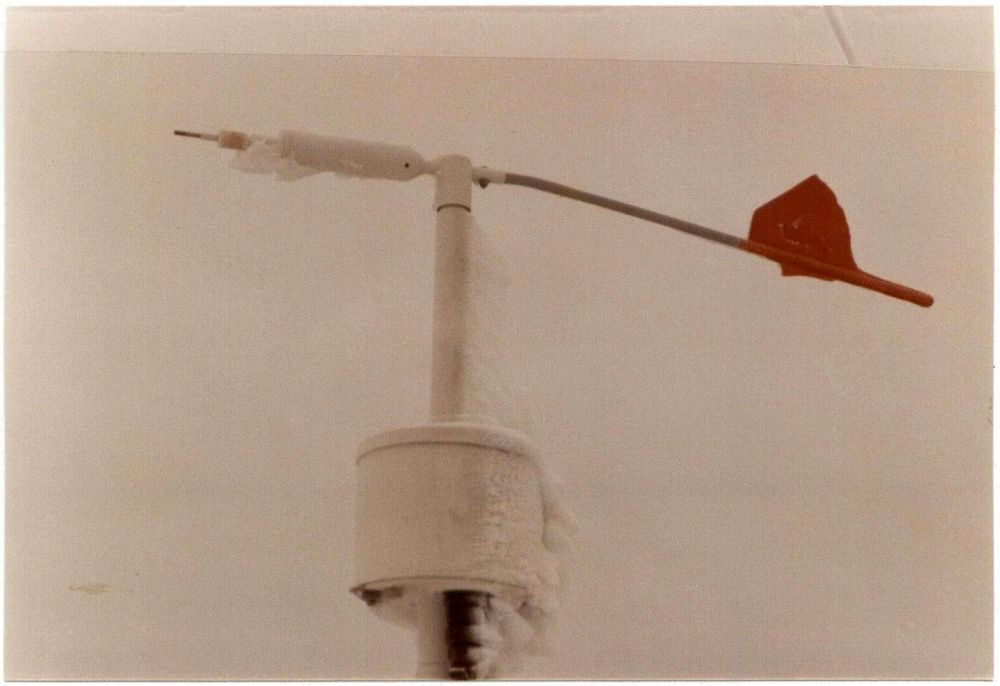

Figure C-4b A Photograph Showing Damage to the Anemometer Caused by Severe Icing Conditions at Dog Mountain

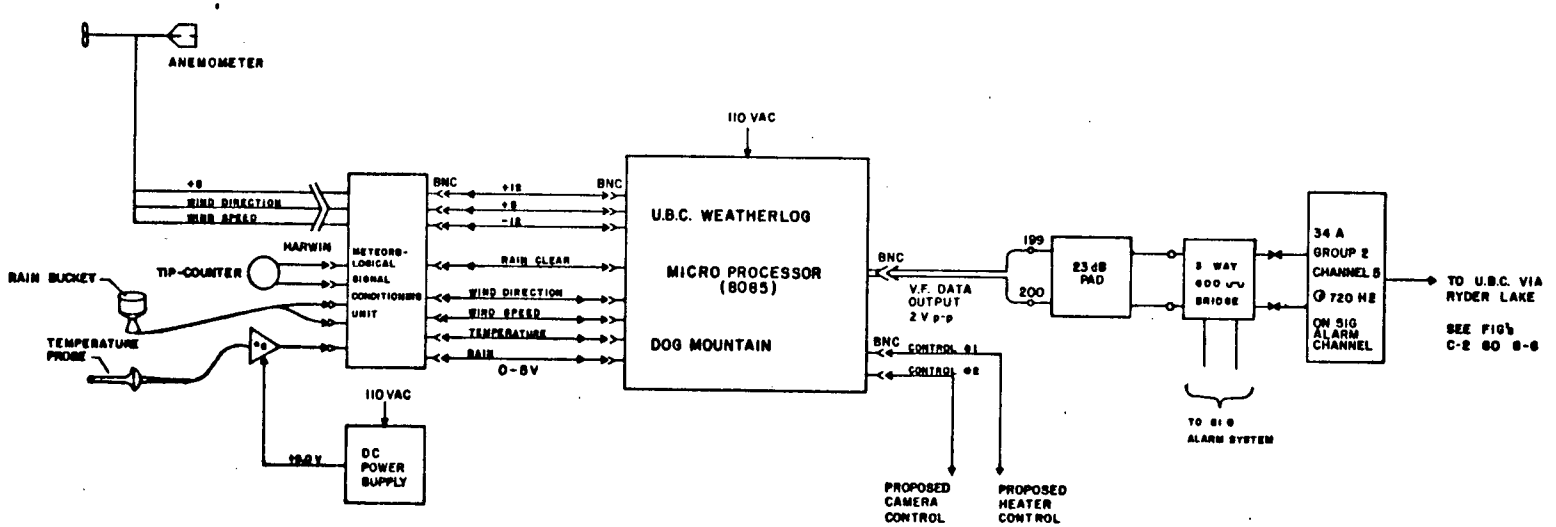

DOG MOUNTAIN SITE EQUIPMENT CONFIGURATION

FIGURE C - 5

ISSUE 1

FEB. 28, 1981

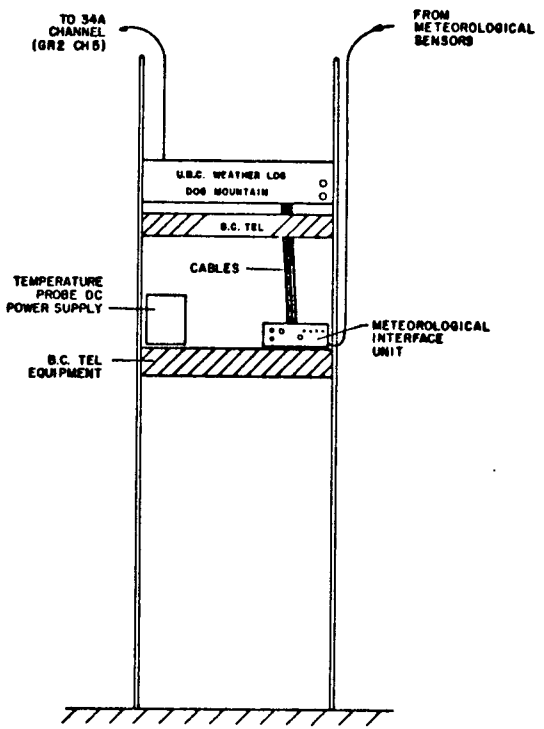

FRONT VIEW OF
THE UBC EQUIPMENT BAY
AT DOG MOUNTAIN

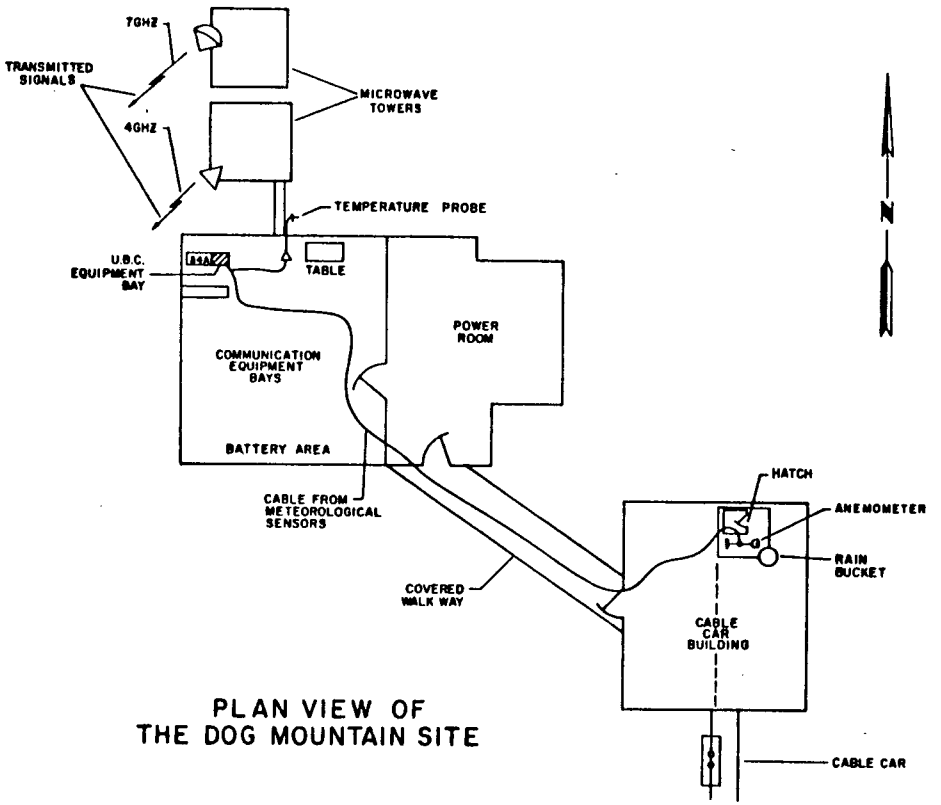

PLAN VIEW OF
THE DOG MOUNTAIN SITE

DOG MOUNTAIN
SITE LAYOUT

FIGURE C-6 | ISSUE 1 | FEB. 28, 1981

C-3 Agassiz Experimental Farm

This site has an elevation of 15m, is 17.8 kilometers from the Ryder Lake receive end and is 200 meters off beam-center. Its primary purpose is to collect meteorological data with particular emphasis on the measurement of rainfall. This site is co-located with the experimental farm's weather station which provides a source of valuable back-up data, as well as gives information on other variables such as pressure and humidity which are not monitored in this experiment. Being situated 610m below beam elevation, melted precipitation rates can be measured using a tipping bucket rain gauge even though the freezing level may be at or below path elevation. The data thus collected are sent to Ryder Lake via a telephone circuit and from there on to UBC, using the statistical multiplex. Refer to Figure C-7 for a site photograph, Figure C-8 for the equipment configuration and Figure C-9 for the site layout.

Figure C-7 Agassiz Experimental Farm Site Photograph

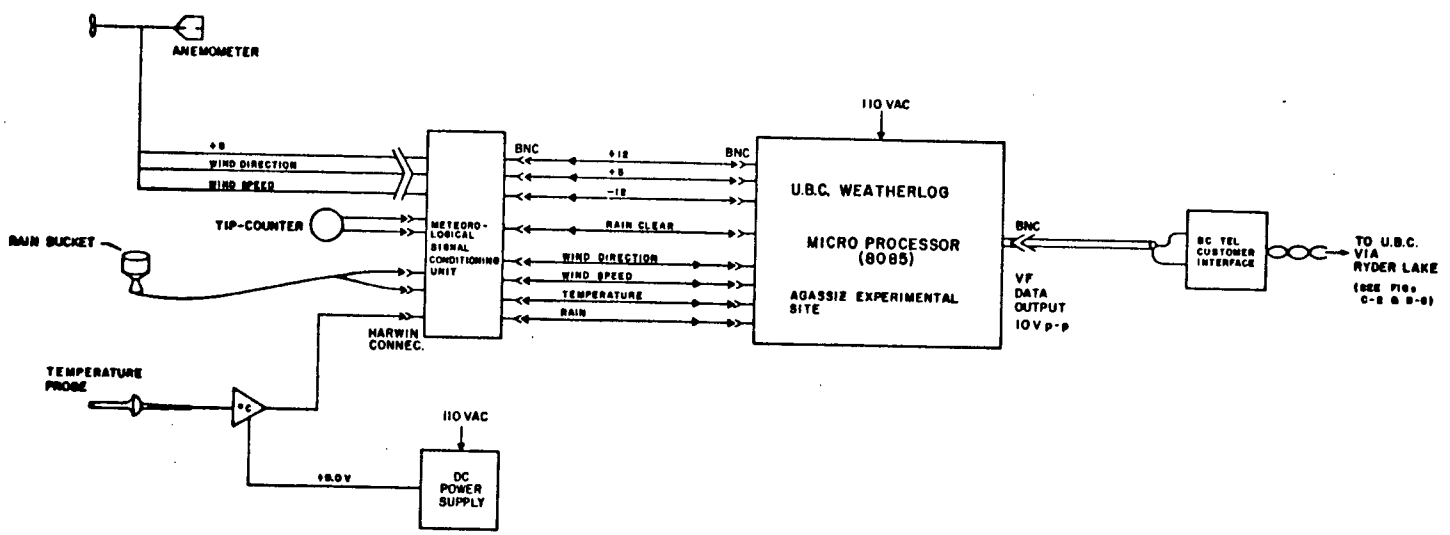

AGASSIZ EXPERIMENTAL FARM SITE EQUIPMENT CONFIGURATION

FIGURE C-8	ISSUE 1
	FEB. 28, 1981

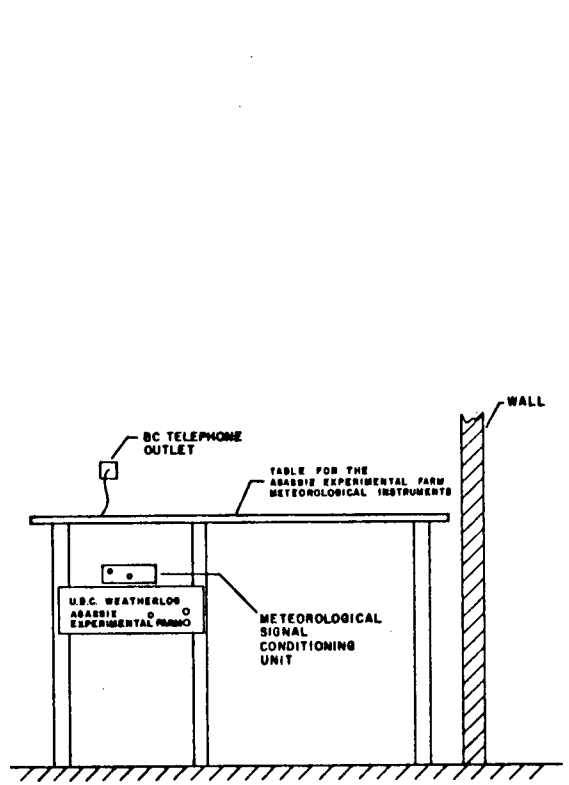

FRONT VIEW OF
THE UBC EQUIPMENT
AT THE AGASSIZ EXPERIMENTAL FARM

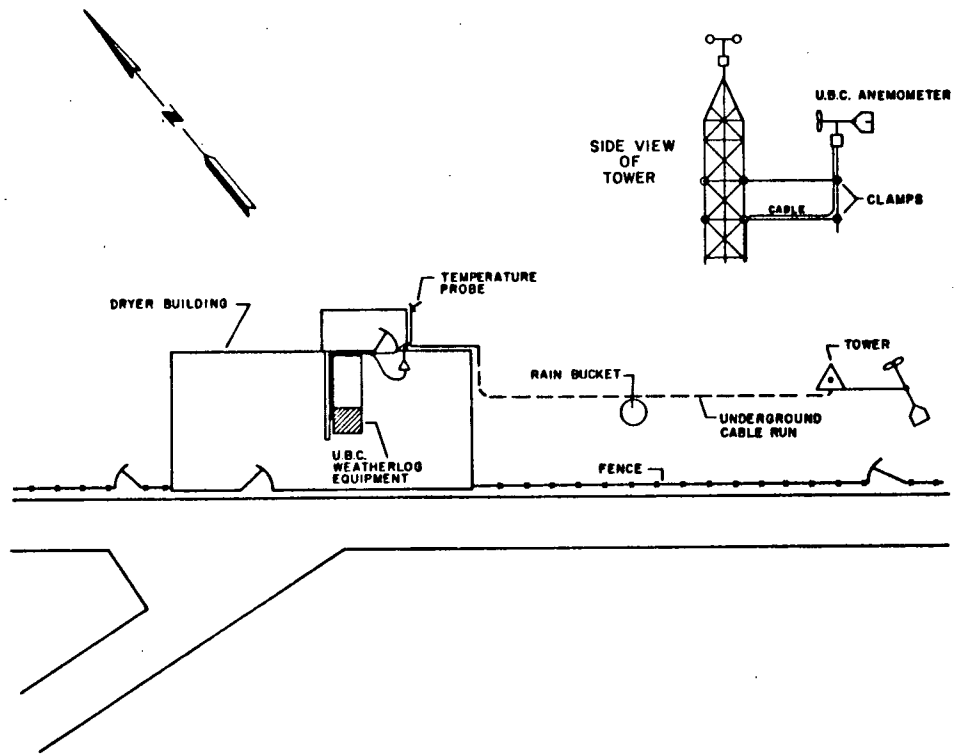

PLAN VIEW OF
THE AGASSIZ EXPERIMENTAL
FARM SITE

AGASSIZ
EXPERIMENTAL FARM
SITE LAYOUT

FIGURE C - 9

ISSUE 1
FEB. 28, 1981

C-4 Ruby Creek

The Ruby Creek Site has an elevation of 31m, is 300m off beam-center and 33.9 kilometers from the Ryder Lake receive end. The site provides for power, a tower and a shelter. It also lies 1158m below beam elevation, making it well suited for use as an intermediate weather station for monitoring melted precipitation rates. The sampled data are sent to Ryder Lake via a VHF radio link and from there it is assigned a data multiplex channel to complete the routing to UBC.

For detailed information, refer to Figure C-10 for a site photograph, Figure C-11 for the site's equipment configuration and Figure C-12 for the site layout.

Figure C-10 Ruby Creek Site Photograph

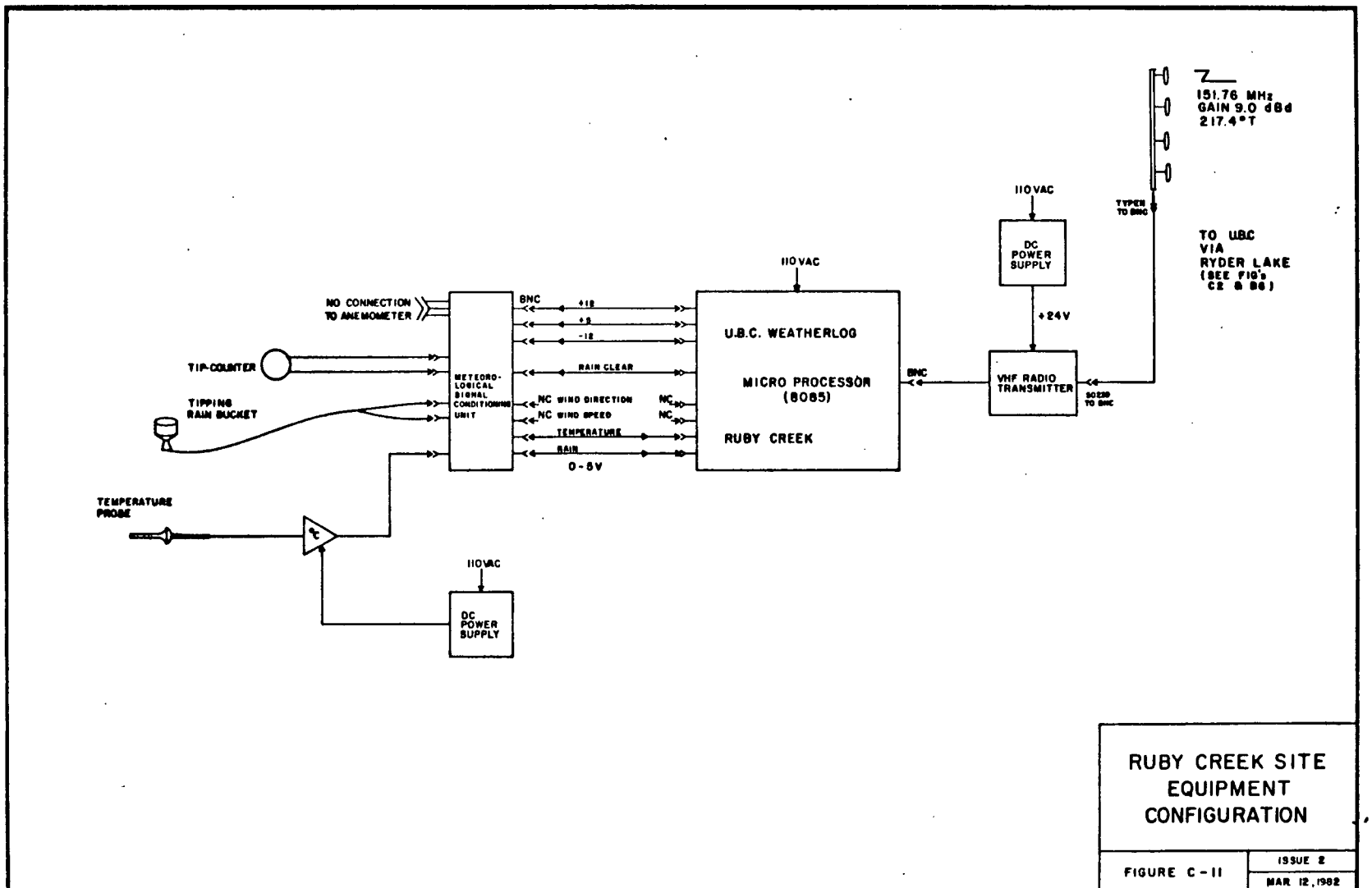

RUBY CREEK SITE EQUIPMENT CONFIGURATION

FIGURE C-11 | ISSUE 2 | MAR 12, 1982

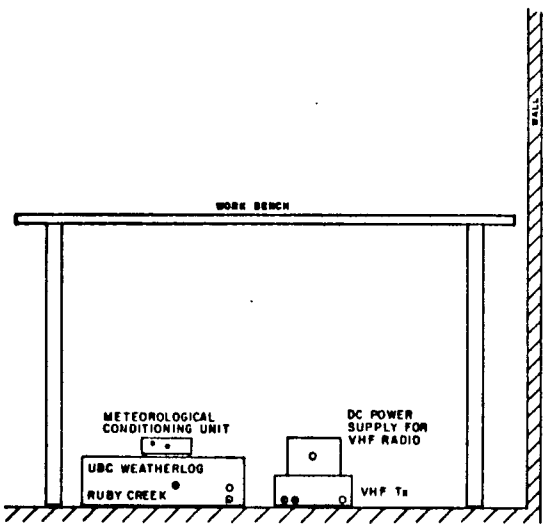

FRONT VIEW OF
THE UBC EQUIPMENT AT
THE RUBY CREEK INSTALLATION

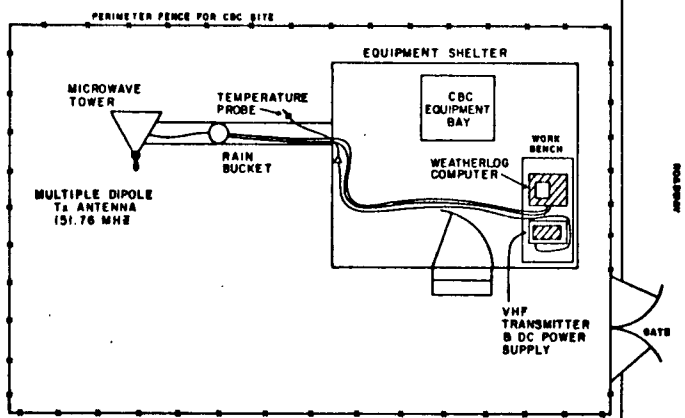

PLAN VIEW OF
THE RUBY CREEK SITE

RUBY CREEK
SITE
LAYOUT

FIGURE C-12 | ISSUE 2 | MAR. 12, 1982

C-5 Bear Mountain

The Bear Mountain site is located at beam elevation on a mountaintop near mid-path. It has a site elevation of 945m and is situated 26.3km from Ryder Lake and 3km to the northwest side of the microwave beam.

The Bear Mountain site is important for investigating the bright band region since it allows an intermediate temperature point to be monitored thus enabling a more accurate temperature gradient profile to be established allowing a more accurate determination of the bright-band thickness. In the final site selection, special consideration has been given to finding a sheltered

Figure C-13

Bear Mountain Site Photograph

location that would minimize misleading readings due to local convection effects. A photograph of the site is illustrated in Figure C-13.

The weather data will be monitored by a battery-powered data acquisition system and transmitted to UBC via a 0.3 Watt VHF radio link to Ryder Lake. The equipment configuration for this system is shown in Figure C-14 and the site layout in Figure C-15.

C-6 University of British Columbia Recording Terminus

The University of British Columbia (UBC) site is located in Room 448 of the Electrical Engineering building and is the terminus for all the data collected. The data which arrive via a telephone circuit, are demultiplexed, coded with the sampling time and condensed for storage on magnetic cassette tape. Facilities are provided for the real time viewing of the incoming data using the video terminal and the chart recorder together with the digital to analog convertor.

A photograph of the UBC terminus is shown in Figure C-16. The equipment configuration is shown in Figure C-17 and the site layout in Figure C-18.

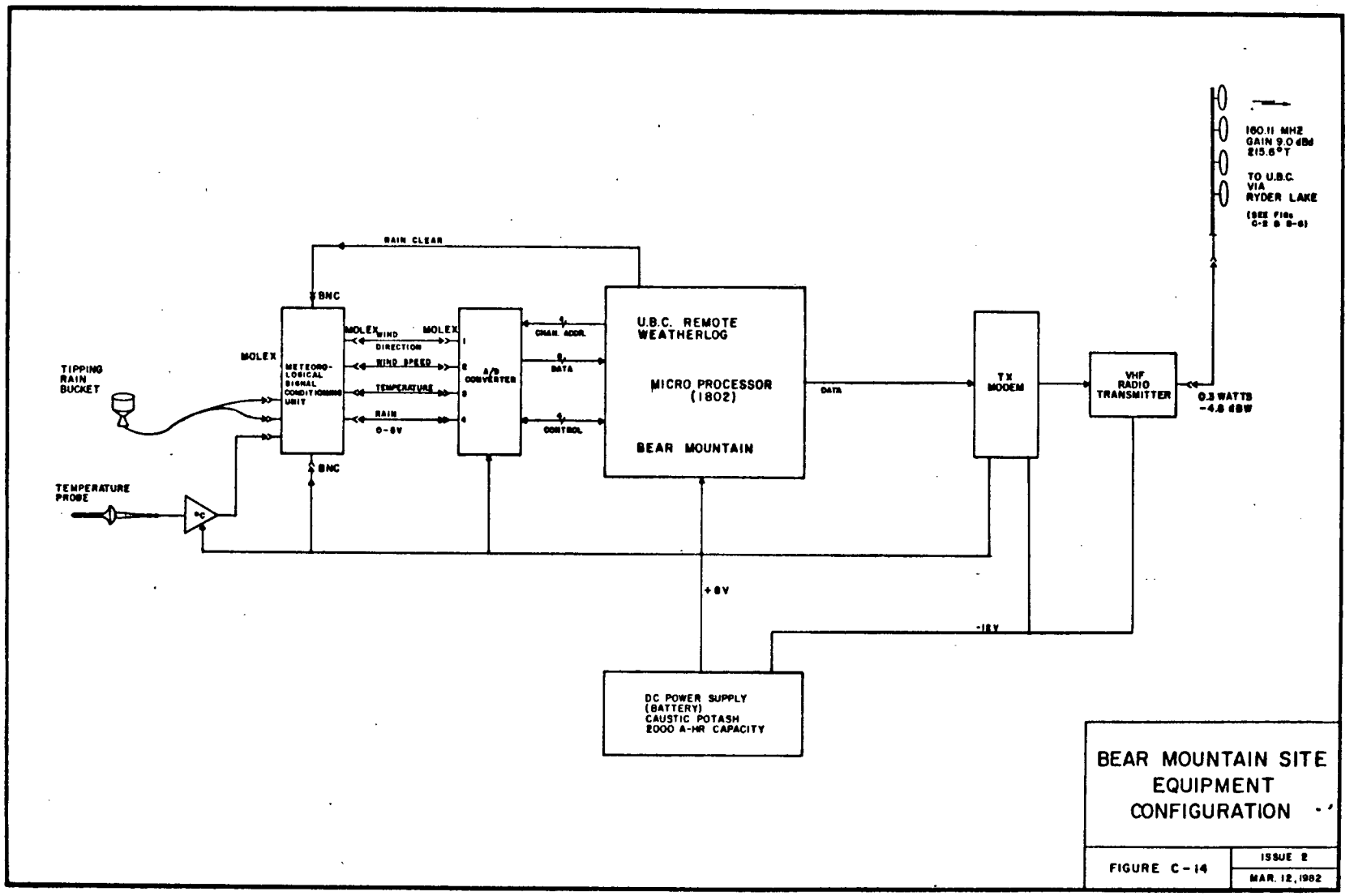

BEAR MOUNTAIN SITE EQUIPMENT CONFIGURATION

FIGURE C-14 | ISSUE 2 | MAR. 12, 1982

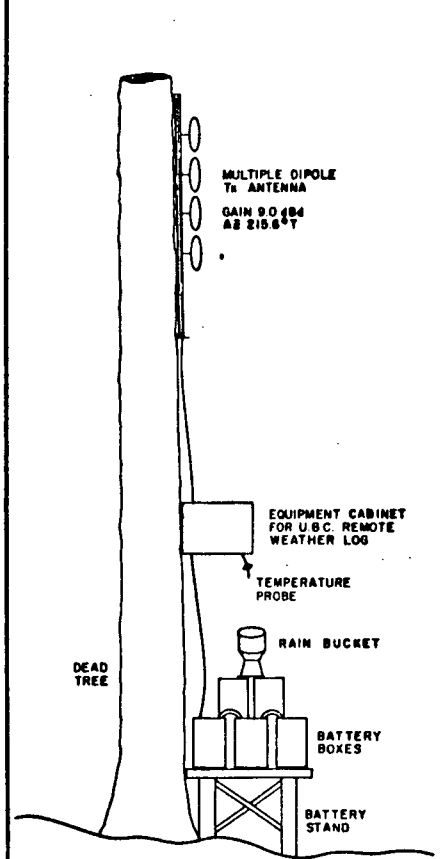

SIDE VIEW OF
EQUIPMENT TREE

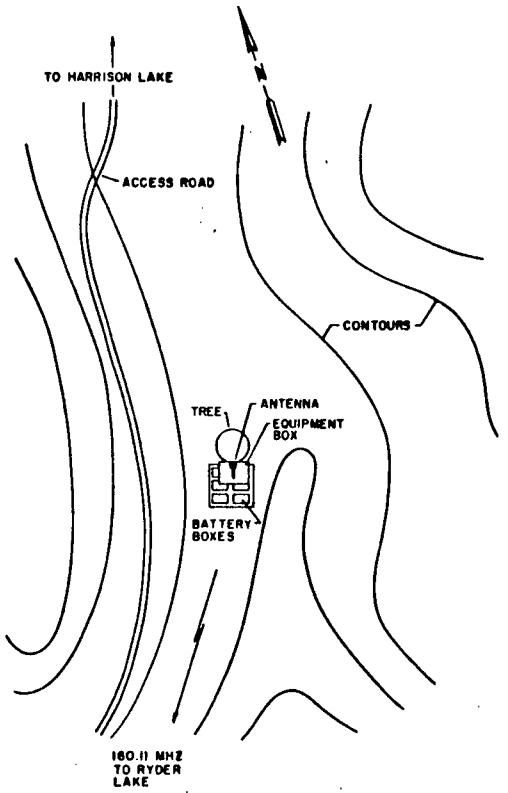

PLAN VIEW OF
THE BEAR MOUNTAIN SITE

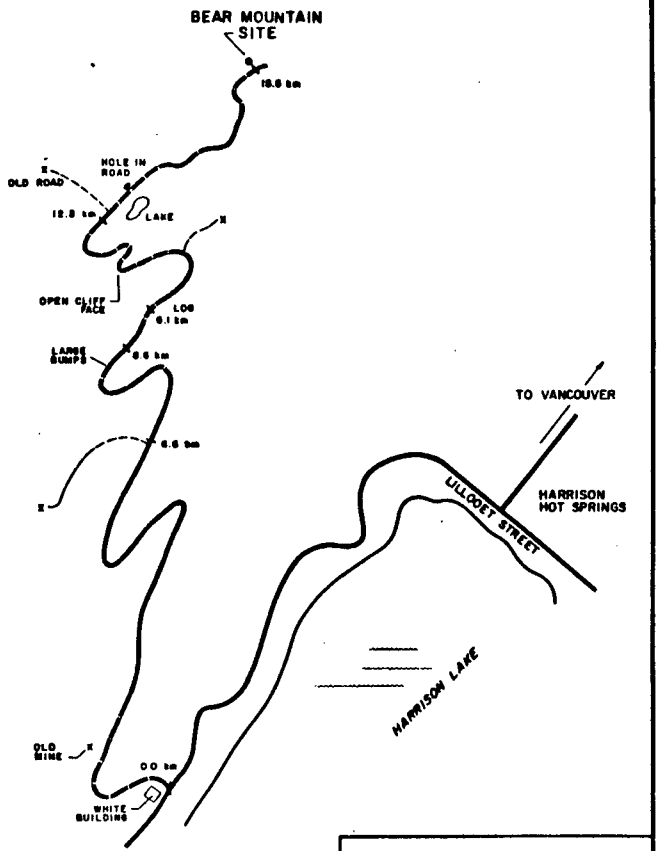

ROAD MAP TO
BEAR MOUNTAIN SITE

BEAR MOUNTAIN
SITE LAYOUT

FIGURE C-15

ISSUE 2
MAR. 12, 1982

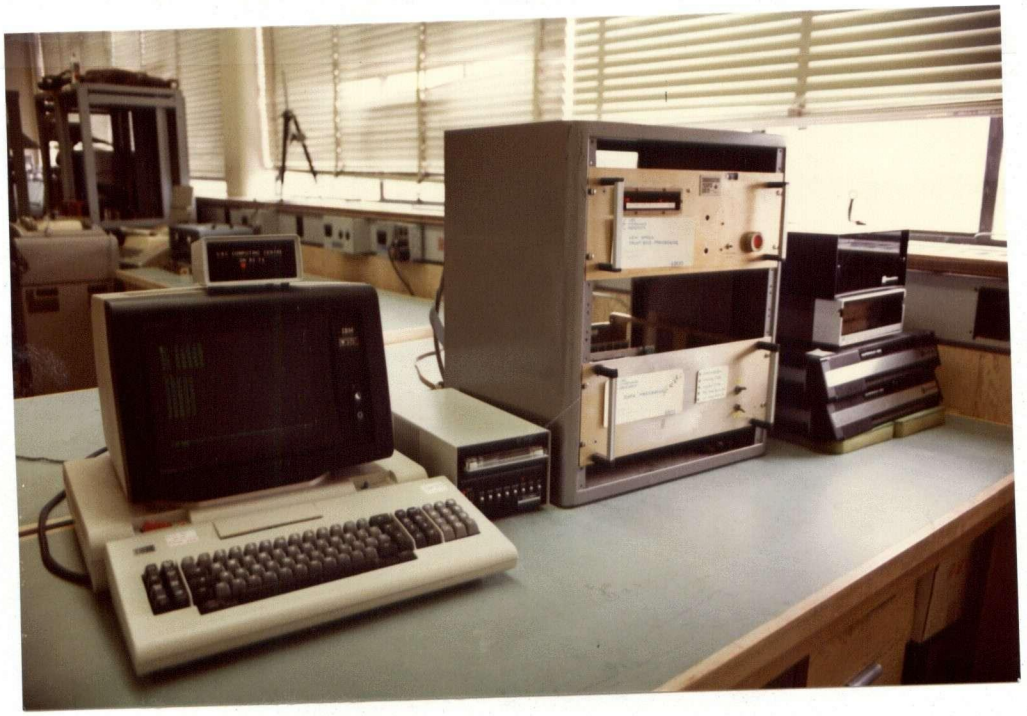

Figure C-16 University of British Columbia Site Photograph

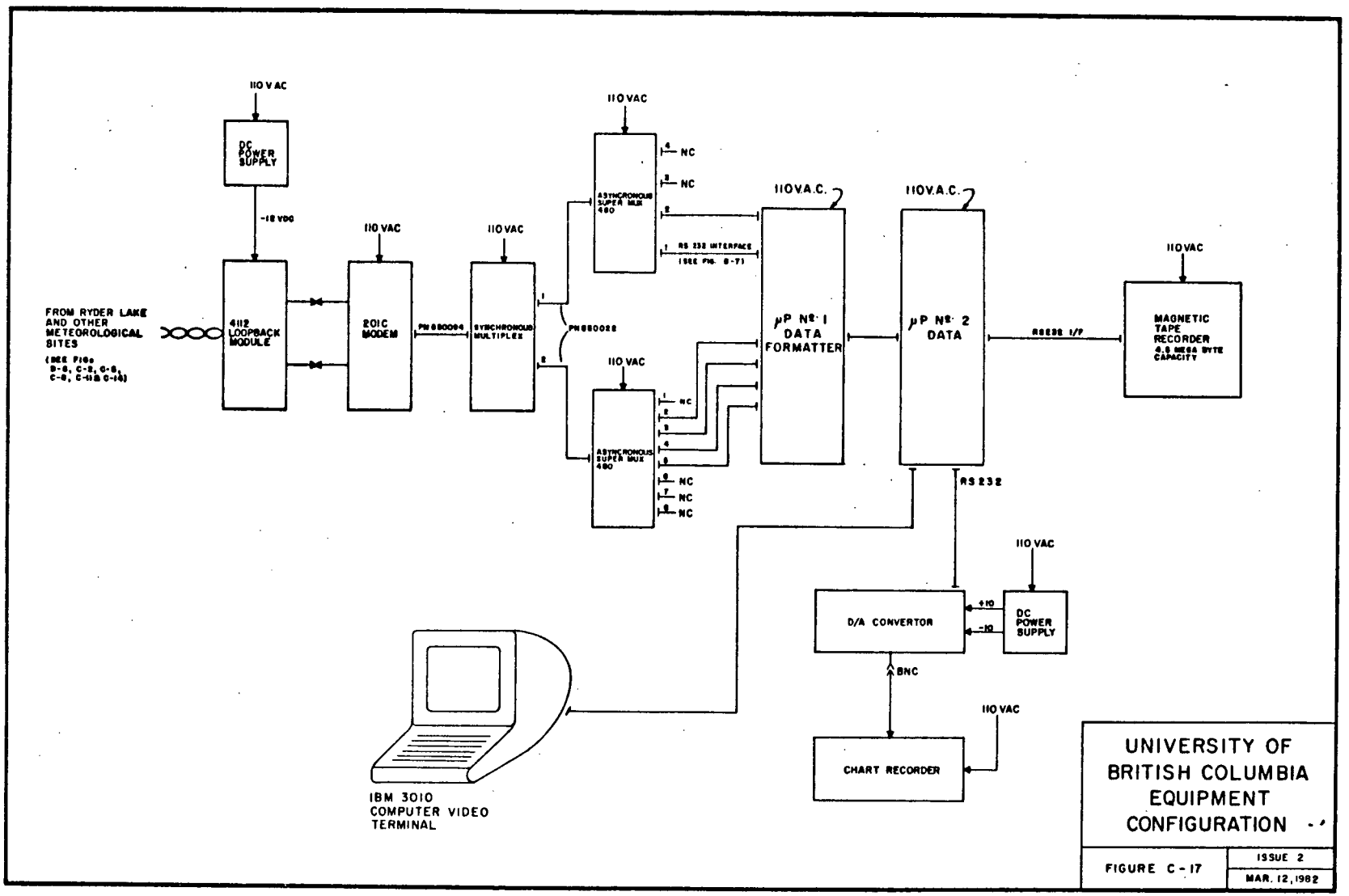
110 VAC
DC POWER SUPPLY
-18 VDC
110 VAC
110 VAC
110 VAC
ASYNCHRONOUS SUPER MUX 480
NC
NC
RS 232 INTERFACE
(SEE PAG. B-7)
110 V.A.C.
110 V.A.C.
110 VAC
FROM RYDER LAKE AND OTHER METEOROLOGICAL SITES
(SEE Figs. B-6, C-2, C-5, C-6, C-8, C-11 & C-14)
4112 LOOPBACK MODULE
201C MODEM
PN 880004
SYNCHRONOUS MULTIPLEX
PN 880002
μP Nº 1 DATA FORMATTER
μP Nº 2 DATA
RS232 I/P
MAGNETIC TAPE RECORDER
4.8 MEGA BYTE CAPACITY
110 VAC
ASYNCHRONOUS SUPER MUX 480
NC
NC
NC
RS 232
110 VAC
D/A CONVERTOR
+10
-10
DC POWER SUPPLY
BNC
110 VAC
CHART RECORDER
IBM 3010 COMPUTER VIDEO TERMINAL
UNIVERSITY OF BRITISH COLUMBIA EQUIPMENT CONFIGURATION
FIGURE C-17
ISSUE 2
MAR. 12, 1982

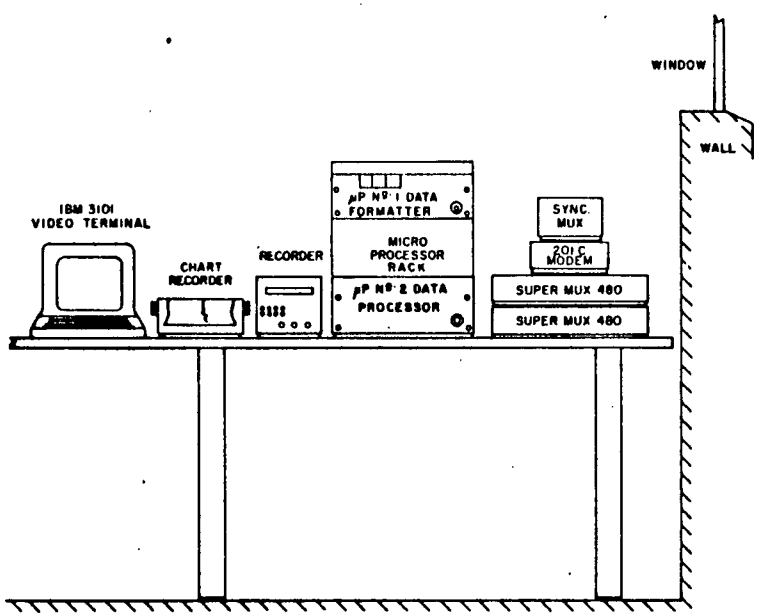

FRONT VIEW OF
THE UBC EQUIPMENT TABLE

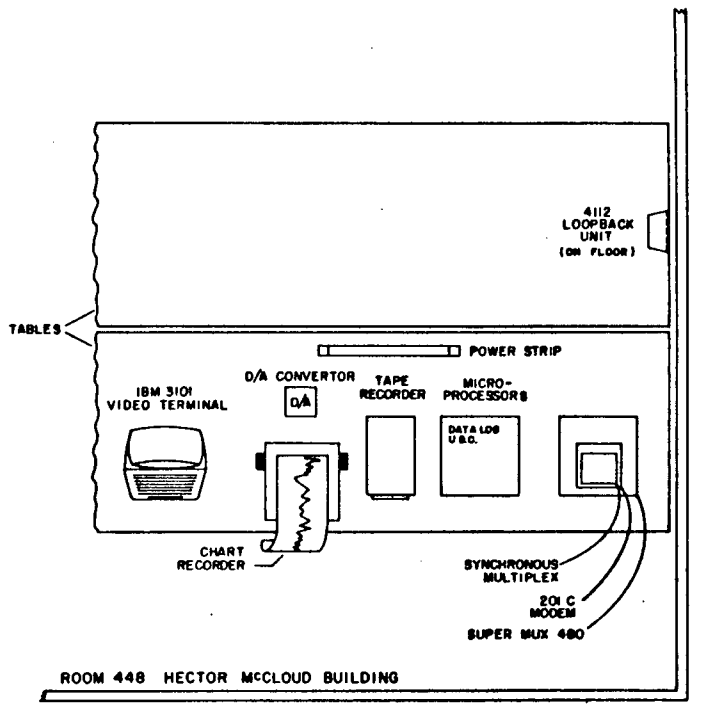

PLAN VIEW OF
THE UBC SITE

UNIVERSITY OF
BRITISH COLUMBIA
SITE LAYOUT

FIGURE C - 18	ISSUE 2
	MAR. 12, 1982

APPENDIX D

METEOROLOGICAL TRANSDUCERS

D-1 The Anemometer

The anemometers used are of the propeller-vane variety capable of measuring both wind speed and wind direction. A photograph of an anemometer is shown in Figure D-1.

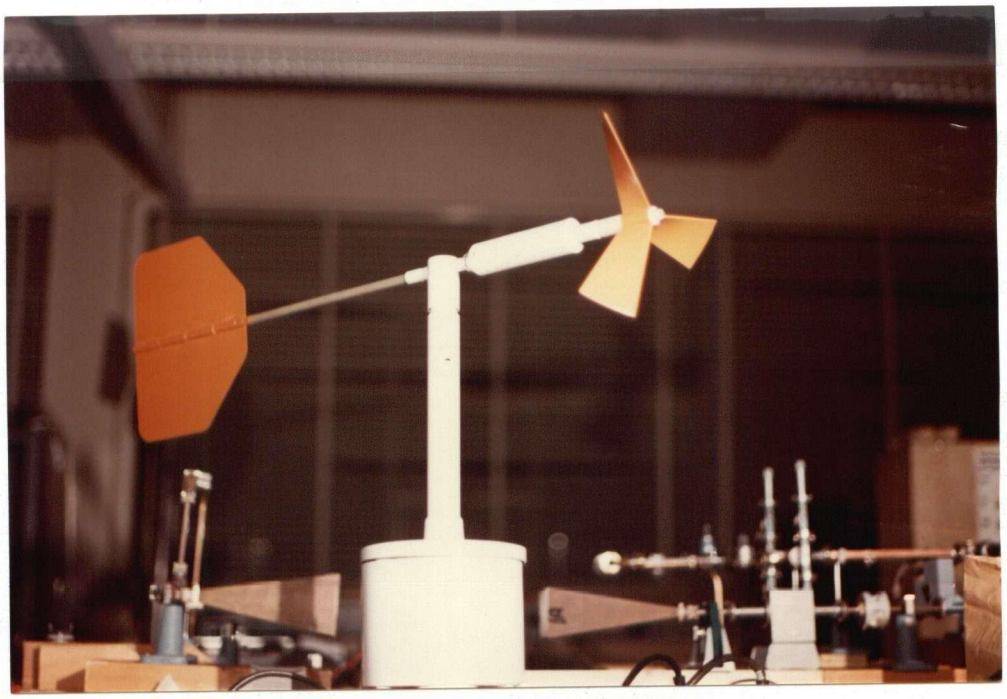

Figure D-1 A Photograph of the Anemometer

To be able to monitor wind speed and wind direction using the anemometer, three separate input and output signals need to be interfaced to the unit, as shown in the circuit and wiring diagram of Figure D-2. These include the potentiometer input excitation voltage for azimuth, its output voltage and the wind speed output voltage derived from the propeller-driven DC generator.

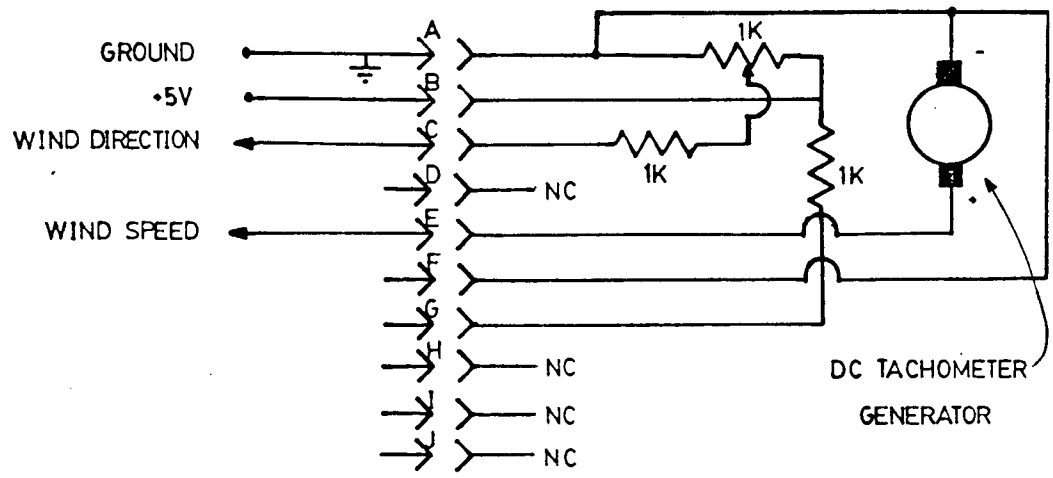

Figure D-2 Anemometer Circuit & Wiring Diagram

These units have proven to work reliably at all sites except for Dog Mountain where severe icing conditions damaged the initial anemometer installation. A radiant heater has been recommended to resolve this problem, as indicated in Appendix C-2.

D-2 The Tipping-Bucket Rain Gauge

The rain gauges used are of the tipping-bucket variety and are capable of measuring point rain rates up to 400 mm/hr. Accurate measurement above this rate is not important due to the low probability of such events in this area.

The rain gauges have a collecting area of 383.6 cm^2 and a nominal tip size of 12.2 grams or 12.2 cubic centimeters of water so that a tip occurs

after each .318 mm of rain. This calibration is done by first pouring a known quantity of water through the bucket and counting the number of tips to give the volume of water per tip. Then, by dividing the volume of water per tip by the collecting area of the bucket, the rainfall per tip, is calculated.

Electrical sensing is accomplished by generating a pulse as the bucket tips by passing a permanent magnet, attached to the bucket's tipping arm, in near proximity to a chassis-mounted reed switch. Rain bucket maintenance has been minimal during the last year of operation, largely due to their plastic corrosion proof construction.

Figure D-3 shows a photograph of the rain bucket and its tipping assembly.

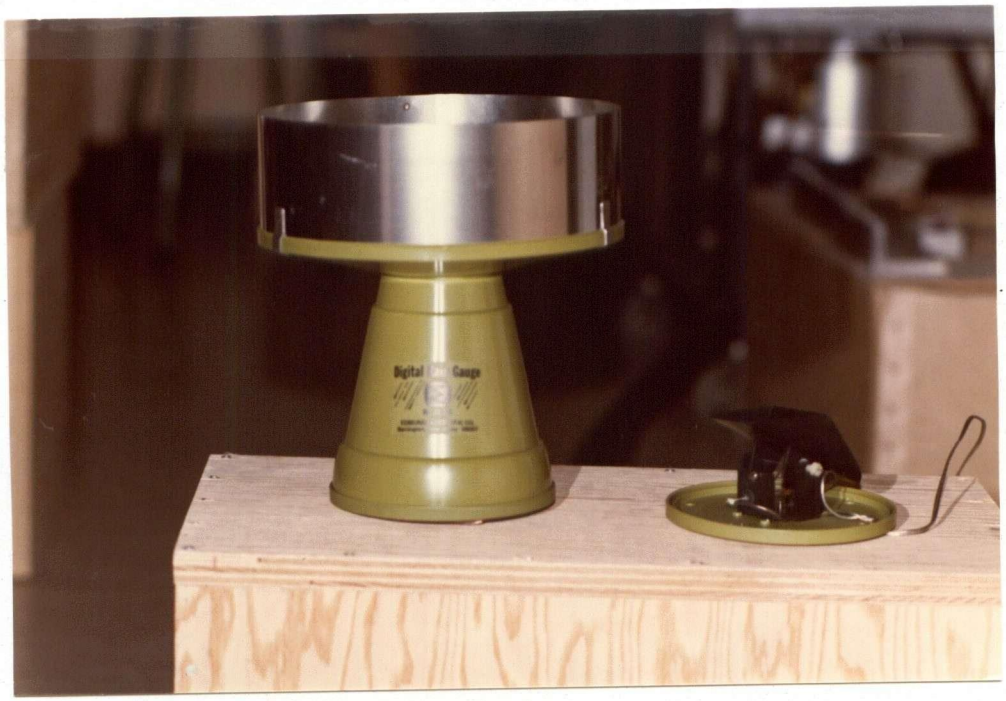

Figure D-3 A Typical Rain Bucket and Tipping Assembly.

D-3 The Temperature Transducer

The operation of the temperature transducer is based upon the linear temperature coefficient of a semi-conductor junction when forward biased with a constant current. The forward voltage which results across the junction varies linearly with temperature and is amplified to produce a DC output voltage of 10 millivolts per degree with separate gain circuits to provide indications in degrees Centigrade or degrees Fahrenheit.

A photograph of the temperature transducer appears in Figure D-4. The temperature sensor is located on the tip of the probe. The tri-position switch allows for selection between an off position, or either the Fahrenheit or centigrade gain circuits. In this experiment the Fahrenheit gain circuit is selected in order to maintain unipolar operation into the conditioning circuits over the desired temperature range of 0°F-64°F, (Appendix E).

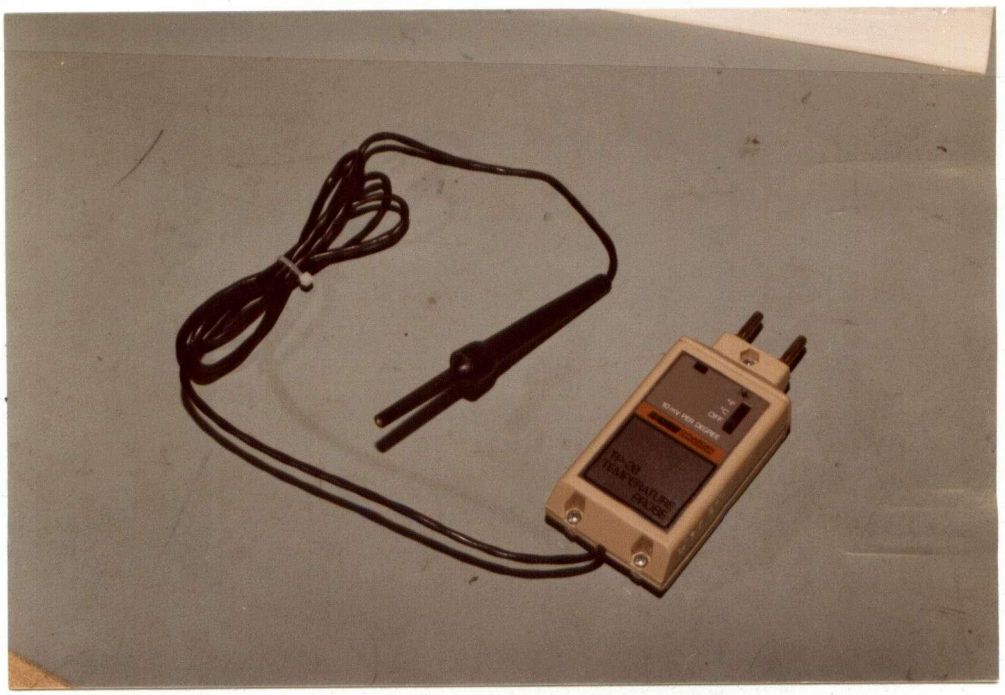

Figure D-4 Photograph of the Temperature Probe

Calibration of the temperature transducer can be accomplished by the following one-point calibration procedure. First the probe is immersed in a cup of semi-melted snow (temperature 32.2°F or 0°C). Then the tri-position switch is used to select both the Fahrenheit and Centigrade gain scales and the output voltages are noted. These voltages represent the freezing point for each scale and the difference between the two readings represents 32.2°. Thus if the Fahrenheit scale is used for monitoring, the lower of the two voltage readings is 0°F and, similarly, if the centigrade scale is used the higher of the two voltage readings is +32.2°C. (This calibration assumes that both the °C and °F gain circuits have been accurately calibrated according to the instruction manual.) Care must be taken to ensure that the temperature probe is installed with an isolated DC power supply since the probe loses calibration when a non-isolated source is used due to a ground loop condition.

Response Time

The response time of the temperature transducer was measured to be 60 degrees Centrigrade per second. This was done by quickly immersing the temperature probe into a cup of cold water after being in a room temperature enviroment and observing the response on a storage oscilloscope.

APPENDIX E

SIGNAL CONDITIONING UNITS

E-1 Meteorological Signal Conditioning Units

The meteorological signal conditioning units provide the interface between the various weather transducer outputs and the + 0-5 volt range analog to digital convertor inputs. The circuit, as presented in Figure E-2, is op-amp derived. Adjustable potentiometers at the front edge of the printed circuit board (see photograph in Figure E-1) provide gain control adjustments for each of the conditioned signals. The input/output connections for the unit are shown in Figure E-3.

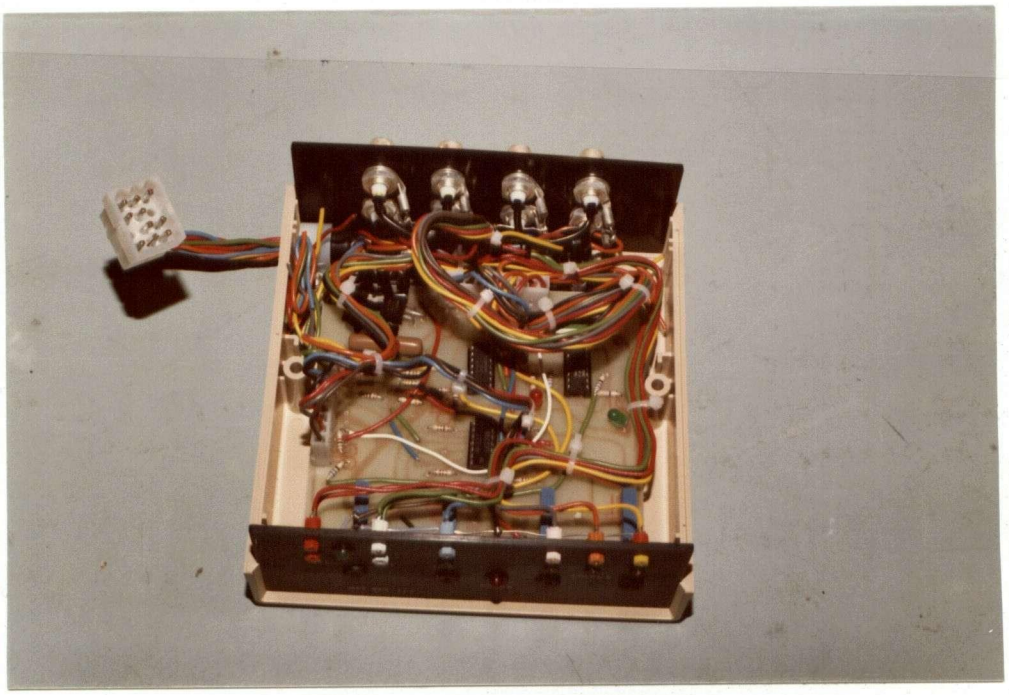

Figure E-1 Top View Photograph of the Meteorological Signal Conditioning Unit.

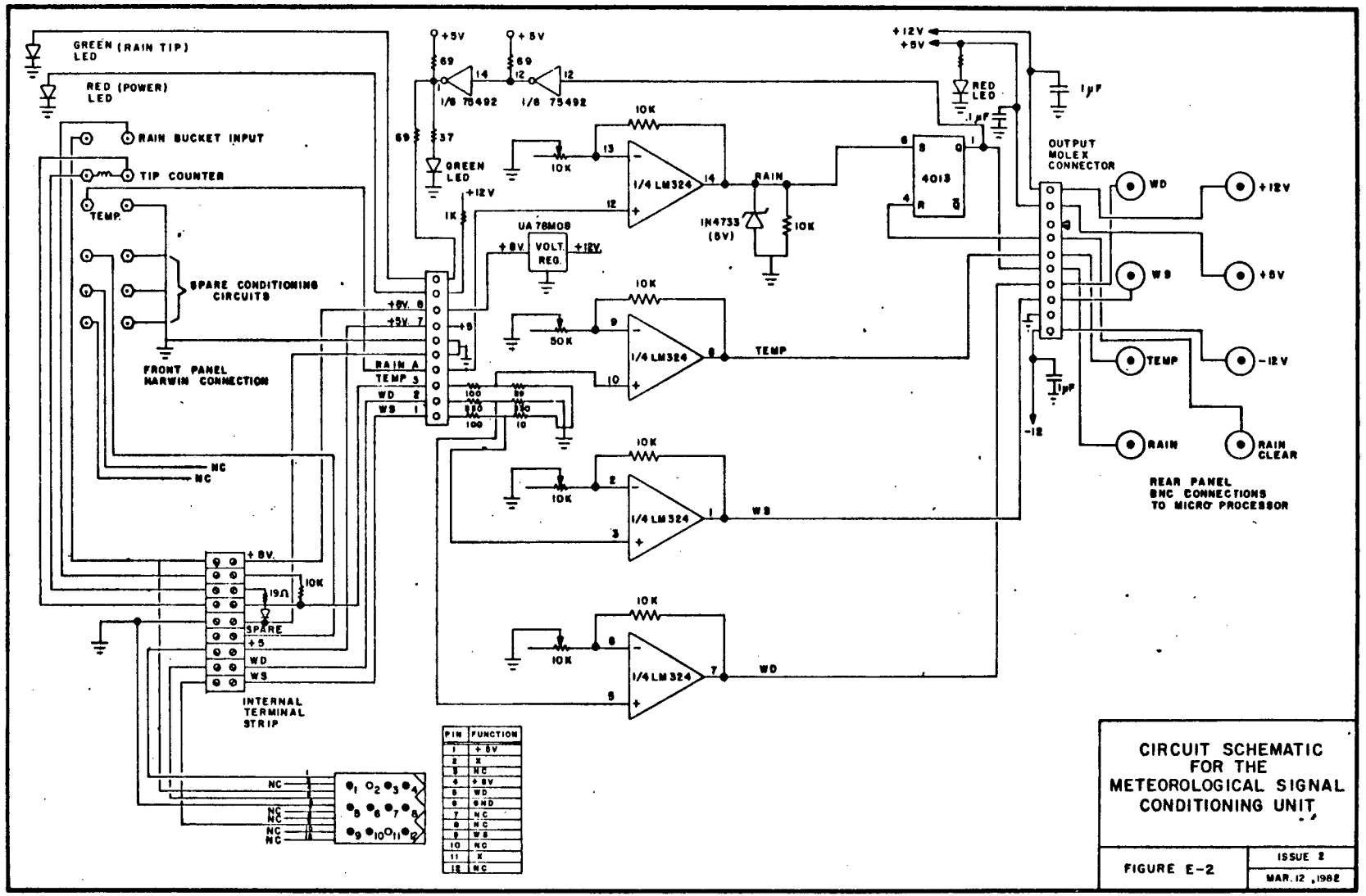

CIRCUIT SCHEMATIC FOR THE METEOROLOGICAL SIGNAL CONDITIONING UNIT

FIGURE E-2

ISSUE 2

MAR. 12, 1982

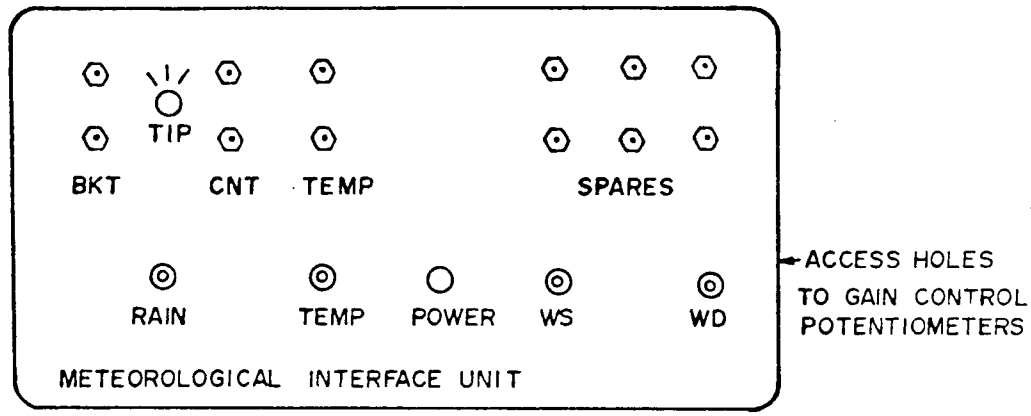

a) FRONT VIEW

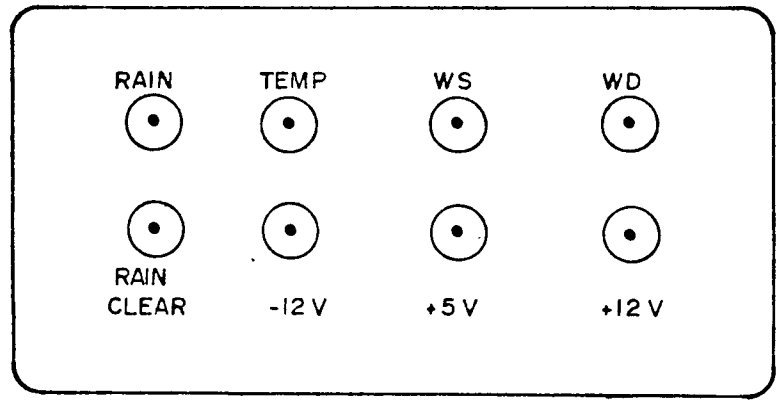

b) REAR VIEW

Figure E-3 Front and Rear Views of the Meteorological Signal Conditioning Unit.

The set-up procedure is best completed in the laboratory before installation and is done through the adjustment of the gain control potentiometers. The procedure to calibrate each meteorological variables is as follows:

i) Rain: Connect the counter and rain bucket leads to the front panel inputs using 'harwin' connectors and observe the output from the rear panel using an oscilloscope. Connect a pulse generator into the rain clear port on the back panel and set it for a several second interval between pulses.

Now adjust the gain of the rain circuit until a bucket tip pulse latches high at the output, indicated by the green LED turning on. Next, observe to see if the pulse from the generator clears the latch. If not, ease off the gain until the latch is cleared. When both a tip of the bucket sets the latch and a pulse from the generator resets it, the rain circuit is ready for operation.

ii) Temperature: Connect the output of the temperature probe into the front panel input of the meteorological conditioning unit using 'harwin' connectors. Ensure that the temperature probe is powered from an isolated -9.0 volt DC power source so that the accuracy of the calibration is maintained. Now place the probe into an ice water mixture and adjust the gain until 32.2^{o}F. on the Fahrenheit scale gives an output of 2.5 volts. The circuit is now ready for operation.

This procedure provides a temperature dynamic range of 0°F (0 volts) to 64.4°F (5.0 volts).

iii) Wind Direction: Connect both the +5 volts azimuth exciter voltage and the wind direction input voltage to the input molex connector (See Figure E-2 for details).

iv) Wind Speed: Connect the windspeed output of the anemometer to the input of the molex connector (See Figure E-2 for details). Now adjust the potentiometer for a gain of 1/2. This is easily accomplished by using a dual trace oscilloscope where the first channel at 1 volt per division monitors the input voltage and the second channel at 0.5 volt per division monitors the output voltage. At ground position align both traces. Now apply a fan to the anemometer propeller and adjust the gain so that the two traces remain superimposed. This procedure allows for wind speeds in excess of 100 kilometers per hour to be monitored and allows the factory calibration graph for output voltage versus wind speed to be read directly by simply dividing the voltage scale in half.

The Bear Mountain Conditioning Card

The circuit schematic for the Bear Mountain signal conditioning card is presented in Figure E-4. As shown, the circuit is basically two parts, the first being a single op-amp differential amplifier to condition the temperature voltage and the second is a voltage follower, S-R latch to condition the bucket tip voltages. The total current consumption is less than 5 ma for this configuration making it well suited for this application.

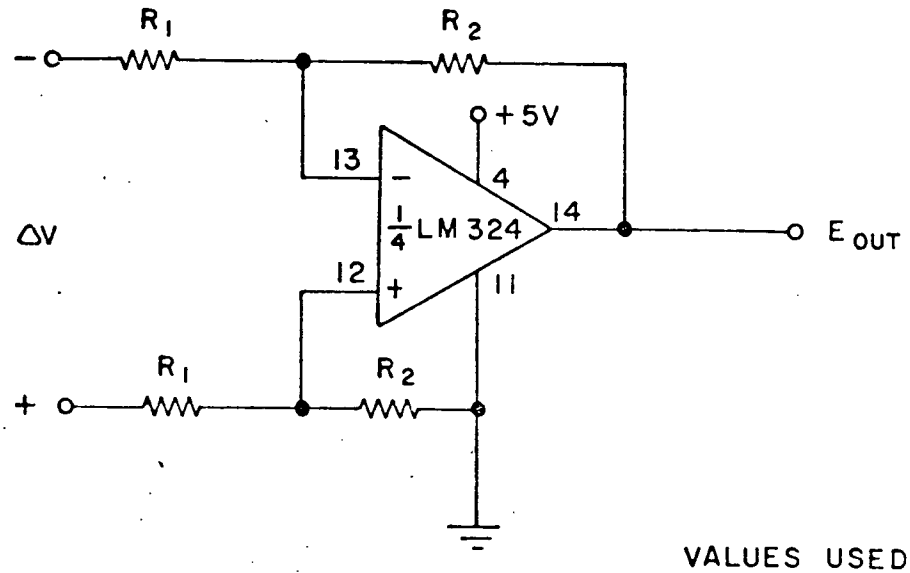

$$\text{GAIN} = \frac{E_{OUT}}{V} = \frac{R_2}{R_1}$$

a) TEMPERATURE CONDITIONING CIRCUIT

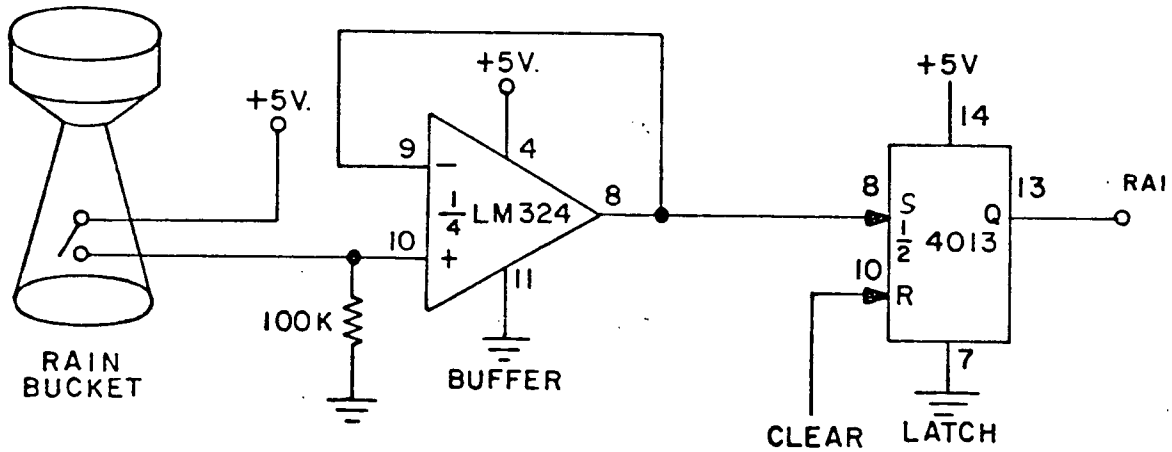

b) RAIN CONDITIONING CIRCUIT

Figure E-4 Circuit Schematic for the Bear Mountain Signal Conditioning Card

E-2 Receiver Signal Conditioning

The receiver signal conditioning unit provides an optimum input range of + 0-5 volt signal to the analog to digital convertor from the 4 and 7 GHz receiver AGC outputs. The circuit schematic for one of the differential amplifier gain blocks used on the receiver conditioning card is shown in Figure E-5. A differential gain block was used for each of the five AGC voltages monitored and all five gain blocks required were incorporated on one card which was mounted on the 6800 mother board. The same card was also used at Ryder Lake to condition the meteorological signals. Table E-1 provides the resistor values used to achieve the optimum gains for each receiver and meteorological signal monitored.

Table E-1 The Resistor Values Used in the Differential Gain Block for Optimum Gain

SIGNAL	R_1,R_4	R_2,R_5	R_6,R_7	R_3	$GAIN_{OPT}$
3550 GHz	20K	50K	25K	100Kpot	- .93
3790 GHz	20K	50K	25K	100Kpot	- 1.26
4010	20K	50K	25K	100Kpot	- 1.40
7142.0	10K	10K	50K	50Kpot	-35.0
7496.2	10K	10K	50K	50Kpot	-50.0
WS	10K	50K	10K	100Kpot	+ 0.5
WD	10K	50K	22K	100Kpot	+ 0.8
TEMP	50K	50K	50K	100Kpot	+ 5.0
RAIN	10K	50K	22K	100Kpot	+ 1.0

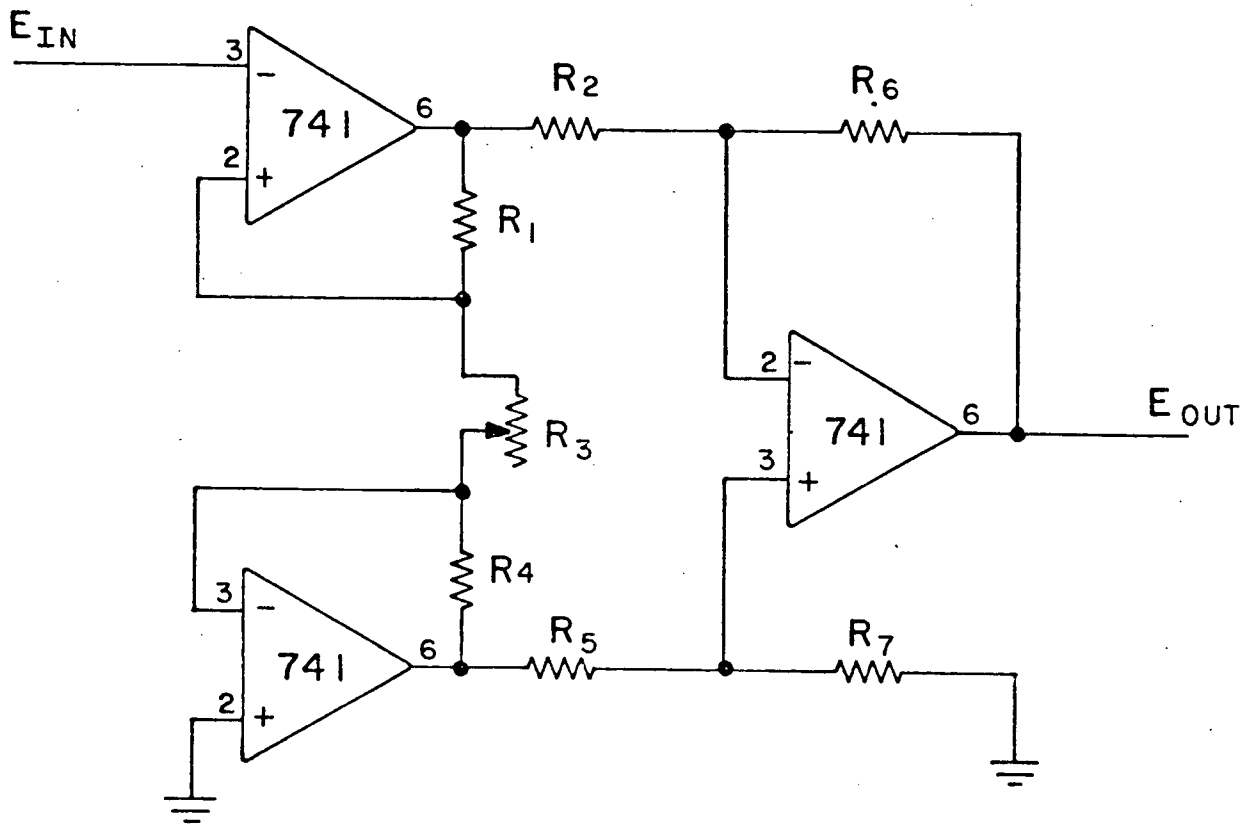

$$GAIN = \frac{E_{OUT}}{E_{IN}} = \left\{ \frac{R_3 + 2R_1}{R_3} \right\} \frac{R_6}{R_2}$$

IF: $R_1 = R_4$; $R_2 = R_5$; $R_6 = R_7$

Figure E-5 Circuit Schematic for One of the Gain Blocks for the Receiver Signal Conditioning Card

Set Up Procedure

Each receiver conditioning circuit is set-up in the same manner. First insert a signal +10dB higher than the normal clear weather received signal levels into the input of each microwave receiver using a microwave signal generator. This provides a safe margin for overfades. At this level, tune the gain of the receiver conditioning unit to match the highest allowable input voltage to the analog to digital convertor. After doing this the receiver signal conditioning unit is now ready to be included as part of the calibration procedure to obtain the AGC curves in Appendix A.

APPENDIX F

ANALOG TO DIGITAL CONVERTOR

Two types of analog to digital (A/D) convertors have been used in this work. The first unit is a 16 channel A/D with 12 bits resolution developed for use with the 6800 system by the Communications Research Centre, Ottawa, and is currently being used in the Ryder Lake microprocessor (see Appendix I). The second unit is a low power consumption 16 channel A/D with 8 bits resolution which has been especially designed for this research, to be used in conjunction with both the RCA 1802 and the INTEL 8085 microprocessors. The remainder of this appendix will deal with this second A/D convertor. Figure F-1 provides photographs of this A/D convertor viewed by itself and as an installed unit.

F-1 Functional Description

The second A/D convertor has the capability of addressing one of sixteen + 0-5 volt analog channels and converting the voltage appearing on the selected channel to a latched hexi-decimal output with values ranging from 00 to FF. Although the 0816 A/D convertor module has the capability of 16 input channels, so far only four conditioned meteorological outputs from the conditioning unit have been connected. These A/D channels are assigned according to the following table:

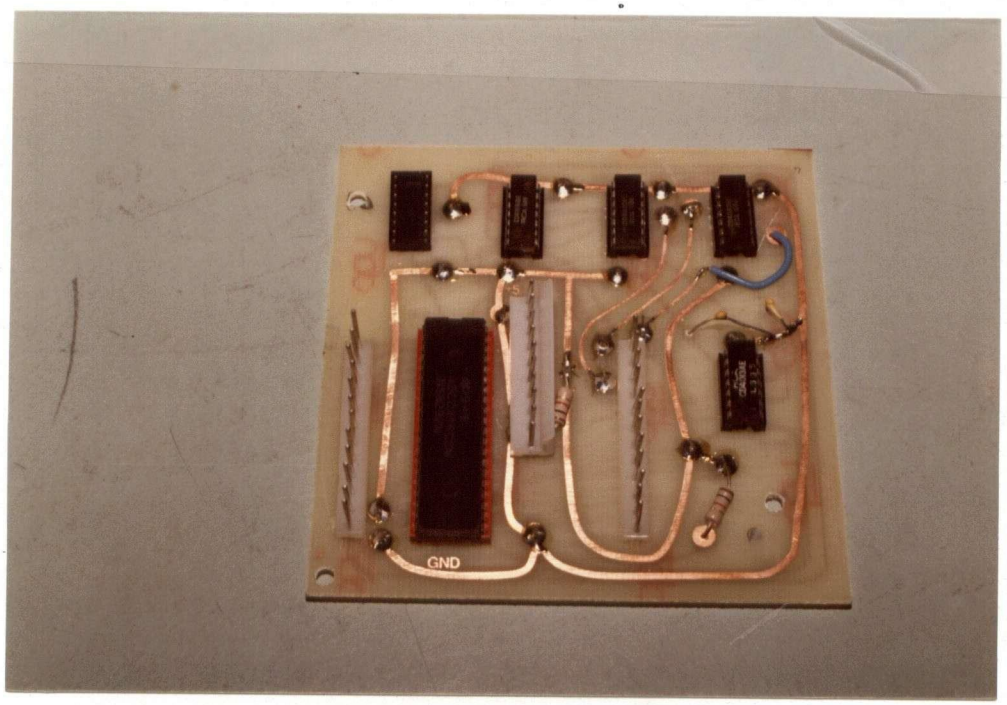

a) Separately

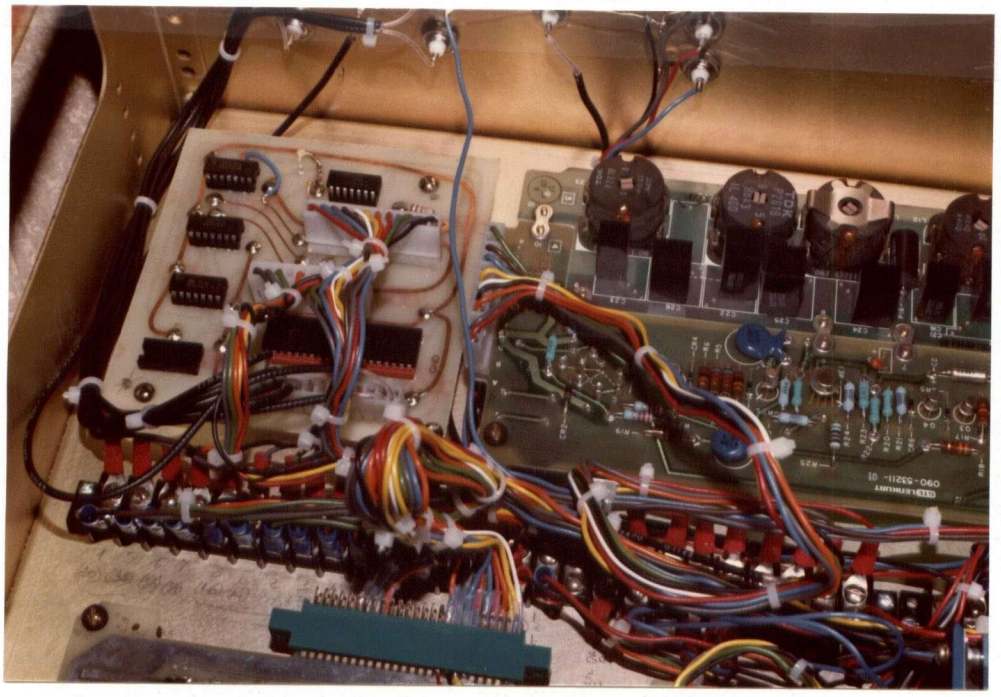

b) Installed

Figure F-1 Photographs showing the A/D Convertor Separately and Installed.

TABLE F-1 A/D Convertor Channel Assignment Table

A/D Channel	Meteorological Variable
3	Wind Direction
4	Wind Speed
5	Temperature
6	Rain
7	Not Defined

When this A/D convertor is used with an 8085 system, control of the channel selection and variable conversion is done through the selection of appropriate software output instructions.

Figure F-2 provides a schematic of the A/D convertor board with the control logic associated with specific output instructions identified. Figure F-3 provides the timing between each of the control signals.

In the design of this A/D board special care has been taken in selecting components with low power consumption to allow direct application of this unit in battery powered sites such as Bear Mountain.

F-2 A/D Convertor Calibration Procedure

Calibration of the A/D convertor is accomplished by sweeping the 0-5 V range of a selected A/D channel with a known voltage and monitoring the value of the hexidecimal output. This procedure is simplified if the test program in Figure F-5 is used. It allows the A/D's hexidecimal output to be viewed directly on an oscilloscope by monitoring the serial output pin (SOD) of the 8085 microprocessor. Figure F-4 provides a sample oscilloscope trace of SOD using the calibration test program.

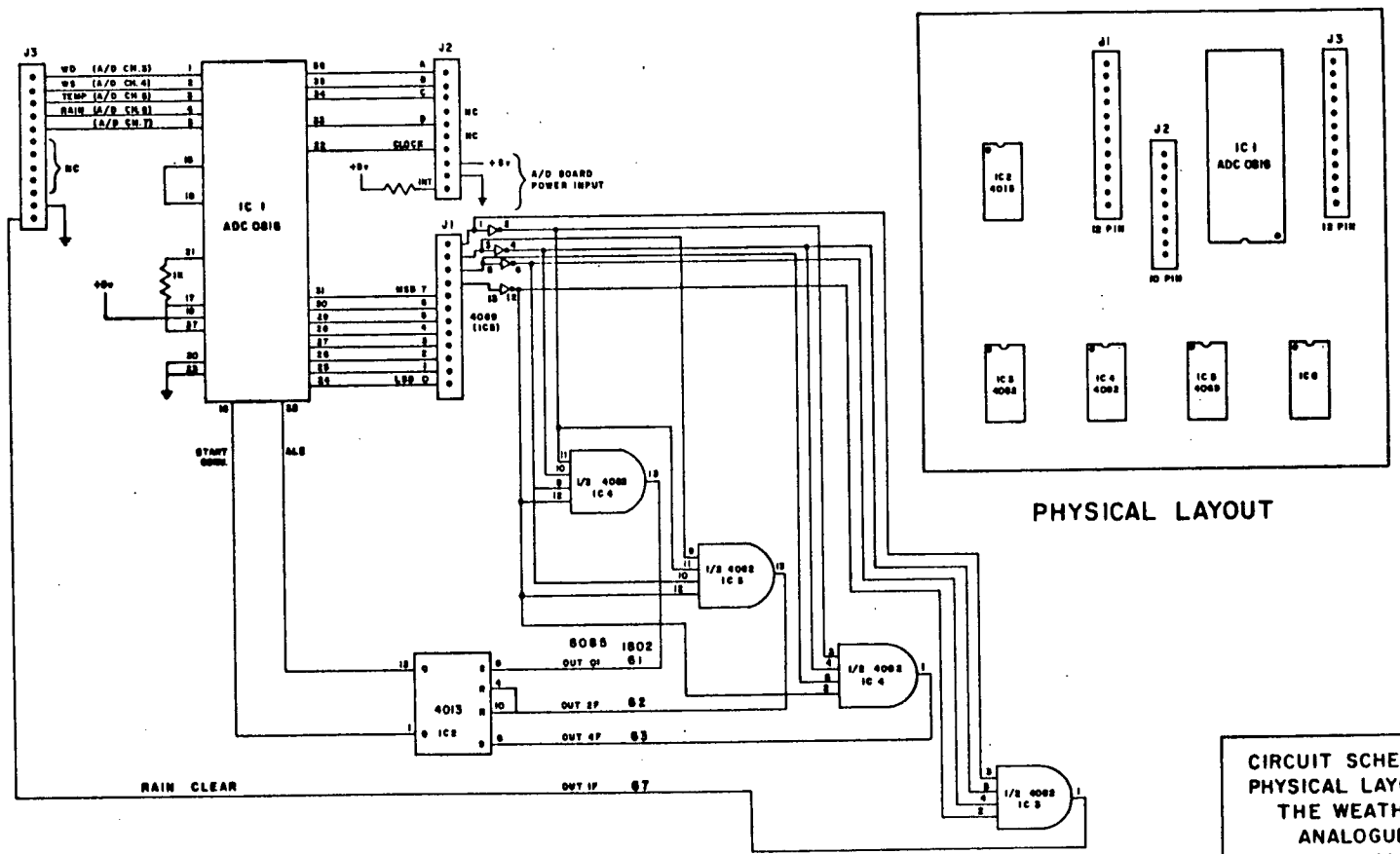

CIRCUIT SCHEMATIC & PHYSICAL LAYOUT FOR THE WEATHERLOG ANALOGUE TO DIGITAL CONVERTOR

FIGURE F-2	ISSUE 2
	MAR. 12, 1982

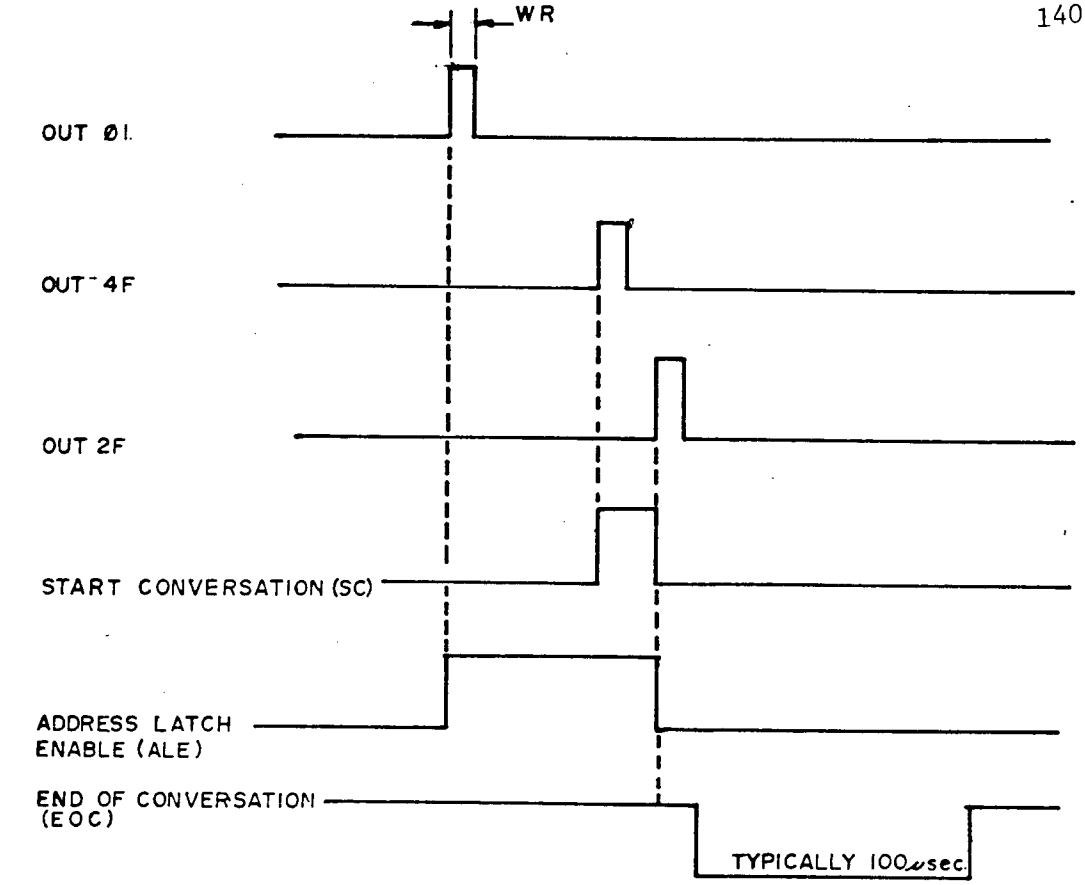

Figure F-3 Control Signal Timing Diagram for the A/D Converter

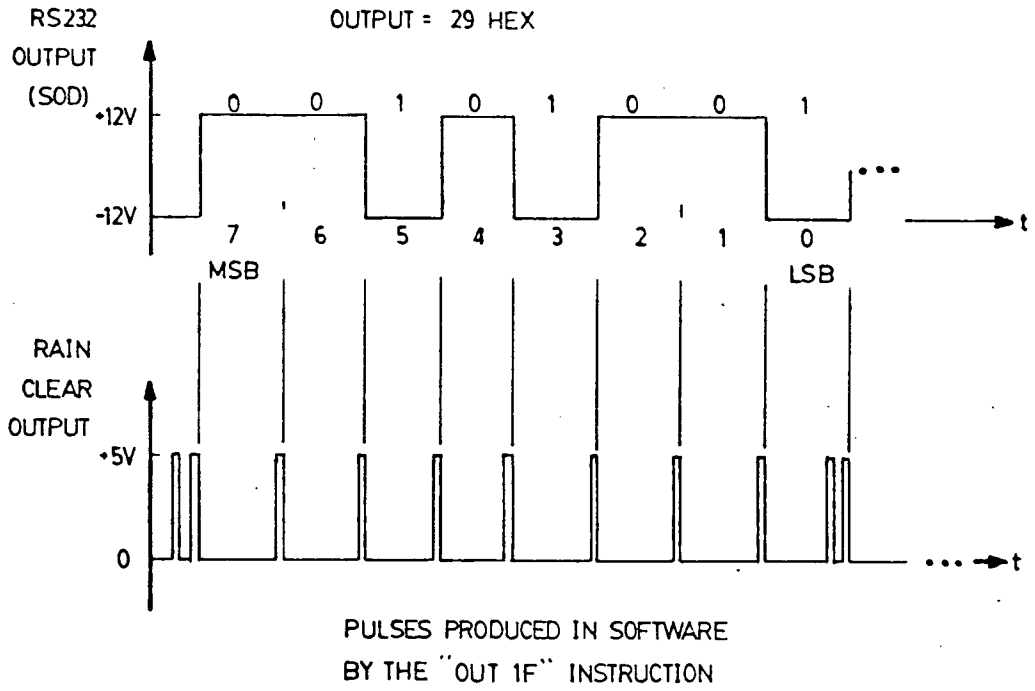

Figure F-4 Sample Oscilloscope Traces of the A/D Output During Calibration

```
Tektronix  8080/8085 ASM V3.1                                   Page    1

00001                   ;*************************************************************
00002                   ;
00003                   ;-------------------------------------------------------------
00004                   ;       THIS PROGRAM READS ONE CHANNEL OF THE A/D AND OUTPUTS THE
00005                   ;       RESULT IN CONTINOUS LOOP FASHION SO THAT THE DATA CAN BE
00006                   ;       READ FROM AN OSCILLOSCOPE. A RAIN CLEAR PULSE IS USED TO MARK
00007                   ;       EACH BIT AND A DOUBLE PULSE IS USED TO INDICATE THE START OF THE
00008                   ;       DATA BYTE. ON THE SCOPE THE DATA APPEARS WITH THE LEAST SIGNIFICANT
00009                   ;       BIT AS THE THE FIRST BIT AT THE LEFT SIDE OF THE DATA BYTE.
00010                   ;
00011                   ;
00012                   ;*************************************************************
00013       0000    >           ORG 000H
00014 0000 C30001   >           JMP MAIN
00015       0100    >           ORG 100H
00016 0100 3E31         MAIN    MVI A,31H
00017 0102 D300                 OUT 00
00018 0104 3E07                 MVI A,07H
00019 0106 30                   SIM
00020 0107 263F                 MVI H,3FH
00021 0109 2E50                 MVI L,50H
00022 010B F9                   SPHL
00023                   ;*************************************
00024                   ;
00025                   ;       DATA CHANNEL ON A/D IS SELECTED
00026                   ;
00027                   ;*************************************
00028 010C 1630                 MVI D,30H
00029 010E 7A                   MOV A,D
00030 010F D301                 OUT 01H
00031 0111 CD5001   >           CALL DELAY
00032 0114 D32F                 OUT 2FH
00033 0116 CD5201   >           CALL DL1
00034 0119 7A           AGAIN   MOV A,D
00035 011A D301                 OUT 01H
00036 011C CD5001   >           CALL DELAY
00037 011F D34F                 OUT 4FH
00038 0121 D32F                 OUT 2FH
00039 0123 CD5201   >           CALL DL1
00040 0126 DB02                 IN 02
00041 0128 DB02                 IN 02
00042                   ;*********************************************************
00043                   ;
00044                   ;       DATA BYTE IS SENT OUT IN A CONTINOUS LOOP FASHION
00045                   ;
00046                   ;*********************************************************
00047 012A 0E08         CC2     MVI C,08H
00048 012C D31F                 OUT 1FH
00049 012E D31F                 OUT 1FH
00050 0130 0F           CC1     RRC
00051 0131 47                   MOV B,A
00052 0132 F640                 ORI 40H
00053 0134 E6C0                 ANI 0C0H

00054 0136 D31F                 OUT 1FH
00055 0138 30                   SIM
00056 0139 78                   MOV A,B
00057 013A 0D                   DCR C
00058 013B C23001   >           JNZ CC1
00059 013E C32A01   >           JMP CC2
00060       0150    >           ORG 150H
00061 0150 00           DELAY   NOP
00062 0151 C9                   RET
00063 0152 1E50         DL1     MVI E,50H
00064 0154 1D           CC9     DCR E
00065 0155 C25401   >           JNZ CC9
00066 0158 C9                   RET
00067
```

Figure F-5 A/D Calibration Program

APPENDIX G

DIGITAL TO ANALOG CONVERTOR

The digital to analog (D/A) convertor has been used in the first phase of this experiment to generate chart recordings of the variables sampled by the data acquisition system and to verify the accuracy of the results processed by the data base management system (Chapter V). The circuit schematic for the D/A unit and its interface to the UBC 6800 microprocessor is presented in Figure G-1.

In the first phase of this experiment the D/A was used in conjunction with the cassette recorder. This was done by first using the recorder to store the time series data as it arrived at UBC from one selected RS 232 data channel. The data thus taken was then read back from the cassette recorder into the UBC 6800 microprocessor which selected a particular variable from the time series data to be outputted through the D/A. This selection process is easily accomplished since each variable arriving on the RS 232 port is assigned a specific position with respect to the sampling-interval synchronization byte. The program for this selection is given in Figure G-2.

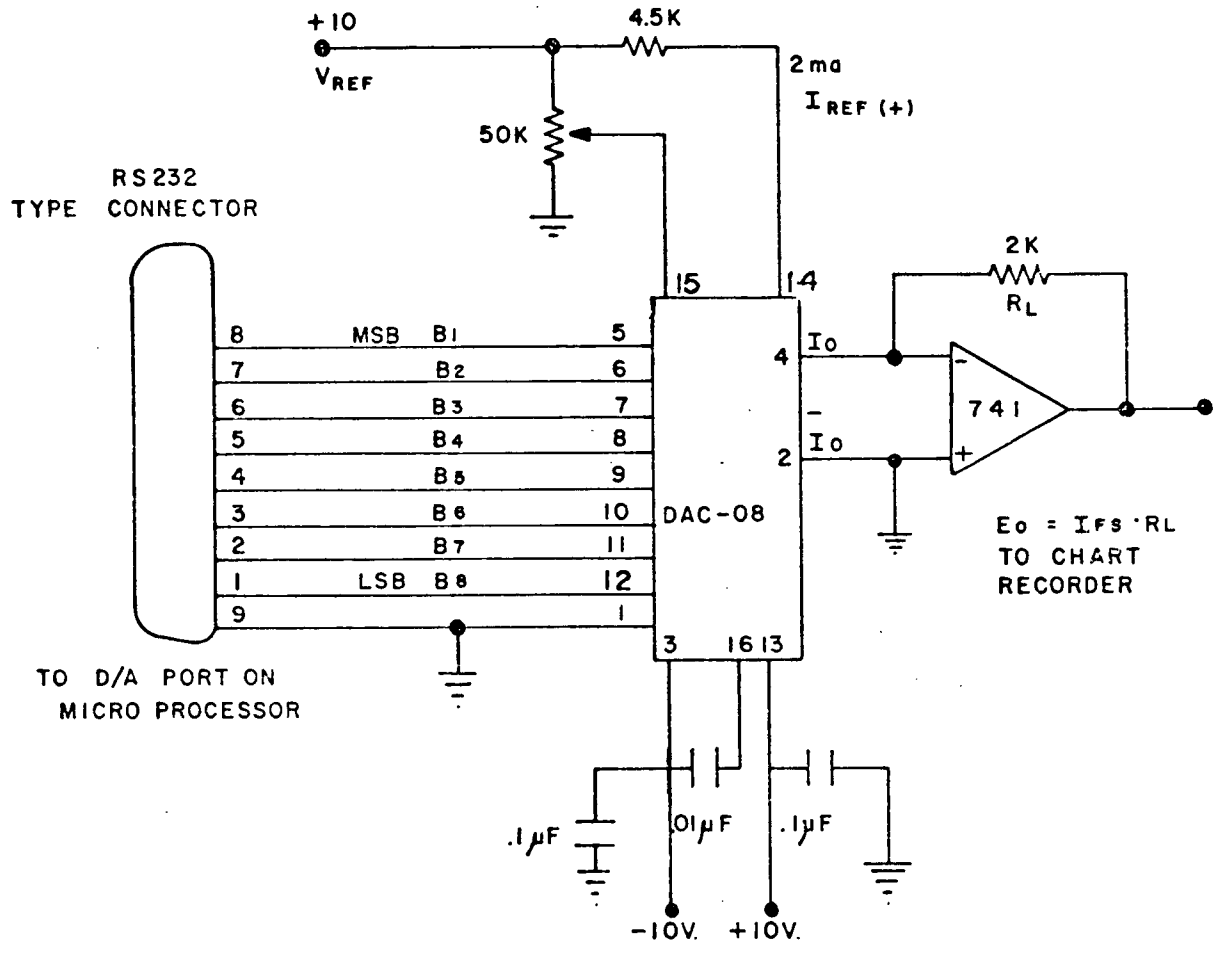

Figure G-1 Circuit Schematic for the D/A Converter

```
;        ******** DA ******************************
;          THIS PROGRAM IS USED TO SELECT TIME-SERIES DATA
;          AS IT ARRIVES AT UBC FROM THE DATA LINK
;          A VARIABLE RELATIVE TO A SYNCHRONIZATION
;          BYTE IS SELECTED FOR OUTPUT TO THE D/A
;          AND THE APPROPIATE VARIABLE IS CHOSEN BY
;          EDITING THE COMMENT STATEMENTS
;
          ORG     0E000H
;VARPTR EQU     0001
;VARPTR EQU     0002
;VARPTR EQU     0003
VARPTR EQU     0004        ; ACTIVATED FOR RAIN OR    RX#4
;VARPTR EQU     0005
STKPTR EQU      0A050H
PIACRA EQU     08011H
PIADRA EQU     08010H      ; PIA REGISTERS
CTR    EQU     0A040H
       CLR     PIACRA
       LDA A #0FFH         ; CLEAR PIA CONTOL REGISTER
       STA A PIADRA        ; SET PIA  AS OUTPUT
       LDA A #04H          ; NON INTERRUPT PORT
       STA A PIACRA
       LDA A #03H          ; RESET ACIA
       STA A 0801EH
       LDA A #015H
       STA A 0801EH        ; COMMAND REGISTER SET UP
       LDS   #STKPTR       ; STACK POINTER
LOOP   LDA A 0801EH        ; LOAD STATUS FROM PORT 7
       LSR A
       BCS   DTOA          ; RDRF      YES GET BYTE
       JMP   LOOP
DTOA   LDA B 0801FH        ; LOAD
       CMP B #0FFH         ; IS IT SYNCH
       BEQ   ZERO          ; YES: RESET COUNTER
       LDA A CTR
       CMP A #VARPTR       ; IS THIS THE VARIABLE
       BEQ   OUTPUT        ; YES: SEND OUT D/A
       INC   CTR
       JMP   LOOP          ; NO: INPUT NEXT VARIABLE
OUTPUT STA B PIADRA        ; SEND OUT D/A
       INC CTR
       JMP LOOP
ZERO   CLR   CTR           ; RESET COUNTER
       INC   CTR
       JMP   LOOP          ; LOOK FOR NEXT BYTE
       END
```

Figure G-2 Listing of the Program to Provide Chart Recordings from the Receiver Data Using the D/A

APPENDIX H

MODEM UNITS

H-1 Modem Transmit Units

A modem transmit unit is included in each of the Dog Mountain, Ruby Creek and Agassiz Experimental Farm Weatherlog Microprocessors. Each unit takes a ±12 volt RS 232 compatible 110 bps serial data stream and encodes this to output a voice frequency FSK modulated signal. The modulated signal is then carried by way of either a VHF or a telephone communications channel to the modem receivers at the Ryder Lake Site. The receive modems are described in section H-2.

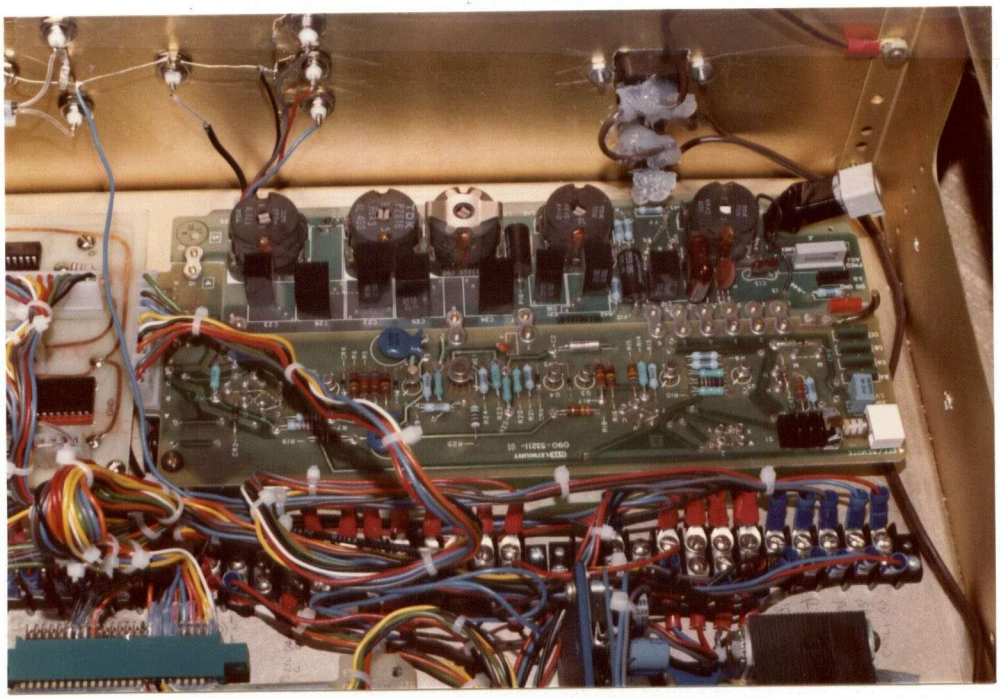

Figure H-1 Photograph of an Intalled Modem Transmit Unit

The centre frequencies for the modems that were available in this project are given in Table H-1 as follows:

Table H-1 Modem Centre Frequency Assignments

Frequency (Hz)	Code	Links Used
480	DA	
720	DB	Dog Mountain
960	DC	Agassiz Experimental Farm, Bear Mountain
1200	DD	Ruby Creek
1440	DE	

Figure H-1 shows a picture of a typical modem transmit unit as installed in a Weatherlog Microprocessor and Figure H-2 gives the interface schematic between the modem transmit unit and the microprocessor.

H-2 Modem Receive Units

All four modem receiver units are located at the Ryder Lake Site (see Appendix C) and have been integrated into one 19" rack mounted unit known as the "UBC Modem Unit". Each modem receiver inputs a voice frequency FSK modulated signal and decodes it into a 110 bps RS 232 compatible output to duplicate the input of the transmit unit (see Section H-1). The RS 232 output from each RS 232 unit is then relayed onto UBC for storage via separate channels on the statistical multiplex.

The physical layout of the "UBC Receiver Modem Unit" depicting front, back and top views is shown in Figure H-3 and a schematic of a typical interface between a modem receiver unit and the RS 232 output connections is given in Figure H-4.

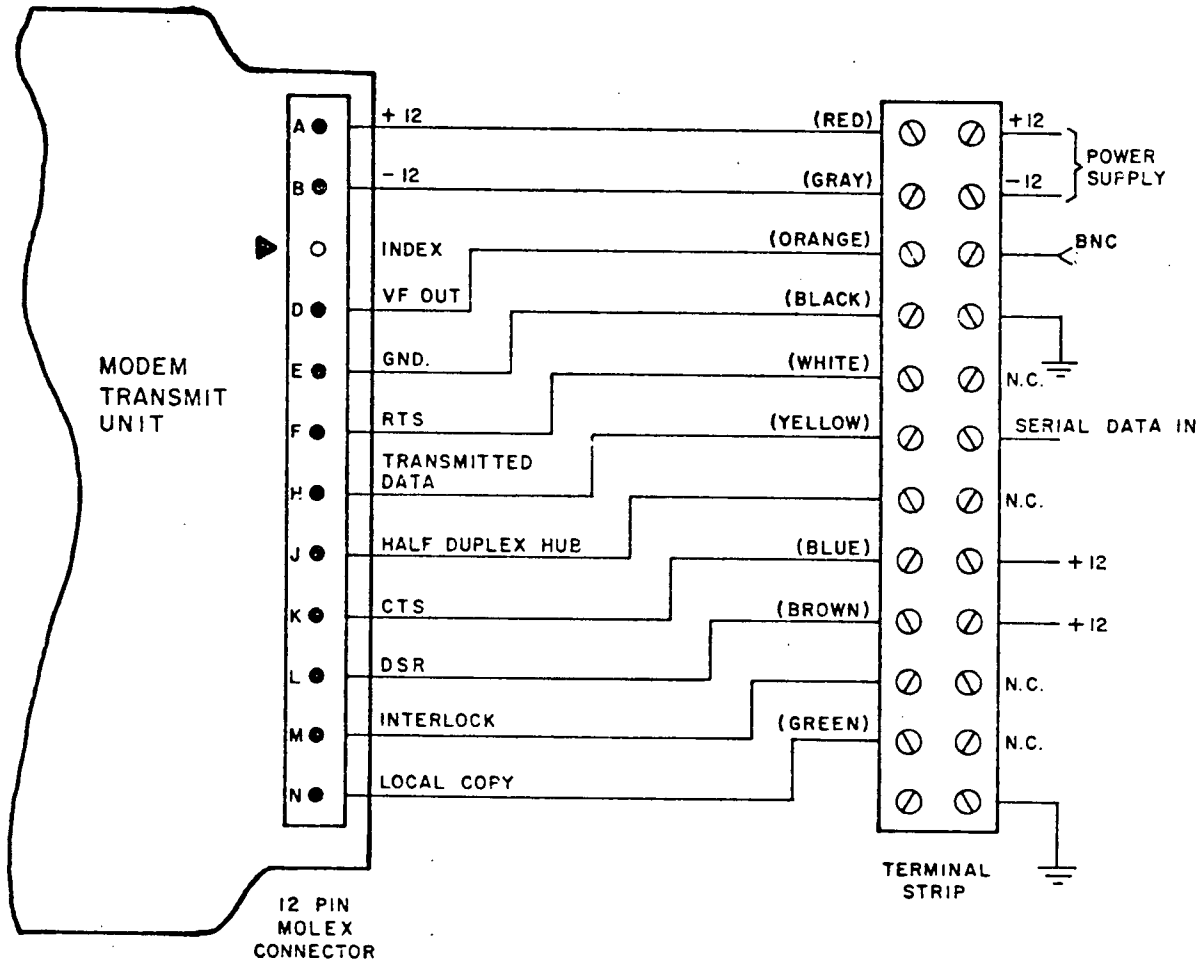

Figure H-2 Interface Schematic for a Weather Log Modem Transmit Unit

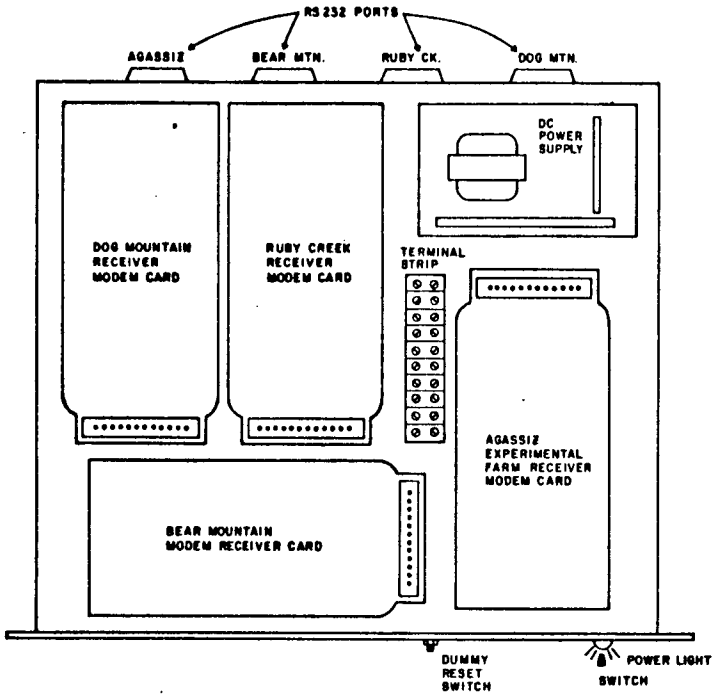

TOP VIEW SHOWING INTERIOR LAYOUT OF THE MODEM UNIT.

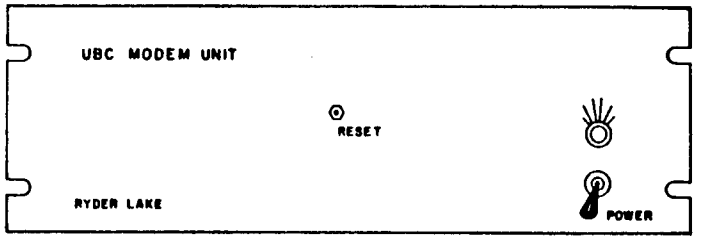

FRONT VIEW

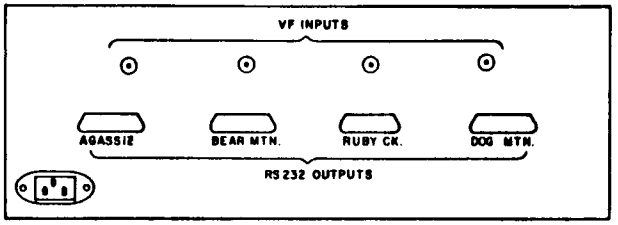

REAR VIEW

PHYSICAL DRAWING OF THE RYDER LAKE RECEIVER UNIT SHOWING TOP, FRONT & REAR VIEWS

FIGURE H-3 | ISSUE 2 MAR 12,1982

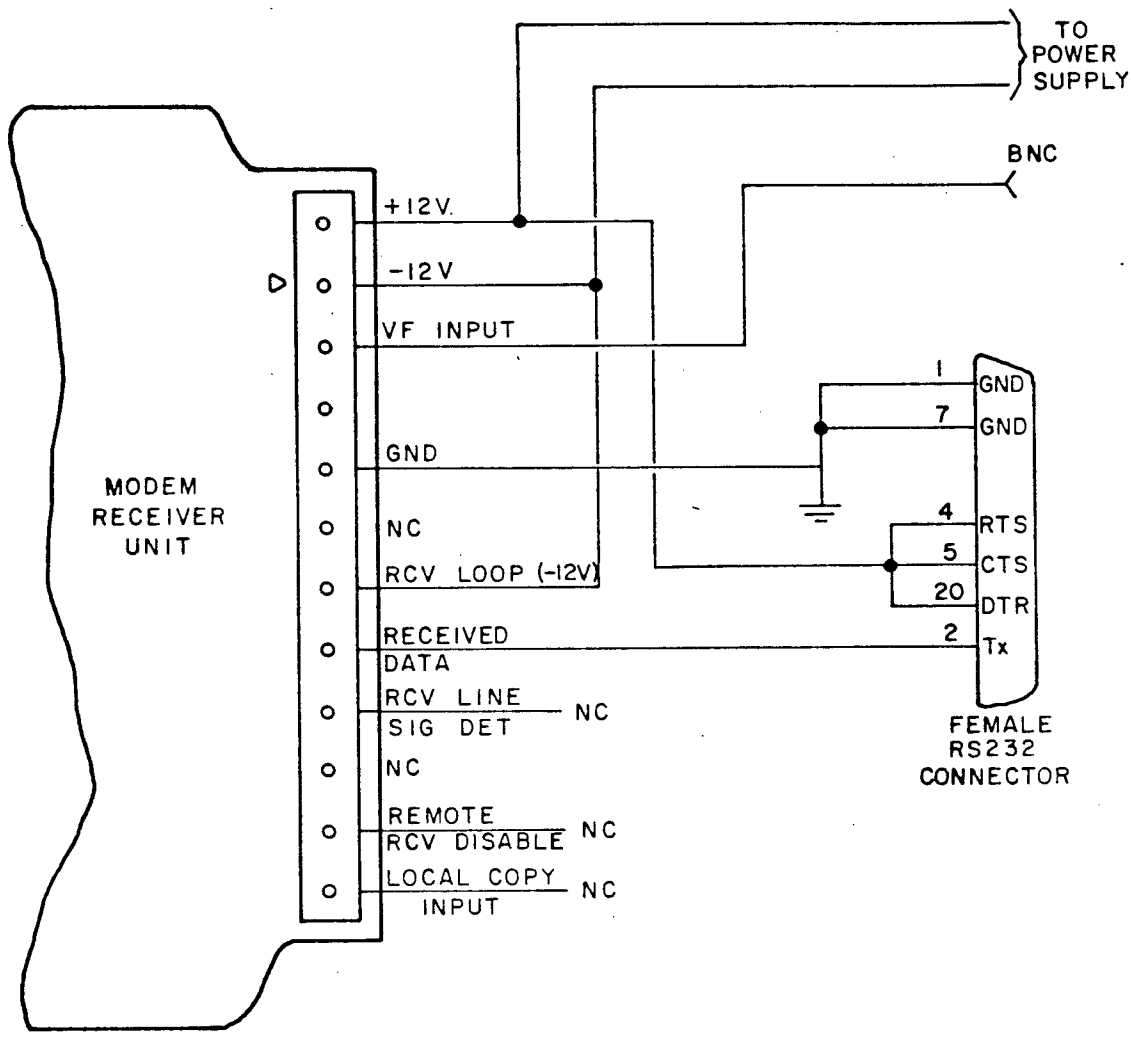

Figure H-4 Interface Schematic for One of the Modem Receiver Units

APPENDIX I

MICROPROCESSOR UNITS

I-1 The UBC Microprocessors

i) General Description

The two UBC microprocessors are both Motorola 6800 based units and are used for the purpose of time correlating the data as it arrives at UBC from the sampling processors along the path. The data formatter unit (μP#1) collects the incoming data, constructs the time series queues and outputs the results each second to the data processor unit (μP#2). The data processor unit then reduces the data to manageable levels by constructing hourly distributions and choosing selected time series intervals for storage onto a 4.5 megabyte capacity cassette recorder. The software routines to do this are discussed in Appendix J.

Two methods have been employed to prevue and test the incoming data stream. The method currently used takes the time series data outputted from the data formatter (μP#1) and resends it using the data processor (μP#2) to a video monitor. A photograph of the video display and discussion of this method is given in Chapter IV. A second method was employed in the first phases of the system integration by reading selected variables from the arriving data streams and outputting these through a digital-to-analog convertor, as described in Appendix G.

The physical layouts for the UBC microprocessors are shown in Figure I-1 and I-2 for the data formatter and data processor respectively. These drawings show the rear termination assignments, the front panel display and the

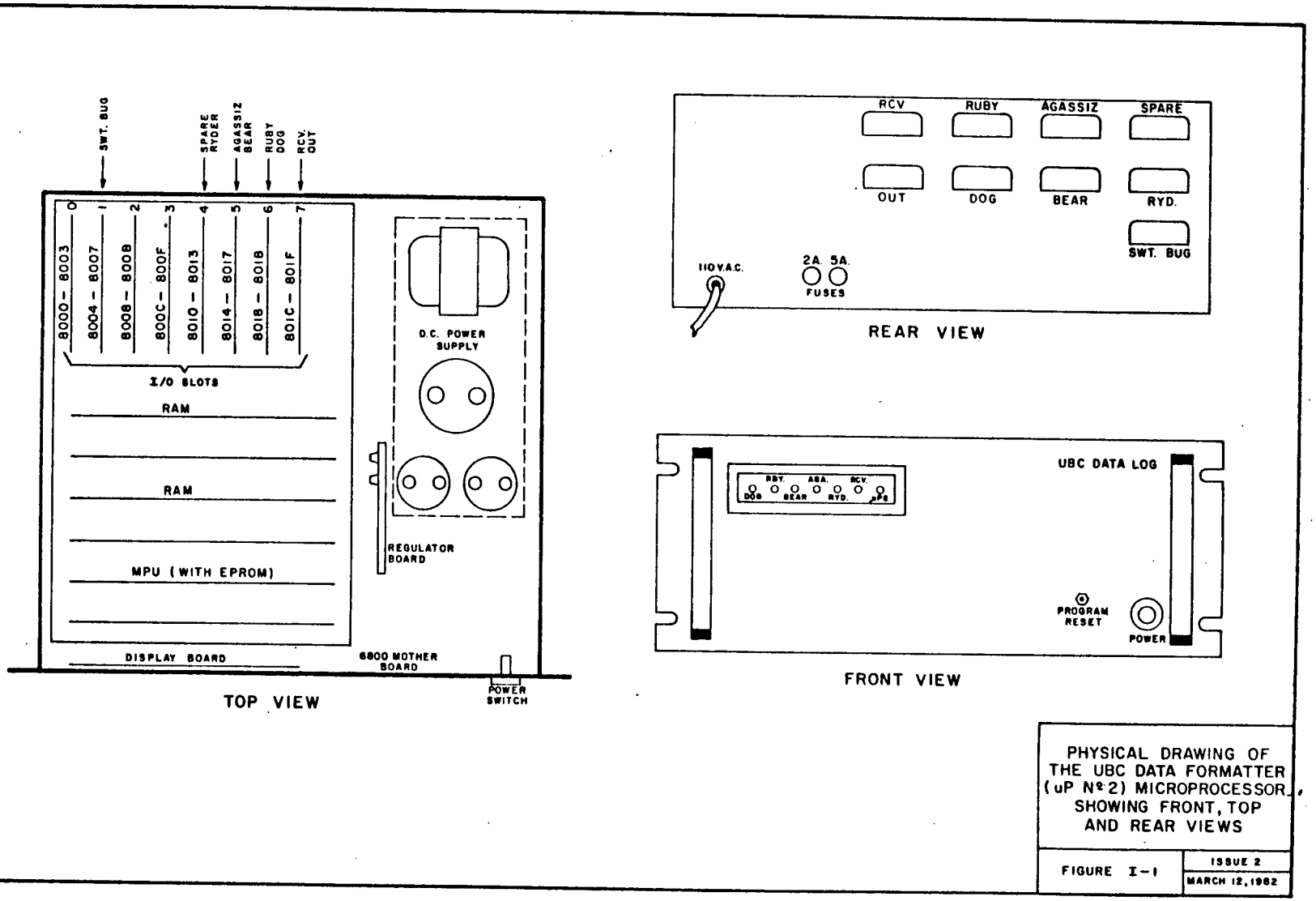

PHYSICAL DRAWING OF THE UBC DATA FORMATTER (uP Nº2) MICROPROCESSOR SHOWING FRONT, TOP AND REAR VIEWS

FIGURE I-1	ISSUE 2
	MARCH 12, 1982

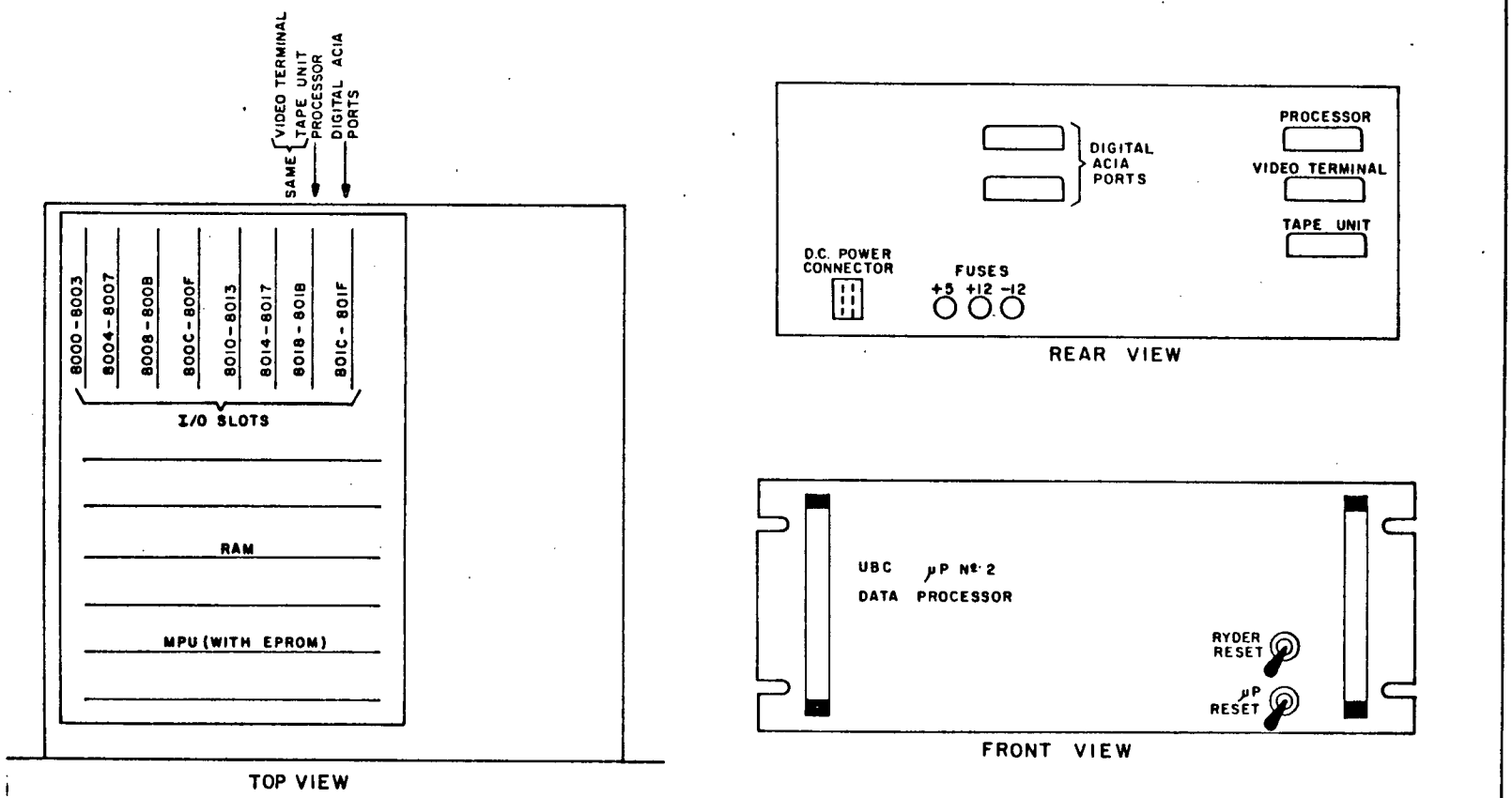

PHYSICAL DRAWING OF THE UBC DATA PROCESSINC (μP Nº 2) MICROPROCESSOR SHOWING FRONT, TOP AND REAR VIEWS -

FIGURE I-2

ISSUE 1
MARCH 12, 1982

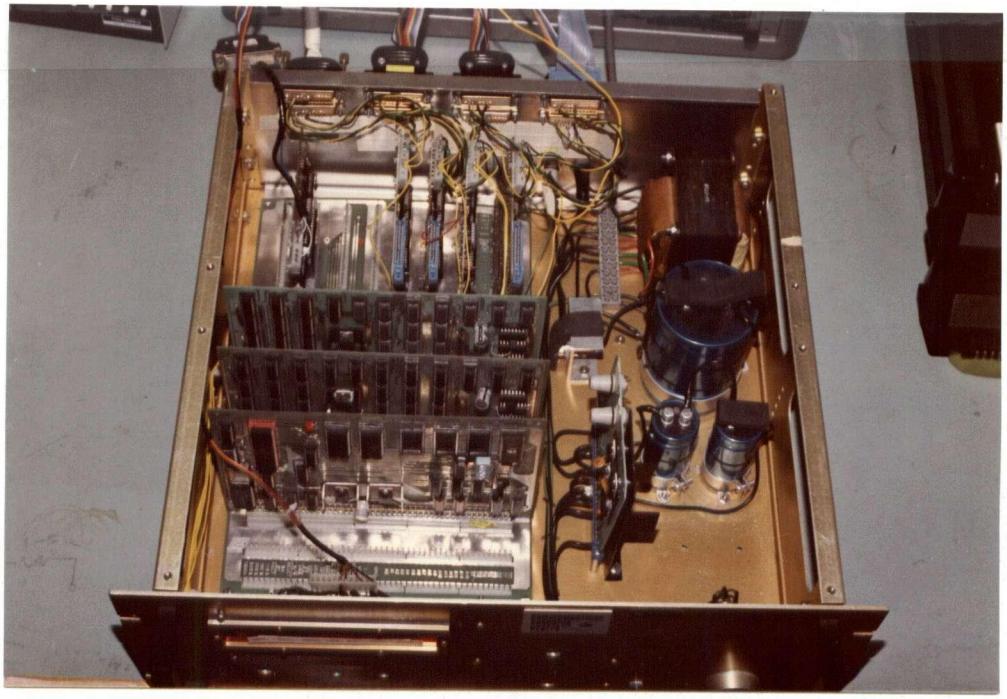

a) The Data Formatter (μP#1)

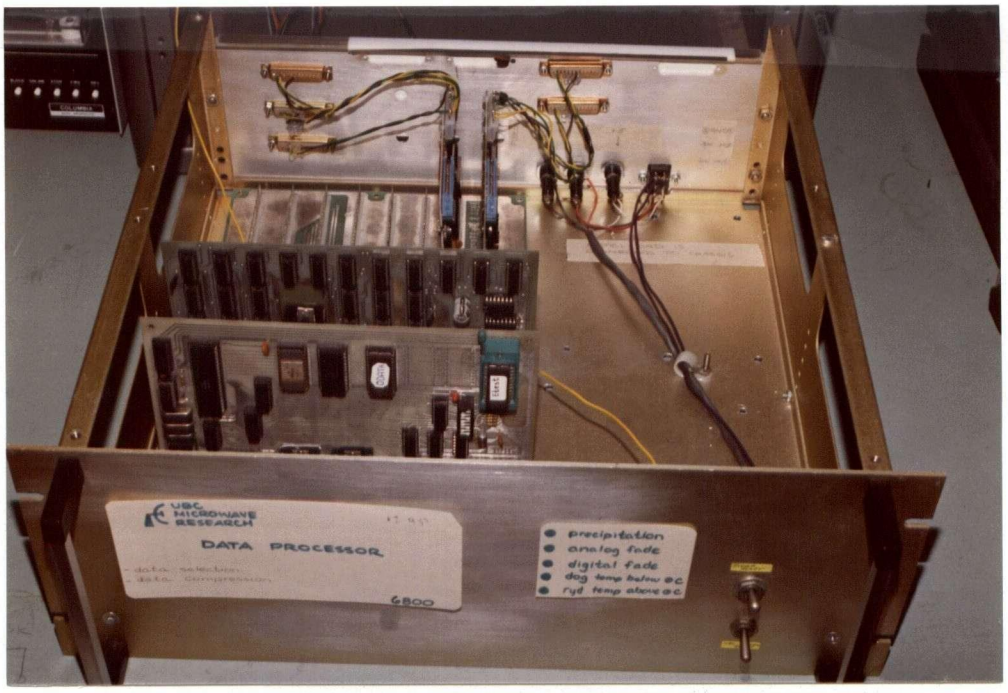

b) The Data Processor (μP#2)

Figure I-3 Photographs Showing the Interior Layout of the Two UBC Microprocessors

processor mother board layouts. A photograph of both microprocessors is given in Figure I-3 illustrating their interior layouts.

An integral part of the UBC unit are the ACIA cards which provide the communications interface between the serial RS 232 input/output ports and the parallel data bus of the microprocessors. Each ACIA card provides an interface to two RS 232 ports according to the assignments shown in Table I-1 and I-2 for μP 1 and 2. Its circuit schematic and physical layout are given in Figure I-4.

Table I-1 I/O Port Address Assignments for the Data Formatter Unit μP#1

I/O PORT #	PORT ADDRESS	FUNCTION	ASSIGNMENT
0	8000		
	8001		
	8002		Not assigned
	8003		
1	8004	PIA I/O Reg.	
	8005	DDR	Terminal
	8006	PIA I/O Reg.	Port PIA
	8007	DDR	
2	8008		
	8009		
	800A		Not assigned
	800B		
3	800C		
	800D		
	800E		Not assigned
	800F		
4	8010	ACIA CMD	Spare I/O Port
	8011	ACIA I/O Reg.	
	8012	ACIA CMD	Ryder Lake
	8013	ACIA I/O Reg.	Meteorological

Table I-1 cont'd.

5	8014	ACIA CMD Reg.	Agassiz Experimental
	8015	ACIA I/O Reg.	Farm
	8016	ACIA CMD Reg.	Bear Mountain
	8017	ACIA I/O Reg.	
6	8018	ACIA CMD Reg.	Ruby Creek
	8019	ACIA I/O Reg.	
	801A	ACIA CMD Reg.	Dog Mountain
	801B	ACIA I/O Reg.	
7	801C	ACIA CMD Reg.	Tape Unit RS232
	801D	ACIA I/O Reg.	Output Port
	801E	ACIA CMD Reg.	Receiver Channel
	801F	ACIA I/O Reg.	from Ryder Lake

Table I-2 I/O Port Address Assignments for the Data Processor Unit μP#2

I/O PORT #	PORT ADDRESS	FUNCTION	ASSIGNMENT
6	8018	ACIA CMD Reg.	Output Port to Video
	8019	ACIA I/O Reg.	Screen and Tape Unit
	801A	ACIA CMD Reg.	Receive from μP#2
	801B	ACIA I/O Reg.	
7	801C	ACIA CMD Reg.	Future
	801D	ACIA I/O Reg.	Digital
	801E	ACIA CMD Reg.	I/O Ports
	801F	ACIA I/O Reg.	

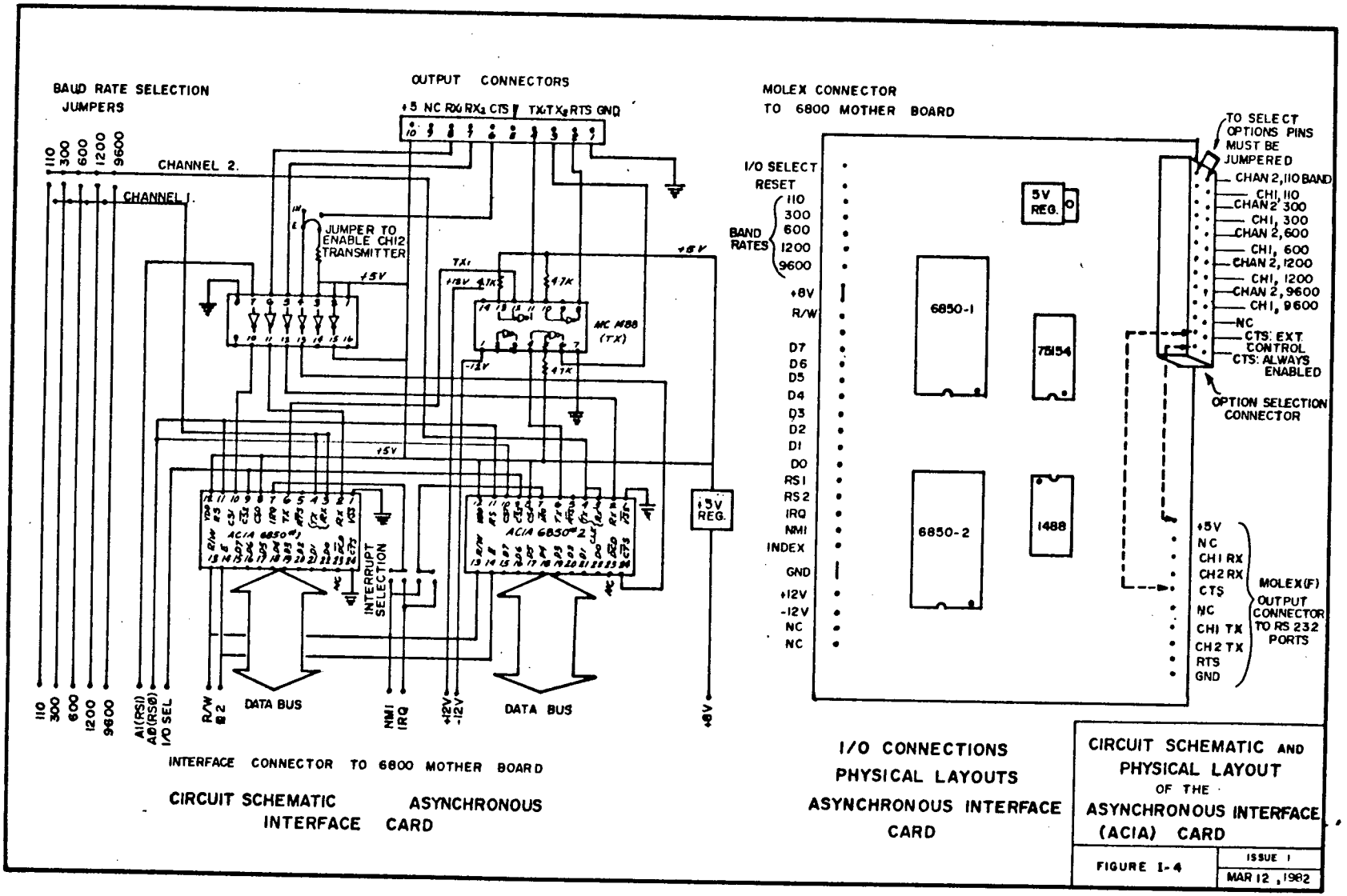

CIRCUIT SCHEMATIC ASYNCHRONOUS INTERFACE CARD

I/O CONNECTIONS PHYSICAL LAYOUTS ASYNCHRONOUS INTERFACE CARD

CIRCUIT SCHEMATIC AND PHYSICAL LAYOUT OF THE ASYNCHRONOUS INTERFACE (ACIA) CARD

FIGURE 1-4

ISSUE 1
MAR 12, 1982

ii) Specifications

a) MPU board

- modified to produce data rates of 110, 300, 600, 1200 and 9600 bps. (μP#1).
- unmodified in μP#2 to give data rates of 110, 300, 600, 1200 and 2400
- if the SWTBUG monitor is to be used switch off both "PROM" dip switches and switch on the "SWT" and "MONITOR" dip switches.
- to use a program in the EPROM, switch on the "LO PROM" or the "HI PROM" dip switch and turn off the "SWT" and "MONITOR" dip switches. The EPROM program then starts in location $E000_{16}$ of the memory space with the interrupt vectors being assigned the following addresses.

Table I-3 6800 Interrupt Vectors

Location	Type of Vector
E7F8	Interrupt Request (IRQ)
E7FA	Non Maskable Interrupt (NMI)
E7FC	Software Interrupt (SWI)
E7FE	Restart

b) ACIA board

- The boards must be strapped according to Figure I-4 to determine their data rates.

c) Regulator board

Input Voltage: ±24V

Output Voltages: +12V
-12V
+14.6V = UD1 (μP#1 only)
-14.6V = UD2 (μP#1 only)

d) Total AC power required

500ma at 110V. A.C.

I-2 The Ryder Lake Microprocessor Unit

The Ryder Lake Microprocessor unit is based on the Motorola 6800. Its purpose is to sample both the received signal levels and the meteorological information from this site and send it to UBC via two separate data channels.

Every 1/10 of a second the received signal levels are sampled and on every tenth sampling interval (i.e. each second) the weather information is also sampled and sent.

The analog-to-digital convertor in this unit is able to resolve to 12 bits which is more than required. Therefore, each sample is first reduced by stripping the four least significant bits before the 8 bit samples are outputted. The channel assignments for the analog-to-digital convertor are provided in Table I-4, as follows:

Table I-4 Analog to Digital (A/D) Convertor Channel Assignments

A/D Channel	Channel Assignment
F	Unassigned
E	Unassigned
D	Rain
C	Temperature
B	Wind Speed
A	Unassigned
9	Wind Direction
8	Unassigned
7	Unassigned
6	Unassigned
5	Unassigned
4	7496 GHz Rx
3	7142 GHz Rx
2	4010 GHz Rx
1	3790 GHz Rx
0	3550 GHz Rx

Figure I-5 provides a drawing showing the hardware assignment slots for the CPU, the ACIA card and the analog-to-digital convertor. Table I-5 provides the I/O port address assignments for the Ryder Lake Unit, as follows:

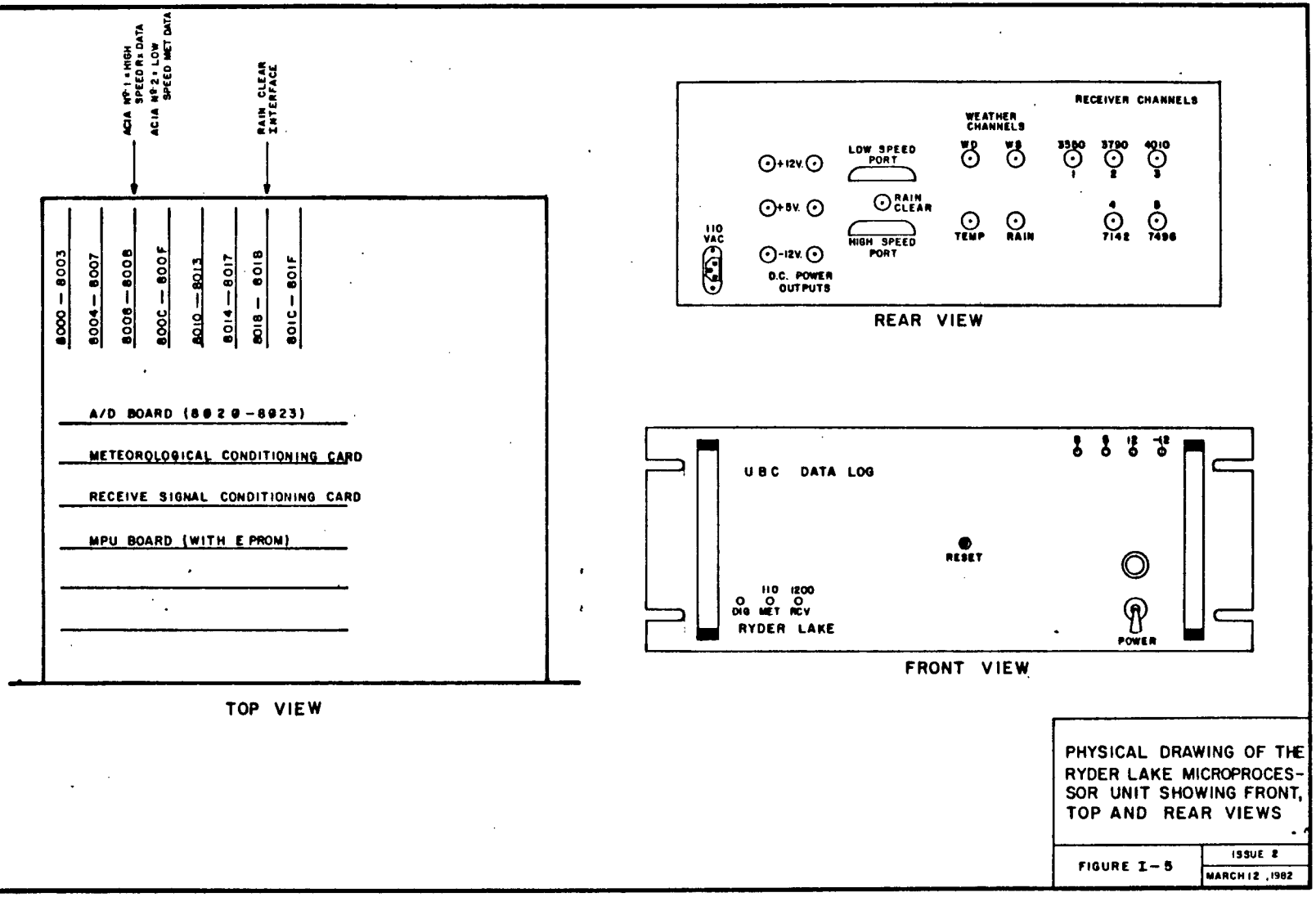

PHYSICAL DRAWING OF THE RYDER LAKE MICROPROCESSOR UNIT SHOWING FRONT, TOP AND REAR VIEWS

FIGURE I-5 | ISSUE 2 | MARCH 12, 1982

Table I-5 I/O Port Address Assignments for the Ryder Lake Unit

I/O PORT #	PORT ADDRESS	FUNCTION	ASSIGNMENT
2	8008	ACIA CMD Reg.	High speed
	8009	ACIA I/O Reg.	Receiver Data
	800A	ACIA CMD Reg.	Low speed
	800B	ACIA I/O Reg.	Meteorological Data
6	8018 to 801B		DC Power Supply Interface

All other I/O port addresses are unassigned.

I-3 The Weatherlog Microprocessor Units

The weatherlog microprocessor units used at Dog Mountain, Ruby Creek and the Agassiz Experimental Farm are based on the INTEL 8085. Their purpose is to sample the meteorological variables of wind speed, wind direction, temperature and rain at one second intervals. The inputs to the microprocessor's A/D channels are 0-5 volts which are provided at the output of the meteorological signal conditioning unit (see Appendix E). The weatherlog microprocessor incorporates a low speed frequency shift keyed modem between the RS 232 output of the 8085 internal processor to the voice frequency 600 ohm unbalanced output of the weatherlog. The FSK output thus derived is then applied to the corresponding channel back to Ryder Lake. From the Ruby Creek location this is via VHF radio, from Dog Mountain this is via the 37A message circuit on the

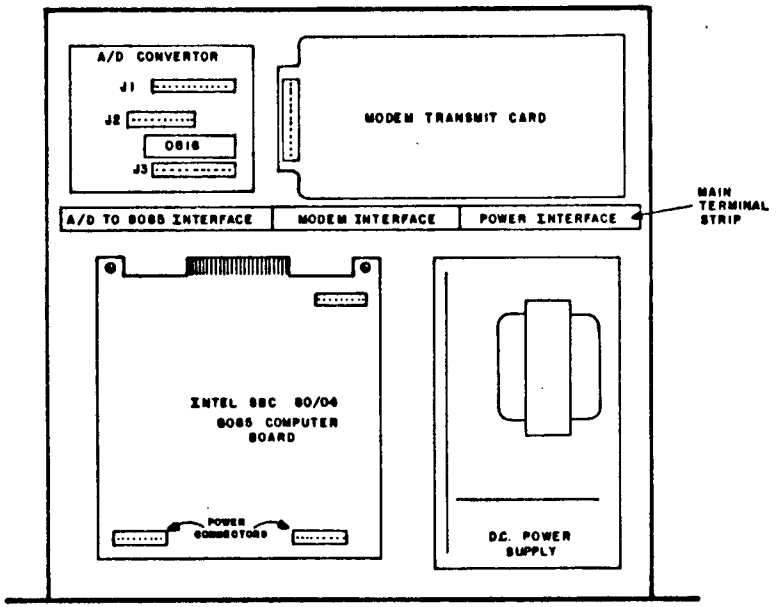

TOP VIEW

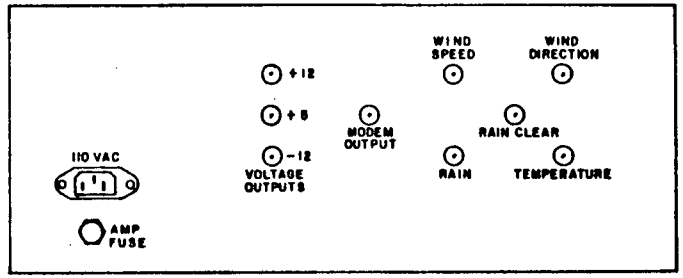

REAR VIEW

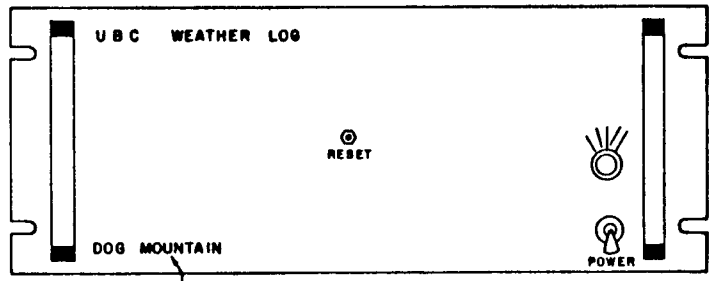

FRONT VIEW

PHYSICAL DRAWING OF THE WEATHER LOG MICRO-PROCESSOR SHOWING FRONT, TOP AND REAR VIEWS

FIGURE I-6

ISSUE 1
MARCH 12, 1982

7 GHz radio and from the Agassiz Experimental Farm this is via a telephone link.

A drawing indicating the positioning within the weatherlog unit of the 8085 computer board, the A/D convertor and the modem transmit card is given in Figure I-6. A photograph of this interior layout is shown in Figure I-7.

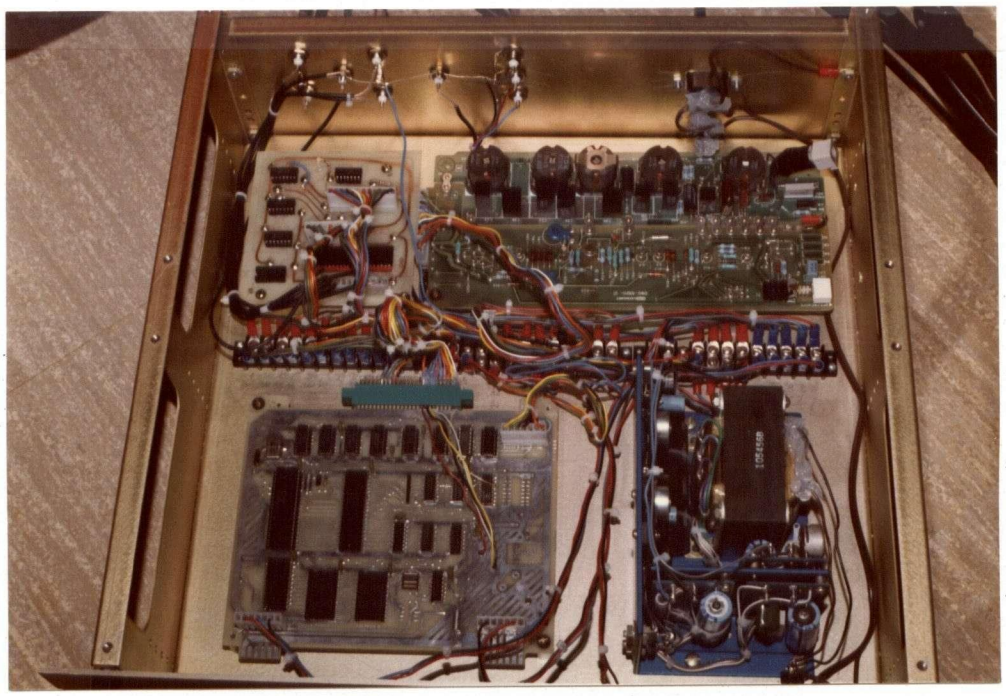

Figure I-7 Photograph showing the Interior Layout of a Typical UBC Weatherlog Microprocessor Unit.

I-4 The Bear Mountain Microprocessor Unit

The purpose of the Bear Mountain Microprocessor is to sample the meteorological variables of temperature and rain once per second and output the data onto the radio link to Ryder Lake.

In designing the microprocessor unit for this site, special care was taken to minimize the power consumption and to choose a technology which could withstand large temperature variations (±40°C). CMOS technology was selected for the microprocessor, the A/D and the signal conditioning unit. The microprocessor is an RCA 1802 and the circuits for the A/D and signal conditioning units are described in Appendices F and E respectively. The total power consumption of the CMOS electronics was 70 ma.

The radio used is a hand-held unit from Motorola specially designed for low power consumption applications. Optimization of the radio's power consumption was achieved through the use of a high gain transmitting antenna and eliminating the power consumption of the radio's final transmitter stage, thus reducing the RF output power from 1.5 watts to 300 mwatts and the radio's current draw to 225 ma.

The expected operational life-time for the Bear Mountain site based on 2000 A-HR caustic potash cells is therefore 1.01 years for the radio battery and 3.23 years for the electronics battery. It is recommended that battery replacement is done by helicopter since the road access is rugged (four wheel drive only) which could damage the cells.

A drawing of the equipment configuration showing the microprocessor, the radio, the A/D and the signal conditioning unit is given in Figure I-8 and a photograph in I-9.

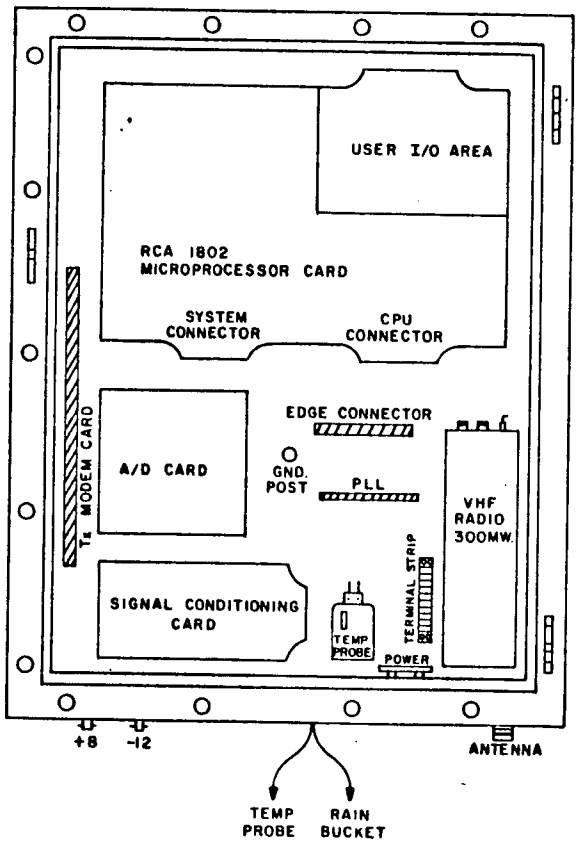

TOP VIEW

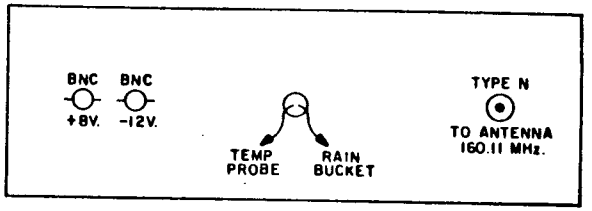

BOTTOM VIEW

PHYSICAL DRAWING OF THE LOW POWER MICROPROCESSOR UNIT - USED AT BEAR MOUNTAIN

FIGURE I-8

ISSUE 2

MARCH 12,1982

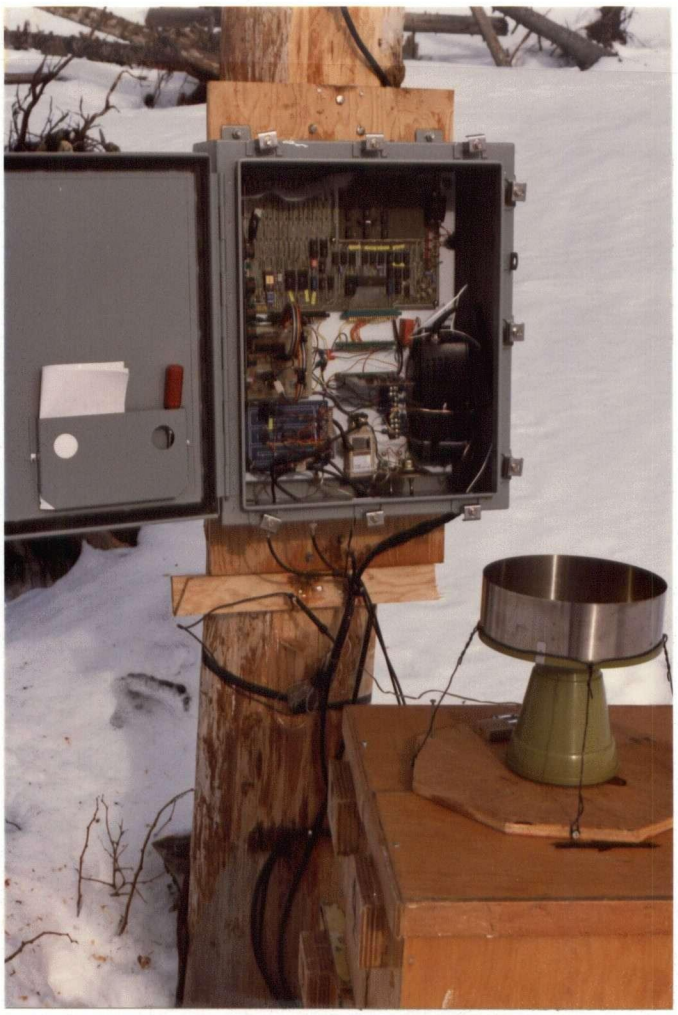

Figure I-9 Photograph showing the Interior Layout of the Bear Mountain Microprocessor Unit

I-5 The NOVA 840 Minicomputer

The purpose of the NOVA 840 minicomputer is to take the data recorded on the cassette tapes and then transfer these data in serial fashion to IBM formatted 800 bpi magnetic tape. Figure I-10 illustrates the equipment arrangement needed to transfer the data.

In order to enter data on the NOVA, an RS 232 to current loop interface was constructed as the NOVA had no RS 232 input ports. The RS 232 to current loop interface schematic is given in Figure I-11.

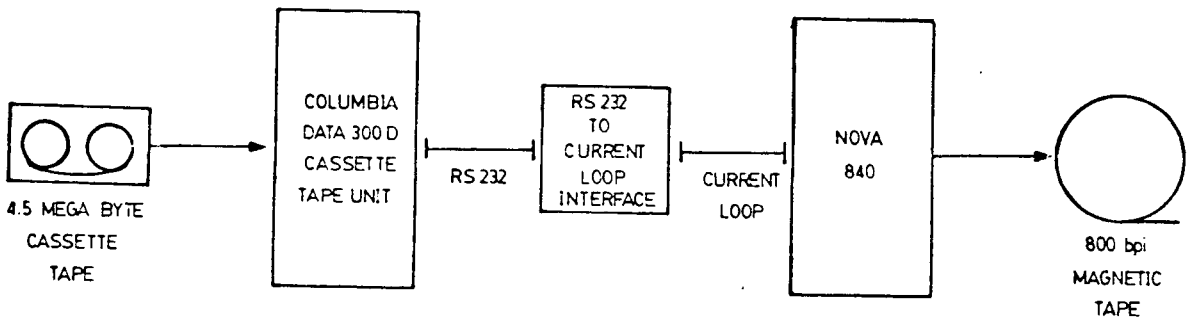

Figure I-10 Equipment Configuration to Transfer Data from the Cassette Tape Drive to the Nova 840 Magnetic Tape Drive.

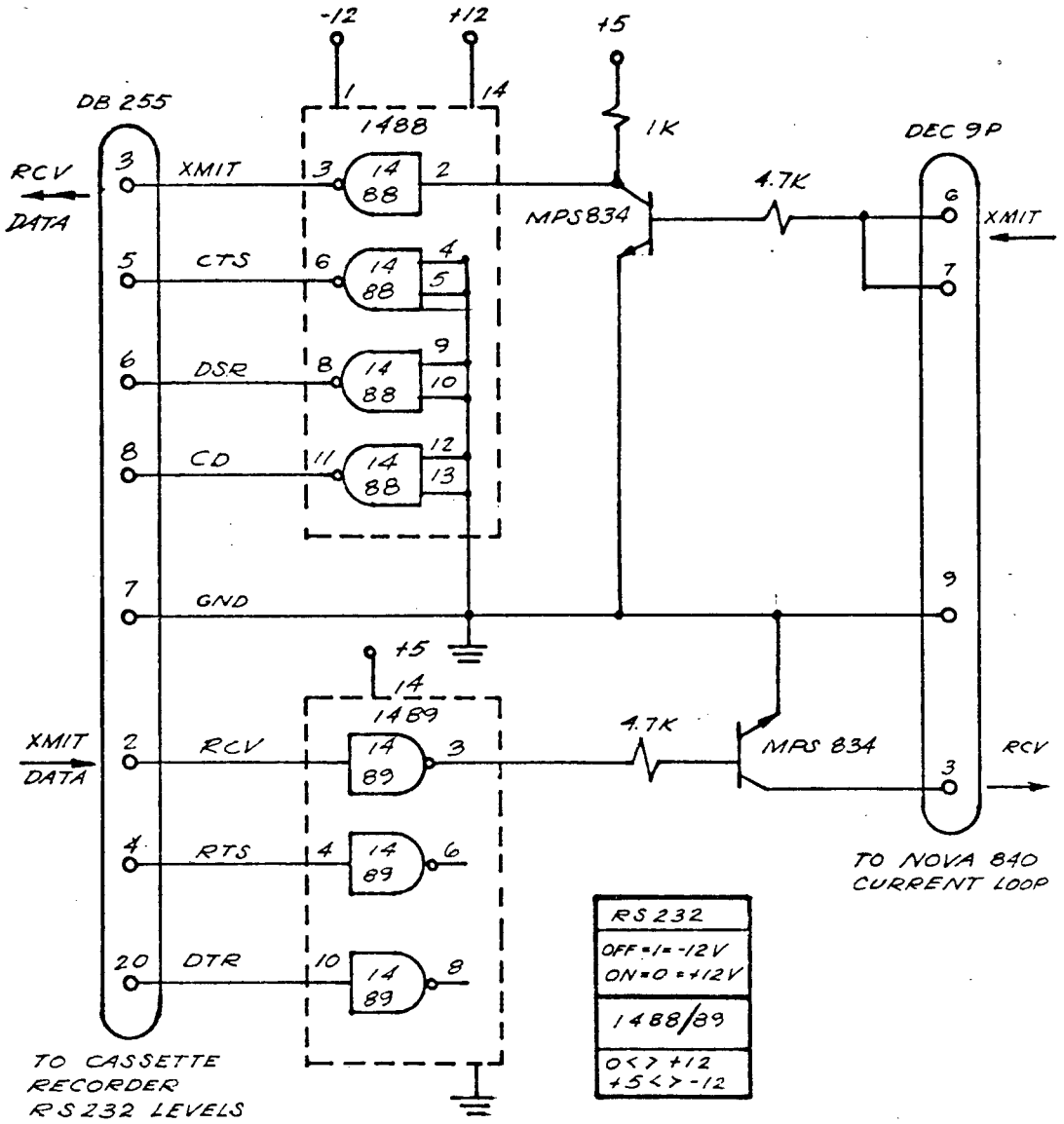

Figure I-11 Circuit Schematic of the RS-232C to Current Loop Interface

APPENDIX J

MICROPROCESSOR SOFTWARE

J-1 The UBC Microprocessors

i) Functional Description

The main function of the UBC 6800 microprocessor software in the data formatter (μP#1) and the data processor (μP#2) is to time-correlate all the field data as these arrives on the data link, output the data for real time viewing on a video monitor, compress it into statistical distributions, select time series segments for storage and finally store the data on magnetic tape using suitable formats. Due to timing constraints and the complexity of incorporating all these tasks under the control of a single CPU, these tasks were distributed between two processors. The first processor, the data formatter or μP#1, has been assigned the tasks of inputting the arriving field data, coding this data to real time, formatting it into buffers and outputting the formatted data once per second to the second CPU. The second processor, the data processor or μP#2 has been assigned the tasks of outputting the data for real time viewing on a video monitor, generating statistical distributions from the data, choosing time series segments and storing these records onto a magnetic cassette recorder in a recoverable format.

The interfaces between both UBC microprocessors, from the statistical multiplex and μP#1, from both microprocessors to the video terminal and from μP#2 to the cassette recorder are all RS232C. The input/output ports are all configured in the software.

The program flow chart for the data formatter (μP#1) is given in Fig. J-1a, a diagram of its buffer memory organization is shown in Figure J-1b and the program flow chart for the data processor (μP#2) is presented in Fig. J-2.

ii) Input/Output Software Design Specifications

I. Received Signal Data

The signal amplitude data arrives at the input of the data formatter (μP#1) in rotational order at one-tenth of a second intervals starting from the lowest frequency receiver. A synchronizing byte (FF) is received after the highest frequency receiver sample arrives and is used to update the software clock on the basis of 10 incoming synch bytes equalling 1 second. After each second the received signal data is dumped to the data processor (μP#2).

The data processor checks the incoming levels for multipath and fading by determining if they exceed a specified range. If this is the case, a time series dump is initiated. The data processor finishes by taking each byte of receiver signal data to update an hourly distribution buffer, to store it in a rotating time series queue and to send it for viewing to a video monitor.

II. Meteorological Data

Each second, four successive bytes arrive on the five input meteorological channels, and immediately following their arrival a synchronizing byte is sent. Their order of arrival is wind direction, wind speed, temperature and rainfall. As each of these samples is received, their position in the data formatter unit's (μP#1) input buffers are updated with the new values and before they are outputted to the data processor

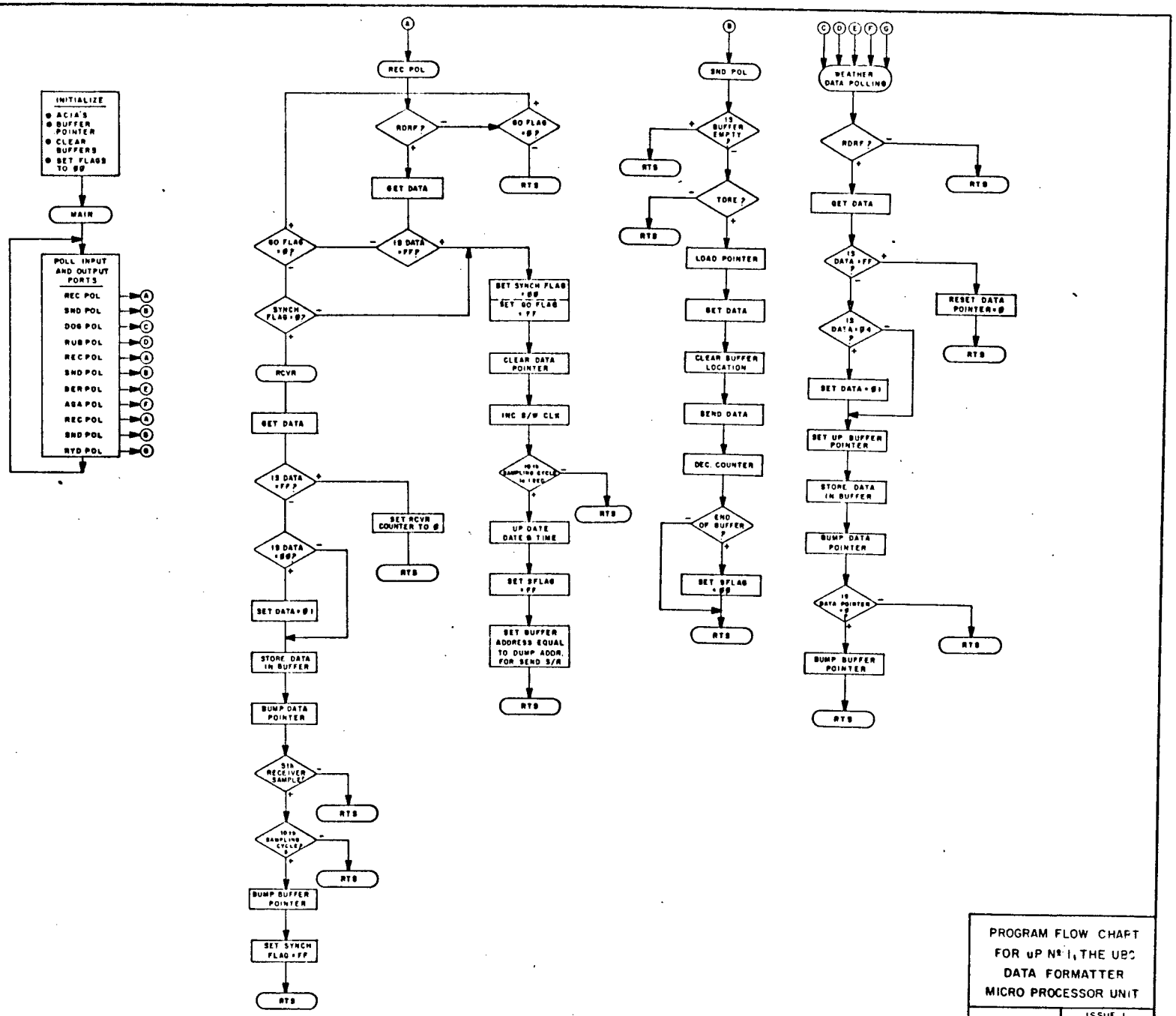

PROGRAM FLOW CHART FOR uP Nº 1, THE UBC DATA FORMATTER MICRO PROCESSOR UNIT

FIGURE J-1a | ISSUE 1 | MARCH 12, 982

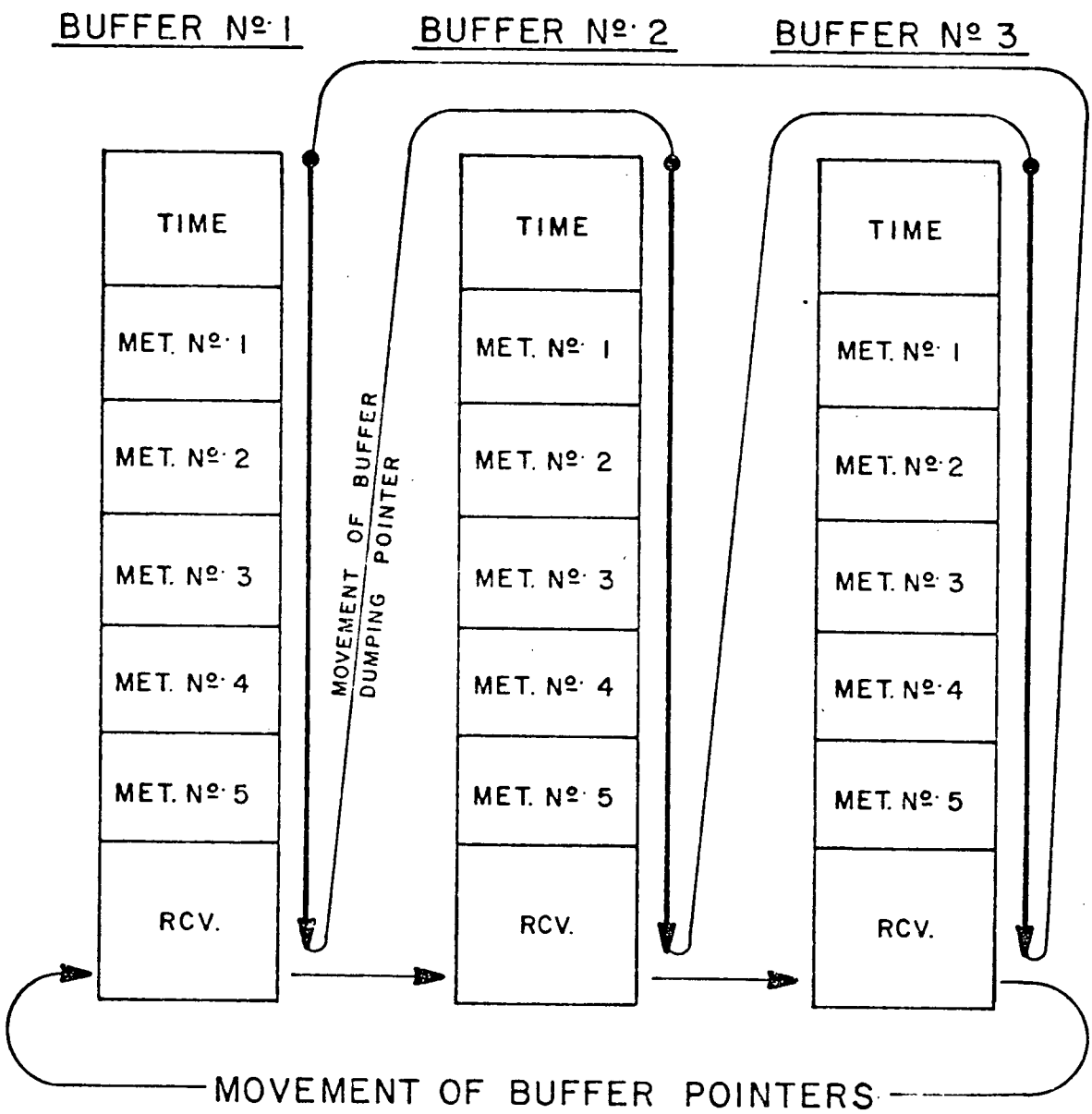

Figure J-1b Data Formatter (μP#1) Buffer Memory Organization

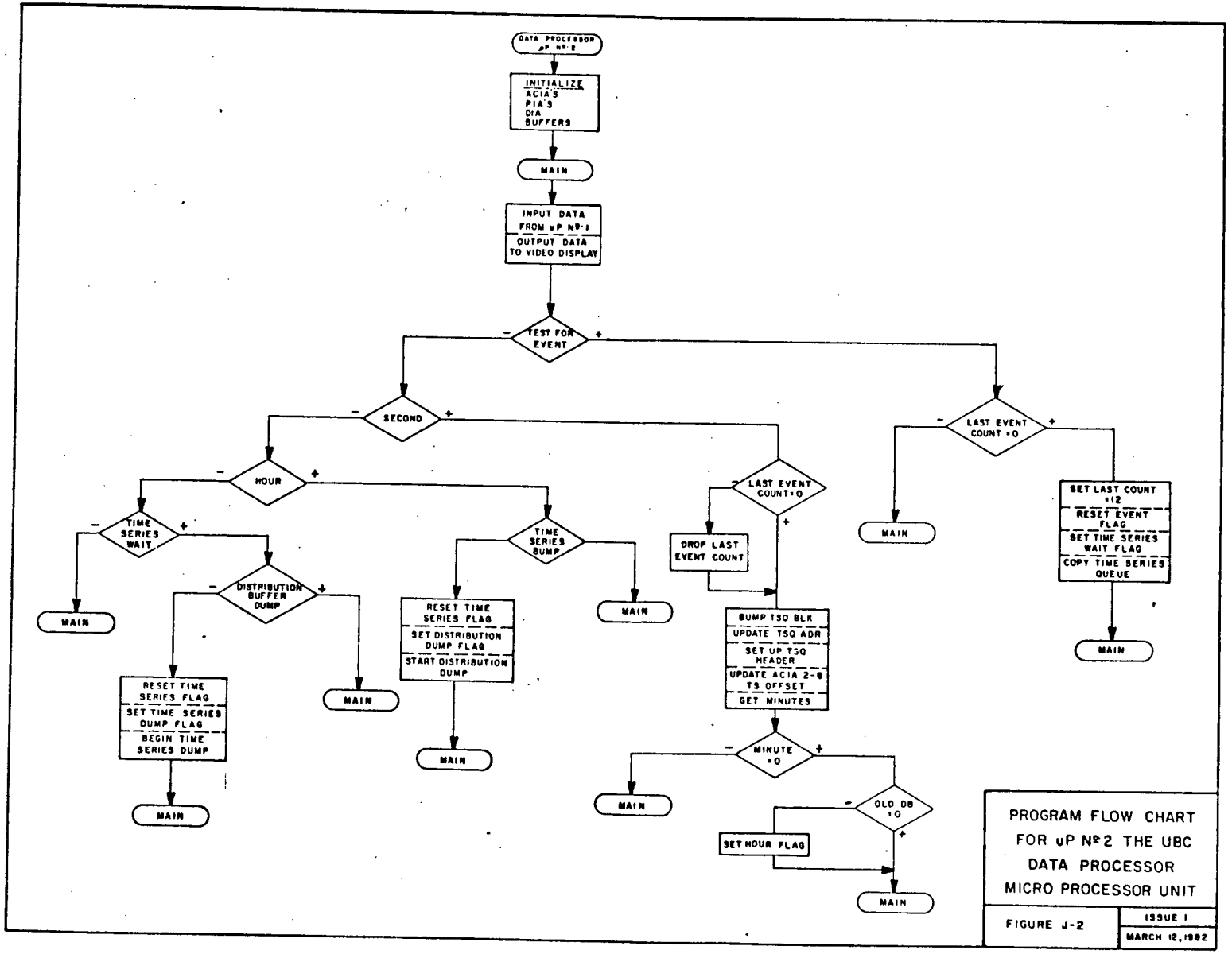
DATA PROCESSOR µP №2
INITIALIZE
ACIA'S
PIA'S
DIA
BUFFERS
MAIN
INPUT DATA FROM µP №1
OUTPUT DATA TO VIDEO DISPLAY
TEST FOR EVENT
SECOND
HOUR
TIME SERIES WAIT
DISTRIBUTION BUFFER DUMP
MAIN
RESET TIME SERIES FLAG
SET TIME SERIES DUMP FLAG
BEGIN TIME SERIES DUMP
MAIN
MAIN
TIME SERIES BUMP
RESET TIME SERIES FLAG
SET DISTRIBUTION DUMP FLAG
START DISTRIBUTION DUMP
MAIN
MAIN
LAST EVENT COUNT=0
DROP LAST EVENT COUNT
BUMP TSQ BLK
UPDATE TSQ ADR
SET UP TSQ HEADER
UPDATE ACIA 2-6 TS OFFSET
GET MINUTES
MINUTE =0
MAIN
OLD DB =0
SET HOUR FLAG
MAIN
LAST EVENT COUNT =0
MAIN
SET LAST COUNT =12
RESET EVENT FLAG
SET TIME SERIES WAIT FLAG
COPY TIME SERIES QUEUE
MAIN
PROGRAM FLOW CHART FOR uP №2 THE UBC DATA PROCESSOR MICRO PROCESSOR UNIT
FIGURE J-2
ISSUE 1
MARCH 12, 1982

(μP#2). The data processor then takes each byte of meteorological data updating its hourly distribution buffer, storing it in a rotating time series queue and outputting it for viewing to a video monitor.

III. Headers and Trailers

Every second the time series queue block is sent by the data formatter (μP#1) after being terminated by two "FF" trailer markers. Immediately following this a header for a new time series queue block is initialized, comprised of data bytes to identify record type, month, day, hour, minute and second.

IV. Criteria to Dump the Distribution Buffer

Every hour the buffer containing the distribution data in the data processor (μP#2) is dumped to the magnetic cassette recorder unless a time series dump is in progress. For this special case, the dump of the distribution buffer waits until the time series queue dump is completed before transferring the distribution data.

The distribution buffer is comprised of five types of data (wind direction, wind speed, temperature, rainfall and receiver amplitude) with five single byte distributions for each meteorological variable type and five double byte distributions for each receiver amplitude. Each meteorological distribution has $40_{16} = 64_{10}$ double byte bins and each receiver amplitude distribution has 128 double byte bins to give the following total memory required for one distribution buffer:

$$5 \times [7 + 4 \times 128 + 256 + 3] = 3890 \text{ bytes}$$

This includes a header of 7 bytes and a trailer of 3 bytes for each variable type. For two distribution buffers twice this number of bytes is required to give a total processor buffer requirement of 7780 bytes. Therefore, at 9600 bps the hourly dump will take 3.2 seconds.

V. Criteria to Dump the Time Series Data

Whenever an event is detected the time series queue is dumped from the buffer in the data processor (μP#2) to the cassette recorder unless a distribution dump is in progress. In this case the time queue is transferred into an output buffer to await completion of the distribution dump. The time series queue (TSQ) is comprised of:

$$12 \times [7 \text{ header} + 5\times4 \text{ meteorological} + 10\times5 \text{ receiver} + 1 \text{ event} + 2 \text{ trailer}] = 960 \text{ bytes}$$

At 9600 bps this will take a minimum of 1.0 seconds to output for storage.

The receiver event flag is tested in the MAIN program. If it is found to be set, the TSQ dump is initialized and the TSQ is copied to an output buffer to first allow completion of other I/O in progress. When a propagation event has been detected, the time series dump flag over the next 12 seconds is disabled so that a dump is not being requested every tenth of a second during the duration of the event.

Another consideration is that a flagged event will not, in general, occur conveniently at the end of an integral second which means when making the TSQ copy to the output buffer typically only 11 complete seconds of data would be transferred. The twelfth second block of data

would normally be incomplete and would consist on the average of five one-tenth of a second receiver sample sets and an incomplete meteorological set. The buffer must therefore be designed to hold 13 seconds to ensure a twelve second record. The resulting TSQ is given in Figure J-3, as follows:

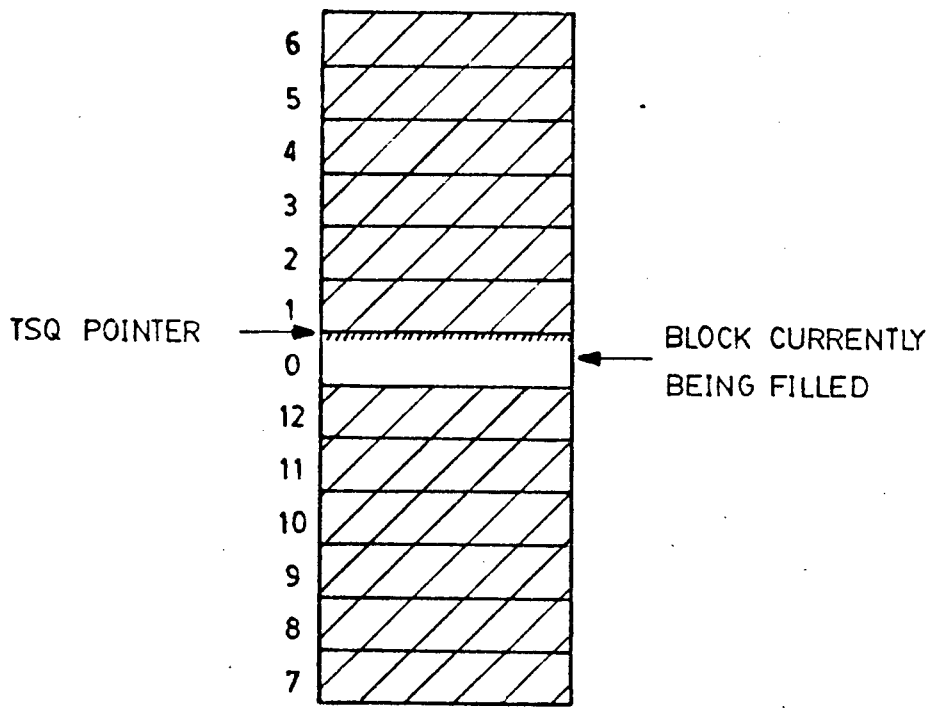

Figure J-3 Diagram Showing the Structure of the Time Series Queue (TSQ)

The TSQ pointer is used to find the first block for dumping and the next block for filling. When the event flag is set, the TSQ starting from the TSQ pointer is dumped. The dump pointer cycles around from the

high address to the low address and then upwards until the most recently completed block is encountered.

VI. Storage Requirements

The question arises as to how much data will be generated for storage. There are basically two types of data series; the first being distribution data recorded at 3890 bytes per hour and the second being TSQ data with a maximum rate of 288,000 bytes per hour but more typically 14,400 bytes per hour at an anticipated event probability of 0.05. Thus the total number of bytes expected to be recorded hourly is 18,290 bytes. At this rate the 4.5 mega byte magnetic cassette cartridges can be expected to last an average of 246 hours, or 10.25 days. This is expected to vary from 15.4 hours where all TSQ data are recorded to 48.2 days when no TSQ data are recorded.

iii) Software Clock

Real time is maintained through a software clock that is incremented upon the arrival of each synch byte and is kept on the basis of a 10 synch bytes equalling one second. The time is stored in RAM locations, 200-204 of the data formatter with the initial time being entered through the "SWTBUG" monitor (see Appendix I-1). Table J-1 gives the RAM time assignments which must be entered in hexedecimal format when initiallized.

Table J-1 RAM Time Assignments (μP#1)

Location	Assignment
0200	Month
0201	Day
0202	Hour
0203	Minute
0204	Second

iv) Data Formats

There are two basic data formats outputted by the data processor (μP#2); a time series format and a distribution series format. The time series format is given in Table J-2 and is repeated for each one second record dumped. A minimum of 12 one second records are dumped preceding an event with new time series records being dumped as long as the event persists. The distribution series format, on the other hand, is given in Table J-3 and is dumped hourly even if no propagation events occur.

Table J-2 Time Series Block Format

Byte	Description	Specific Comments
1	Record Type	FE = Time Series Block
2	Months	BCD
3	Days	BCD
4	Hours	BCD
5	Minutes	BCD
6	Seconds	BCD
7	Gauge Status	HEX
8	Wind Direction	Dog Mountain
9	Wind Speed	Dog Mountain
A	Temperature	Dog Mountain
B	Rainfall	Dog Mountain
C	Wind Direction	Ruby Creek
D	Wind Speed	Ruby Creek
E	Te-perature	Ruby Creek
F	Rainfall	Ruby Creek
10	Wind Direction	Bear Mountain
11	Wind Speed	Bear Mountain
12	Temperature	Bear Mountain
13	Rainfall	Bear Mountain
14	Wind Direction	Agassiz Experimental Farm
15	Wind Speed	Agassiz Experimental Farm
16	Temperature	Agassiz Experimental Farm
17	Rainfall	Agassiz Experimental Farm
18	Wind Direction	Ryder Lake
19	Wind Speed	Ryder Lake
1A	Temperature	Ryder Lake
1B	Rainfall	Ryder Lake
1C	Receiver 1	3550 MHz First 100 msec.
1D	Receiver 2	3790 MHz First 100 msec.
1E	Receiver 3	4010 MHz First 100 msec.
1F	Receiver 4	7142 MHz First 100 msec.
20	Receiver 5	7496.5 MHz First 100 msec.

Table J-2 Time Series Block Format (cont'd.)

Byte	Description	Specific Comments
21-25		Second 100 msec.
26-2H		Third 100 msec.
2B-2F		Fourth 100 msec.
30-34		Fifth 100 msec.
35-39		Sixth 100 msec.
3A-3E		Seventh 100 msec.
3F-43		Eighth 100 msec.
44-48		Ninth 100 msec.
49-4D		Tenth 100 msec.
4E	EVENT INDICATOR	cc = Fade 99 = Rain
4F-50	EOB TRAILER	Two consecutive FF's

Table J-3 Data Format for the Distribution Buffer

Byte	Description	Specific Comments
0	Record Type (FD)	FD = Distribution Series
1	Month	BCD
2	Day	BCD
3	Hour	BCD
4	Minute	BCD
5	Second	BCD
6	Data Type (01)	Data Type Control Word
7-86	Dog Mountain	Wind Direction Distribution
87-106	Ruby Creek	" " "
107-186	Bear Mountain	" " "
187-206	Agassiz Exp. Farm	Wind Direction Distribution
207-286	Ryder Lake	" " "
287	FF	Trailer
288	FF	"
289	FF	"

Table J-3 Data Format for the Distribution Buffer (cont'd.)

Byte	Description	Specific Comments
28A	Record Type (FD)	Header
28B	Month	"
28C	Day	"
28D	Hour	"
28E	Minute	"
28F	Seconds	Header
290	Data Type (02)	"
291-310	Dog Mountain	Wind Speed Distribution
311-390	Ruby Creek	" " "
391-410	Bear Mountain	" " "
411-490	Agassiz Exp. Farm	Wind Speed Distributions
491-510	Ryder Lake	" " "
511	FF	Trailer
512	FF	"
513	FF	"
514	Record Type (FD)	Header
515	Month	"
516	Day	"
517	Hour	"
518	Minute	"
519	Second	Header
51A	Data Type (04)	"
51B-59A	Dog Mountain	Temperature Distribution
59B-51A	Ruby Creek	" "
51B-69A	Bear Mountain	" "
69B-71A	Agassiz Exp. Farm	Temperature Distribution
71B-79A	Ryder Lake	" "
79B	FF	Trailer
79C	FF	"
79D	FF	"
79E	Record Type (FD)	Header
79F	Month	"
780	Day	"
781	Hour	"
782	Minute	"

Table J-3 Data Format for the Distribution Buffer (cont'd.)

Byte	Description	Specific Comments
783	Second	Header
784	Data Type (08)	"
7A5 824	Dog Mountain	Rainfall Distribution
825-8A4	Ruby Creek	" "
8A5-924	Bear Mountain	" "
925-9A4	Agassiz Exp. Farm	Rainfall Distribution
9A5-A24	Ryder Lake	" "
A25	FF	Trailer
A26	FF	"
A27	FF	"
A28	Record Type (FD)	Header
A29	Month	"
A2A	Day	"
A2B	Hour	"
A2C	Minute	"
A2D	Second	Header
A2E	Data Type (10)	"
A2F-B2E	Receiver 1 (3550 MHz)	Received Signal Distribution
B2F-C2E	Receiver 2 (3790 MHz)	" " "
C2F-D2E	Receiver 3 (4010 MHz)	" " "
D2F-E2E	Receiver 4 (7142 MHz)	Received Signal Distribution
E2F-F2E	Receiver 5 (7496 MHz)	" " "
F2F	FF	Trailer
F30	FF	"
F31	FF	"

J-2 The Ryder Lake 6800 Microprocessor Software

The purpose of the Ryder Lake software is to coordinate the sampling for both the meteorological variables and receiver signal amplitudes and transmit these on two links; a low speed (110 bps) link and a high speed (1200 bps) link respectively to UBC. The software flow chart to do this is given in Figure J-4. The program starts by initializing the ACIA I/O ports and A/D and

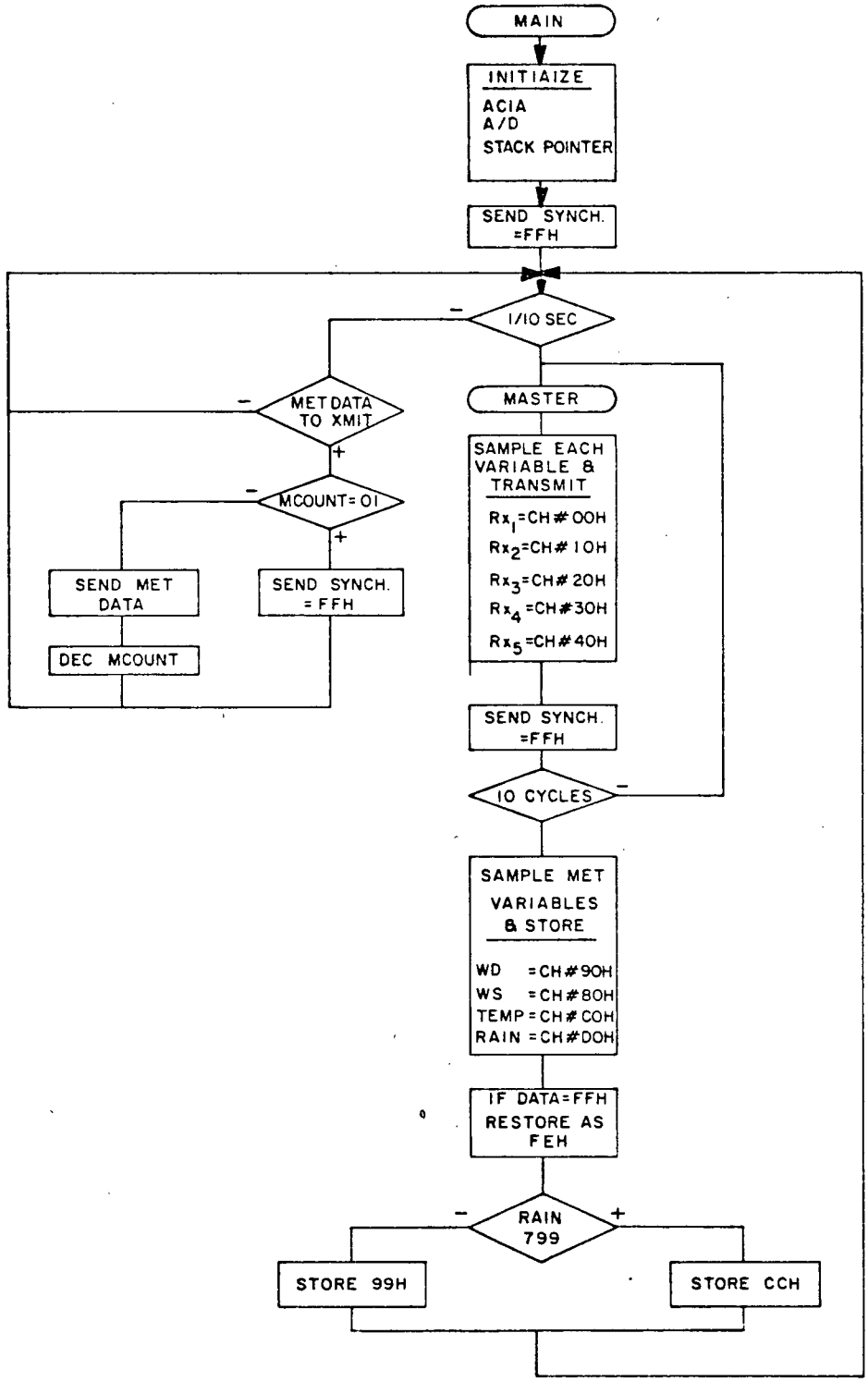

Figure J-4 Data Acquisition Flow Chart for the Ryder Lake Datalog 6800 Microprocessor.

then waits to sample data. The basic sampling interval is 1/10 of a second at which time the receivers are sampled and their data sent. Every tenth interval, that is for each second, the meteorological variables are sampled and the data transferred to an output buffer for transmission. In this way the received signal levels are sent as soon as they are sampled, whereas the meteorological data are sent, one at a time, from an output buffer. The ACIA output ports at Ryder Lake are configured for one start and one stop bit which are matched by the UBC microprocessor data formatter input ports.

J-3 The Weatherlog 8085 Microprocessor Software

The purpose of the weatherlog software is to coordinate a one second A/D sampling interval of the four meteorological variables: wind speed, wind direction, temperature and rain, and then send these data on the communication channel to UBC at a rate of 110 bps. The weatherlog software flow chart is given in Figure J-5 and is the same for the Dog Mountain, the Ruby Creek and the Agassiz Experimental Farm site locations. As shown, the program starts by initializing the stack pointer, the A/D channels and the software delay loop. Then after each second the variables are sampled and outputted through the SOD pin of the 8085 microprocesor to the communications link. This cycle is repeated every second which is determined by a program delay loop. If any software changes are made to the main program software the delay loop must be recalibrated. This is facilitated by monitoring the rain clear output connector of the microprocessor (see Figure I-6) and using a frequency meter to measure the sampling interval.

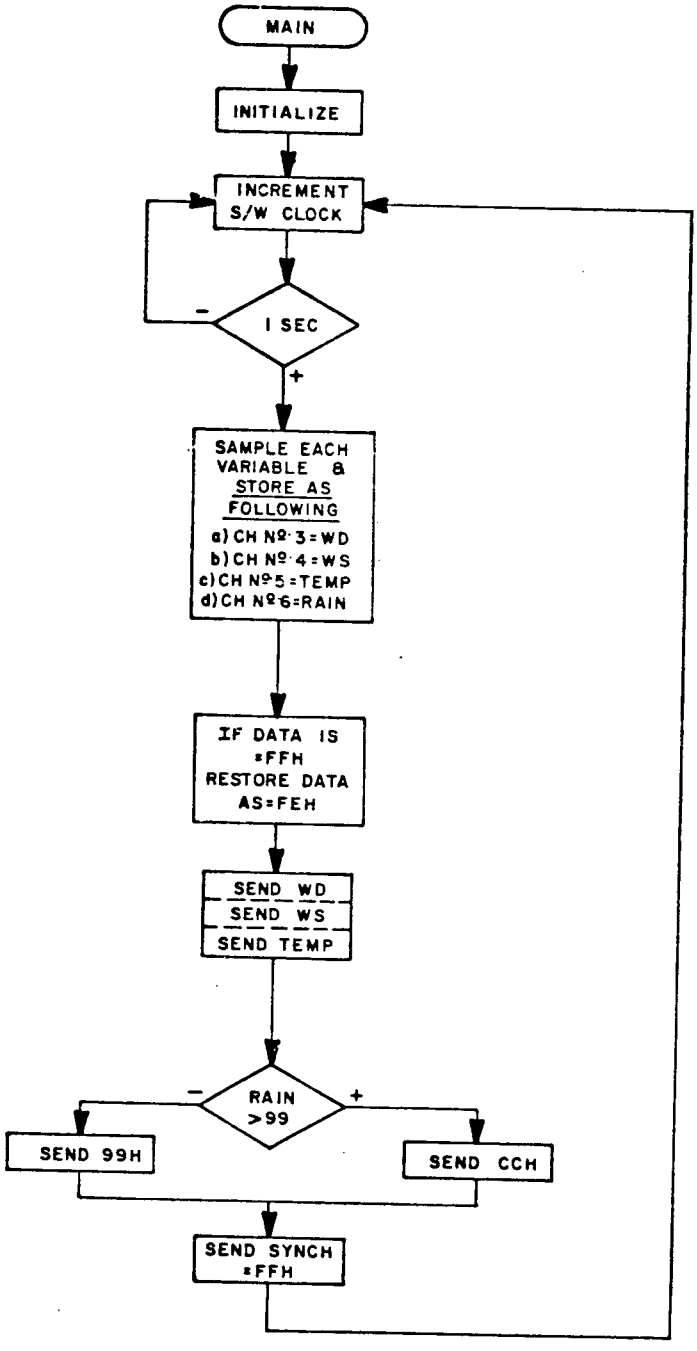

Figure J-5 Program Flow Chart for the UBC Weatherlog 8085 Data Acquisition Microprocessors

J-4 The Bear Mountain 1802 Microprocessor Software

Functionally, the Bear Mountain RCA 1802 microprocessor software shown in the flow chart of Figure J-6, is the same as the 8085 weatherlog. The only differences are in the method by which the timing for the one second sampling interval and the 110 bps data stream are derived. Instead of using software derived delay loops as is done in the 8085 system the 1802 software relies on externally derived interrupt pulses to establish sampling intervals and transmission timing.

J-5 The NOVA 840 Minicomputer Data Transfer Software

The purpose of this software is to transfer data from the magnetic cassette recorder to the magnetic reel-to-reel tape on the NOVA 840. The software flow chart for this data transfer operation is given in Figure J-7. After initialization, the program first requests a block of data (2k bytes) from the cassette recorder by issuing an ASCII control command. The NOVA then converts the data to EBCDIC characters and outputs the block to the magnetic tape. After transferring one block another is requested for transfer and the process is repeated.

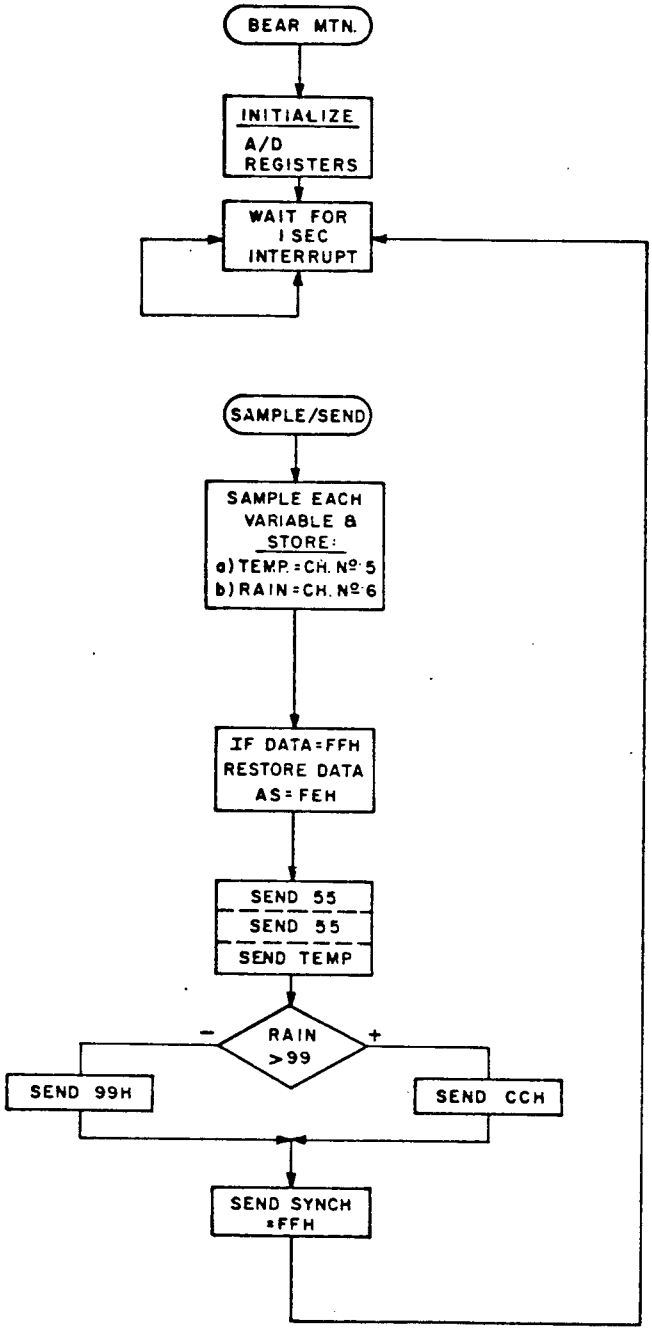

Figure J-6 Data Acquisition and Control Program Flow Chart for the Remote Bear Mountain 1802 Microprocessor Unit

J-4 The Bear Mountain 1802 Microprocessor Software

Functionally, the Bear Mountain RCA 1802 microprocessor software shown in the flow chart of Figure J-6, is the same as the 8085 weatherlog. The only differences are in the method by which the timing for the one second sampling interval and the 110 bps data stream are derived. Instead of using software derived delay loops as is done in the 8085 system the 1802 software relies on externally derived interrupt pulses to establish sampling intervals and transmission timing.

J-5 The NOVA 840 Minicomputer Data Transfer Software

The purpose of this software is to transfer data from the magnetic cassette recorder to the magnetic reel-to-reel tape on the NOVA 840. The software flow chart for this data transfer operation is given in Figure J-7. After initialization, the program first requests a block of data (3k bytes) from the cassette recorder by issuing an ACSII control command. The NOVA then converts the data to EBCDIC characters and outputs the block to the magnetic tape. After transferring one block another is requested for transfer and the process is repeated.

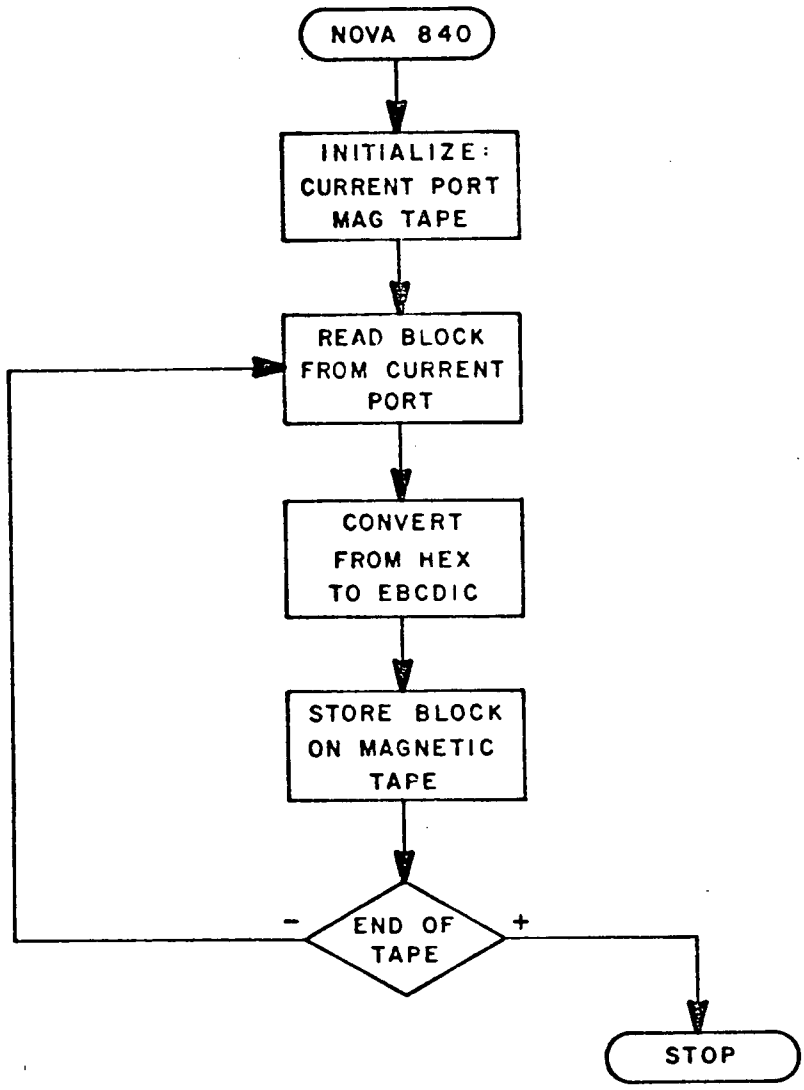

Figure J-7 Program Flow Chart to Transfer Data from Cassette Tapes to Magnetic Tape Using the Nova 840.

APPENDIX K

THE BRIGHT BAND PROPAGATION EXPERIMENT'S DATA BASE MANAGEMENT SYSTEM

K-1 Introduction

This appendix gives the documentation to facilitate program development and maintenance of the data base management system (DBMS) used in this bright band propagation experiment. As described in Chapter IV, the data acquisition system generates sufficiently large volumes of data to make the bright band research project impractical unless a computerized data reduction, storage and analysis system is utilized. Thus the data handling function performed by DBMS is an integral part of this research project since it is responsible to provide the data analysis and graphical outputs which are used to draw the experimental conclusions.

K-2 The System

DBMS is a sequential system where the input is raw experimental data and the output is given as a presentation of graphical results via plotting routines. A functional flowchart relative to the bright band experiment showing their developmental status to the completion of this thesis work is given in Figure K-1.

In terms of DBMS development, the entry procedure is complete, and an integrated plotting package which includes routines to plot attenuation with path average rain rate, individual rain rates, site temperature, site differential temperature, differential temperature, temperature gradient and wind

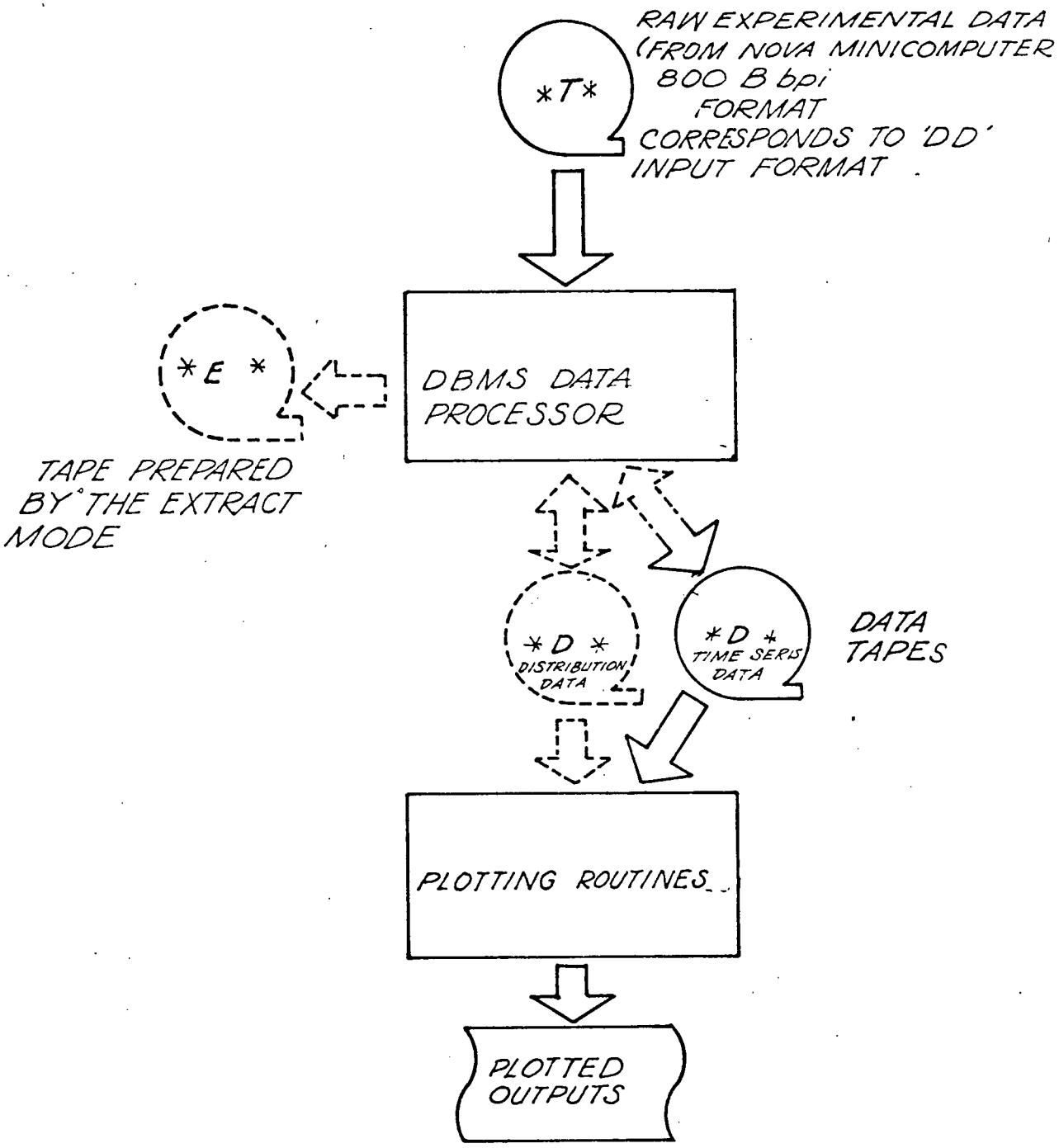

Figure K-1 DBMS Functional Flow Chart Showing Completion Status

speed as a function of time, have been finished. Several DBMS packages are still under development and these include the "SCAN" function, the "EXTRACT" function and several "PLOT" routine options.

A detailed description of the major system software packages which comprise DBMS are dealt with in the following sections. These include the main DBMS program, the bright band "ENTER" function, the data directory, and the "PLOT" routine options. All these system packages use the Fortran IV-G compiler.

K-3 DBMS Main

The DBMS main program initializes the system and delegates program control to user requested operating modes as shown in its software flow chart given in Figure K-2. At the present time the "ENTER" and "PLOT" modes are fully integrated into DBMS, however, it is anticipated that the "SCAN" and the "EXTRACT" mode will be incorporated into the system during the next phase of this research program.

K-4 "ENTER"

"ENTER" is a conversion algorithm designed to convert recorded hex values to floating point engineering units for analysis. When the "ENTER" option is envoked the disc file or tape containing the hex information is read, converted to engineering units and then outputted to a temporary disc file, "-DATA". These data can then be analyzed using "PLOT" or stored to permanent disc files or on magnetic tape using MTS "FILESAVE".

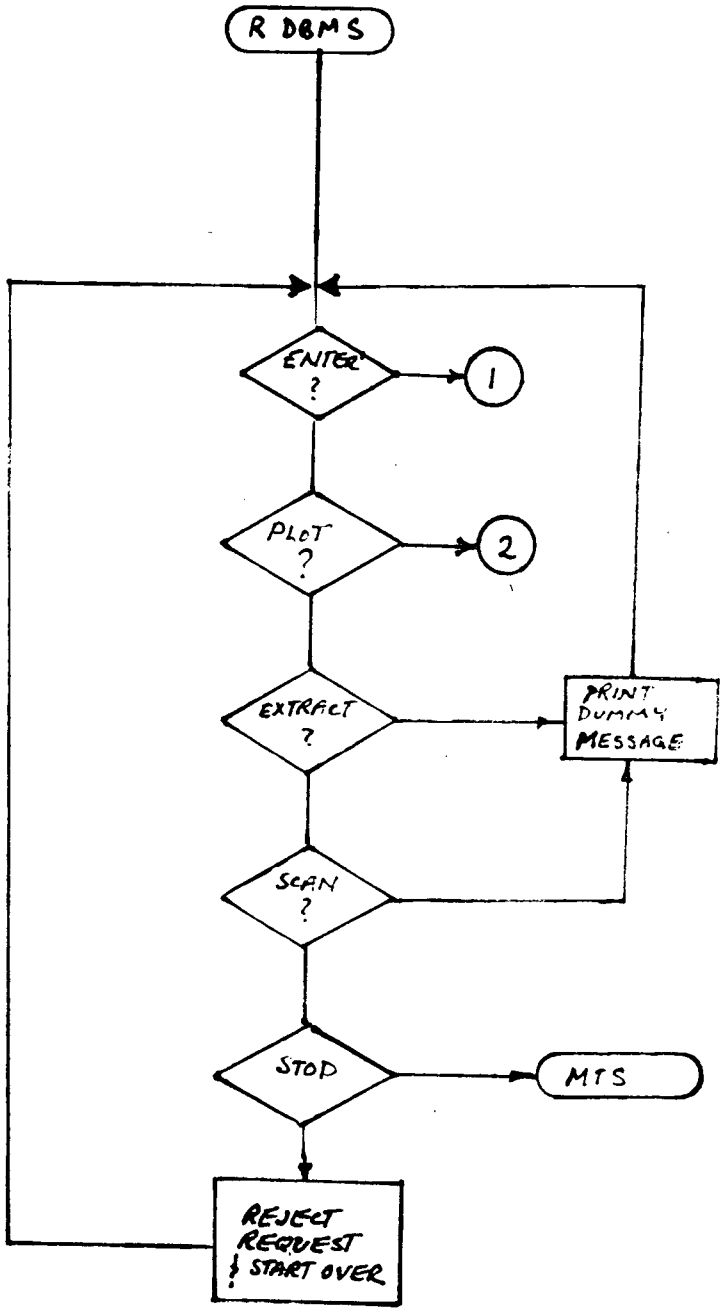

Figure K-2 DBMS Main Program Flow Chart

K-5 The Data Directory

Each of the formats into and out of the DBMS entry procedure are specified by a data directory. Each item in the directory is separately and parametically defined so changes can be made to it without changing the executable software. Since the data directory defines the DBMS input and output formats, it is central to the development of new entry procedures for other experiments.

A listing of the data directory used in the entry procedure for the bright band experiment is given in Table K-1. The lettered labels for the column headings can be defined in more detail, as follows:

A. Record sequence number; a label (not entered as part of the data directory),

B. Field Name; descriptor of the data elements,

C. Tape Type Number; 1 for output and 2 for input tape,

D. Variable Type Number; "1" for 2 byte or 1 half-word size and "2" for 4 byte or 2 half-word size data fields,

E. Starting byte position of this field in the data record,

F. Ending byte position of this field in the data record,

G. Field extraction parameter; gives the optional default specification,

H. Data variable encoding format.

Table K-1 Data Directory for the Time Series Format

A	B	C	D	E	F	G	H
1	Record Type	2	1	1	2		BCD
2	Month	2	1	3	4		BCD
3	Days	2	1	5	6		BCD
4	Hours	2	1	7	8		BCD
5	Minutes	2	1	9	10		BCD
6	Seconds	2	1	11	12		BCD
7	Gaugestatus	2	1	13	14		HEX
8	Dog-Wind DN	2	1	15	16	00	HEX
9	Dog-Wind SP	2	1	17	18	00	HEX
10	Dog-Temp	2	1	19	20	00	HEX
11	Dog-Rain	2	2	21	22	00	HEX
12	RBY-Wind DN	2	1	23	24		HEX
13	RBY-Wind SP	2	1	25	26	00	HEX
14	RBY-Temp	2	1	27	28	00	HEX
15	RBY-Rain	2	2	29	30	00	HEX
16	Bar-Wind DN	2	1	31	32	00	HEX
17	Bar-Wind SP	2	1	33	34	00	HEX
18	Bar-Temp	2	1	35	36	00	HEX
19	Bar-Rain	2	2	37	38	00	HEX
20	AGZ-Wind DN	2	1	39	40	00	HEX
21	AGZ-Wind SP	2	1	41	42	00	HEX
22	AGZ-Temp	2	1	43	44	00	HEX
23	AGZ-Rain	2	2	45	46	00	HEX
24	RLK-Wind DN	2	1	47	48	00	HEX
25	RLK-Wind SP	2	1	49	50	00	HEX
26	RLK-Temp	2	1	51	52	00	HEX
27	RLK-Rain	2	2	53	54	00	HEX
28	01-RX1:3550	2	1	55	56		HEX
29	01-RX2:3790	2	1	57	58		HEX
30	01-RX3:4010	2	1	59	60		HEX
31	01-RX4:7142	2	1	61	62		HEX
32	01-RX5:7496	2	1	63	64		HEX
33	02-RX1:3550	2	1	65	66		HEX
34	02-RX2:3790	2	1	67	68		HEX
35	02-RX3:4010	2	1	69	70		HEX

Table K-1 Data Directory for the Time Series Format (cont'd.)

A	B	C	D	E	F	G	H
36	02-RX4:7142	2	1	71	72		HEX
37	02-RX5:7496	2	1	73	74		HEX
38	03-RX1:3550	2	1	75	76		HEX
39	03-RX2:3790	2	1	77	78		HEX
40	03-RX3:4010	2	1	79	80		HEX
41	03-RX4:7142	2	1	81	82		HEX
42	03-RX5:7496	2	1	83	84		HEX
43	04-RX1:3550	2	1	85	86		HEX
44	04-RX2:3790	2	1	87	88		HEX
45	04-RX3:4010	2	1	89	90		HEX
46	04-RX4:7142	2	1	91	92		HEX
47	04-RX5:7496	2	1	93	94		HEX
48	05-RX1:3550	2	1	95	96		HEX
49	05-RX2:3790	2	1	97	98		HEX
50	05-RX3:4010	2	1	99	100		HEX
51	05-RX4:7142	2	1	101	102		HEX
52	05-RX5:7496	2	1	103	104		HEX
53	06-RX1:3550	2	1	105	106		HEX
54	06-RX2:3790	2	1	107	108		HEX
55	06-RX3:4010	2	1	109	110		HEX
56	06-RX4:7142	2	1	111	112		HEX
57	06-RX5:7496	2	1	113	114		HEX
58	07-RX1:3550	2	1	115	116		HEX
59	07-RX2:3790	2	1	117	118		HEX
60	07-RX3:4010	2	1	119	120		HEX
61	07-RX4:7142	2	1	121	122		HEX
62	07-RX5:7496	2	1	123	124		HEX
63	08-RX1:3550	2	1	125	126		HEX
64	08-RX2:3790	2	1	127	128		HEX
65	08-RX3:4010	2	1	129	130		HEX
66	08-RX4:7142	2	1	131	132		HEX
67	08-RX5:7496	2	1	133	134		HEX
68	09-RX1:3550	2	1	135	136		HEX
69	09-RX2:3790	2	1	137	138		HEX
70	09-RX3:4010	2	1	139	140		HEX

Table K-1 Data Directory for the Time Series Format (cont'd.)

A	B	C	D	E	F	G	H
71	09-RX4:7142	2	1	141	142		HEX
72	09-RX5:7496	2	1	143	144		HEX
73	10-RX1:3550	2	1	145	146		HEX
74	10-RX2:3790	2	1	147	148		HEX
75	10-RX3:4010	2	1	149	150		HEX
76	10-RX4:7142	2	1	151	152		HEX
77	10-RX5:7496	2	1	153	154		HEX
78	EVENT FLAG	2	1	155	156		HEX
79	FF END OF BLOCK	2	1	157	158		HEX
80	FF "	2	1	159	160		HEX

K-6 "PLOT"

"PLOT" is an integrated interactive plotting package specifically designed for presenting the recorded measurements in a graphical time series format. The plotting options developed in work are as follows:

1. Rain rate and one receiver signal versus time;
2. Temperature -
   a) site temperature and one receiver signal versus time,
   b) site differential temperature and one receiver signal versus time,
   c) site to site differential temperature and one receiver signal versus time,
   d) temperature gradient and one receiver level versus time;
3. Site windspeed and one receiver level versus time;
4. Two receiver signals versus time (one second average);
5. High resolution two receiver levels versus time (all 1/10 second sample points).

In all these plot options the scales and offsets are interactively adjustable.

The "PLOT" package takes source data in engineering units from the "-DATA" tempory file, processes it for the plotter into another temporary file called "-PLOT#". The plot can then be previewed using PLOTSEE and routed for output to the CALCOMP plotters or to a printronix printer (RMPROUTE=PTRXPLOT for the best output). A sample plotting rum is given in Figure K-3.

```
        PROPAGATION DATA PLOTTING SYSTEM
        ********** **** ******** ******

SELECT OUTPUT OPTION REQUIRED (ENTER FUNCTION NUMBER)

  (1) TIME SERIES PLOT OF ONE RECEIVER SIGNAL STRENGTH
      AND ONE RAIN RATE

  (2) TIME SERIES PLOT OF ONE RECEIVER SIGNAL STRENGTH
      AND ONE OF SEVERAL TEMPERATURE DISPLAY OPTIONS

  (3) TIME SERIES PLOT OF ONE RECEIVER SIGNAL STRENGTH
      AND WIND SPEED

  (4) TIME SERIES PLOT OF TWO RECEIVER SIGNAL STRENGTHS

  (5) INTERIM VERSION OF TEMPERATURE GRADIENT PLOT

4.

ENTER CODE FOR SOURCE FILE DESIRED:
     1 => TEST SCRATCH FILE "-DATA"
     2 => PERMANENT DISK FILE "D001.DAT"
1.
ENTER STARTING RECORD NO. TO BE PLOTTED: (I6)
1.
ENTER NO. OF RECORDS TO BE PLOTTED: (I6)
8000.
PLOT WILL DISPLAY  8000 RECORDS, STARTING WITH NO.     1
ARE DEFAULT VALUES OF FIRST RX. SIGNAL LEVEL DISPLAY OK?
     ORIGIN VALUE =  -40.00
     INCREMENT    =    5.00
     ENTER "<CR>" OR "NO"
NO
ENTER ORIGIN VALUE: (F5.0)
-65..
ENTER INCREMENT VALUE: (F5.0)
5..
ARE DEFAULT VALUES OF SECOND RX. SIGNAL LEVEL DISPLAY OK?
     ORIGIN VALUE =  -40.00
     INCREMENT    =    5.00
     ENTER "<CR>" OR "NO"
NO
ENTER ORIGIN VALUE: (F5.0)
-50..
ENTER INCREMENT VALUE: (F5.0)
5..
ENTER DISPLAY RESOLUTION CODE:
     1 => ONE PLOTTED POINT PER SECOND
     2 => TEN PLOTTED POINTS PER SECOND
1.
ARE DEFAULT VALUES OF TIME AXIS DISPLAY OK?
     ORIGIN VALUE =    0.0
     INCREMENT    =    1.00
     ENTER "<CR>" OR "NO"
NO
ENTER ORIGIN VALUE: (F5.0)
0..
ENTER INCREMENT VALUE: (F5.0)
10..
FOR FIRST RECEIVER CHANNEL:
ENTER RECEIVER NUMBER TO BE SELECTED:
     1 => 3550 MHZ.          2 => 3990 MHZ.
     3 => 4010 MHZ.          4 => 7142 MHZ.
     5 => 7496 MHZ.
3.
FOR SECOND RECEIVER CHANNEL:

5.
TYPICAL RESULTS: (INCHES)

  SEQ. NO.          X          RX. #1          RX. #2

      1           1.00           5.88            1.82
   1201           3.00           5.83            0.27
   2401           5.00           5.50            0.44
   3601           7.00           5.86            1.45
   4801           9.00           5.69            0.91
   6001          11.00           5.74            0.88
   6002          11.00           5.74            0.92

 SUCCESSFULLY READ   8001 DATA RECORDS
 PLOTTING WILL TAKE APPROX.    3 MIN.  53 SEC. AND   14 INCHES OF PAPER.
 MAXIMUM Y VALUE IS APPROX.   10 INCHES.
   0 MIN   51 SEC, OR  22% OF TOTAL PLOT TIME IS WITH PEN UP.
 SUCCESSFUL PLOT.
#Execution Terminated
# $16.13,  $41.87T
#SET RMPROUTE=PTRXPLOT
#   $.01,  $41.89T
#R *PLOTSEE O=-PLOT#
#Execution Begins
```

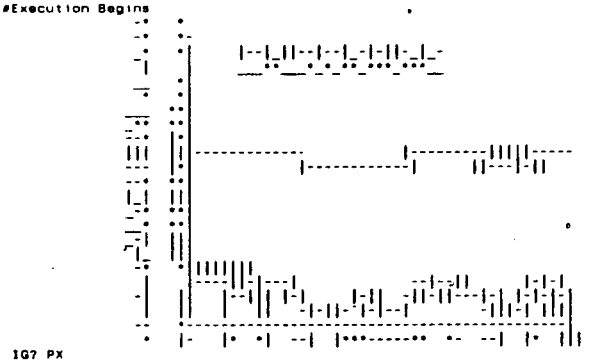

```
 IG? PX
 *RMPRINT* assigned job number 462548
 Printronix plot generation done.
 IG? PX
 Printronix plot generation done.
 IG? PX
 Printronix plot generation done.
 IG?
 End of plots. Last chance to use *IG.
 IG?
#*RMPRINT* RM462548 released to PTRXPLOT 6 pages PRIORITY=NORMAL

  DEVICETYPE=PTRX
#Execution Terminated
```

Figure K-3 Sample Plotting Run

REFERENCES

1. Van Trees, H., Hoversten, E., and McGarty, T., "Communications Satellites: Looking into the 1980's", IEEE Spectrum, pp. 43-51, Dec. 1977.

2. GTE Lenkurt, Engineering Considerations for Microwave Communication Systems, 1970.

3. Silverthorn, D., and Tetarenko, R., "Microwave Radio Spreads TV", Telesis, vol. 5, pp. 209-213, 1976.

4. HervieUx, P., "RD-3: an 8 GHz Digital Radio System for Canada", Telesis, vol. 4, pp. 53-59, 1975.

5. Anderson, C., Barber, S., and Patel, R., "Propagation Experiments Show Path to Success", Telesis, vol. 6, pp. 180-185, 1977.

6. Stephansen, E., "Review of Clear-Air Propagation on Line-of-Sight Radio Paths", URSI Symposium on Effects of the Lower Atmosphere on Radio Propagation at Frequencies Above 1 GHz", Lennoxville, Quebec, Canada, 26-30 May, 1980.

7. Dougherty, H., "A Survey of Microwave Fading Mechanisms Remedies and Applications", ESSA Technical Report ERL69-WPL4, Boulder Co., NTIS Access No. COM-71-50288, Mar. 1968.

8. Segal, B., and Barrington, R., "The Radio Climatology of Canada - Tropospheric Refractivity Atlas for Canada", Communications Research Centre, Ottawa, CRC Rpt. #1315, Dec. 1977.

9. Bean, B., Cahoon, B., Samson, C., and Thayer, G., "A World Atlas of Atmospheric Radio Refractivity", Boulder Co. ESSA Monograph 1, NTIS Access No. AD648-805, 1966.

10. International Radio Consultive Committee (CCIR), XIVth Plenary Assembly, Koyoto, Japan, vol. V, 1978.

11. Bullington, K., "Radio Propagation Fundamentals", BSTJ, vol. 36, pp. 593-627, May 1957.

12. Ryde, J., and Ryde, D., General Electric Corporation Report, #7831, 1941; #8516, 1944; #7831, 1941; #9670, 1945.

13. Ryde, J.W., "The Attenuation and Radar Echos Produced at Centimetre Wave-Lengths by Various Meteorological Phenomena", Rpt. of the Physics Society, London and the Royal Meteorological Soc. entitled "Meteorological Factors in Radio-Wave Propagation".

14. Medhurst, R.C., "Rainfall Attenuation of Centimeter Waves: Comparison of Theory and Measurement", IEEE Trans. Ant. & Prop., vol. AP-13, vol. 4, pp. 550-564, 1965.

15. Robertson, S., and King, A., "The Effect of Rain Upon the Propagation of Waves in the 1 and 3 Centimeter Regions", Proc. IRE, vol. 34, pp. 178P-180P, 1946.

16. Okamura, S., Funakawa, K., Uda, H., Kato, J., and Oguchi, T., "On the Measurement of Attenuation by Rain at 8.6 mm Wave Length", J. Radio Research Labs (Tokyo), vol. 6, pp. 255-267, April 1959.

17. Robinson, N., "Measurements of the Effect of Rain, Snow and Fogs on 8.6 mm Radar Echos", Proc. IEE, vol. 102, pt. B, pp. 709-714, Sept. 1955.

18. Funakawa, K., and Kata, J., "Experimental Studies of Propagation Characters of 8.6 mm Wave on a 24 km Path", J. Radio Research Labs (Tokyo), vol. 9, pp. 351-367, Sept. 1962.

19. Crane, R., "Propagation Phenomena Affecting Satellite Communication Systems Operating in the Centimeter and Millimeter Wavelength Bands", Proc. IEEE, vol. 59, pp. 173-188, Feb. 1971.

20. Rodgers, C.V., and Olsen, R.L., "Calculation of Radio Wave Attenuation Due to Rain at Frequencies up to 1000 GHz", Communications Research Centre (Canada), Rpt. #1299, 1976.

21. Crane, R.K., "Attenuation Due to Rain - A Mini Review", IEEE Trans. Antennas and Propagation, AP-23, pp. 750-752, 1975.

22. Olsen, R.L., Rodgers, D.V., and Hodge, D.B., "The aR^b Relation in the Calculation of Rain Attenuation", IEEE Trans. on Antennas and Propagation, AP-26, pp. 218-239, 1978.

23. Laws, J.O., and Parsons, D.A., "The Relation of Drop Size to Intensity", Amer, Geophys. Union Trans., vol. 22, pp. 452-460, 1943.

24. Marshall, J., and Palmer, W., "The Distribution of Raindrops with Size", J. Meteorology, vol. 5, pp. 165-177, 1948.

25. Joss, J., Thams, J., and Waldvogel, A., "The Variation of Raindrop Size Distributions at Lacarno", in Proc. of the Intl. Conf. on Cloud Physics, Toronto, Canada, pp. 369-373, 1968.

26. Fedi, F., and Mandarini, P., "Influence of Spacing and Integration Time of the Raingauges on the Attenuation Rain Rate Relationship", J. Rech. Atm., vol. 8, #1-2, 1974.

27. Semplak, R., and Keller, H., "A Dense Network for Rapid Measurement of Rainfall Rate", BSTJ, pp. 1745-1756, July-Aug. 1969.

28. GTE Lenkurt, "Antenna Decoupling Due to Non-Selective Power Fading", Demodulator, vol. 27, #3, pp. 1-6, Mar. 1978.

29. DeLange, O., "Propagation Studies of Microwave Frequencies by Means of Very Short Pulses", BSTJ, vol. 31, #1, pp. 91-103, Jan. 1952.

30. Meadows, R., Lindgren, R., and Samuel, J., "Measurement of Multipath Propagation Over a Line-of-Sight Radio Link at 4 Gc/s Using Frequency Sweep Technique", Proc. IEE, vol. 113, #1, pp. 41-48, Jan. 1966.

31. Rummler, W., "Extentions of the Multipath Fading Channel Model", Intl. Conf. on Commun., vol. 2, Boston, Mass., pp. 32.2.1-32.2.5, June 1979.

32. Sasaki, O., and Akiyama, T., "Multipath Delay Characteristics on Line-of-Sight Microwave Radio System", IEEE Trans. on Commun., vol. COM-27, #12, pp. 1876-1886, Dec. 1979.

33. Sanberg, J., "Extraction of Multipath Parameters from Swept Measurements on a Line-of-Sight Path", IEEE Trans. Ant. and Prop., vol. AP.

34. Martin, L., "Etude de la Selective des Evanouissements dus aux Trajets Multiple", URSI Comm. F. Symposium, Lennoxville, Quebec, Canada, pp. 3.5.1-3.5.5, May 1980.

35. Bello, P., Pickering, L., and Boardman, C., "Multipath Over LOS Channels Study", Rpt. by CNR INC for Rome Air Development Center, Air Force Systems Command, Griffiss Air Force Base, N.Y. 13441, Aug. 1977.

36. Barnett, W., "Multipath Propagation at 4, 6 and 11 GHz", BSTJ, vol. 51, #2, pp. 321-361, Feb. 1972.

37. Weibel, G., and Dressel, H., "Propagation Studies in Millimeter-Wave Link Systems", Proc. IEEE, vol. 55, pp. 497-513, Apr. 1967.

38. Vigants, A., "Number and Duration of Fades at 6 and 4 GHz", BSTJ, vol. 50, #3, pp. 815-841, Mar. 1971.

39. Watson, P., "Survey of Measurements of Attenuation by Rain and Other Hydrometeors", Proc. IEE, vol. 123, pp. 863-871, 1976.

40. Oomori, T., and Aoyagi, S., "A Presumptive Formula for Snowfall Attenuation of Radio Waves", Elec. & Comm. in Japan, vol. 54-B, #9, pp. 34-39.

41. Kolosov, M.A., Poshidaer, V.N., Sokolov, A.V., and Sukhoniu, E.V., "The Prediction of Millimetre Radio Wave Attenuation in Precipitation", IVCRM Colloquim, Nice, France, Preprints paper IV-12, Oct. 1973.

42. McCormick, K.S., "A Comparison of Precipitation Attenuation and Radar backscatter Along Earth-Space Paths", IEEE Trans. Ant. and Prop., AP-20, #6, pp. 747-755, 1972.

43. Goldhirsh, J., "Attenuation of Propagation Through Rain for an Earth-Satellite Path Correlated with Predicted Values Using Radar", IEEE Trans. Ant. and Prop., AP-24, pp. 800-806, 1976.

44. Dissanayake, A.W., and McEwan, J.J., "Radar and Attenuation Properties of Rain and Bright Band", IEE Antennas and Propagation Conf. Proc., London, Eng., Nov. 1978.

45. Goldhirsh, J., "A Review on the Application of Nonattenuating Frequency Radars for Estimating Rain Attenuation and Space Diversity Peformance", IEEE Trans. on Geoscience Elec., vol. GE-17, #4, pp. 218-239, 1979.

46. Goldhirsh, J., "Prediction of Slant Path Rain Attenuation Statistics at Various Locations", Radio Sc., vol. 12, #5, pp. 741-747, 1977.

47. Hendry, A., Antar, Y., Schlesak, J., and Olsen, R., "Melting Layer Attenuation at 28.56 GHz from Simultaneous Comstar Beacon and 16.5 GHz Diversity Radar Observations", presented at IEE Second Intl. Conf. on Antennas and Propagation, U. of York, U.K., Apr. 13-16, 1979.

48. Watson, P., McEwan, N., Dissanayake, A., and Haworth, D., "Attenuation and Cross-polarization Measurements at 20 GHz Using the ATS-6 Satellite with Simultaneous Radar Observations", IEEE Trans. Ant. & Prop., AP-27, pp. 11-17, 1979.

49. Nishitsuji, A., and Matsumoto, A., "The Character of Falling Snow", from SHF and EHF Propagation in Snow Districts, Momograph Series of the Research Inst. of Applied Electricity, Hokkaido U., Sapporo, Japan, vol. 19, pp. 63-78, 1971.

50. Nishitsuji, A., and Matsumoto, A., "Calculation of Radiowave Attenuation Due to Snowfall", ibid., pp. 63-78, 1971.

51. Nishitsuji, A., and Matsumoto, A., "Problems on the Radio Wave Attenuation in Millimeter and Microwave Regions at Snowfall", ibid., pp. 79-91, 1971.

52. Mason, B., The Physics of Clouds, Oxford University Press, Amen House, London, 1957.

53. Pruppacher, H., and Klett, J., Microphysics of Clouds and Precipitation, D. Reidel Publishing Co., Dordrecht, Holland, 1978.

54. Hallgren, R., and Hosler, C., "Preliminary Results on the Aggregation of Ice Crystals", Physics of Precipitation, Geophysical Monograph #5 NAS-NRC #746, pp. 257-263, 1959.

55. Rogers, R., A Short Course in Cloud Physics, Pergamon of Canada Ltd., Toronto, Canada, 1976.

56. Ludlarn, F., Clouds and Storms, The Pennsylvania State U. Press, 1980.

57. Owen, N., "Digital Radio Test at 8 GHz, Big Sicker-Vancouver", B.C. Telephone Co. Rpt., Exp. Proj. 000723, Jan. 1981.

58. Dept. of Communications, "Application Procedures for Planned Radio Stations Above 890 MHz in Terrestrial Fixed Service", RSP-113, Issue 2, Sept. 1975.

59. Kheirallah, H., Segal, B., and Olsen, R., "Application of Synthetic Storm Data to Evaluate Path Average Rain Rate Techniques for Predicting Rain Attenuation Statistics", Proc. URSI Commission F Open Symposium, Lennoxville, Quebec, Canada, pp. 2.10.1-2.10.6, 1980.

60. Drafuca, G., J. Rech. Atmos., vol. 8, pp. 399-441, 1974.

61. Bertook, E., DeRenzis, G., and Drufuca, G., Proc. URSI Commisssion F Open Symposium, La Baule, France, pp. 295-300, 1977.

62. Watson, P., Ahmed, H., and Papaioannou, G., IEE Conf. Proc. 169, part 2, pp. 92-96, 1978.

63. Annual Meteorological Summary for 1978, 1979, 1980: Agassiz Experimental Farm, Atmospheric Environment Service, Environment Canada.

64. Van der Star, J., and Kharadly, M., "Measurements of Copolar Attenuation Through the Bright Band at 4 and 7 GHz", Annales des Telecommunications, vol. 36, #1-2, Feb. 1981.

65. Van der Star, J., and Kharadly, M., "Measurement of Copolar Attenuation Through the Bright Band at 4 & 7 GHz", Proc. URSI Commission F Open Symposium, Lennoxville, Quebec, Canada, pp. 4.8.1-4.8.3, 1980.

66. McNicol, J., Rain Attenuation at 74 GHz, M.A.Sc. Thesis, Dept. of Electrical Engineering, The University of British Columbia, Mar. 1977.

67. Bullington, K., "Radio Propagation for Vehicular Communications", IEEE Trans. on Behicular Technology, vol. VT-26, #4, pp. 295-308, Nov. 1977.

68. Okumura et al., "Field Strength and it's Variability in VHF and UHF Land-Mobile Radio Service", Review of Tokyo Elec. Comm. Lab., vol. 16, pp. 835-873, Sept.-Oct. 1978.

69. Shepherd, N., "VHF and UHF Propagation", General Electric Datafile Bulletin #10003-1, July 1962.

70. Peters, B., An Experimental Investigation of Dual-Polarized Atmospheric Propagation at 73 GHz, Ph.D. Thesis, Dept. of Electrical Engineering, The University of British Columbia, April 1982.

71. Thomson, D., Coulter, R., and Warhaft, Z., "Simultaneous Measurements of Turbulence in the Lower Atmosphere Using SODAR and Aircraft", Fourth Symposium on Meteorological Observations & Instrumentation of the American Meteorological Society, Denver, Colorado, April 10-14, 1978.